Secretion from the *Leishmania* flagellum as a potential mechanism of virulence factor delivery

Makin, Laura
St Edmund Hall
University of Oxford

A thesis submitted for the degree of
DPhil
Michaelmas term 2017

List of contents

List of Tables

List of Figures

1. Introduction

2. Materials and Methods

3. Subcellular origin and structure of *L. mexicana* EVs

4. Biochemical and molecular characterisation of *L. mexicana* EVs

5. Biological effects of *L. mexicana* promastigotes and EVs on macrophages

6. Discussion

List of abbreviations

AB	Add-back
AP-1	Activator protein 1
BiP	Binding immunoglobulin protein
BMDM	Bone marrow-derived macrophage
Cas9	CRISPR-associated gene 9
CXCL	C-X-C motif chemokine
DC	Dendritic cell
DIC	Differential interference contrast
DIF	Differentiating *Leishmania*
EF	Elongation factor
eGFP	Enhanced Green Fluorescent Protein
EM	Electron microscopy
Erk	Extracellular signal-related kinase
ESCRT	Endosomal sorting complex required for transport
eYFP	Enhanced Yellow Fluorescent Protein
EV	Extracellular vesicle
FCS	Foetal calf serum
FM	Flagellar membrane
FP	FP
GO	Gene ontology
GPCR	G protein-coupled receptor
GPI	Glycophosphatidylinositol
GT2	Glucose transporter 2
HRP	Horseradish peroxidase
IFN	Interferon
IL	Interleukin
iPSC	Induced pluripotent stem cell
JNK	c-Jun N-terminal kinase
Kb	Kilobase pairs
kDa	Kilodaltons
Log	Logarithmic
LPG	Lipophosphoglycan
LPS	Lipopolysaccharide
M199	Medium M199 (for promastigote culture)
MAPK	Mitogen-activated protein kinase
mCh	mCherry fluorescent protein
M-CSF	Macrophage colony-stimulating factor
mNG	mNeon Green fluorescent protein
MOI	Multiplicity of infection
MS	Mass spectrometry
NFκB	Nuclear factor kappa-light-chain-enhancer of activated B cells
NK	Natural killer
NTA	Nanoparticle tracking analysis
ORF	Open reading frame
PAMP	Pathogen-associated molecular pattern
PBS	Phosphate-buffered saline
PCR	Polymerase chain reaction

PF	Paraformaldehyde
PFR	Paraflagellar rod
PM	PM
PPG	Proteophosphoglycan
PRO	Promastigote
PRR	Pattern recognition receptor
PV	Parasitophorous vacuole
SAP	Secreted acid phosphatase
SEM	Standard error of the mean
sgRNA	Single guide RNA
SHP-1	Src homology region 2 domain-containing phosphatase 1
SM5.5	Schneider's Drosophila Medium, pH 5.5
SMP1	Small myristoylated protein 1
SNARE	Soluble N-ethylmaleimide-sensitive factor activating protein receptor
TEM	Transmission electron microscope
TGN	Trans-Golgi network
Th	T helper
TLR	Toll-like receptor
TNF	Tumour necrosis factor
T7 RNAP	T7 RNA polymerase
UA	Uranyl acetate
WB	Western blot
WCL	Whole cell lysate
WT	Wild type

List of species

C. elegans	*Caenorhabditis elegans*
C. reinhardtii	*Chlamydomonas reinhardtii*
C. fasciculate	*Crithidia fasciculate*
D. melanogaster	*Drosophila melanogaster*
L. braziliensis	*Leishmania braziliensis*
L. donovani	*Leishmania donovani*
L. infantum	*Leishmania infantum*
L. major	*Leishmania major*
L. mexicana	*Leishmania mexicana*
L. panamensis	*Leishmania panamensis*
L. pifanoi	*Leishmania pifanoi*
L. tarentolae	*Leishmania tarentolae*
T. brucei	*Trypanosoma brucei*

List of appendices

(Supplied digitally and can be accessed online at the Oxford University Research Archive)

Appendix 1. Triplicate data PRO DIF EV label-free MS. This Excel workbook shows TriTrypDB accession numbers for all *L. mexicana* proteins from the 3 biological repeats of the PRO and DIF EV MS analyses as identified by a MS/MS ion search using Mascot software against an *L. mexicana* genome (Fiebig et al., 2015).

Appendix 2. GO term enrichment in PRO and DIF EV MS data. This Excel workbook shows the GO term enrichment analysis of proteins present in every PRO repeat and every DIF repeat.

Appendix 3. Proteins found in all PRO repeats, all DIF repeats and all repeats of EV MS data. This Excel workbook shows TriTrypDB accession numbers for the 56 proteins found in all PRO EV repeats, the 127 proteins found in all DIF repeats and the 37 proteins found in all 6 repeats, as shown in Fig. 4.5F.

Appendix 4. Proteins selected for fluorescent tagging based on PRO and DIF EV MS analyses. This Excel worksheet shows the proteins which have been selected for fluorescent tagging, as shown in Table 4.5, with extra columns giving more information about each protein: which terminus of the protein was tagged and why, flagellar enrichment, presence in other proteomes, InterPro annotation, conservation, presence of GPI anchors and signal peptides, molecular weight, transmembrane domains and GO term analyses. Proteins which were successfully tagged at either terminus to produce drug resistant cell lines are shown in green (36). Proteins where tagging was attempted but unsuccessful are shown in black (7). 5 additional proteins are shown which were selected for fluorescent tagging but tagging was not actually attempted for reasons which are stated (red). Note that C terminal tagging is the default.

Abstract

Protozoa of the *Leishmania* genus are transmitted between mammalian hosts by the sandfly and cause the neglected tropical disease leishmaniasis. Upon injection into the mammalian host by the sandfly promastigote-form parasites are phagocytosed by macrophages, where they differentiate into amastigotes. Although many virulence factors are known to modulate macrophage signalling pathways to favour infection, the delivery mechanisms are largely unknown. During differentiation to amastigotes the promastigote flagellum shortens dramatically and the fate of the excess flagellar membrane is unknown. Here we investigate the possibility that during *Leishmania mexicana* differentiation, shedding of the flagellar membrane is a source of extracellular vesicles (EVs) which provide a virulence factor delivery mechanism. The kinetics and structural mechanisms of EV release from promastigotes were investigated by live cell imaging and by measuring the concentration of shed EVs. Isolated EVs from a differentiating parasite culture or a control promastigote parasite culture were analysed by fluorescence and electron microscopy and mass spectrometry. To study the biological effects of EVs, macrophages were exposed to isolated EVs or live promastigotes and cytokine secretion was quantified by ELISA. An *LPG1* null mutant was used to assess the contribution of virulence factor lipophosphoglycan (LPG) to the observed effects. Known protein virulence factors and LPG are present in *L. mexicana* EV fractions as well as known flagellar proteins. We show that there is a link between *L. mexicana* flagellar shortening and EV release, which is a recently discovered phenomenon in *Chlamydomonas* and mammalian cell research. We find that isolated EVs and live promastigotes induce changes in secreted cytokine levels from human and murine macrophages, including a substantial and previously unreported suppression of CXCL10, a chemokine which plays a protective role in *Leishmania* infection. LPG contributes to the effects observed on cytokine production, and EVs may be an important delivery mechanism for LPG.

Thesis word count (excluding figures, tables, bibliography and appendices): 49,667

Declaration: All work in this thesis has been carried out by Laura Makin and has not been previously submitted for any other degree. One figure has been previously published (Figure 4.12, Beneke et al., 2017) in an open access paper and this work was fully produced by Laura Makin.

1. Introduction

1.1. Known effects of *Leishmania* on the host immune response

1.1.1. *Leishmania* parasites cause a range of human diseases

Around twenty species of the protozoan parasite *Leishmania* cause a spectrum of human and animal diseases known as leishmaniases, ranging from the visceral form, which is fatal in 95% of cases unless treated, to the most prevalent and relatively mild cutaneous form (WHO, 2017). The parasite is spread between mammalian hosts by over ninety species of phlebotomine sandfly (WHO, 2017). The disease is classed as one of the neglected tropical diseases which mostly affect the world's poorest people; there are approximately one million new cases and 20,000 deaths per year according to the latest World Health Organisation figures. The *Leishmania* species studied here is *Leishmania mexicana* (*L. mexicana*), the most common cause of cutaneous leishmaniasis in South America (Kevric et al., 2015). This form of the disease presents as skin lesions which can cause disfigurement and social isolation; the lesions are usually self-healing within several months, but can also present as chronic or diffuse forms (Kassi et al., 2008). For all forms of leishmaniasis, most current drug regimes span several days to a month and cannot be taken orally, making administration in resource-poor settings challenging (de Menezes et al., 2015). This situation has been improved by the addition of a liposomal amphotericin B to the list of available drugs, which can be administered in a single dose, however this treatment is only effective for visceral leishmaniasis and only in certain geographical areas (Sundar and Singh, 2016). Further adding to the difficulty in controlling leishmaniasis, there is no human

vaccine and in some areas zoonotic reservoirs exist (Lima et al., 2013, Roque and Jansen, 2014).

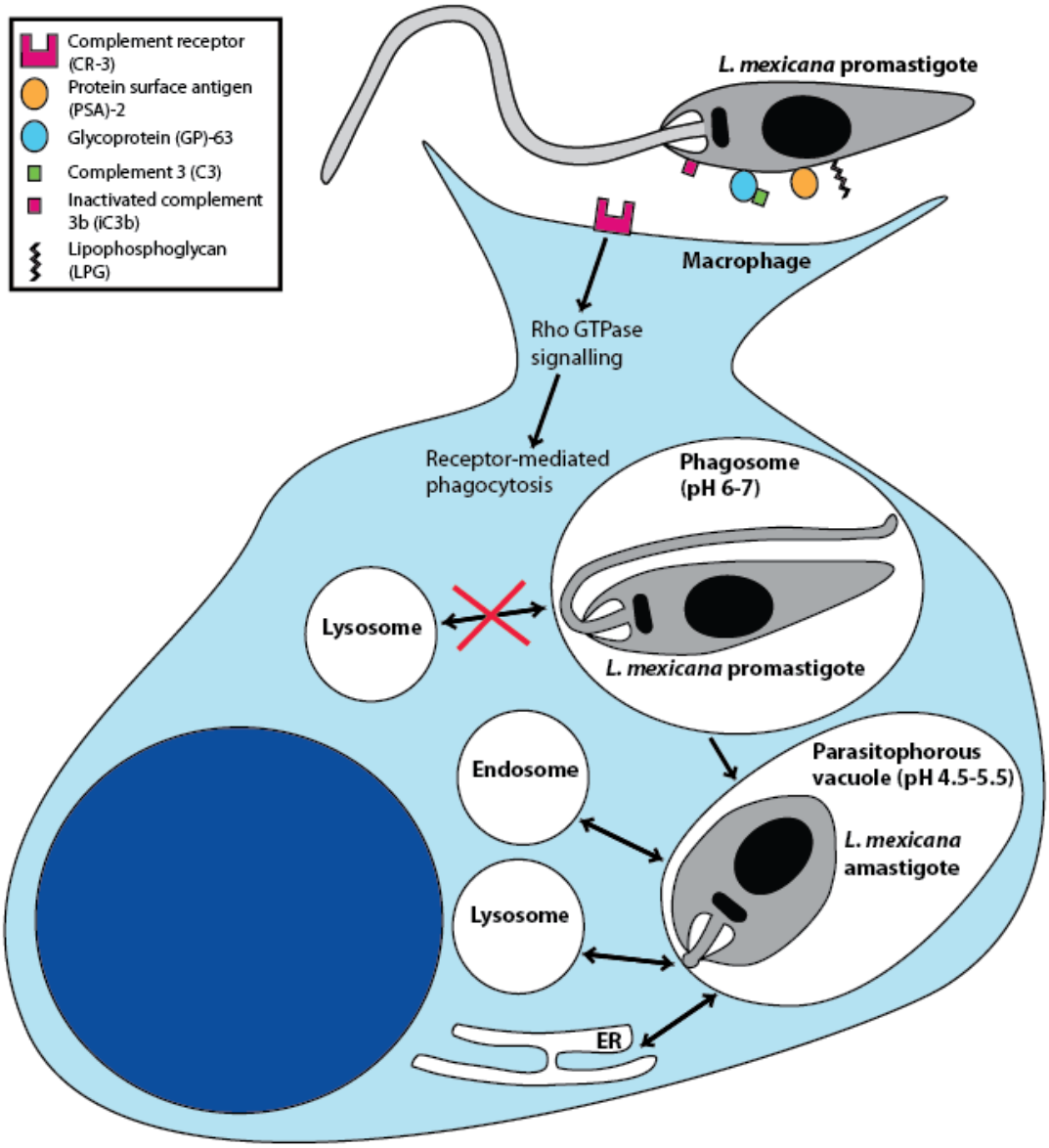

Figure 1.1. Macrophage uptake and differentiation of *L. mexicana* promastigotes. Following injection of promastigotes by the sandfly into the mammalian host, parasite and host factors on the parasite surface interact with macrophage receptors including complement receptor 3, triggering Rho GTPase-dependent actin filament rearrangement in the macrophage. The parasites are subsequently taken up via receptor-mediated phagocytosis. During promastigote to amastigote differentiation the phagosome resists fusion with lysosomal

compartments and retains a near-neutral pH. Mature, amastigote-containing parasitophorous vacuoles (PVs) have lowered pH and interact with many cellular compartments. A single amastigote within the PV is shown here, but during infection many amastigotes can occupy the same PV.

During their life cycle, *Leishmania* spp. alternate between two morphological forms: elongated promastigotes that live in the sandfly vector and small round amastigotes, which replicate in the mammalian host (see Figure 1.2 for a summary of the life cycle). In the sandfly the parasites progress through a series of distinct promastigote morphologies, alternating between replicating and non-replicating stages (Gossage et al., 2003, Rogers et al., 2002). The flagellum of promastigotes is long and motile and used for swimming and attachment in the insect vector. Upon uptake by phagocytes in the mammalian host, infectious metacyclic promastigotes morphologically differentiate over the course of 16 h to the amastigote form, which have a short immotile flagellum which structurally resembles sensory cilia (Gluenz et al., 2010), and shorter rounder cell body (Wheeler et al., 2015). During the initial stages of infection, the parasites are taken up primarily by neutrophils in the first 24 h and subsequently accumulate in macrophages, the primary host cell, over the course of several days (Peters et al., 2008). Parasites are taken up by macrophages via receptor-mediated phagocytosis, which is dependent on surface-anchored parasite factors, notably the zinc metalloprotease glycoprotein GP63 (also called leishmanolysin) and lipophosphoglycan (LPG), and interactions between parasite-bound complement factors and macrophage complement receptors (CRs) (Ueno and Wilson, 2012) (Figure 1.1). Initially following promastigote uptake, fusion between the phagosome and lytic compartments is limited, leading to a delay in acidification while promastigote to

amastigote differentiation takes place (Desjardins and Descoteaux, 1997, Moradin and Descoteaux, 2012) (Figure 1.1). Once differentiated, *L. mexicana* amastigotes reside in the low pH environment of multi-occupancy parasitophorous vacuoles (PVs) within macrophages (Benchimol and de Souza, 1981) (Figure 1.1). The PV is a modified membrane-bound phagosomal compartment (Figure 1.1) which contains both host and parasite factors (Ndjamen et al., 2010). Once differentiation is complete, *L. mexicana* replication within PVs is slow, with a doubling time of around 12 days in murine infection (Kloehn et al., 2015). Amastigotes egress from host macrophages and infect new macrophages to propagate the infection (Real et al., 2014).

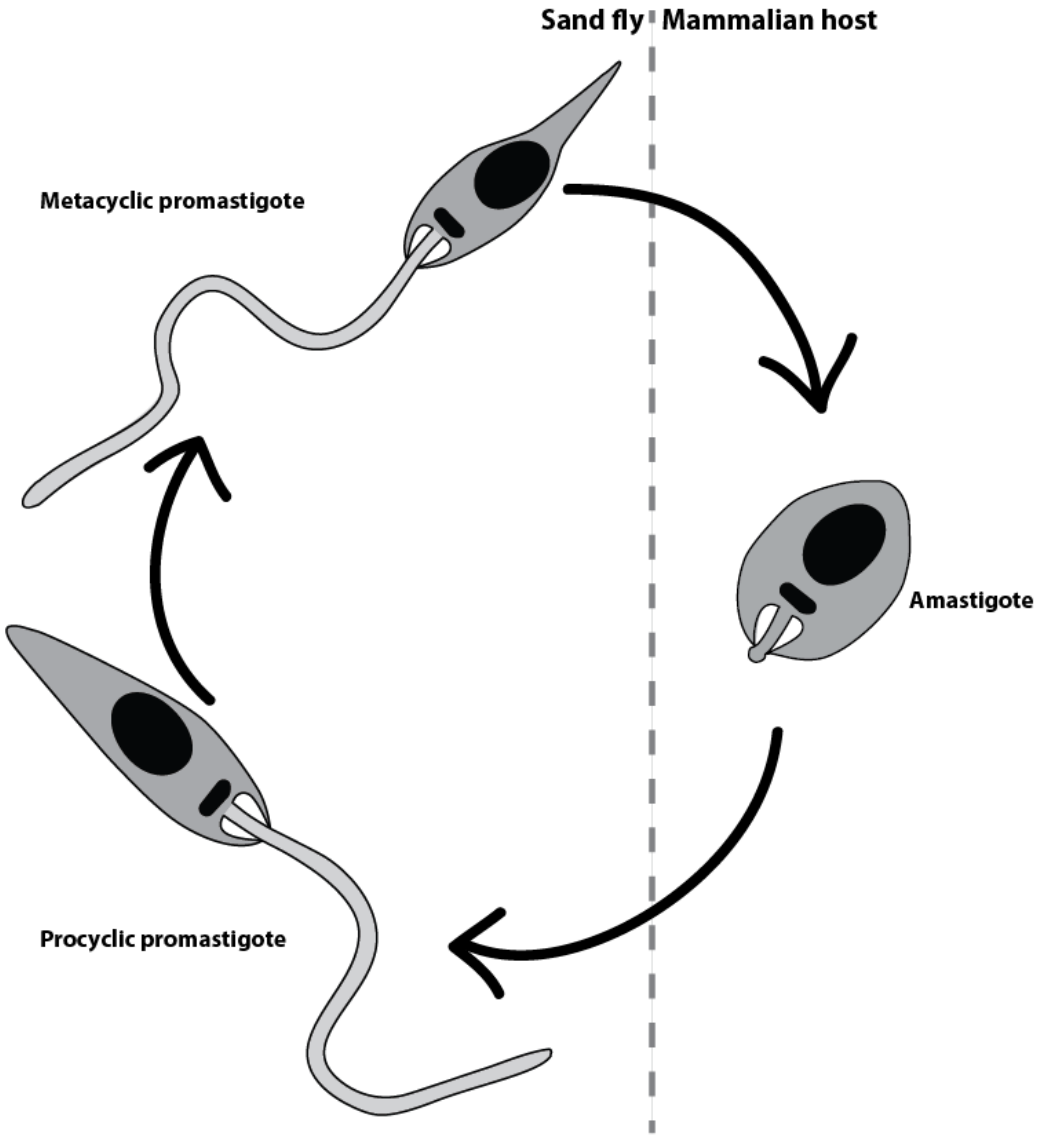

Figure 1.2. The *Leishmania* life cycle. This schematic shows a simplified version of the major *Leishmania* life cycle stages. Procyclic promastigotes replicate in the sandfly midgut then migrate up to the thoracic midgut and stomodeal valve where they differentiate to infective metacyclic promastigotes, which are non-replicative. They are egested by the sandfly during the bite to a mammalian host, where they are phagocytosed by host macrophages and differentiate to replicative amastigotes which cause the disease leishmaniasis. When a sandfly bites, a pool of blood containing amastigotes is created and ingested. The amastigotes differentiate back to procyclic promastigotes and escape from the bloodmeal, and the life cycle continues.

1.1.2. The immune response in self-healing and persistent *Leishmania* infection

The immune response to *Leishmania* infection is highly complex and depends on host status and the *Leishmania* species; there is still much that we do not understand, particularly for human infection. In mice there is clear evidence that a T helper 1 (Th1) response controls infection while a Th2 response is permissive (Wang et al., 1994, Kopf et al., 1996). The early work establishing this Th1/Th2 paradigm was done mostly in *L. major* murine studies. Production of interleukin (IL)-12 and interferon (IFN)-γ defines the Th1 response leading to parasite clearance, and IL-4 classically defines the non-healing Th2 response (Heinzel et al., 1989). However, subsequent studies have called into question whether IL-4 itself is necessary for the establishment of a non-healing Th2 response (Mohrs et al., 2000), or whether the non-healing phenotype is simply a lack of an effective Th1 response. It has been suggested that IL-4 is not essential, since IL-4-deficient mice are not necessarily resistant to infection (Noben-Trauth et al., 1996). Furthermore, high levels of IL-4 have been shown to exacerbate cutaneous but not visceral murine infection, showing the paradigm is not universal. In visceral infection, there is strong evidence that IL-10 and transforming growth factor (TGF)-β, rather than IL-4, play an important role in promoting *Leishmania* infection (Saha et al., 2007). The use of susceptible BALB/c mice in the initial studies establishing the Th1/Th2 paradigm is significant, since this strain of mice is known to have defects in the Th1 response (Barbi et al., 2008). IL-13 also seems to play an important role in establishing the non-healing Th2 response which may be independent of IL-4, since normally-resistant C57BL/6 mice which were induced to overexpress IL-13 were rendered susceptible to *L. major* infection (Matthews et al., 2000).

The early conclusions drawn about the Th1/Th2 paradigm do not necessarily apply to *L. mexicana* infection in all cases, since this parasite species is able to induce non-healing disease in many mouse strains resistant to *L. major* (McMahon-Pratt and Alexander, 2004). However, the general conclusions that IL-12 is protective (Rodriguez-Sosa et al., 2001) and IL-4 is conducive to a non-healing response (Satoskar et al., 1997) also appear to be true for *L. mexicana* infection of mice.

For all *Leishmania* species, an IL-12-driven Th1 response does appear to be protective and the importance of Th1 cytokines for parasite clearance is widely accepted; this response ultimately leads to parasite clearance through IL-12 and IFNγ-dependent enhancement of macrophage parasite killing (Alexander and Bryson, 2005). The crucial role for IFNγ in mounting an effective response to *L. major* infection was shown through infection of normally-resistant mice which lack IFNγ; these mice were no longer resistant, even though other Th1 cytokines were produced and significant levels of Th2 cytokines were not, showing that IFNγ is perhaps the most important cytokine in the healing response (Swihart et al., 1995). IFNγ also has a crucial role in clearing murine visceral leishmaniasis (Lehmann et al., 2000). The role of IL-12 in driving the Th1 response was shown through injection of IL-12 at the same time as *L. major* infection of BALB/c mice, leading to enhanced parasite control (Von Stebut et al., 2003). Similar effects have also been shown by injection of C-X-C motif chemokine (CXCL)-10, another Th1-associated cytokine (Vasquez and Soong, 2006).

IL-10 and TGFβ are both correlated with persistence of human visceral leishmaniasis (Saha et al., 2007) and IL-10 is also correlated with non-healing human cutaneous leishmaniasis (Castellano et al., 2009, Salhi et al., 2008). Studies in mice have shown

that this correlation is likely directly due to IL-10 action, since IL-10 KO mice are better able to clear parasites and increased levels of IL-10 leads to increased susceptibility to infection (Maspi et al., 2016). However, IL-10 is often also present alongside a robust Th1 response to regulate excessive tissue damage due to inflammation, therefore high IL-10 levels do not necessarily preclude a healing response (Gomes-Silva et al., 2007, Abdoli et al., 2017).

In contrast to murine infection, in humans the Th1/Th2 paradigm is less clear-cut and certainly less well studied (Ajdary et al., 2000, Rogers and Titus, 2004). However, it does seem that, as for murine infection, Th1-type cytokines are important for clearance of infection (Gaafar et al., 1995) and IL-4 correlates with persistence of cutaneous lesions (Ajdary et al., 2000). It is thought that chronic *Leishmania* infection in humans tends to induce an immunosuppressive environment characterised by Th2 or mixed Th1/Th2 responses (Shio et al., 2012, Salhi et al., 2008) and high expression of anti-inflammatory cytokines IL-10 and TGFβ (Anderson et al., 2008, Saha et al., 2007, Salhi et al., 2008). The effects of host cytokine levels on *Leishmania* infection are summarised in Table 1.1. Several studies also show that induction as well as inhibition of pro-inflammatory cytokines such as IL-8, IL-12 and IFNγ occurs during early infection (Teixeira et al., 2006, Matte and Olivier, 2002) in cell types including macrophages, and this early inflammation may help establish the disease. Further studies are needed to determine to what extent the Th1/Th2 paradigm applies to human infection with different *Leishmania* species.

Table 1.1. Summary of the roles of host cytokines in *Leishmania* infection persistence or clearance. The main published effects of host cytokines on *Leishmania* infection are summarised.

Host cytokine	Effect on *Leishmania* infection	References
IL-12	Promotes parasite clearance and a protective Th1 response.	(Vargas-Inchaustegui et al., 2009) (Alexander and Bryson, 2005) (Rodriguez-Sosa et al., 2001) (Whitaker et al., 2008)
IFNγ	Promotes parasite clearance by enhancing macrophage killing of parasites as part of a protective Th1 response.	(Vargas-Inchaustegui et al., 2009, Murray et al., 2013) (Alexander and Bryson, 2005) (Halliday et al., 2016) (Swihart et al., 1995) (Becker et al., 2003)
IL-10	High levels of IL-10 correlate with parasite persistence in mice and humans. IL-10 may also be needed to restrict tissue damage.	(Kropf et al., 2004) (Saha et al., 2007) (Gallego et al., 2011) (Maspi et al., 2016) (Ibraim et al., 2013, Rojas-Bernabe et al., 2014) (Whitaker et al., 2008)
IL-4	Levels of IL-4 correlate with parasite persistence in cutaneous infection of humans and mice.	(Heinzel et al., 1989) (Satoskar et al., 1997) (Abou Fakher et al., 2009) (Ajdary et al., 2000)
IL-13	High levels of IL-13 are associated with the non-healing Th2 response.	(Matthews et al., 2000)
TGFβ	High levels of TGFβ are associated with non-healing visceral infection in humans.	(Saha et al., 2007)

1.1.3. Known effects of promastigote *Leishmania* infection on macrophage cytokine secretion

The systemic cytokine response to *Leishmania* infection has been extensively studied, as discussed above in *Section 1.1.2*. In addition, significant efforts have been made to determine the cytokine responses of individual cell types, including the primary host cell: macrophages. Macrophages are an important source of many cytokines including tumour necrosis factor (TNF)-α, IL-12 and IL-10 (Arango Duque and Descoteaux, 2014), and their direct contact with the *Leishmania* parasites which infect them makes

them a key target for parasite modulation of the cytokine response. Increases in the secretion of a large number of mostly pro-inflammatory cytokines from unstimulated macrophages has been documented in response to infectious stationary phase promastigotes (Filardy et al., 2014, Arango Duque et al., 2014). Although amastigotes are also used for experimental macrophage infection, the scope of this discussion is limited to promastigote infection and the early establishment of infection, i.e. up to one week following infection. This is because we are interested in the early delivery of virulence factors to prepare the host macrophage for infection. It should be noted that stationary phase *Leishmania* promastigotes are often used for infection studies since this population is enriched for infective metacyclic parasites (up to 50%) (Sacks et al., 1985); purified metacyclic parasites are not used in this study because this requires extra density gradient separation steps (Spath and Beverley, 2001). Upon infection of unstimulated resident macrophages from C57BL/6 mice with stationary phase *L. major* promastigotes TNFα, IL-6, TIMP-1, IL-1ra (an anti-inflammatory cytokine), G-CSF, TREM, CXCL1, MIP-1α, MIP-1β, MCP-1, and MIP-2 were all upregulated (Filardy et al., 2014). It is not clearly understood why *Leishmania* parasites would induce the production of pro-inflammatory cytokines which are associated with resistance to infection (Teixeira et al., 2014), but it is possible that early inflammation may promote host cell recruitment and help establish the infection. It is also possible that it may represent an effective host response to *Leishmania* infection. Another study confirmed that TNFα and IL-6 secretion were increased after infection of unstimulated murine bone marrow-derived macrophages (BMDMs) with *L. major* or *L. donovani* promastigotes (Arango Duque et al., 2014). In contrast, a study carried out in human THP-1 macrophages found that TNFα secretion

was unchanged after infection with *L. donovani* promastigotes, while IL-8 secretion was increased (Silverman et al., 2010a). This discrepancy may be accounted for by differences between murine and human responses. IL-8 is a chemoattractant for neutrophils, the main reservoir of *Leishmania* parasites in the initial days of infection (Peters et al., 2008); IL-8 is therefore an important chemokine in the establishment of *Leishmania* infection. The gene encoding IL-8 is absent in mice (Mestas and Hughes, 2004). There could be several reasons, aside from parasite and host species, why an increase in TNFα was not observed in all studies. One important parameter which varies between different studies is the infection time, which is important because each cytokine has its own secretion kinetics (Lacy and Stow, 2011, Stow et al., 2009, Arango Duque and Descoteaux, 2014, Eichelbaum and Krijgsveld, 2014); it is therefore unlikely that at any chosen time point all the cytokines of interest will be at peak secretion.

In *Leishmania* infection studies, macrophages are commonly treated with lipopolysaccharide (LPS) and/or IFNγ to induce a pro-inflammatory 'classically activated' phenotype which is accompanied by the increased production of many cytokines including TNFα, IL-12 and IL-10 (van Wilgenburg et al., 2013). This treatment allows the study of macrophages in an inflammatory environment mimicking what might be present during infection, although a wider range of activated macrophage subtypes are also likely to be present during infection (Martinez and Gordon, 2014). Using this experimental setup, several cytokines have been found to be inhibited by *Leishmania* promastigote infection. The production of IL-12, a key driver of the Th1 response which promotes parasite clearance as discussed above in *Section 1.1.2*

(Ghalib et al., 1995, Strauss-Ayali et al., 2005), was found to be completely inhibited when murine granuloma macrophages were simultaneously infected with *L. major* promastigotes and stimulated with LPS and IFNγ (Belkaid et al., 1998). IL-12, as well as IL-17, IL-3, IL-4, IL-6 and IL-13, was also found to be inhibited when peritoneal murine macrophages were infected with *L. major* or *L. amazonensis* parasites with simultaneous LPS stimulation (Lapara and Kelly, 2010). The inhibitory effect on IL-12 was further confirmed in *L. mexicana*, where BMDMs from C57BL/6 mice were infected with stationary phase promastigotes with LPS stimulation (Cameron et al., 2004). Inhibition of IL-12 by *Leishmania* promastigotes is therefore a well-documented effect, and is in line with the Th1/Th2 paradigm which implies that inhibition of this Th1-type cytokine would favour the parasite (Von Stebut et al., 2003). It is perhaps surprising, given the strong correlation of IL-10 with persistent *Leishmania* infection (Castellano et al., 2009, Salhi et al., 2008, Saha et al., 2007), that increased production of this cytokine from macrophages in response to promastigotes has not been observed. It is important to bear in mind, however, that macrophages are only one source of IL-10 in systemic infection. In fact *Leishmania* infection has been shown to modulate IL-10 production by another cell type, dendritic cells (DCs), (Silverman et al., 2010b) and by macrophages in response to the amastigote form of the parasite (Yang et al., 2007b).

1.1.4. *Leishmania* virulence factors and their delivery

While many effects of *Leishmania* infection on macrophage cytokine release have been documented, the exact parasite factors which elicit these effects and how are less well understood. Virulence factors can be defined as a protein or other factor such as a glycoconjugate, which when inhibited reduces the ability of a pathogen to

colonise, survive and/or replicate in its host. Furthermore, a virulence factor can be distinguished from a housekeeping gene (which may also be essential for survival in the host) by their ability to interact with host factors and many of them directly modulate or help to evade the host immune response. Many of the best studied virulence factors are bacterial proteins which are secreted into the host environment using specialised secretion systems (Green and Mecsas, 2016). A small number of *Leishmania* virulence factors have been identified for over a decade including GP63 (Thiakaki et al., 2006, Russell and Wilhelm, 1986, Button and McMaster, 1988), LPG (Spath et al., 2000, King et al., 1987, Kaneshiro et al., 1986), cysteine peptidases (Buxbaum et al., 2003) and heat shock proteins (HSPs) (Hubel et al., 1997). Studies using KO cell lines have shown that parasites lacking any of these factors have impaired virulence in mice: GP63 (Thiakaki et al., 2006); LPG (Spath et al., 2000); cysteine peptidases (Buxbaum et al., 2003); HSPs (Hubel et al., 1997). Although, as will be discussed later, parasite dependence on these factors can vary between *Leishmania* species. The best studied of these factors by far are GP63 and LPG, both of which are highly expressed on the promastigote surface and are greatly reduced in the amastigote stage (Abu-Dayyeh et al., 2010, Bahr et al., 1993). Both are surface expressed molecules which are linked to the membrane via a GPI anchor, although secreted forms also exist of both factors (Yao et al., 2003, Ilg et al., 1994). LPG is a glycoconjugate with phosphoglycan repeats (see Chapter 5 Introduction), the structure of which varies between species and life cycle stage (Forestier et al., 2014). GP63 is a multigene family of functional metalloprotease glycoproteins (Yao et al., 2003).

As discussed in *Section 1.2*, LPG and GP63 have both been implicated in the modulation of various host macrophage pathways which could lead to changes in cytokine secretion. However, the delivery mechanisms of these virulence factors have remained elusive until recently, since *Leishmania* species lack specialised virulence delivery systems analogous to bacterial secretion systems (Green and Mecsas, 2016). Several recent papers have convincingly shown that GP63 is delivered to host cells via extracellular vesicles (EVs) and is subsequently detected in the host cytoplasm where many of its host targets are located (See *Section 1.2*) (Gomez et al., 2009, Atayde et al., 2015, Silverman and Reiner, 2011). The trafficking pathways which allow EV-associated GP63 to reach the macrophage cytoplasm are unknown. Recent proteomic and functional studies of *Leishmania* EVs have proposed that EVs are likely to be the major delivery mechanism for virulence factors (Silverman et al., 2010a, Silverman and Reiner, 2011). Indeed, as discussed in *Section 4.1.1*, there is good evidence showing that some virulence factors, including GP63, elongation factor (EF)-1α and HSPs (Silverman et al., 2010a, Hassani et al., 2014), are EV cargo. Evidence supporting their presence in *Leishmania* EVs includes Western blots (WBs) showing that that they are protected from tryptic digest in EV-enriched samples, and that these virulence factors are enriched in the same density gradient fractions as those enriched for EVs (Silverman et al., 2010a, Hassani et al., 2014). However, whether EVs are the sole mechanisms for delivery of these factors and whether other important virulence factors, such as LPG, are delivered via EVs remain open questions. In addition, for *Leishmania* factors which have been less well studied in the context of EVs and which have been assigned as EV cargo mostly on the basis of mass spectrometry (MS), such as cysteine peptidases (Atayde et al., 2015), it is not clear whether these factors are

indeed EV-associated or freely secreted. There are factors such as the phosphoglycoprotein secreted acid phosphatase (SAP) which are known to be secreted freely into the surrounding medium (Ilg et al., 1991), but the contribution of this route to virulence factory delivery is largely unknown.

1.1.5. Diverse roles of extracellular vesicles across eukaryotes

Intercellular communication via EVs is now recognised as a widespread phenomenon across mammalian cells, archaea, bacteria and protozoa (Kim et al., 2014, Raposo and Stoorvogel, 2013, Brown et al., 2015, Schorey et al., 2015). There are three broad classes of EV defined thus far: microvesicles (MVs), apoptotic bodies and exosomes (Colombo et al., 2014). These classes are often confused in the literature and it is common not to differentiate between MVs and exosomes when referring to EVs. Most studies of EVs as intercellular messengers are restricted to MVs and exosomes, although recently several studies have assigned biological roles to apoptotic bodies (Guenat et al., 2017, Zhu et al., 2017, Zweemer et al., 2017). The scope of this study does not include apoptotic bodies, however, since the existence of an apoptotic pathway and in particular apoptotic bodies in *Leishmania* spp. is unclear (Zangger et al., 2002). It is important to consider exosomes and MVs separately due to their different routes of biogenesis: MVs are released at the plasma membrane (PM) by outward budding and exosomes are released by the fusion of multi-vesicular bodies (MVBs) with the PM to release intraluminal vesicles (ILVs) (Raposo and Stoorvogel, 2013). These biogenesis mechanisms are summarised in Figure 1.3. In addition to their different biogenesis mechanisms, exosomes and MVs can be differentiated to a certain extent based on size; exosomes are relatively uniform at 40-100 nm in diameter, whereas MVs are more heterogeneous with diameters ranging from 40-

1000 nm (Livshits et al., 2015). Apoptotic bodies are larger at 500-2000 nm and can contain cellular organelles (Ihara et al., 1998). The overlapping size distribution of the different classes of EVs makes it impossible to separate them based on size alone. Thus far, there are no widely recognised markers to distinguish between the EV classes. Although research with this goal is ongoing (Kowal et al., 2016), it seems unlikely that any such markers would be widely applicable to different cell types or species (discussed further in Chapter 4). Therefore, unless special care has been taken to determine the subcellular origin of a particular population of EVs, it is perhaps best to refer to isolated vesicles as EVs rather than a particular subset.

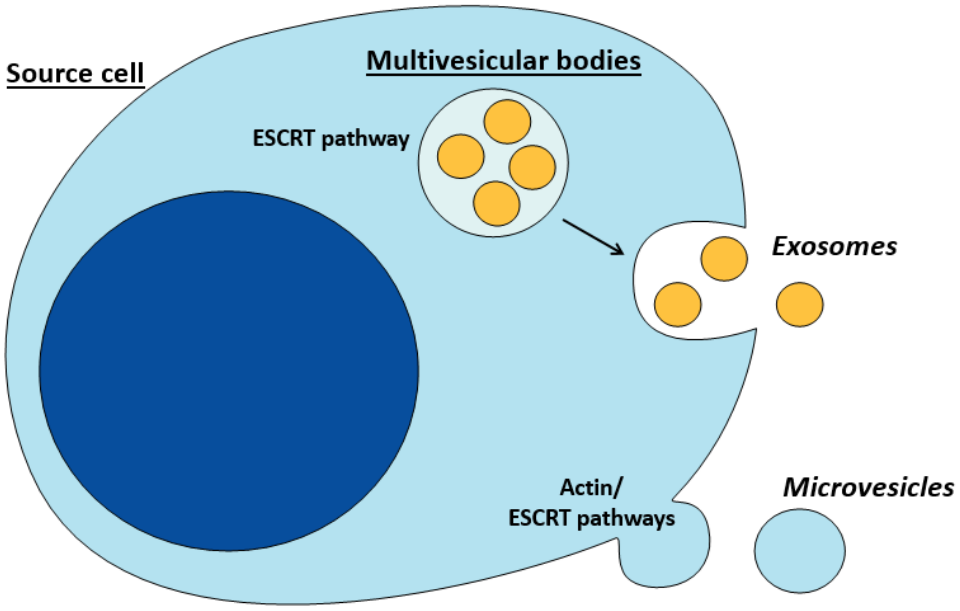

Figure 1.3. Exosome and microvesicle biogenesis. A schematic of a generic cell is shown. Exosomes are released when MVBs fuse with the plasma membrane releasing intraluminal vesicles. Microvesicles bud directly from the plasma membrane. Both processes involve components of the ESCRT complex to induce membrane curvature and scission and actin-dependent pathways have been implicated in microvesicle biogenesis.

The documented roles of EVs are diverse, thanks to their ability to deliver specific protein and RNA cargo (Ramachandran and Palanisamy, 2012, Lawson et al., 2017), and have been reviewed extensively (Lawson et al., 2017, Nazimek et al., 2015, Rodriguez and Prados-Rosales, 2016, Beer and Wehman, 2017, Raposo and Stoorvogel, 2013, Schorey et al., 2015). Much effort has gone into identifying EV cargo to try and elucidate how EVs mediate intercellular communication. Extracellular vesicles have been found to contain RNAs which could influence transcription in the target cell including mRNAs, miRNAs and even tRNAs, as well as proteins including T cell antigens, enzymes and major histocompatibility complexes (MHCs) I and II (Thery et al., 2002a). Relatively little is known about how vesicles carry this cargo to other cells; this could include fusion with the target cell membrane, endocytosis or surface receptor interactions (Mulcahy et al., 2014). EVs can also have their effect in the extracellular matrix (Muralidharan-Chari et al., 2009) or on the surface of the cell from which they were released (Wood et al., 2013). Studies of EV function in mammalian systems have been the most extensive, with known functions ranging from modulation of the immune response through presentation of antigens to T cells (Robbins and Morelli, 2014), to regulation of tumour metastasis (Sullivan et al., 2017) and conference of drug resistance to tumour cells (Samuel et al., 2017b). EVs have been shown to regulate *Drosophila melanogaster* development via the delivery of signalling proteins Wnt and Hedgehog (Beer and Wehman, 2017). In *Caenorhabditis elegans*, EVs have been shown to mediate aspects of mating behaviour via the delivery of polycystins to the environment (Wang et al., 2014).

The function of EVs has also been studied in single-celled eukaryotes including *Chlamydomonas reinhardtii*, where EVs are responsible for the delivery of a protease required for hatching of daughter cells from a shared cell wall (Wood et al., 2013). This study was the first to examine the function of a specific subset of microvesicles: flagellar EVs. The significance of flagellar EVs first came to attention due to the fact that the cell body of *C. reinhardtii* is encased in a cell wall and it has been shown that the flagellar membrane is the main source of EVs in this organism (Wood and Rosenbaum, 2015). This discovery raised questions about the universal importance of the flagellum as a source of EVs and whether they could be functionally different from EVs derived from the cell body membrane. Since then flagellar EVs have been studied in *C. elegans* (Wang et al., 2014)*, Trypanosoma brucei* (Szempruch et al., 2016b) and mammalian cells (Nager et al., 2016), as discussed in greater detail in *Section 3.1.1*, suggesting that they could be a widespread phenomenon across eukaryotes.

A small number of studies have examined the role of EVs in the interaction between host and protozoan parasite and this topic has been recently reviewed (Szempruch et al., 2016a, Marti and Johnson, 2016). There are broadly three mechanisms by which EVs can modulate host-pathogen interactions. Firstly, EVs can be used for parasite-parasite communication to enhance fitness; an example of this is transfer of the protein serum resistance-associated antigen (SRA), which confers resistance to cell lysis by trypanosome lytic factors in human serum, from resistant to non-resistant *T. brucei* species via EVs (believed to be flagellar-derived) (Szempruch et al., 2016b). Secondly, EVs from parasitized host cells can modulate infection; EVs from the malaria parasite *P. falciparum*-infected erythrocytes can activate macrophages and induce the

production of cytokines including IL-10 (Mantel et al., 2013). Finally, EVs released directly from the parasite can exert effects on the host; *Leishmania* spp. EVs have several documented effects on the immune response. In addition to the effects of *Leishmania* EVs on host cytokine production and transcription factors which are discussed in detail below (*Section 1.2*), when injected into mice prior to infection, both *L. major* and *L. donovani* EVs lead to increased parasite burden and a Th2-skewed immune response (Silverman et al., 2010b). *L. major* infection of mice was also exacerbated when isolated EVs were co-injected simultaneously with infectious parasites, a situation thought to mimic the *in vivo* setting since *Leishmania*-derived EVs have been isolated from sandfly inocula (Atayde et al., 2015). This strongly suggests that *Leishmania* EVs have immunosuppressive properties which favour infection. However, other studies suggest their effects may be more nuanced; injection of isolated *Leishmania* EVs into mice induces recruitment of immune cells, in particular host macrophages and neutrophils, to a greater extent than parasites alone (Hassani et al., 2014). This seemingly pro-inflammatory effect of EVs could aid the establishment of infection via the recruitment of host cells to parasitize, alongside their ability to favour infection via the induction of anti-inflammatory cytokines. Specific effects of *Leishmania* EVs on host intracellular pathways have also been reported: incubation of *L. major* EVs with macrophages leads to the cleavage of several protein tyrosine phosphatases (PTPs) including Src homology region 2 domain-containing phosphatase (SHP)-1, in a GP63-dependent manner (Hassani et al., 2014).

1.2. EV biogenesis mechanisms

1.2.1. ESCRT pathway

ESCRT proteins are involved in a variety of processes such as cytokinesis abscission and MVB formation, which all involve membrane curvature induction and abscission (reviewed in (Hurley, 2015)). The process is usually dependent on mono- or Lys 63 linked- ubiquitination of the cytosolic tails of transmembrane proteins (Raiborg and Stenmark, 2009). The ESCRT pathway is implicated in both exosome release via MVB formation (discussed below) as well as microvesicle release by facilitating outward PM budding (Kieffer et al., 2008).

Table 3.1. Presence of ESCRT components in *Leishmania*. The presence (tick) or absence (cross) of *S. cerevisiae* ESCRT components in *L. major*, as determined by BLAST analysis, is shown. This data is taken from an evolutionary study by Leung et al. (Leung et al., 2008).

ESCRT component	Present in *Leishmania*
ESCRT 0	
Hse1	×
Vps27	×
ESCRT I	
Vps37	✓
Vps28	✓
MVB12	×
Vps23	✓
ESCRT II	
Vps36	✓
Vps22	✓
Vps25	✓
ESCRT III	
Vps20	✓
Vps32	✓
Vps2	✓
Vps24	✓
CHMP7	×
ESCRT III-associated	
Vps31	✓
Vps4	✓
Vta1	✓
Vps46	✓
Vps60	✓

The ESCRT pathway comprises complexes 0, I, II and III, as well as associated proteins (Hurley, 2015), most of which have high identity homologs in *Leishmania* spp. although ESCRT 0 components are absent (Table 3.1). Knockdown of Tsg101 leads to reduced microvesicle secretion from murine T cells, as well as failure to package T cell receptor into microvesicles (Choudhuri et al., 2014), suggesting a role for ESCRT proteins in cargo selection as well as EV biogenesis. Tsg101 knockdown, as well as

knockdown of ESCRT 0 proteins HRS and STAM1, also leads to reduced EV release in HeLa cells (Colombo et al., 2013). In murine T cells disruption of ESCRT protein vacuolar protein sorting (Vps)-4 function leads to an accumulation of microvesicles at the PM which fail to be released, consistent with the role of Vps4 in disassembly of ESCRT III complexes allowing membrane scission to take place. Vps4 is essential in almost all ESCRT-dependent processes so far studied (Kieffer et al., 2008, Stuchell-Brereton et al., 2007, Obita et al., 2007) and has a reciprocal best BLAST homolog in *Leishmania* spp. (LmxM.08_29.2500). Overexpression of a dominant negative form of Vps4 (E235Q) induces defects in MVB cargo sorting and trafficking in *L. major* similar to those seen in budding yeast, as well as reduced ability to differentiate and infect murine macrophages (Besteiro, Williams et al. 2006).

1.2.2. The role of MVBs in exosome release and their presence in *Leishmania*

MVBs were initially observed by EM studies of mammalian cells in the 1950s (Palade, 1955). Classical MVBs have since been well studied in mammalian cells and yeast and are characterised by the presence of ILVs, ESCRT components and Rabs, in particular Rab7 (reviewed in (Hanson and Cashikar, 2012)). Late endosomes contain activated signalling proteins such as receptor-ligand complexes which are either recycled back to the PM, or internalised into ILVs as the endosome matures into a MVB. MVBs fuse with the PM to release exosomes or with lysosomes where the contents of ILVs are degraded. Canonical mammalian MVBs are 100-600 nm across with ILVs ~50 nm across. Both tetraspanin association and ubiquitination are implicated in targeting proteins to ILVs (Hanson and Cashikar, 2012).

The function, structure and even presence of MVBs in *Leishmania* are poorly studied. Single membrane-delimited organelles containing variable numbers of relatively

homogeneous vesicles (<100 nm across) were first observed in *L. donovani* promastigotes in 1969 and defined as MVBs based on their similar appearance to mammalian MVBs (Djaczenko et al., 1969). Since then, MVBs have been mentioned in several ultrastructural *Leishmania* studies (Hentzer and Kobayasi, 1977, Garcovich et al., 1975, Vannier-Santos et al., 1995) but no detailed analysis of their biogenesis and function has taken place.

A recent study in *L. mexicana* has identified a compartment called the multivesicular tubule (MVT) which appears to have lysosomal function (Mullin et al., 2001) and has only been described in *Leishmania* spp.. Time-lapse labelling with membrane dye FM 4-64 suggests that the MVT is a terminal compartment since the dye accumulates and remains in the MVT. The collapse of the MVT upon treatment with an inhibitor of vacuole-type H^+ ATPases suggests that the MVT is a lysosome-like compartment (Mullin et al., 2001). Surprisingly, in log phase promastigotes the MVT has a relatively high pH and low lytic capacity which increases greatly upon entry into stationary phase (Mullin et al., 2001). The tubule extends along the majority of the cell and contains small 30-50 nm vesicles reminiscent of ILVs in MVBs. *Leishmania* endosomes are also structurally different to their mammalian equivalents, having a tubulo-vesicular structure (Weise et al., 2000). The presence of the MVT is reliable and is observed under many conditions since its first description by Mullin et al. (Besteiro et al., 2006, Ghedin et al., 2001, Dodge et al., 2004, Sahin et al., 2008). It has been observed that between the MVT and the Golgi are a series of MVBs which are morphologically similar to mammalian MVBs (Mullin et al., 2001); possibly these structures are analogous to the MVB-like structures observed in earlier studies

(Djaczenko et al., 1969). Their function is unclear; the authors propose that the MVBs carry material from the Golgi to the MVT in an analogous way to mammalian MVBs carrying material from the Golgi and PM to lysosomal compartments.

Although it is assumed that *Leishmania* releases MVB-derived exosomes (Silverman et al., 2010a, Silverman and Reiner, 2011, Silverman et al., 2010b), in the study by Mullin et al. (2001) MVBs were not observed close to or fusing with the flagellar pocket (FP) (Mullin et al., 2001). An array of regularly spaced (~20 nm apart) sub-pellicular microtubules spans the inner face of the cell body membrane (Gull, 1999), excluding the FP, and the FP is the only site which is thought to allow endo- and exocytosis in kinetoplastids (reviewed in (Overath et al., 1997)). Whether *Leishmania* MVBs fuse with surface membranes to release exosomes remains unclear. EM artefacts are a particular issue with MVBs; the internal structures are often poorly preserved using conventional methods (Hanson and Cashikar, 2012). Indeed, Mullin et al. observed that some *Leishmania* cells contained a series of MVB-like structures in place of a MVT (Mullin et al., 2001), which may be an artefact of sample processing for EM. Another study in *L. mexicana* observed MVB-like structures only in mutant cells which lack AP-1, a membrane trafficking protein, and this was assumed to be the result of MVT fragmentation. In the related parasite *T. brucei,* 'MVBs' were observed only in mutant (trans-splicing deficient) or stressed cells (Eliaz et al., 2017). MVBs were observed in a more *in vivo* context in both *L. major* and *L. infantum* promastigotes in the sandfly midgut (Atayde et al., 2015), and in this context MVBs were also observed fusing with the FP.

An alternative approach to looking for MVB-like structures by EM is functional conservation. One of the best studied signals targeting proteins to ILVs is ubiquitination, including monoubiquitiniation and K63-linked polyubiqutination (Hanson and Cashikar, 2012, Piper and Lehner, 2011). Evidence that there is ubiquitin-dependent targeting to degradative vesicular compartments in *Leishmania* comes from *L. mexicana* studies where the surface membrane protein myo-inositol transporter was fused to monoubiquitin leading to its accumulation in the MVT (Vince et al., 2011).

One of the only well-documented markers for MVBs in mammalian cells is Rab7 (Hanson and Cashikar, 2012). Rab7 immunofluorescence in *L. major* showed the protein localises to a region between the nucleus and kinetoplast (Denny et al., 2002) which is thought to correspond to the site of endocytosis from the FP in trypanosomatids. Although it was not possible to determine by light microscopy, it is possible based on its cellular location that the observed localisation of Rab7 in *L. major* corresponds to the MVB-like structures which are sometimes observed in this region by EM (Mullin et al., 2001). Rab7 localised to undefined locations adjacent to CPB-positive late endocytic compartments immuno-gold labelling experiments; it was not possible to determine, however, whether membranous structures corresponding to MVBs or the MVT were present at these locations (Denny et al., 2002).

Another defining feature of MVBs is dependence on ESCRT complexes as well as the ATPase Vps4 to drive ILV formation, and their disruption leads to impaired ILV formation (Hanson and Cashikar, 2012). In *L. major* a dominant negative version of Vps4 was overexpressed, leading to accumulation of the mutated protein in

endosomal compartments and preventing normal trafficking of membrane dye to the MVT (Besteiro et al., 2006). These results are consistent with the effects of mutating VPS4 in yeast and mammalian cells (Lin et al., 2005, Babst et al., 1998), suggesting that functional dependence on ESCRT in endosomal trafficking in *Leishmania* is conserved. Overall, certain MVB functions and characteristics appear to be conserved in *Leishmania*, but whether MVBs themselves are present at all and whether the MVT represents the functional equivalent of mammalian MVBs or other endocytic compartments remains unclear.

1.2.3. Ceramide-dependent multivesicular body formation

An ESCRT-independent mechanism for MVB formation involves conversion of sphingomyelin to ceramide resulting in lipid microdomain coalescence and inward curvature of endosomal membranes. Sphingomyelinase (SMase) is an essential enzyme for catalysing ceramide production in mammals (Trajkovic, Hsu et al. 2008), therefore the absence of sphingomyelin in *Leishmania* spp. (Kaneshiro et al., 1986) suggests that this pathway may be absent. However, since the major form of sphingolipid in *Leishmania* spp. is inositol phosphorylceramide rather than sphingomyelin and ceramide, it is possible that a different enzyme fulfils the role of sphingomyelinase in MVB formation. For example, a *Leishmania* protein with homology to human neutral SMase, ISCL (Inositol phosphoSphingolipid phospholipase C-Like), has sphingomyelinase activity as well as inositol phosphorylceramide hydrolase activity. It seems that *Leishmania* spp. are able to utilise mammalian host sphingomyelin; interestingly, ISCL sphingomyelinase activity specifically is required for amastigote proliferation in a mouse model (Zhang, Xu et al. 2012). Conversely, only the inositol phosphorylceramide hydrolase activity of ISCL specifically is needed for

promastigote survival, suggesting that sphingomyelin is not essential in the sandfly host (Zhang, Xu et al. 2012). Knockdown of one of the upstream synthetic enzymes of sphingolipids in *Leishmania*, SPT2, leads to accumulation of ILV-like vesicles in internal vacuoles and the FP (Zhang, Showalter et al. 2003) suggesting a possible increase in MVB formation. This could be due to defects in the proper trafficking or degradation of MVBs. Overall, it is not clear how specific lipids such as sphingomyelin contribute to MVB formation and exosome release in *Leishmania*.

1.2.4. Tetraspanins' role in extracellular vesicle formation

Tetraspanins are a variable superfamily of proteins characterised by four transmembrane domains and four to six conserved extracellular cysteine residues. The many mammalian superfamily members (>30) regulate diverse processes including cell adhesion, membrane fusion and protein trafficking (reviewed in (Charrin et al., 2014)). They form tetraspanin-enriched membrane microdomains and the tetraspanin peripherin-2/rds plays a role in induction of membrane curvature (Khattree, Ritter et al. 2013) which may be important in EV biogenesis (Andreu and Yanez-Mo 2014). Tetraspanins CD63, CD9 and CD81 (Kowal et al., 2016) have been used as EV markers, although the exact roles of tetraspanins in EV biology are largely speculative. CD9 KO in murine DCs leads to defects in exosome release via an unknown mechanism (Chairoungdua et al., 2010). It seems likely that tetraspanins play a role in cargo selection due to their large number of interacting protein partners including adhesion molecules and, interestingly, RNA binding proteins (Hemler, 2008). While mammalian genomes encode many tetraspanins, there is only one gene encoding a protein with a predicted tetraspanin domain, which has no mammalian orthologues based on BLAST searches, in *L. mexicana* (LmxM.32.0170). This protein is

uncharacterised and it would be interesting to see whether the level of EV release is affected in KO parasites.

1.2.5. Actin

Actin and actin-binding proteins are commonly found in EV proteomes (Thery et al., 2002b) and actin-dependent mechanisms are proposed for microvesicle and exosome biogenesis. Knockdown of cortactin, which promotes actin polymerisation, leads to decreased exosome release from mammalian cancer cells (Sinha et al., 2016). Interestingly, actin has been implicated in flagellar microvesicle release (Nager et al., 2016) (discussed in the following section). Concerning microvesicle biogenesis generally, actin and Arf6–dependent PM budding is one of the few well-studied mechanisms. Arf6 is a small PM-associated GTPase whose activation upon binding GTP leads to phospholipase D (PLD) and subsequently Erk recruitment to the PM. Phosphorylation and activation of myosin light chain kinase by recruited Erk induces acto-myosin driven outward membrane budding and abscission (Muralidharan-Chari, Clancy et al. 2009). The presence of this pathway in *Leishmania* spp. is hard to determine due to the presence of large families of small GTPases and their GEFs (guanine-nucleotide exchange factors) which have highly similar functional groups. PLD is not encoded by *L. mexicana* whereas there is a good Erk1 homolog.

Another actin-dependent mechanism for microvesicle release involves membrane nanotubes which dissociate into EVs, depending on complex interactions between contractile forces, the underlying cytoskeleton and membrane composition (Jelercic and Gov, 2015). This process is known as pearling. Pearling has been studied in the context of intestinal microvilli, which are ~100 nm thick surface membrane projections (by comparison the *Leishmania* flagellum is ~300 nm across) supported

internally by actin-rich bundles. Upon myosin-1a activation, a membrane binding motor protein, with ATP, microvillar membrane is translocated to the + end tips of microvilli (McConnell and Tyska 2007). EVs are simultaneously shed from the microvillar tips, resulting in maintenance of microvillar length. The authors propose a model whereby the acto-myosin-driven contractile force exerted on the translated membranes combined with the loss of membrane contact with the actin cytoskeleton at the microvillar tip leads to instability and vesiculation. Membranes can also undergo pearling upon loss of contact with the cortical actin cytoskeleton in a myosin-independent manner, without the requirement for a contractile force (Heinrich, Ecke et al. 2014). Most studies, however, find that tensile or contractile forces contribute to pearling (McConnell and Tyska 2007, Yue, Zhang et al. 2014, Jelercic and Gov 2015), although tension could be induced by osmotic pressure rather than protein machinery (Yue, Zhang et al. 2014). In some cases, additional protein machinery such as dynamin is required for membrane scission, but actin polymerisation itself can drive membrane scission in a dynamin-independent manner (Kirkham and Parton 2005, Romer, Pontani et al. 2010). Membrane cholesterol and sphingolipid content (Varkey, Isas et al. 2010) and curved BAR domain proteins (Kishimoto, Sun et al. 2011) can also contribute to nanotube formation and dynamics. In summary, while interplay between the different factors contributing to pearling is complex, the intrinsic ability of membranes to form nanotubes which undergo vesiculation is evident. Could there be an analogous form of pearling in *Leishmania*? In that case, would the nanotube undergoing vesiculation be the flagellum itself, with budding from the tip (with the flagellum being analogous to the intestinal microvilli described above), or nanotubes branching off the flagellum or cell body?

1.2.7. Exocyst complex

The exocyst is an octameric complex involved in vesicle tethering and has been implicated in EV release although its role in this process is poorly understood (reviewed in (Martin-Urdiroz et al., 2016)). In the fungus *Cryptococcus neoformans* knockdown of exocyst component Sec6 leads to abolishment of EV release (Panepinto et al., 2009). All eight exocyst components were identified in human urinary EVs by MS (Chacon-Heszele et al., 2014). Interestingly, in Madin-Carby Canine Kidney (MDCK) cells exocyst components primarily localised to primary cilia (Rogers et al., 2004, Chacon-Heszele et al., 2014) and EVs on the ciliary surface (Chacon-Heszele et al., 2014), suggesting a possible link with ciliary EV release and/or function.

1.3. Known effects of *Leishmania* EVs on host cytokine secretion

In the last decade, the small number of studies on *Leishmania* EVs, mostly carried out by Silverman et. al., have revealed several effects on host cell cytokine secretion. One study was carried out using EVs from *L. donovani* promastigote cultures where the pH was slowly dropped to pH5.5 at 37°C over 24 h, conditions which presumably induced promastigote to amastigote differentiation (Silverman et al., 2010b). Human blood monocytes were pre-treated with these EVs then infected with promastigotes for 12 h, and subsequently IFNγ-stimulated for a further 24 h. Under these conditions IL-10 and IL-8 increased and TNFα decreased (Silverman et al., 2010b). *L. donovani* EVs were also incubated with human blood monocyte-derived DCs overnight before inducing DC maturation for a further 48 h. Under these conditions IL-12, TNFα and IL-10 secretion were inhibited, although it is worth noting that very high EV concentrations of up to 100 µg/ml were required to induce significant effects (Silverman et al.,

2010b). In the same study mice were pre-injected with *L. donovani* EVs twice over 5 weeks prior to infection with promastigotes for a further 5 weeks before harvesting splenocytes for cytokine analysis. EV-treated mice had higher levels of IFNγ, IL-10, IL-17 and unchanged TNFα compared to control infected mice. In addition, the EV-treated mice had higher parasite burdens than control mice, again suggesting that *Leishmania* EVs promote infection (Silverman et al., 2010b). In summary, a single study showed the ability of *Leishmania* EVs to either up- or down-regulate both pro-inflammatory cytokines such as IFNγ and TNFα and anti-inflammatory IL-10 under different conditions.

A second study by Silverman et al. also confirmed the ability of *Leishmania* EVs to induce IL-8 production (Silverman et al., 2010a). This time, *L. major* and *L. donovani* EVs were isolated from 24 h cultures at 37°C at either pH5.5 or 7. EVs were incubated with THP-1 macrophages and IL-8 production was increased while TNFα production was unchanged (Silverman et al., 2010a). Interestingly, EVs from both *Leishmania* species and pH conditions had similar effects.

Finally, Olivier et al. published the first study of *Leishmania* EVs which are released from promastigotes in the sandfly midgut (Atayde et al., 2015). Stationary phase *L. major* promastigotes were co-injected into mice footpads with EVs which were either isolated from the infected sandfly midgut or from 4 h *in vitro* cultures at 37°C. The mRNA levels of several cytokines in the draining lymph nodes were measured at 5 weeks post-infection: IL-2, IL-4, IFNγ, IL-17a, IL-23 and IL-10 secretion were increased compared to the non-EV-treated controls (Atayde et al., 2015). Interestingly, *in vivo* and *in vitro* isolated EVs had similar effects on cytokine production, providing the first

evidence that *in vitro* isolated *Leishmania* EVs may function similarly to EVs produced *in vivo*. The fact that macrophage IL-8 secretion is increased by *Leishmania* EVs, as well as by promastigote infection (Silverman et al., 2010a), suggests that there may be similarities between the biological effects of *Leishmania* EVs and their cells of origin. However, extensive studies to directly compare the effects of *Leishmania* promastigotes and EVs on macrophage cytokine secretion have not yet been carried out; whether *Leishmania* EVs, like promastigotes, can induce TNFα and IL-6 secretion and inhibit IL-12 secretion has yet to be well established.

1.4. Known mechanisms of macrophage cytokine secretion regulation and their manipulation by *Leishmania* infection

While the biological effects of secreted cytokines on target cells and inflammation have been extensively studied (Kelso, 1998), the mechanisms of release and regulation are much less well understood, as will be discussed in this section. Similarly, while the effects of *Leishmania* infection and EVs on cytokine secretion have been well documented as discussed above in *Sections 1.1.3* and *1.1.6* respectively, in many cases the specific parasite factors and macrophage targets responsible remain elusive. Cytokine secretion by macrophages can be induced in response to pro-inflammatory stimuli such as LPS (Medzhitov and Horng, 2009), requiring signal transduction leading to either *de novo* gene expression or post-transcriptional regulation. Most signalling pathways leading to regulation of macrophage cytokine secretion studied thus far have been shown to be pattern recognition receptor (PRR)-dependent (Moreira et al., 2008, Boonstra et al., 2006, Gais et al., 2010). Downstream of protein expression, the physical release of cytokines via classical or non-classical secretion is now being recognised as a key regulatory step (Murray and Stow, 2014). Classical secretion is via fusion of Golgi-derived vesicles with the PM (see *Section 1.2.6*) and non-classically secreted proteins have no recognisable signal peptide and are secreted by mechanisms including EV release (Stow et al., 2009). For only a subset of cytokines, including TNFα and IL-6 (Stow et al., 2009, Neininger et al., 2002, Arango Duque et al., 2013), are we beginning to build up a detailed picture of their secretion pathways and modes of upregulation in response to stimuli such as LPS. It is becoming clear that understanding the secretion mechanisms of one cytokine cannot necessarily help us draw conclusions about others since the mechanisms uncovered so far have varied greatly (Stow et al., 2009). It is also evident that conclusions cannot be made about

cytokine secretion pathways in one cell type from studies that have been carried out in another (Stow et al., 2009, Boonstra et al., 2006), therefore our discussion of cytokine secretion by macrophages will largely be restricted to macrophage literature.

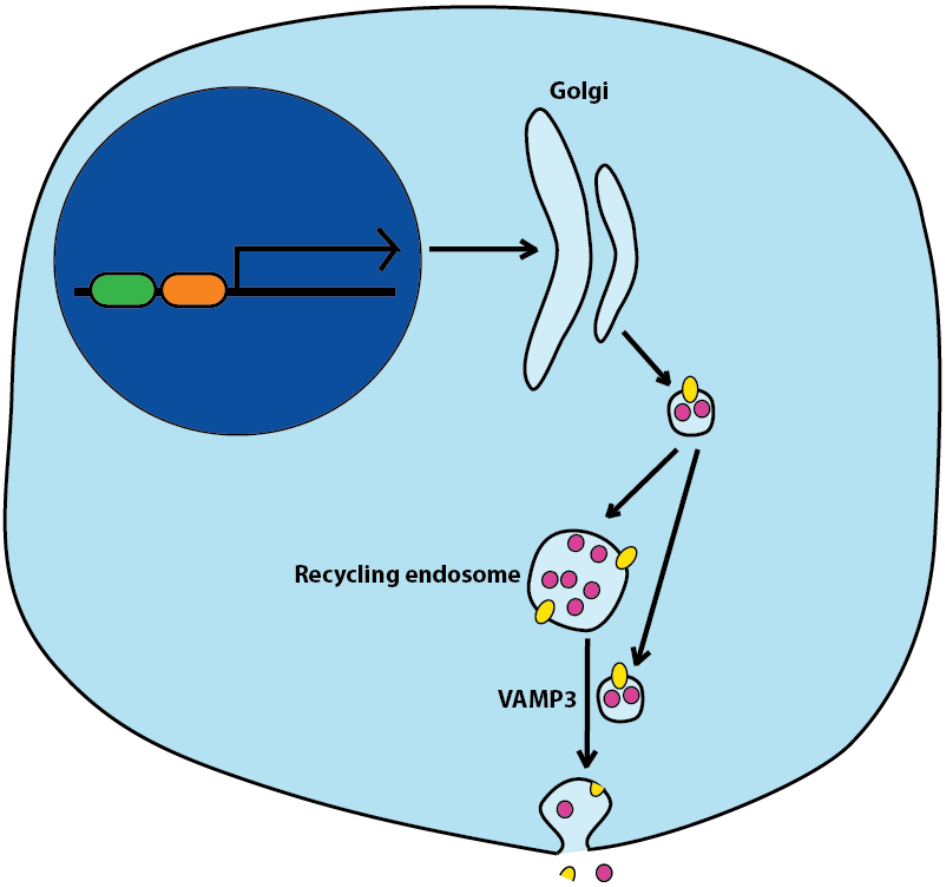

Figure 1.4. Macrophage cytokine secretion. Cytokines are transcribed in the nucleus then translated in the ER before being trafficked to the Golgi. Vesicles bud from the trans face of the Golgi containing soluble cytokines such as IL-10 and IL-6 and/or membrane-bound pro-cytokines such as pro-TNFα. These vesicles are trafficked to the plasma membrane either via the recycling endosome (e.g. IL-6, TNFα and IL-10) or not (e.g. IL-10) and this involves specific membrane tethering complexes including the SNARE VAMP3. When cytokine-containing secretory vesicles fuse with the plasma membrane cytokines such as IL-10 and IL-6 are released directly. Pro-TNFα is cleaved by TNFα-converting enzyme (TACE) allowing the release of soluble TNFα.

1.4.1. Surface receptors

The first points of contact between an external stimulus or pathogen and macrophages are surface receptors. A small number of studies show that ligation of macrophage surface receptors can modulate cytokine secretion in response to pro-inflammatory stimuli (Gerber and Mosser, 2001), or even induce cytokine secretion independently (Boonstra et al., 2006). Ligation of FcγR, an IgG antibody receptor expressed on macrophages, by addition of E-IgG (IgG-opsonised erythrocytes) led to specific suppression of IL-12 secretion and enhancement of IL-10 secretion when murine BMDMs were stimulated with LPS, a toll-like receptor (TLR)-4 agonist (Gerber and Mosser, 2001). IL-12 suppression, but not IL-10 enhancement, was also seen in response to CR ligation, by addition of E-C3b/i in the presence of LPS stimulation (Gerber and Mosser, 2001). Interestingly, these results were not dependent on phagocytosis since latex beads could not replicate the effects. The molecular mechanisms behind the ability of FcγR and CR ligation to modulate cytokine secretion remain unknown. It was also shown that CD40 ligation induced IL-10 secretion in the absence of additional stimuli, showing that TLR-independent pathways for cytokine induction exist (Boonstra et al., 2006).

The finding that macrophage surface receptor ligation can modulate cytokine secretion is important for host-pathogen interaction studies, since during infection TLR agonists and other pathogen factors are likely to be present alongside surface receptor ligands, either for host cell invasion or due to opsonisation. *Leishmania* opsonisation has indeed been found to influence cytokine secretion by the macrophages they infect; un-opsonised *L. amazonensis* amastisotes do not induce IL-10 secretion in murine BMDMs whereas IgG-opsonised amastigotes do (Yang et al.,

2007b). It was shown using wild type (WT) versus FcγR null macrophages that this effect was dependent on the IgG receptor FcγR (Yang, Mosser et al. 2007. Furthermore, the fact that inhibition of Syk, a tyrosine kinase involved in FcγR-mediated signalling, suppresses IL-10 secretion in this context (Yang, Mosser et al. 2007) provides a clue about the signalling pathways downstream of surface receptors which can modulate cytokine secretion, although much remains to be elucidated. In addition to FcγR, *Leishmania* parasites also use CRs as surface receptors during promastigote entry into macrophages (Ueno and Wilson, 2012). Both GP63 and LPG on the promastigote surface bind C3b which can be presented as a ligand for CR1 (Ueno and Wilson, 2012). GP63 cleaves C3b to generate iC3b which can then bind to CR3 to facilitate parasite uptake (Ueno and Wilson, 2012, Russell, 1987). However, the downstream signalling pathways and possible effects on cytokine production in *Leishmania* infection are yet to be uncovered. Overall, the impact of parasite-surface receptor interactions on *Leishmania*-induced cytokine secretion remains poorly studied.

1.4.2. Pattern recognition receptors and their adaptors

Most of the signalling pathways leading to regulation of macrophage cytokine secretion studied thus far have been shown to be dependent on PRRs, particularly TLRs (Moreira et al., 2008, Boonstra et al., 2006, Gais et al., 2010). TLRs bind to pathogen-associated molecular patterns (PAMPs) such as LPS or cytosolic DNA and initiate signalling cascades via adaptor proteins myeloid differentiation primary response (MyD)-88 or TIR-domain-containing adapter-inducing interferon-β (TRIF) leading to cellular responses including cytokine secretion (Boonstra et al., 2006). It was shown using BMDMs from MyD88 and TRIF KO mice, that CpG and LPS signal via

MyD88 to induce IL-10 secretion and that LPS and Poly I:C (a TLR3 agonist) signal via TRIF (Boonstra et al., 2006).

The most studied PAMP-PRR interaction is LPS signalling via TLR4, which is known to induce increased secretion of many pro-inflammatory cytokines such as TNFα, IL-6 and CXCL10, as well as anti-inflammatory cytokines including IL-10 (Ma et al., 2001, Rossol et al., 2011). Other PRRs also induce cytokine secretion; in murine BMDMs, unmethylated CpG motifs signal through TLR9 and MyD88 to induce IL-10 secretion (Boonstra et al., 2006). It was also shown using BMDMs from KO mice that NOD2 (a cytoplasmic PRR of the Nod-like receptor class) and TLR2 are needed for IL-10 production induced by purified pneumococcal cell wall (PnCW) (Moreira et al., 2008). In addition, PnCW-induced TNFα, IL-6, IL-1α and IL-12 production were all found to be TLR2-dependent (Moreira et al., 2008). Finally, signal transduction via TLR3 was shown to induce IL-10 production (Boonstra et al., 2006). These results show that macrophages can transduce signals from a range of PAMPs to induce the same cytokine response, reflecting the need to mount an innate immune response to diverse pathogens.

Table 1.2. Summary of *Leishmania* effects on host signalling. The main published effects of *Leishmania* infection or *Leishmania* factors on host MyD88 and TLR signalling are listed.

Macrophage effector	*Leishmania*-dependent effects	Reference
MyD88	KO mice are more susceptible to *L. braziliensis* infection	(Vargas-Inchaustegui et al., 2009)
	WT but not KO mice produce TNFα in response to purified *L. major* LPG	(de Veer et al., 2003)
	The amastigote glycoconjugate P8 PGLC induces TLR4- and MyD88- dependent IL-12 and TNFα production (*L. pifanoi*)	(Whitaker et al., 2008)
TLR2	KO mice are less susceptible to infection (*L. braziliensis* and *L. donovani*)	(Vargas-Inchaustegui et al., 2009, Murray et al., 2013)
	KO mice are more susceptible to infection (*L. mexicana* and *L. major*)	(Halliday et al., 2016)
	LPG signals via TLR2 in human and murine macrophages	(Ibraim et al., 2013, Rojas-Bernabe et al., 2014)
	LPG-TLR2 complex formation confirmed in NK cells (*L. major*)	(Becker et al., 2003)
	Leishmania SIR2RP1 protein induces TLR2-depedent IL-12 and TNFα secretion in DCs (*L. infantum*)	(Silvestre et al., 2009)
TLR4	KO mice are more susceptible to *L. major* infection	(Kropf et al., 2004)
	KO macrophages have strikingly higher *L. panamensis* infection levels	(Gallego et al., 2011)
	LPG signals via TLR4 in human and murine macrophages	(Ibraim et al., 2013, Rojas-Bernabe et al., 2014)
	The amastigote glycoconjugate P8 PGLC induces TLR4- and MyD88- dependent IL-12 and TNFα production (*L. pifanoi*)	(Whitaker et al., 2008)
TLR9	KO mice are more susceptible to *Leishmania* infection (*L. major*)	(Abou Fakher et al., 2009)
	LPG reduces TLR9 expression, possibly via TLR2 signalling (*L. major*)	(Srivastava et al., 2013)
	CpG repeats in *Leishmania* DNA are a TLR9 agonist leading to a protective immune response (*L. major*)	(Abou Fakher et al., 2009)
TLRs 1, 2, 3 and 4	*L. panamensis* infection induces increased expression of these TLRs in macrophages	(Gallego et al., 2011)

The published effects of *Leishmania* infection on MyD88 and TLR signalling are numerous and sometimes conflicting; the main effects are summarised in Table 1.2.

The adaptor protein MyD88 is important in *Leishmania* infection, as shown by the fact that MyD88 KO mice are more susceptible to infection (Vargas-Inchaustegui et al., 2009). The requirement for MyD88 in parasite clearance during murine infection appears to be due to TLR-dependent induction of Th1 cytokines, particularly IL-12, which normally leads to parasite clearance in resistant C57BL/6 mice; MyD88 KO mice secrete only low levels of IL-12 in response to infection (Muraille et al., 2003). Macrophage-specific MyD88 likely plays an important role in murine resistance to *Leishmania* infection since macrophages are a major source of IL-12 (Wang et al., 1999), however the involvement of macrophages in these studies was not shown directly. MyD88 is known to play a role in LPG-dependent macrophage signalling, since murine macrophages from MyD88 KO mice are unable to produce TNFα in response to purified *L. major* LPG unlike their wild-type counterparts (de Veer et al., 2003).

The importance of TLRs in *Leishmania* infection is demonstrated by infection of TLR KO mice and macrophages compared to WT controls. It is fairly well established that TLR9- (Abou Fakher et al., 2009) and TLR4- deficient (Murray et al., 2013, Kropf et al., 2004) mice are more susceptible to *Leishmania* infection, showing a protective role for these TLRs. This protective role can also be seen at the macrophage level: *L. panamensis*-infected TLR4 KO human macrophages have strikingly higher infection levels than WT in the first 24 h post-infection (Gallego et al., 2011). Surprisingly, some studies indicate that TLR2-deficient mice are less susceptible to infection (Murray et al., 2013, Vargas-Inchaustegui et al., 2009). However, a different study showed a protective role for both TLR2 and TLR4: *L. major* promastigote-infected TLR2 and TLR4

KO mice had larger lesions than control mice (Halliday et al., 2016). The same study also showed a protective role for TLR2, but not TLR4, in *L. mexicana* murine infection, although substantial differences were only visible at around 10-12 weeks post infection and the difference no more than two-fold (Halliday et al., 2016). What could account for these apparently different roles for TLR2? The same mouse model, using WT and TLR2 KO C57BL/6 mice, was used for all the murine infection studies investigating the role of TLR2, but different *Leishmania* species were used (Halliday et al., 2016, Vargas-Inchaustegui et al., 2009, Murray et al., 2013). A protective role of TLR2 was shown for *L. major* and *L. mexicana* infection (Halliday et al., 2016) and the opposite was shown for *L. donovani* (Murray et al., 2013) and *L. braziliensis* (Vargas-Inchaustegui et al., 2009) infection. In addition to *Leishmania* species, the infection level measure varies between studies; parasite load in the liver is commonly used to measure *L. donovani* infection (Murray et al., 2013), while lesion size and parasite load are used for cutaneous infection (Vargas-Inchaustegui et al., 2009, Halliday et al., 2016). This latter consideration is particularly important when comparing results from different studies, since lesion size and parasite load do not always correlate; one study showed that *L. braziliensis* lesions in TLR2 KO mice were smaller than in control mice while there was no difference in parasite load (Vargas-Inchaustegui et al., 2009). A careful comparison in a single study of infection levels of both macrophages and mice infected with several *Leishmania* species is required to help resolve the confusion surrounding the role of TLR2. However, it is clear from numerous studies that *Leishmania* infection is modulated by TLR signalling and therefore parasite factors must exist to regulate TLRs directly or indirectly.

One way in which *Leishmania* modulates TLR signalling is by upregulating expression of TLRs themselves. *L. panamensis* infection of human macrophages induces increased protein expression of TLRs 1, 2, 3 and 4, but not 9 (Gallego et al., 2011), and upregulated TLR2 expression was also reported in response to purified *L. donovani* antigens (Srivastava et al., 2012). The mechanisms of TLR upregulation were not investigated.

Thus far, few parasite factors have been proposed as TLR ligands and the best studied of these is LPG. LPG signals through surface receptors TLRs 2 and 4 in murine (Srivastava et al., 2013, Ibraim et al., 2013) and human macrophages (Rojas-Bernabe et al., 2014) and these studies were carried out using purified LPG from *L. major*, *L. infantum* and *L. braziliensis* and *L. mexicana* respectively. *L. major* LPG-TLR2 complex formation has been directly shown in human natural killer (NK) cells by immunoprecipitation (Becker et al., 2003), and blocking experiments with phosphoglycan-specific antibodies showed that TLR2 is likely to recognise the phosphoglycan repeat domain of LPG (Becker et al., 2003). Whether LPG interacts directly with TLR4 or TLR9 is unknown. TLR9 recognises intracellular CpG motif-containing DNA and promotes a protective anti-leishmanial response (Abou Fakher, Rachinel et al. 2009). LPG appears to modulate TLR9 expression, possibly via TLR2 (Srivastava et al., 2013). This was shown using high versus low LPG-expressing parasites to infect macrophages and it was observed that the high LPG parasites reduced TLR9 mRNA expression more than the low LPG parasites and that the reduction in TLR9 expression was reversed by adding anti-TLR2 antibodies, suggesting a TLR2 and LPG-dependent mechanism for TLR9 downregulation (Srivastava et al.,

2013). TLR9 downregulation correlated with IL-10 and TGFβ secretion but dependency on reduced TLR9 signalling was not directly shown (Srivastava et al., 2013). However, the two parasite strains with high and low LPG may have other unknown differences in virulence factor expression which could account for these effects. Given the documented protective role for TLR9 in *Leishmania* infection (Abou Fakher, Rachinel et al. 2009), it would make sense that there are parasite mechanisms to downregulate TLR9 signalling, although the exact mechanism of suppression requires further study.

Two studies which used either macrophages from KO mice (Ibraim et al., 2013) or anti-TLR antibodies incubated with human macrophages (Rojas-Bernabe et al., 2014) showed that blocking either TLR2 or TLR4 had the same effects on LPG-dependent changes in cytokine production. These studies were carried out using purified LPG from *L. infantum* and *L. braziliensis,* and *L. mexicana* respectively. However, evidence that TLR2 and TLR4 signal differently in response to LPG comes from another study in which TLR-deficient peritoneal murine macrophages were incubated with purified LPG from *L. amazonensis* and found that p38, c-Jun N-terminal kinase (JNK) and inhibitor of kappa B (IκB)-α activation was dependent on TLR4 but not TLR2 (Nogueira et al., 2016). Therefore, the same controversy over whether TLR2 and TLR4 play conflicting roles in infection is apparent at the level of response to LPG.

The different reported roles of TLR2 in infection may be partially explained by its downstream signalling pathways; effects which are conducive to and deleterious to *Leishmania* infection have both been shown. Different studies suggest that LPG-TLR2 interactions can lead to mitogen-activated protein kinase (MAPK) activation (Rojas-

Bernabe et al., 2014), NF-κB nuclear translocation (Becker et al., 2003) and transcription of inflammatory cytokines (Gaafar et al., 1995). These effects are presumed to lead to enhanced *Leishmania* clearance, although this was not shown directly. On the other hand, LPG-TLR2 signalling has been proposed to down-regulate TLR9 signalling leading to reduced anti-leishmanial responses (Srivastava et al., 2013). Whether these events can occur simultaneously under the same conditions is unknown, but it is possible that the balance of these effects could determine the overall effect of TLR2 on disease outcome under different conditions.

A small number of other factors have been proposed as TLR ligands during *Leishmania* infection. Direct binding of *Leishmania* DNA to TLR9 has been proposed: it was shown using TLR9-deficient DCs from mice that both *L. major* parasites and isolated DNA induce IL-12, IL-6 and IFNγ mRNA expression in a TLR9-dependent manner (Abou Fakher et al., 2009). Isolated mammalian DNA does not induce the same effects and the effect of *Leishmania* cells or isolated DNA was abolished by DNAse treatment, suggesting that CpG repeats in *Leishmania* DNA are the likely ligand for TLR9 (Abou Fakher et al., 2009). Further studies are required to determine whether *Leishmania* DNA could also trigger cytokine secretion via TLR9 in macrophages.

P8 proteoglycolipid complex (P8 PGLC) is a glyconjugate which is highly expressed on the *Leishmania* amastigote surface (Whitaker et al., 2008). IL-12 and TNFα are upregulated in macrophages in response to purified P8 PGLC (Whitaker et al., 2008). It was shown using BMDMs from KO mice that this cytokine induction is TLR4- and MyD88-dependent but not TLR2-dependent (Whitaker et al., 2008). TLR4 is also important for TNFα induction by amastigotes (Whitaker et al., 2008). Parasite burden

is slightly increased in amastigote-infected TLR4 KO mice compared to WT mice, which is likely to be the result of decreased pro-inflammatory cytokine release in the absence of TLR4 signalling (Whitaker et al., 2008). Direct TLR4-P8 PGLC interaction is not shown in this study and there is no use of P8 PGLC-deficient parasites to demonstrate the importance of this factor during infection, therefore more research is needed to determine whether P8 PGLC is a true TLR4 ligand.

The silent information regulator 2 related protein 1 (SIR2RP1) protein induces IL-12 and TNFα secretion in DCs from B57BL/6 WT mice, and this effect is abrogated in DCs from TLR2 KO mice (Silvestre et al., 2009). Interestingly, although SIR2RP1 also induces IL-12 and TNFα secretion in macrophages, there was no difference in cytokine secretion between the infected WT and TLR2 KO macrophages, suggesting that SIR2RP1 signals via a different unknown receptor in macrophages. Whether SIR2RP1 directly binds ILR2 in DCs remains unknown.

One study has proposed a mechanism of parasite-induced TLR modulation whereby host factors are the TLR ligand. Inhibitor of serine peptidase 2 (ISP2) KO *L. major* parasites have lower survival in macrophages and this effect is dependent on TLR2 and neutrophil elastase (NE), a serine peptidase released from neutrophils during *Leishmania* infection (Faria et al., 2011). Therefore, it is suggested that NE signals through TLR4 to induce parasite killing, and that the *L. major* protein ISP2 can counteract this effect through NE inhibition (Faria et al., 2011). However, it was not shown whether NE is a direct ligand for TLR4 or whether ISP2 is able to directly inhibit NE, although it does have serine peptidase inhibiting activity. In fact, a recent report shows that NE induces TLR4 activation indirectly by cleaving the fibronectin variant

containing the extra domain A (FNIII EDA), revealing a cryptic binding site (Julier et al., 2015). Furthermore, this study shows that NE alone cannot activate TLR4 as determined by a HEK cell NFκB activation readout (Julier et al., 2015). Whether FNIIIEDA is the TLR4 ligand acting downstream of NE in *Leishmania* infection remains to be investigated. If this is the case this shows that *Leishmania* parasites have developed elaborate ways to modulate TLR signalling.

These experiments were carried out in either murine or human cells; care must be taken when inferring effects between the two species. Although the overall TLR signalling outcomes are similar many specific differences in induced genes and sensitivity have been reported (Schroder et al., 2012, Vaure and Liu, 2014, Ariffin and Sweet, 2013, Reynolds and Haniffa, 2015).

1.4.3. Regulation of cytokine expression through MAPKs and other downstream signalling pathways

MAPKs fall into three classes: extracellular signal-related kinase (Erk)-1/2, JNKs and p38. They are typically activated at the PM by small GTPases in response to surface receptor-transduced stimuli, including PAMP-TLR interactions (Arthur and Ley, 2013). MAPKs play an important role in cytokine induction and regulation, both via activation of transcription factors to regulate *de novo* gene expression (Arthur and Ley, 2013) and via post-transcriptional control (Tiedje et al., 2014). In IL-8 gene expression for example, p38, Erk1/2 and JNK pathways have all been shown to contribute through transcription factor activation (Hoffmann et al., 2002). It was shown using specific inhibitors that p38 MAPK signalling is required for LPS-induced IL-10 expression in THP-1 macrophages (Ma et al., 2001).

MAPK signalling downstream of TLRs is complex and different agonist-TLR complexes signal via one or more of the MAPK classes to varying extents (Peroval et al., 2013). For instance, one study has shown that Erk1/2 is not a downstream effector of TLR2 for PnCW-dependent IL-10 secretion in murine BMDMs (Moreira et al., 2008). However, Erk1/2 is involved in the TLR2-dependent IL-10 response to zymosan (Slack et al., 2007). These data show that TLR2 signalling can induce IL-10 secretion with different intermediate signalling pathways depending on the context.

Signalling pathways other than MAPKs also regulate cytokine expression. The second messenger molecule cyclic adenosine monophosphate (cAMP) inhibits inflammatory gene expression (among other functions), including TNFα, in murine macrophages (Wall et al., 2009). This was shown to be mediated by activated protein kinase A (PKA) which regulates cytokine gene expression via unknown mechanisms (Wall et al., 2009). SHP-1, a protein tyrosine phosphatase, has been extensively studied as a negative regulator of T cell receptor signalling (Stefanova et al., 2003). SHP-1 also appears to play a role in cytokine secretion in macrophages, since LPS-stimulated macrophages from SHP-1 KO mice have enhanced TNFα production and reduced IL-10 production (Okenwa et al., 2013). SHP-1 knockdown is also able to reduce IL-10 production and enhance TNFα production. There seem to be at least two pathways governing IL-10 production in murine macrophages, since p38 signalling also induces LPS-dependent IL-10 production in a SHP-1-independent manner (Okenwa et al., 2013). Pyk2 (a focal adhesion proline-rich tyrosine kinase) and Src (a protein tyrosine kinase) are also activated downstream of SHP-1 to induce IL-10 gene expression (Okenwa et al., 2013).

These studies highlight the complexity and redundancy of signalling pathways which regulate cytokine secretion. Therefore they offer many targets which could be modulated by pathogens to alter cytokine production. Both general *Leishmania* infection and the specific parasite factors EF-1α, GP63 and LPG have been found to target these pathways and MAPK regulation by trypanosomatid parasites has been recently reviewed (Soares-Silva et al., 2016).

Conflicting studies exist as to whether live *Leishmania* promastigotes induce MAPK activation. In contrast to a study which finds that *L. donovani* parasites do not induce activation of the three MAPKs (Prive and Descoteaux, 2000), another found that activation of Erk1/2, p38 and JNK in BMDMs is increased by *L. mexicana* infection (Shweash et al., 2011). In addition, *L. major* infection of macrophages induces JNK activation, and importantly KC cytokine secretion by these macrophages was found through the use of inhibitors to be JNK-dependent (Filardy et al., 2014).

These discrepancies could be due to the effect of different *Leishmania* species, although another study found that *L. donovani* did not evade p38 activation altogether, rather there was initial p38 activation in response to infection which disappeared within 18 h (Junghae and Raynes, 2002); whether this subsequent downregulation of p38 is due to parasite-driven mechanisms is unclear. Inhibition of IFNγ-dependent Erk activation in *L. donovani* infection was found to be dependent on SHP-1 (Forget et al., 2006). Studies carried out in *L. donovani* have shown that SHP-1 can be bound and activated by parasite EF-1α; direct interaction between *Leishmania* but not host EF-1α and SHP-1 was shown and *Leishmania* EF-1α increased SHP-1 phosphatase activity both *in vitro* and in macrophages (Nandan et al., 2002). Since EF-

1α-SHP-1 interactions have not been studied in other *Leishmania* species, it is possible that this mechanism is specific to or upregulated in *L. donovani*, which may explain the different levels of MAPK activation between *Leishmania* species.

Leishmania virulence factors GP63 and LPG have also been found to target SHP-1 and MAPKs. *L. major* GP63 is able to cleave SHP-1 *in vitro*, and the resulting cleavage fragments from infected B10R murine macrophages have higher phosphatase activity than SHP-1 from uninfected macrophages or macrophages infected with GP63 KO parasites (Gomez et al., 2009). While it is known that downregulation of SHP-1 in *Leishmania* infection leads to increased release of pro-inflammatory cytokines (Okenwa et al., 2013), the exact effects of *Leishmania* EF-1α- and GP63- dependent SHP-1 upregulation on macrophage cytokine release have not been addressed. The fact that SHP-1 is upregulated by *Leishmania* factors via at least two different mechanisms perhaps highlights the importance of SHP-1 activity in *Leishmania* infection. This idea is supported by the fact that SHP-1 KO macrophages and mice have dramatically lower parasite loads when infected with *L. major* compared to controls (Forget et al., 2001).

While the effects of *Leishmania*-dependent MAPK regulation on macrophage cytokine release requires further study, some effects have been reported. Although Erk MAPKs were found not to play a role in uninfected murine macrophages in LPS-induced IL-10 secretion (Moreira et al., 2008), in *L. amazonensis*-infected macrophages Erk1/2 activation leads to phosphorylation of histone H3 at the IL-10 promoter leading to recruitment of specificity protein 1 (Sp1) and IL-10 transcription (Yang et al., 2007b). It can be speculated that this Erk1/2-dependent cytokine regulation benefits the

parasite since high IL-10 levels are associated with non-resolving infection, and indeed it was shown that Erk1/2 inhibition reduced lesion size in infected mice (Yang et al., 2007b). However, it cannot be concluded from this study whether it was the loss of Erk1/2-dependent IL-10 production which specifically led to reduced lesion size; the loss of other Erk1/2-dependent effects may have driven the reduction in infectivity.

Purified LPG from *L. donovani* (Balaraman et al., 2005) and *L. major* (de Veer et al., 2003) induces phosphorylation and activation of p38 and Erk1/2 leading to increased production of pro-inflammatory cytokines in murine macrophages, and *L. mexicana* LPG (Rojas-Bernabe et al., 2014) induced the same responses in human macrophages. In live *L. donovani* cells, however, LPG was found to have the opposite effect; *LPG1* and *LPG2* KO parasites, which are unable to produce LPG, induce robust Erk1/2 activation whereas WT parasites do not (Prive and Descoteaux, 2000), suggesting a suppressive role for LPG. These conflicting results support the idea that purified LPG and live parasite-associated LPG may function differently in several respects. However, another study showed the same increase in IL-12 production induced by both purified and cell-associated *L. major* LPG under the same conditions (Favila et al., 2015); more studies comparing the effects of purified versus cell-associated LPG under the same conditions would be valuable to the field.

One possible explanation for conflicting results between cell-associated and purified LPG could be the absolute amount of purified LPG added to host cells compared to the amount of LPG that would be present if whole promastigotes were added. Working on the basis that 1 mg of LPG can be isolated from 10^{10} *L. major* promastigotes (Opat et al., 1996), most studies appear to add roughly the same

amount of LPG, ± 10-fold, to target cells as would be delivered with a live *Leishmania* multiplicity of infection (MOI) of around 10 (Favila et al., 2015). However, even if the absolute concentrations of LPG present when either purified LPG or live cells are used in experiments, it is highly likely that soluble versus surface-immobilised LPG behave differently and can interact with their binding partners to different extents. This could be due, for example, to the GPI anchor being inaccessible when LPG is membrane-bound or the presence of other membrane-associated *Leishmania* factors alongside membrane-bound LPG which could modulate the interaction of LPG with host receptors. Increases in LPG dose generally leads to increases in its effects (Rojas-Bernabe et al., 2014, Favila et al., 2015).

In summary, while direct regulation of host SHP-1 by *Leishmania* EF-1α and GP63 has been demonstrated, the downstream effects on cytokine production require investigation. On the other hand, many effects of *Leishmania* infection on MAPK activation have been reported, but the exact regulatory mechanisms remain unclear. Conflicting roles for LPG in MAPK regulation have been shown from studies using purified LPG or whole cells, and determining the exact molecular target of LPG which governs these effects would be a valuable step forward. In many cases, *Leishmania*-driven MAPK regulation remains to be linked to downstream changes in cytokine production by macrophages and thus requires further study.

1.4.4. Transcriptional regulation of cytokine production

The extent to which cytokines rely on *de novo* gene expression for their induction in response to stimuli varies. In general, the secretion of cytokines such as IL-6 and TNFα which are released very quickly (within 2 h) following stimulation, for example by LPS,

is heavily dependent on post-transcriptional control of pre-existing mRNAs (Stow et al., 2009, Neininger et al., 2002). Whereas for cytokines such as IL-10, which are released later, *de novo* transcription is essential for proper induction (Slack et al., 2007). In every case, a mixture of *de novo* gene expression and post-transcriptional control are likely to contribute to different extents to cytokine induction, as has been shown for IL-8 where both levels of control play important roles (Hoffmann et al., 2002, Winzen et al., 1999). In general, while many transcription factors are known to regulate cytokine production, the mechanisms of transcriptional regulation of particular cytokines are poorly understood and in most cases a cytokine is under the transcriptional control of several transcriptional activators and/or repressors. Different classes of transcription factors in macrophages exist with distinct properties governing their potential control mechanisms. Class I transcription factors, including NFκB and interferon regulatory factors (IRFs), are constitutively expressed but need to be activated, so control mechanisms can include regulation of coactivators or inhibitors, such as the NFκB inhibitor IκB, and regulation of nuclear translocation (Medzhitov and Horng, 2009). Class II TFs are *de novo* synthesised so here regulation could include transcriptional regulation and they are usually constitutively nuclear once expressed; ATF3 belongs to this class and often acts as a suppressor of LPS-induced genes (Medzhitov and Horng, 2009). Finally, the class III lineage-specific factors are constitutively expressed and active in the nucleus but their control of specific genes is still inducible. Lineage-specific TFs which are expressed in macrophages include PU.1, C/EBPβ, IRF8 and RUNX1 (Medzhitov and Horng, 2009). NFκB is one of the best studied transcription factors and has been shown to induce the transcription of most LPS-induced genes (Medzhitov and Horng, 2009) including

CXCL1 (Kanayama, Inoue et al. 2015), CXCL10 (Brownell, Bruckner et al. 2014) and CXCL11 (Yang, Wei et al. 2007). Many cytokine promoters have NFκB binding sites, including CXCL10 (Fukumoto et al., 2012) and IL-8 (Jundi and Greene, 2015). The IL-8 promoter also has activator protein (AP)-1 and C/EBPbeta binding sites, although NFκB in particular is essential for its transcription (Hoffmann et al., 2002).

Of course, other transcription factors also have documented roles in cytokine gene expression. CXCL10 transcription can also be suppressed by AP-1 and C/EBP-β, and activated by IRF3 (Brownell, Bruckner et al. 2014). The CXCL10 promoter has both interferon-sensitive response elements (ISREs) and NFκB-binding sites. LPS-induced CXCL10 transcription is dependent on endogenous LPS-induced IFNβ, which activates STAT1/STAT2/IRF-9 complex-dependent transcription from the ISRE in the CXCL10 promoter (Fukumoto et al., 2012). This result is supported by the fact that LPS-induced expression of CXCL10 is impaired in STAT1-deficient mice (Fukumoto et al., 2012). Interestingly, suppression of CXCL10 gene expression was achieved by secreted parasitic products from *Spirometra erinaceieuropaei* by targeting multiple points in the pathway: IFNβ transcription and STAT1 S727 phosphorylation were suppressed leading to decreased transcription from the CXCL10 ISRE (Fukumoto et al., 2012).

While most cytokine genes seem to be under the control of several transcription factors, one study has shown by truncating the IL-10 promoter that only the Sp1 transcription factor binding site is needed for LPS-induced IL-10 production in THP-1 cells (Ma et al., 2001). However, this analysis was done using a plasmid construct, so conceivably other transcriptional activators would be required in the context of chromatin. There are many coactivators of Sp1, as with other transcription factors,

including CRSP, Rb, hTAFII 130, and their modulation can also lead to cytokine regulation. Sp1 has also been shown to play a role in IL-10 production in murine macrophages (Brightbill et al., 2000).

In addition to transcription factors, chromatin remodelling is a key regulatory mechanism for cytokine gene expression and the roles of histone modifications in the regulation of cytokine expression are beginning to be uncovered. Histone deacetylation within the IL-8 promoter leads to suppression of gene expression (Jundi and Greene, 2015). Reversing these mechanisms, for example through HDAC inhibition or HAT upregulation, leads to derepression of IL-8 transcription (Jundi and Greene, 2015). Histone H3 phosphorylation at serine 10 as a result of p38 signalling leads to NFκB recruitment, which can induce transcription of NFκB-dependent cytokines (Medzhitov and Horng, 2009). Histone H2A ubiquitination, which is mediated by the histone H2A ubiquitin ligase 2A-HUB, inhibits CXCL10 expression in macrophages (Medzhitov and Horng, 2009, Zhou et al., 2008). Histone 3 Lys27 trimethylation can also lead to repression of LPS-induced genes (Medzhitov and Horng, 2009, De Santa et al., 2007). Furthermore, chromatin remodelling complexes, which move nucleosomes to alter promoter accessibility, such as SWI/SNF also have a role in regulating accessibility of cytokine promoters (Medzhitov and Horng, 2009).

Studies on transcription factor regulation by *Leishmania* factors have mostly focussed on NFκB and AP-1, both of which are important regulators of the macrophage pro-inflammatory response (Ricote et al., 1998, Lawrence and Natoli, 2011). Several reports have shown that NFκB is activated in response to purified LPG using both luciferase assays for transcriptional activity in RAW-ELAM cells (de Veer et al., 2003)

and WBs (Becker et al., 2003) to confirm nuclear translocation. Similarly, the transcription factor AP-1 is activated in response to purified LPG (Balaraman et al., 2005). However, comparing the effects of WT versus LPG null parasites suggests that live parasite-associated LPG does not activate AP-1 (Contreras et al., 2010) and NFκB (Prive and Descoteaux, 2000). It should be noted, however, that this may not be true under all conditions and for all combinations of *Leishmania* species and host cell. Furthermore, the effects of *Leishmania* infection on NFκB transcription are complex, as discussed below in this section.

Leishmania infection of macrophages induces the GP63-dependent cleavage of the NFκB subunit p65, resulting in a p35 fragment which translocates as a novel dimer with p50 to the nucleus and is still able to bind the NFκB consensus DNA binding site (Gregory et al., 2008). The authors postulate that this novel NFκB dimer could still be transcriptionally active, although this was not shown directly and the p35 fragment is predicted not to retain the p65 transactivation domain (Gregory et al., 2008). Both *L. major* EVs (Hassani et al., 2014) and the *L. mexicana* secreted proteome (Hassani et al., 2011) also induce nuclear translocation of this novel form of NFκB, and they also induce more nuclear translocation of the p50/p50 and p50/p65 forms compared to live cells. GP63 has also been reported to degrade and reduce the nuclear translocation of AP-1; drastically reduced AP-1 binding to macrophage nuclear DNA was shown in response to WT but not GP63 KO *L. donovani*, *L. mexicana* and *L. major* cells (Contreras et al., 2010). Furthermore, a direct role for GP63 in the downregulation of AP-1 is supported by the fact that GP63 and the AP-1 subunit c-Jun interact in immunoprecipitation studies and GP63 can cleave purified c-Jun *in vitro*

(Contreras et al., 2010). Reduced AP-1 activity is also apparent in response to both *L. major* EVs (Hassani et al., 2014) and the *L. mexicana* secreted proteome (Hassani et al., 2011), although to a lesser extent than induced by live parasites. Whether these differences between secreted factors and live cells is due to differences in the dose of GP63 is unclear.

Other studies using WT versus KO parasites state that NFκB (Cameron et al., 2004) and AP-1, in addition to STAT1a, activity is reduced in a cysteine peptidase b (CPB)-dependent manner (Abu-Dayyeh et al., 2010), in conflict with the GP63-dependency discussed above. CPB is a protein which is upregulated in the amastigote form of the parasite (Souza et al., 1992). These discrepancies are likely to be explained by the recent discovery that in *L. mexicana* CPB is required for the expression of WT levels of GP63, since GP63 expression is lower in CPB KO parasites (Casgrain et al., 2016). Given the lack of studies showing direct interaction between CPB and transcription factors, while there is evidence for direct cleavage of AP-1 by GP63 (Contreras et al., 2010), it seems likely that the effect of CPB KO parasites on transcription factors is due to the indirect effects on GP63 activity. This hypothesis is further supported by evidence that GP63 but not CPB is required for p65 cleavage in response to *Leishmania* infection (Gregory et al., 2008). However, the ability of both promastigotes and amastigotes to efficiently reduce NFκB and AP-1 activity is inconsistent with GP63-dependency since amastigotes express greatly reduced amounts of GP63 (Abu-Dayyeh et al., 2010).

These results suggest that *Leishmania* EVs and live cells reduce AP-1 activity and modulate NFκB activity. The exact downstream effects on cytokine expression remain largely unknown. An important unanswered question is whether the novel p35/p50

form of NFκB can initiate transcription and if so does it have a different set of transcriptional targets from the conventional complexes. In addition, the roles of GP63 and CPB in the downregulation of macrophage transcription factors need to be further investigated considering the newly acquired knowledge that CPB regulates GP63 expression. The ability of these parasite factors to cleave transcription factors should be tested systematically *in vitro*, and whether the same factor is responsible for transcription factor degradation in response to promastigote and amastigote infection should be addressed. Finally, while one study has found that *L. donovani* infection induces changes in macrophage DNA methylation (Marr et al., 2014), the effect of *Leishmania*-dependent chromatin remodelling on cytokine expression remains understudied. Further research in this area could yield new insights into *Leishmania*-dependent cytokine regulation.

1.4.5. Post-transcriptional regulation of cytokine expression

Regulation of mRNA stability and translation efficiency is a key mechanism of cytokine control, particularly for cytokines such as TNFα and IL-6 which are among the first to be released after LPS stimulation and pre-existing pools of mRNA are the main source of translated cytokine. (Stow et al., 2009, Neininger et al., 2002)

MAP kinase-activated protein kinase 2 (MK2) is a serine/threonine kinase downstream of p38 signalling which plays an important role in post-transcriptional cytokine regulation. This is supported by the fact that MK2-deficient mice are unable to induce normal levels of TNFα, IFNγ, IL-1 and IL-6 in response to LPS (Neininger et al., 2002). Splenocytes from MK2 KO mice are unable to induce TNFα in response to LPS, unless the AU-rich element (ARE) in the TNFα 3’ UTR is deleted (Neininger et al.,

2002). AREs are important regions for the post-transcriptional control of several cytokines, including TNFα, IL-8 and IL-10 (Winzen et al., 1999, Anderson, 2008, Gais et al., 2010). Although the exact mechanisms are unknown, there appears to be at least two ways in which MK2 modulates cytokine expression via ARE elements: MK2 regulates IL-6 mRNA stability via ARE-like regions in the 3' UTR, and regulates TNFα translation via the ARE elements in 3' UTR (Neininger et al., 2002). Upstream of TNFα regulation, MK2 is activated by TLR4-dependent signalling via TRIF and p38 (Gais et al., 2010). IL-8 mRNA stabilisation via an ARE element is also mediated by the p38-MK2 pathway (Winzen et al., 1999). It remains unclear whether MK2 interacts directly with ARE elements, it is perhaps more likely that MK2 phosphorylates other RNA-binding proteins; ARE regions are bound by lots of positive and negative regulating proteins which modulate stability and/or translation and kinases such as MK2 can regulate their activity (Anderson, 2008).

Although this area is not well studied, small non-coding RNAs (ncRNAs), such as micro (mi)RNAs or small interfering (si)RNAs, bind and regulate cytokine transcripts by specifically targeting them to the RISC machinery for degradation (known as RNA interference or RNAi), or by modulating the efficiency of translation or poly(A) tail shortening (Agrawal et al., 2003). miRNAs and siRNAs are cleaved from double-stranded or hairpin RNAs into shorter ~20-25 nucleotide fragments (Agrawal et al., 2003). miR369 has been shown to bind TNFα 3' UTR (Anderson, 2008). miR155 reduces IL-4, IL-5 and IL-10 expression in T cells (Anderson, 2008) and is also present in macrophages (Testa et al., 2017), although it is not clear if its effects are direct or indirect. Evidently, miRNAs have the potential to regulate cytokine production, both

by regulating the degradation of cytokine mRNA and by targeting other mRNAs encoding regulators of cytokine secretion.

Hypothetically, *Leishmania* infection could regulate post-transcriptional control of cytokines by modulating host mechanisms or by delivering parasite ncRNAs and mRNAs. The former has been more extensively studied; several changes in the levels of host ncRNAs in response to *Leishmania* infection have been documented, although in most cases the mechanisms are unknown. miRNAs targeting components of MAPK signalling pathways are deregulated in *L. major* and *L. donovani*-infected macrophages (Geraci et al., 2015). miR120 is upregulated in *L. major*-infected murine macrophages, and suppression of this miRNA led to a decrease in parasite load (Frank et al., 2015), indicating the importance of this miRNA in promoting infection. A screen of 365 human miRNAs found that 64 macrophage miRNAs are consistently deregulated in response to *L. major* infection during the first 24 h (Lemaire et al., 2013). Interestingly, several of the deregulated miRNAs are documented to modulate TLR signalling. qRT-PCR confirmed that the levels of five deregulated miRNAs which target chemokine mRNAs negatively correlate with their target chemokine mRNA level. *Leishmania*-induced upregulation of at least one of the miRNAs, miRNA-210, is dependent on the transcription factor hypoxia-inducible factor (HIF)-1α, which is known to regulate transcription of this miRNA. However, it is not known how *Leishmania* regulates this transcription factor and it was not shown directly whether *Leishmania* infection does increase HIF-1α activation. miR-210 targets and inhibits the NFκB signalling pathway in macrophages (Qi et al., 2012, Zhang et al., 2015).

Infection of RAW macrophages with *L. donovani* decreases expression of the endosomal sorting complex required for transport (ESCRT) protein hepatocyte growth factor-regulated tyrosine kinase substrate (HRS), leading to inhibition of MVB formation (Bose et al., 2017). MVBs are emerging as an important site for dissociation of RISC complexes and recycling of RNAi machinery (Lee et al., 2009, Gibbings et al., 2009). Consistent with this, mRNA and protein expression is affected in the infected macrophages (Bose et al., 2017), including increased IL-6 mRNA expression. It should be noted that inhibition of the ESCRT complex would lead to pleiotropic cellular defects in membrane trafficking, cytokinesis etc., therefore further experiments are needed to determine whether changes in mRNA levels are due to RNAi regulation or to global cellular changes as a result of ESCRT inhibition.

Degradation of the essential RNAi component Dicer by *L. donovani* has been documented. GP63 is probably the mediator; GP63 induces the same Dicer cleavage *in vitro* as the cleavage observed *in vivo* in infected Huh7 liver cells (Ghosh et al., 2013). Dicer cleavage likely leads to global down-regulation of RNAi, including the post-transcriptional control of cytokines, although this was not investigated. The specific accumulation of pre-miR122 and a decrease in the level of miR-122 was observed (Ghosh et al., 2013). More research is needed to confirm whether GP63 directly cleaves Dicer and what global effects Dicer cleavage has on *Leishmania* infection. Crucially, to what extent does Dicer cleavage contribute to the global changes in gene expression, and cytokine gene expression in particular, observed in *Leishmania*-infected cells (Fernandes et al., 2016, Ovalle-Bracho et al., 2015, Dillon et al., 2015)?

Leishmania could also modulate macrophage post-transcriptional control by delivering its own ncRNAs to target host mRNAs for silencing or its own mRNAs to be transcribed by the host cell. Delivery of parasite ncRNAs to host cells via EVs is relatively well documented and has been the subject of recent reviews (Bayer-Santos et al., 2017, Lefebvre and Lecuyer, 2017), although thus far, very few specific parasite ncRNAs have been studied and found to modulate host gene expression. In mammalian cells, EVs deliver mRNAs and miRNAs which are functional in the target cell (Ramachandran and Palanisamy, 2012), suggesting that the same may be true of parasite-derived RNAs in host macrophages, although there are no specific examples yet. Importantly, essential RNAi machinery is partially absent or non-functional in several trypanosomatid species, including *T. cruzi*, *L. mexicana* and *L. donovani*, but is present in *L. braziliensis* (Lye et al., 2010). Species with non-functioning RNAi do not generate conventional miRNAs or siRNAs. Interestingly, even in mammalian species with intact RNAi machinery, the majority of RNAs identified in EVs are ncRNAs derived from rRNA and tRNAs, with typically only ~10% of RNAs being mRNAs or miRNAs (Miranda et al., 2014, Li et al., 2014, Nolte-'t Hoen et al., 2012). Despite this, most mammalian studies have focussed on the functional significance of mRNA and miRNA EV cargo (Ramachandran and Palanisamy, 2012). Whether rRNA- and tRNA- derived RNAs are able to mediate post-transcriptional regulation in the target cell is beginning to be uncovered. tRNA-derived small RNAs (tsRNAs) are ~32 nucleotide fragments of mature tRNAs. They bind Argonaute proteins, an essential part of the RNAi machinery, and modulate siRNA- and miRNA- dependent RNAi efficiency by competing for Argonaute binding (Haussecker et al., 2010). In fact, two abundant tsRNAs found in *T. cruzi* EVs, $TsRNA^{Thr}$ and $TsRNA^{Leu}$, were individually transfected into HeLa cells and the

mRNA levels of 23 host genes, including cytokines CXCL1 and CXCL2, were more than 3-fold up- or down- regulated (Garcia-Silva et al., 2014). These are currently the only specific parasite ncRNAs with documented effects on host cells.

The few *Leishmania* and *T. cruzi* studies on EV RNA cargo have also found that the majority of RNAs are rRNA- and tRNA- derived, with even lower proportions of mRNAs than in mammalian studies (Garcia-Silva et al., 2014, Bayer-Santos et al., 2014, Lambertz et al., 2015). *L. braziliensis* but not *L. donovani* EVs contain a very small number of siRNAs, consistent with their having intact RNAi machinery (Lambertz et al., 2015). However, for both species the majority (>90%) of RNAs were derived from rRNAs, intergenic unannotated regions and tRNAs (Lambertz et al., 2015). The intergenic RNAs appear to be novel transcripts which do not encode open reading frames (ORFs) (Lambertz et al., 2015). Microscopy of THP-1 macrophages incubated with *Leishmania* EVs with fluorescently labelled RNA cargo showed that RNA is delivered to the host cytoplasm, suggesting they have the potential to target host transcripts (Lambertz et al., 2015). Only very few mRNA reads were detected in this study (Lambertz et al., 2015), in contrast to mammalian studies where mRNAs form a small but significant fraction of RNAs (Miranda et al., 2014, Li et al., 2014, Nolte-'t Hoen et al., 2012). This could be because only 59% of *L. donovani* reads and 23% of *L. braziliensis* reads aligned with their reference genomes, therefore a large fraction of reads remain unannotated (Lambertz et al., 2015). Around 900 novel previously unannotated mRNA transcripts were recently discovered in an RNAseq analysis of *L. mexicana* (Fiebig et al., 2015), supporting the idea that there may also be unannotated

mRNAs encoded in the *L. donovani* and *L. braziliensis* genomes which have been missed in genomic alignments.

The fact that the RNA composition of mammalian and trypanosomatid EVs resembles the composition of whole cells (Miranda et al., 2014, Li et al., 2014, Nolte-'t Hoen et al., 2012, Lambertz et al., 2015, Bayer-Santos et al., 2014) (the approximate distribution of RNA in S. cerevisiae is 80% RNA, 15% tRNA and 5% mRNA), raises the possibility that whole cell contamination or debris form a significant fraction of the EV samples being analysed. There is evidence from *Leishmania* studies suggesting this is not the case. The presence of a subset of intergenic RNAs in EVs was confirmed by Northern blot and compared to whole cells; the RNAs were present in both samples but at different lengths, suggesting selective packaging into (or selective degradation inside) EVs (Lambertz et al., 2015). Furthermore, tsRNAs were detected by Northern blot in EVs and were enriched in EVs compared to whole cells when equal amounts of RNA were loaded (Lambertz et al., 2015). Searches of tsRNA sequences against the human genome did not correspond to any ORFs but there were matches in intergenic regions (Lambertz et al., 2015). It is possible these tsRNAs could be functional since mammalian ncRNAs are thought to regulate transcription by binding intergenic regulatory sites, although this has not been well studied (Jacquier, 2009).

The fact that the predominant RNA species identified in both mammalian and trypanosomatids are ncRNAs derived from rRNAs and tRNAs is an interesting observation, perhaps suggesting conservation of EV cargo. Future studies should focus on the functional importance of these novel ncRNAs. Thus far, it seems highly likely based on one *Leishmania* study and several mammalian studies that *Leishmania*

EVs deliver RNA to host macrophages, but specific host targets and potential effects on cytokine regulation are yet to be discovered.

1.4.6. Vesicle release

Macrophages have no secretory granules, therefore cytokines are released either via constitutive release of vesicles from the trans-Golgi network (TGN) which go on to fuse with the PM, or in the case of cytokines such as IL-1 which have no classical signal peptide they are secreted via non-classical, poorly understood pathways (Lacy and Stow, 2011). Arfs, Rabs, adaptor proteins and golgins all contribute to protein cargo sorting at the TGN (Murray and Stow, 2014). GFP-tagging and overexpression of TNFα has shown that its secretion by the constitutive pathway is more complex than direct delivery in vesicles from the TGN to the PM (Stow et al., 2009): TNFα is trafficked from the TGN in dynamic tubulovesicular transporters to recycling endosomes before being trafficked to the PM. Since TNFα is initially produced as a transmembrane protein, its ectodomain must then be cleaved by TACE or ADAM to release the extracellular cytokine (Stow et al., 2009). Several other cytokines, including IL-6 and IL-10, are also secreted via the recycling endosome in macrophages (Murray and Stow, 2014, Stow et al., 2009). Macrophage cytokine secretion is summarised in Figure 1.4.

While there is constant low level cytokine secretion via the constitutive pathway, there is significant scope for regulation. Many components of constitutive secretion pathways are upregulated in response to LPS including golgins, Rabs and soluble N-ethylmaleimide-sensitive factor activating protein receptors (SNAREs) (Murray and Stow, 2014). The golgin p230, several Rabs, several SNAREs and synaptotagmins (Syts) all positively regulate TNFα secretion (Murray and Stow, 2014). SNAREs mediate

membrane fusion by bringing opposing membranes together (Pagan et al., 2003). Rabs are small GTPases which recruit a range of tethering proteins and SNAREs to mediate vesicular trafficking (Murray and Stow, 2014).

Golgins are coiled coil proteins which are recruited to the TGN and mediate the release of tubular vesicles. The golgin p230 is recruited to the TGN by Arl1 and coats tubular vesicles carrying TNFα to the recycling endosome (Lieu et al., 2008). Knockdown of p230 in RAW cells reduces TNFα trafficking to the cell surface, while non-specific protein release, such as MHC II surface expression, is unaffected (Lieu et al., 2008). Macrophages of p230 KO mice also have impaired TNFα secretion. LPS treatment of RAW macrophages leads to increased numbers of p230-positive tubular vesicles and increased TNFα release. Interestingly, the increase in TNFα trafficking in response to LPS does not seem to be due to increased p230 expression since this remains constant (Lieu et al., 2008); it could be due to enhanced recruitment of p230 to the TGN by another factor. IL-10, like TNFα, is mostly secreted via the recycling endosome on p230-labelled carriers and p230 is essential for this process. IL-10 is also secreted by transport directly from the TGN to the PM on golgin-97 positive tubules (Murray and Stow, 2014).

Classically secreted cytokines are trafficked from the Golgi complex to the recycling endosome which is dependent on the SNAREs syntaxin6, syntaxin7, Vti1b and VAMP3 (Murray et al., 2005b). Subsequent fusion of vesicles from the recycling endosome with the PM is dependent on the SNAREs VAMP3, Syntaxin 4 and synaptosomal-associated protein 23 (SNAP23) (Murray et al., 2005a). In order to increase secretion of a cytokine via the constitutive pathway, there must be both increased cytokine

transcription and/or translation and increased expression of the correct SNAREs. The density of SNAREs on subsets of vesicles can modulate their propensity for secretion, allowing fine-tuning of cytokine secretion (Stow et al., 2009). LPS up-regulates macrophage SNARE expression through both transcriptional and post-transcriptional regulation (Stow et al., 2009). Several studies have convincingly shown that altering levels of SNARE expression can alter the level of cytokine secretion. Syntaxins are SNAREs which are usually presented on the target membrane side. Increased Syntaxin 4 surface expression is observed on RAW macrophages following LPS stimulation and overexpression of syntaxin 4 in macrophages leads to increased TNFα surface delivery (Pagan et al., 2003). Syntaxin 4 knockdown in RAW cells leads to decreased TNFα surface delivery (Pagan et al., 2003). Another study confirmed that knockdown of syntaxin 4 leads to a reduction in TNFα secretion (Stow et al., 2009). In addition, expression of both SNAREs syntaxin 6 and Vti1b increases following macrophages LPS activation and overexpression of either protein leads to increased TNFα secretion (Murray et al., 2005b).

Syts interact with SNAREs to regulate vesicle fusion, sometimes in a calcium-dependent manner. Syt XI is expressed by macrophages and localises to recycling endosomes (Arango Duque et al., 2013). Syt XI knockdown leads to slightly increased IL-6 and TNFα secretion in murine macrophages and overexpression to decreased levels (Arango Duque et al., 2013). Syt XI has no functional calcium-binding domain and does not seem to bind SNAREs. It is unclear how it negatively regulates IL-6 and TNFα release; it could be through hindering vesicle fusion.

The ability of *Leishmania* infection to target vesicle release mechanisms has been relatively well studied, mostly focussing on the roles of GP63 and LPG. A recent study using immunofluorescence showed that following infection LPG and GP63 are rapidly distributed across the macrophage, confirming that these parasite factors are likely to be able to interact with host vesicle trafficking pathways (Matte and Descoteaux, 2016). *Leishmania* infection alters the cellular distribution of Syt V in an LPG-dependent manner, reducing its localisation to *L. donovani*-containing PVs in the first 2 h post-infection (Vinet et al., 2009). Syt V phagosomal localisation is also reduced following LPG-zymosan uptake compared to zymosan uptake alone (Vinet et al., 2009). The role of Syt V has not been investigated directly but it localises to the recycling endosome and phagocytic cup and therefore may have a role in cytokine secretion (Murray and Stow, 2014).

Syt XI is targeted by *Leishmania* infection in what appears to be a GP63-dependent manner. WT promastigote infection of BMDMs leads to a decrease in cellular Syt XI levels (Arango Duque et al., 2014). WBs show the appearance of Syt XI degradation products in the presence of WT but not GP63 KO parasites (Arango Duque et al., 2014). Further confirming the role of GP63, purified Syt XI is cleaved by incubation with WT but not GP63 KO parasites and this effect is inhibited by a Zn^{2+} ion chelating agent, which inhibits Zn metalloproteases including GP63 (Arango Duque et al., 2014). *L. major* and *L. donovani* promastigotes induce IL-6 and TNFα secretion from BMDMs in a GP63-dependent manner (Arango Duque et al., 2014). Syt XI knockdown was able to partially restore IL-6 and TNFα secretion in GP63 KO *Leishmania*-infected macrophages, suggesting that GP63-dependent loss of Syt XI is at least partially

responsible for the increased secretion of these cytokines (Arango Duque et al., 2014). This is consistent with the known inhibitory role of Syt XI in IL-6 and TNFα secretion (Arango Duque et al., 2013).

The SNAREs VAMP3 and VAMP8 are degraded in a GP63-dependent manner by *L. mexicana* (Casgrain et al., 2016)*, L. major* and *L. donovani* infection of murine BMDMs (Matheoud et al., 2013). However, direct cleavage by GP63 was not shown. VAMP3 is involved in vesicle trafficking of cytokines from the recycling endosome to the PM, therefore its cleavage is likely affect macrophage cytokine secretion (Matheoud et al., 2013), but this was not addressed in these studies.

Multiple studies show the ability of *Leishmania* parasites to regulate vesicle trafficking pathways (Ndjamen et al., 2010, Matte and Descoteaux, 2016, Scianimanico et al., 1999, Desjardins and Descoteaux, 1997); thus far this has mostly been studied in the context of the PV. It is possible that these known mechanisms may also play as yet unknown roles in the regulation of macrophage cytokine release, in addition to the new mechanisms which are being discovered such as Syt XI cleavage.

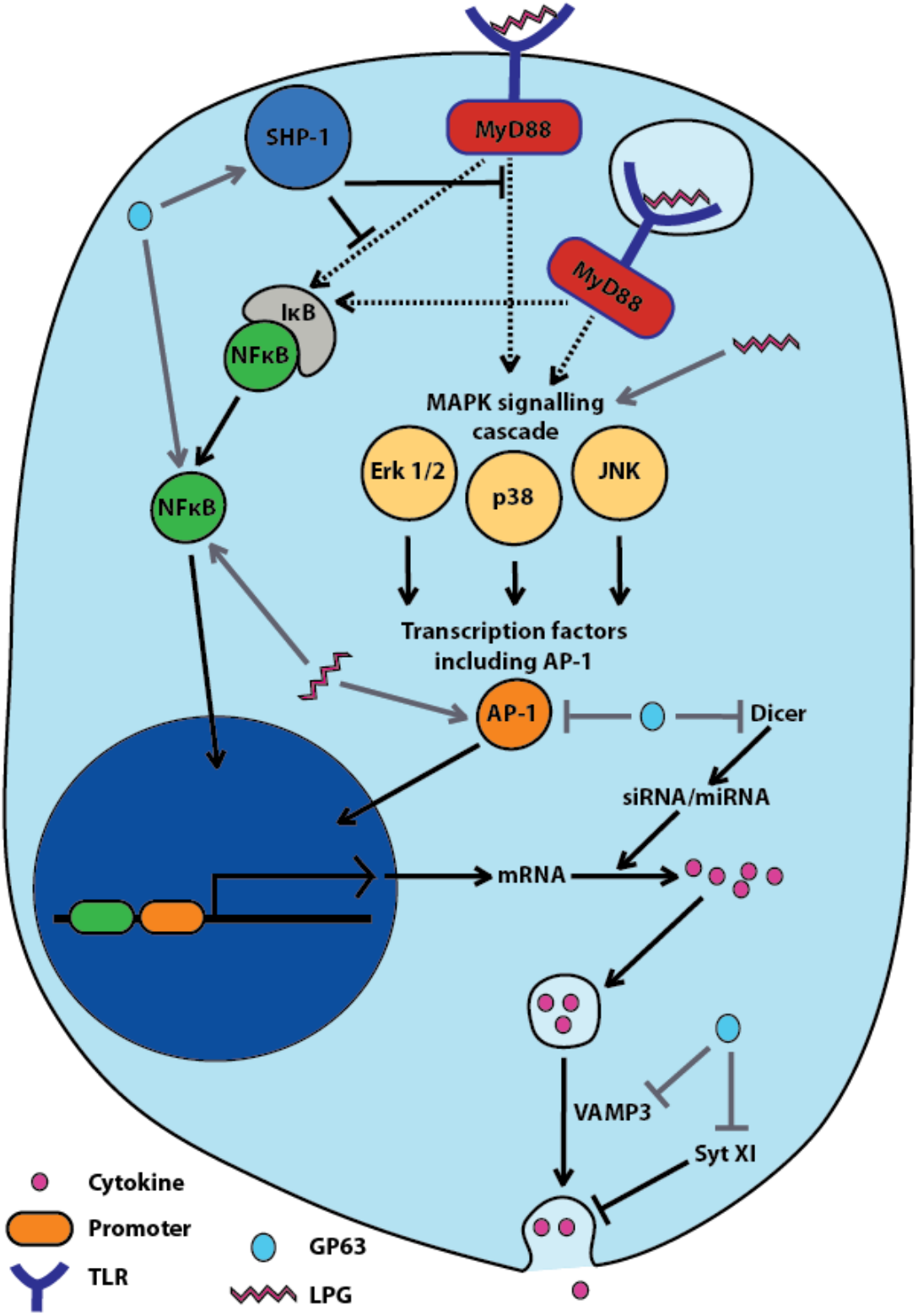

Figure 1.5. Effects of LPG and GP63 on macrophage signalling pathways. A schematic of a macrophage is shown with some of the key signalling pathways leading to cytokine secretion highlighted. The known effects of the *Leishmania* virulence factors LPG and GP63 on these

pathways are indicated. TLRs on either the PM or endosomes are bound by PAMPS, including LPG which signals via TLR2 and TLR4 and downregulates TLR9. TLRs then signal via MyD88 to initiate both MAPK (via a phosphorylation cascade of MAP kinases) and NFκB (via the release of inhibitory IκB) activation. SHP-1 inhibits these events and is activated by GP63-mediated cleavage. Purified LPG upregulates MAPK signalling via unknown mechanisms. One or more of the MAPKs Erk1/2, JNK and p38 activate transcription factors including AP-1. NFκB and AP-1 are both cleaved by GP63 and upregulated by purified LPG. Transcription factors including NFκB and AP-1 mediate cytokine transcription and mRNAs are exported to the cytoplasm. mRNA stability and translation efficiency are modulated by miRNAs and siRNAs produced by Dicer, which is cleaved by GP63. Once translated, classically secreted cytokines are trafficked via the Golgi and recycling endosome to the PM. Vesicle trafficking is mediated by SNAREs including VAMP3, which is cleaved by GP63. Fusion of cytokine-containing vesicles with the PM is inhibited by Synaptotagmin XI, which is also cleaved and inhibited by GP63.

Black lines: macrophage signalling events. **Grey lines:** LPG- and GP63- dependent effects. **Bar headed arrows:** inhibitory effect. **Arrows:** positive effect or complex regulation. **Dashed lines:** additional signalling steps are present but not shown.

1.3. Aims

Recent research has shown that *Leishmania* EVs are an important delivery mechanism for virulence factors to the host and that they are able to modulate the host immune response. The subcellular origin of these EVs remains unknown, and the overarching aim of this thesis is to determine the subcellular origin of *Leishmania* EVs, and in particular to investigate whether the flagellum is a source of EVs. We aim to further address this question in the context of early time points corresponding to the establishment of infection, specifically focussing on the period of flagellar shortening during promastigote to amastigote differentiation. We hypothesise that this is a crucial time for virulence factor delivery to render the host more susceptible to infection, and that there could be a link between flagellar shortening and virulence factor delivery via flagellar EV release. This idea will be investigated.

Furthermore, we aim to perform a broad analysis of the effects of *Leishmania* promastigotes and EVs on macrophage cytokine analysis. This will provide a valuable direct comparison of the immunomodulatory effects of *Leishmania* promastigotes versus EVs. To our knowledge, only one previous study has addressed the effects of *Leishmania* EVs on macrophage cytokine production and found that IL-8 production is increased (Silverman et al., 2010a); the parasite factors responsible for this effect remain unknown. To gain further insights into this, we will also investigate parasite factors present as EV cargo which could be responsible for any changes in cytokine secretion observed.

2. Materials and methods

L. mexicana cell culture, cell lines and their characterisation

2.1. *L. mexicana* cell culture

Promastigote form *L. mexicana* (WHO strain MNYC/BZ/62/M379) and genetically modified derivatives (Table 2.1) were grown at 28°C in M199 medium (Life Technologies) with 2.2 g/L $NaHCO_3$, 0.005% haemin, 40 mM 4-(2-Hydroxyethyl)piperazine-1-ethanesulfonic acid pH 7.4 and 10% foetal calf serum (FCS). Stationary phase promastigotes were collected 5 days after seeding logarithmic phase promastigotes at a density of 1×10^5 cells/ml. Axenic promastigote to amastigote differentiation was induced by resuspending promastigotes in Schneider's Drosophila Medium (Life Technologies) with 5.34 g/L 2-(N-morpholino)ethanesulfonic acid hydrate and 10% FCS, adjusted with concentrated hydrochloric acid to pH 5.5 (medium SM5.5) and culturing in vented flasks at 34°C and 5% CO_2. Relevant selection drugs (Melford Laboratories Ltd.) were added to the medium at: 32 µg/ml Hygromycin B, 20 µg/ml Puromycin Dihydrochloride, 5 µg/ml Blasticidin S Hydrochloride, 40 µg/ml G-418 Disulfate, 50 µg/ml Nourseothricin Sulfate (NTC) and 25 µg/ml Phleomycin. Cell culture densities were measured using a CASY model TT cell counter (Roche Diagnostics) with a 60 µm capillary and exclusion of particles with a pseudo-diameter below 2.0 µm.

Table 2.1. Details of all *L. mexicana* cell lines used. The cell line name, origin, description and resistance markers are shown.

Cell line	Origin	Genetic modifications	Drug selection
WT	WHO strain MNYC/BZ/62/M379	None	None
SMP1::mCh	Previously generated in the Gluenz lab	mCherry gene and resistance cassette inserted at 3' end of endogenous SMP1 (LmxM.20.1310) locus.	G418
SMP1::eYFP	Previously generated in the Gluenz lab	eYFP gene and resistance cassette inserted at 3' end of endogenous SMP1 (LmxM.20.1310) locus.	Phleomycin
SMP1::mCh-GT2::eGFP:TY	Previously generated in the Gluenz lab	mCherry gene and resistance cassette and eGFP:TY and resistance cassette inserted at 3' end of endogenous SMP1 (LmxM.20.1310) and GT2 (LmxM.36.6290) loci respectively.	G418, Phleomycin
Cas9 T7	Previously generated in the Gluenz lab (Beneke et al., 2017)	Cas9 and T7 RNA polymerase genes inserted into WT cell line.	Hygromycin, NTC
Cas9 T7 (p)	Previously generated in the Gluenz lab (Beneke et al., 2017)	Cas9 T7 cell line was passaged through BMDMs by Jessica Valli and differentiated back to promastigotes.	Hygromycin, NTC
Cas9 T7 SMP1::mCh	Previously generated in the Gluenz lab (Beneke et al., 2017)	mCherry gene and resistance cassette inserted at 3' end of endogenous SMP1 (LmxM.20.1310) locus in Cas9 T7 cell line.	Hygromycin, NTC, G418
ΔLPG1	Generated in the Gluenz lab by Laura Makin (Beneke et al., 2017)	Cas9 T7 (p) cell line with both *LPG1* alleles replaced with drug resistance cassettes.	Blasticidin, Neomycin, Hygromycin, NTC
***LPG1* add-back**	Generated in the Gluenz lab by Laura Makin (Beneke et al., 2017)	*ΔLPG1* cell line expressing an ectopic copy of *LPG1*.	Hygromycin, NTC, Phleomycin
EV biogenesis and flagellar length control protein knockout cell lines	Generated in the Gluenz lab by Laura Makin	Both alleles of gene of interest replaced with drug resistance cassettes in cell line Cas9 T7 SMP1::mCh.	Hygromycin, NTC, G418, Blasticidin, Puromycin
mNG-tagged candidate EV-associated protein cell lines	Generated in the Gluenz lab by Laura Makin	An mNeonGreen gene and drug resistance cassette inserted at the 5' end of at least one allele of the gene of interest in cell line Cas9 T7 SMP1::mCh.	Hygromycin, NTC, G418, Blasticidin
mNG-tagged adenylyl cyclases	Generated in the Gluenz lab by Laura Makin	An mNeonGreen gene and drug resistance cassette inserted at the 3' end of at least one allele of the gene of interest in cell line Cas9 T7 SMP1::mCh.	Hygromycin, NTC, G418, Blasticidin
eYFP-tagged candidate EV-associated protein cell lines	Generated in the Gluenz lab by Laura Makin	An eYFP gene and drug resistance cassette inserted at the 3' end of one allele of the gene of interest in cell line Cas9 T7 SMP1::mCh.	Hygromycin, NTC, G418, Blasticidin

2.2. Genetic modification of *L. mexicana* cell lines

2.2.1. Generation of knockout cell lines

Gene deletions were performed in the *L. mexicana* Cas9 T7 cell line (and derivatives thereof), which express both Cas9 nuclease, to allow cleavage of specific genomic sites in the presence of single guide (sg)RNA, and T7 RNA polymerase, to allow the *in vivo* transcription of sgRNAs from DNA templates. See (Beneke et al., 2017) for details.

Generation of *ΔLPG1* and *LPG1* AB cell lines was done by Laura Makin, as described in (Beneke et al., 2017).

To generate a knockout, Blasticidin and Neomycin knockout constructs were amplified from pTBlast and pTNeo plasmids (Figure 2.1A) in polymerase chain reaction (PCR) reactions each containing 15 ng of pT plasmid, 0.2 mM dNTPs, 2 µM each of the forward and reverse primers, 1 unit of Expand High Fidelity polymerase (Roche), 3% DMSO, 1.5 mM $MgCl_2$, 1x Expand High Fidelity buffer (Roche), topped up to 40 µl with ddH_20. Thermocycling conditions were: 5 min at 94°C, 40 cycles of 30 s denaturation at 94°C, 30 s annealing at 65°C and 2 min 40 s extension at 72°C, followed by a 7 min extension at 72°C. sgRNA DNA templates were amplified (Figure 2.1C) in PCR reactions each containing 0.2 mM dNTPs, 2 µM each of the forward and reverse primers, 0.6 units of Expand High Fidelity polymerase (Roche) and 1x Expand High Fidelity buffer (Roche), topped up to 20 µl with ddH_2O. The thermocycling conditions were: 30 s at 98°C, 35 cycles of 10 s denaturation at 98°C, 30 s annealing at 60°C and 15 s extension at 72°C, followed by a 10 min extension at 72°C.

L. mexicana Cas9 T7 (p) logarithmic stage promastigotes were transfected with the pTBlast and pTNeo constructs and the 5' and 3' sgRNAs simultaneously using Amaxa Nucleofector IIb (Lonza) programme X-001. 35 µl each of the pTBlast and pTNeo constructs and 15 µl each of the 5' and 3' sgRNA constructs were pooled to a total volume of 100 µl and sterilised by heating at 95°C for 5 min. A negative control using sterile ddH_2O instead of donor DNA was included for all transfections. The pooled constructs were added to 100 µl of cell suspension containing 1.10^7 cells in Tb-BSF buffer (Schumann Burkard et al., 2011) final concentrations 66.7 mM Na_2HPO_4, 23.3 mM NaH_2PO_4, 5 mM KCl, 50 mM HEPES pH7.3, 143 µM $CaCl_2$) with $CaCl_2$ final concentration 0.15 mM, topped up with ddH_2O. The transfected cells were selected using G418 and blasticidin in M199 medium. The resulting drug resistant population was cloned out in the presence of these drugs in supplemented M199 medium (M199 medium (Life Technologies), 2.2 g/L $NaHCO_3$, 0.005% haemin, 40 mM 4-(2-Hydroxyethyl)piperazine-1-ethanesulfonic acid pH 7.4, 100 µM adenine hemisulphate, 1.2 µg/ml biopterin and 20% FCS).

All other knockout cell lines (EV biogenesis and flagellar length control proteins) were generated in the same way, except that Cas9 T7 SMP1::mCh cells were transfected with pTBlast and pTPuro constructs and drug selection was carried out using blasticidin and puromycin.

For PCR screening of all knockout cell lines to check for the loss of the ORF of interest and the correct genomic integration of the drug resistance constructs, genomic DNA was prepared using DNeasy kits (Qiagen). The PCR reactions each contained 1x Expand High Fidelity buffer (Roche), 0.2 µM dNTPs, 1 µM each of forward and reverse

primers, 0.6 units of Expand High Fidelity polymerase (Roche), topped up with ddH_20 to 20 µl. The thermocycling conditions were: 5 min at 94°C, 30 cycles of 30 s denaturation at 94°C, 5 s annealing at 60°C and 50 s extension at 72°C, followed by a 7 min extension at 72°C.

All primers for knockout were designed using an online resource for CRISPR Cas9 genome editing in *L. mexicana* and other kinetoplastids LeishGEdit (Beneke; 2017) and the primers for knockout screening were designed by Tom Beneke in the Gluenz lab using open-source Primer3 software (Untergasser et al., 2012) with some modifications. The following parameters were used: the 5'UTR forward primer (for drug cassette integration verification) was designed to anneal within a 250bp window, between 150-400bp upstream of the ORF start codon. ORF forward primer and ORF reverse primers (to verify the loss of ORF) were designed to anneal anywhere in the ORF, resulting in an amplicon with a product size from 100bp to 350bp. All three primers were designed with a target annealing temperature of 60°C and a GC content from 30-70%. Three common reverse primers were used to amplify from within the drug resistance gene ORFs for drug cassette integration verification:

pTBlast: 5' CCGTTGCTCTTTCAATGAGGGTG 3'

pTNeo: 5' GTCTTGACAAAAAGAACCGGGC 3'

pTPuro: 5' TCAATGTGTCGATCTGGGTCAAC 3'

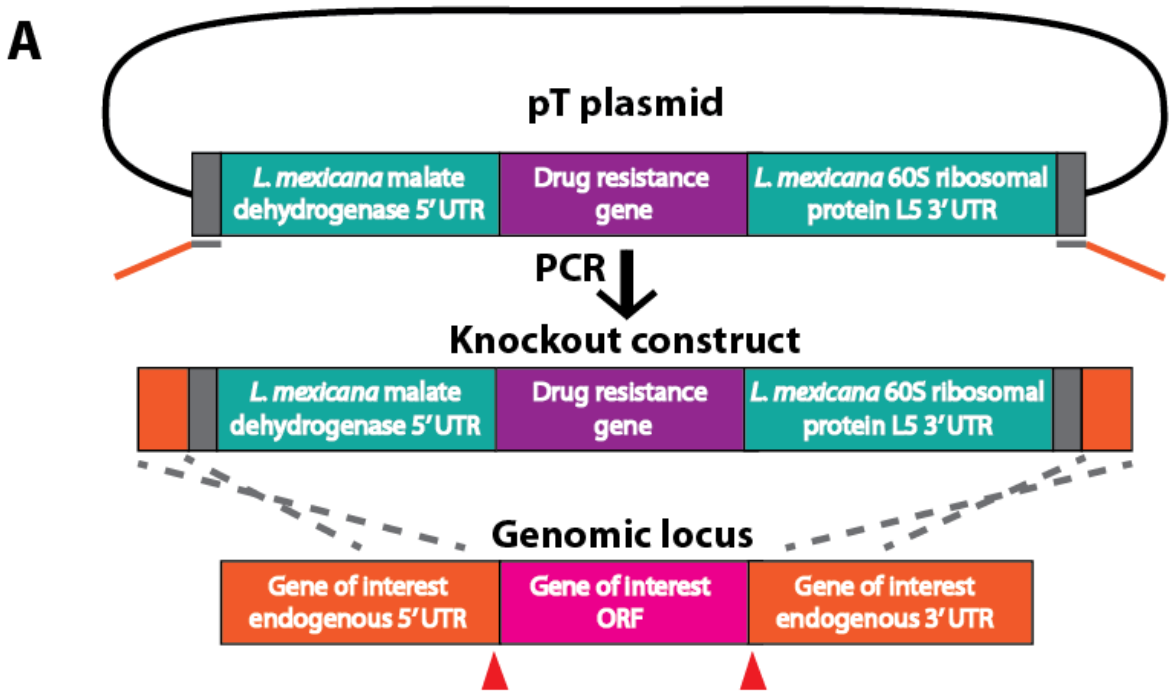
A
pT plasmid
L. mexicana malate dehydrogenase 5′ UTR
Drug resistance gene
L. mexicana 60S ribosomal protein L5 3′ UTR
PCR
Knockout construct
L. mexicana malate dehydrogenase 5′ UTR
Drug resistance gene
L. mexicana 60S ribosomal protein L5 3′ UTR
Genomic locus
Gene of interest endogenous 5′ UTR
Gene of interest ORF
Gene of interest endogenous 3′ UTR

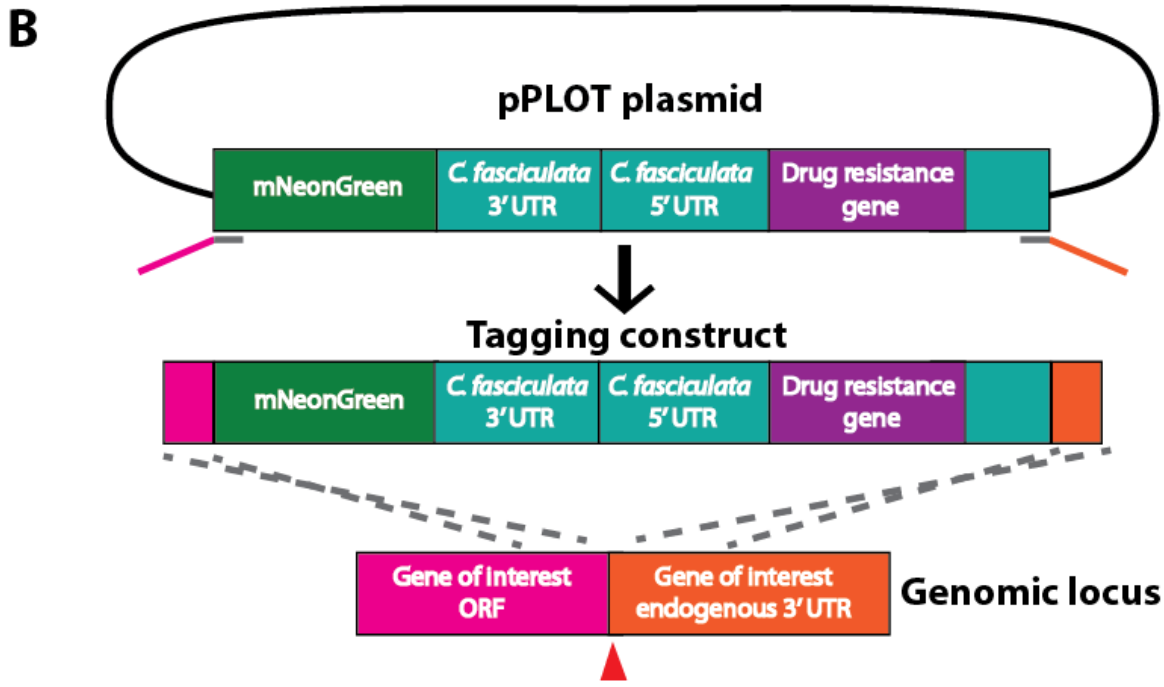
B
pPLOT plasmid
mNeonGreen
C. fasciculata 3′ UTR
C. fasciculata 5′ UTR
Drug resistance gene
Tagging construct
mNeonGreen
C. fasciculata 3′ UTR
C. fasciculata 5′ UTR
Drug resistance gene
Gene of interest ORF
Gene of interest endogenous 3′ UTR
Genomic locus

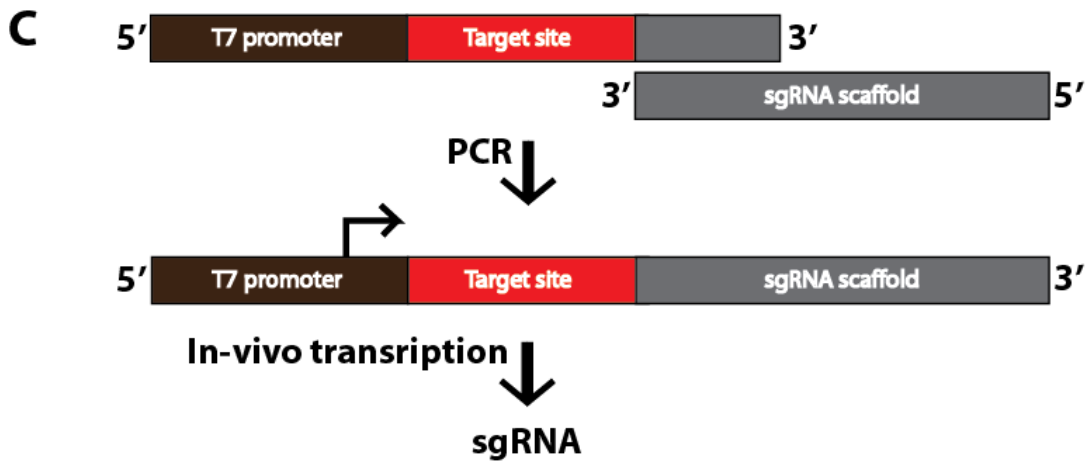

Figure 2.1. Genetic manipulation using Crispr Cas9. A) The schematic illustrates gene knockout which was used to replace both alleles of a gene of interest with resistance genes. Primers with overhangs containing 30 bp homology to the UTRs of the gene of interest (orange) were used to PCR amplify a resistance gene cassette from the pT plasmid. The ORF of interest was excised by Cas9 nuclease which was targeted to sites immediately upstream and downstream of the ORF of interest by 5′ and 3′ sgRNAs respectively (DNA cuts are indicated by red triangles). The linear knockout construct was used to repair the locus, replacing the ORF of interest with a resistance gene cassette. **B)** This schematic illustrates C terminal fluorescent tagging, however the principal is the same for N terminal tagging. Primers with overhangs containing 30 bp homology to the end of the ORF of interest (pink) and the start of the 3′ UTR of the gene of interest (orange) were used to PCR amplify an mNeonGreen gene and resistance gene cassette from the pPLOT plasmid. A double-stranded break was introduced into the locus by Cas9 nuclease which was targeted to a site immediately downstream of the ORF of interest by a 3′ sgRNA. The linear tagging construct was used to repair the locus, introducing an in-frame mNeonGreen gene at the 3′ end of the ORF of interest followed by a resistance gene cassette. C) Two short overlapping primers were fused by PCR amplification to produce a double-stranded template DNA (Bassett, 2014). Once transfected into an *L. mexicana* cell expressing T7 polymerase the template is transcribed *in vivo* from the T7 promoter (arrow) to produce an sgRNA containing a 20 nucleotide homology

site for targeting to the gene of interest (red) and the sgRNA scaffold for Cas9 nuclease recruitment (grey).

2.2.2. Generation of *LPG1* add-back cell line

The *LPG1* CDS was amplified using primers with overhangs to introduce Spe I and Psp XI sites at the 5' and 3' ends respectively. Both the PCR product and pRM005 vector (Figure 2.2) were digested with Spe I and Psp XI restriction enzymes and 5' phosphate of the digested plasmid was removed using alkaline phosphatase. The digested PCR product and plasmid were incubated overnight at 4°C with T4 ligase at an insert:backbone molecular ratio of 7:1 (Beneke et al., 2017). Sure2 competent *E. coli* cells were transformed with the resulting construct by heat shock for 45 s at 42°C and selected at 37°C on agar plates containing 100 µg/ml ampicillin. Selected colonies were expanded in LB broth with ampicillin at 37°C then the plasmid was purified using a QIAprep Spin Miniprep kit (Qiagen) before being linearised by digestion with Pac I. The final construct was ethanol precipitated, resuspended in 10 µl sterile ddH_20 and transfected into 1.10^7 *L. mexicana ΔLPG1* clone F3 cells. The transfection was carried out as already described (*Section 2.2.1*), except that 10 µl of DNA construct was added to 95 µl of resuspended cells. The transfected cells were placed under drug selection in M199 medium plus phleomycin for selection of the AB construct and hygromycin to select for the retention of the Cas9 construct.

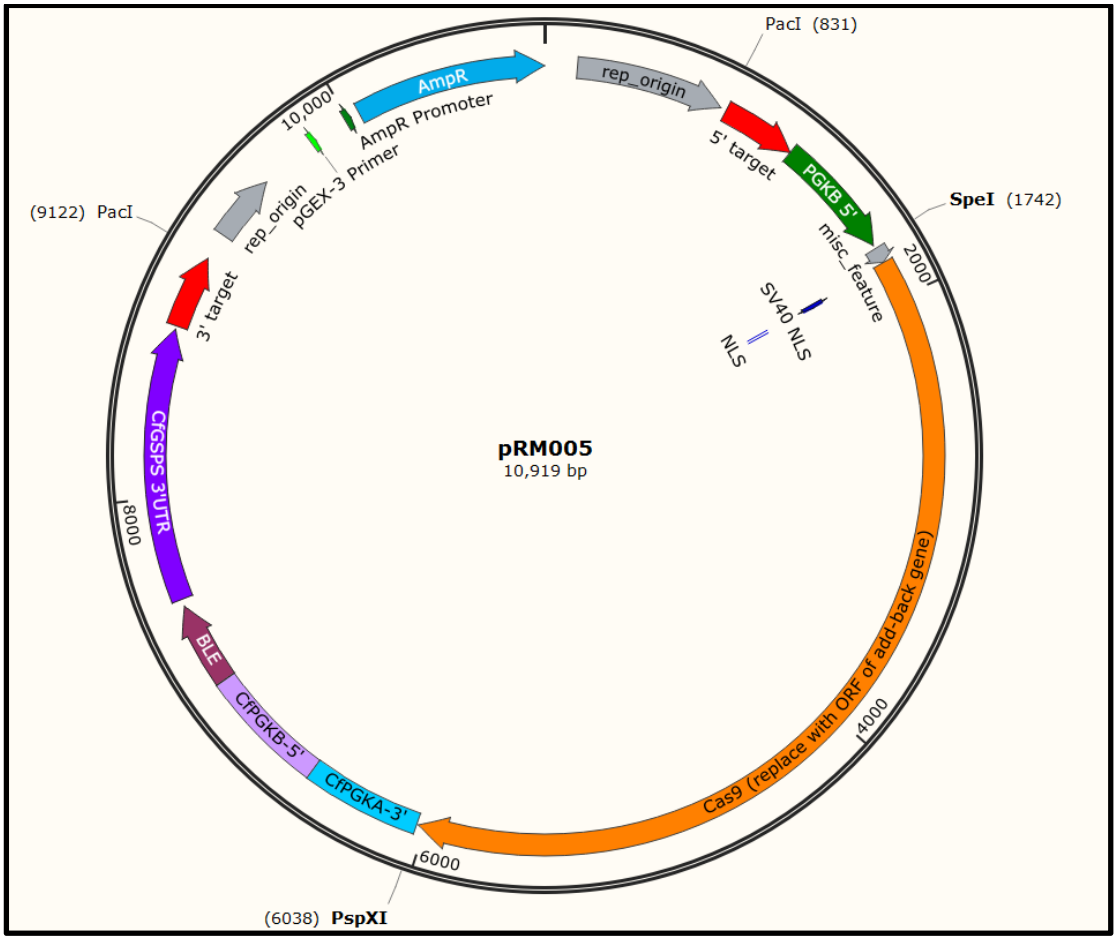

Figure 2.2. Plasmid pRM005 for add-back generation. Plasmid map showing the vector used for generation of the *LPG1* AB cell line. The Cas9 gene (orange) was excised by restriction digest using the Psp XI and SPe I sites and the *LPG1* ORF was cloned in. Before transfection into *L. mexicana* cells the plasmid was linearised and the ampicillin resistance cassette was excised by restriction digest with Pac I. The 5' and 3' target sites (red) have homology to the *Leishmania* β-tubulin array.

2.2.3. Generation of fluorescently tagged cell lines

Cell lines with a gene encoding a fluorescent protein inserted in-frame at the 5' or 3' end of the endogenous ORF of interest were generated using one of two published methods:

1) Crispr Cas9-mediated tagging to allow insertion of a linear construct with short 30 bp homology arms (Beneke et al., 2017)(Figure 2.1B)

2) Fusion PCR-mediated tagging to allow insertion by homologous recombination of a linear construct with long 500 bp homology arms (Dean et al., 2015)(Figure 2.3).

For the first method, constructs were amplified from the pPLOT plasmid in PCR reactions each containing 30 ng of pPLOT plasmid, 0.2 mM dNTPs, 2 µM each of the forward and reverse primers, 1 unit of Expand High Fidelity polymerase (Roche), 1x Expand High Fidelity buffer (Roche), topped up to 30 µl with ddH_20. Thermocycling conditions were: 5 min at 94°C, 40 cycles of 30 s denaturation at 94°C, 30 s annealing at 65°C and 2 min 15 s extension at 72°C, followed by a 7 min extension at 72°C. sgRNA constructs were PCR amplified as described in the Crispr Cas9 knockout method (*Section 2.2.1*). The entire construct and sgRNA PCR products for each target gene were pooled and sterilised by heating at 95°C for 5 min ready for transfection. The transfections were carried out using *L. mexicana* Cas9 T7 SMP1::mCh as already described (*Section 2.2.1*). The transfected cells were placed under drug selection in M199 medium plus blasticidin. All primers were designed using online resource LeishGEdit.net (Beneke;, 2017).

For the fusion PCR method, firstly, 500 bp homology arms were PCR amplified from *L. mexicana* genomic DNA; each reaction contained 160 ng of genomic DNA, 0.2 mM dNTPs, 2 µM each of the forward and reverse primers, 3% DMSO, 2.5 units of Expand High Fidelity polymerase (Roche), 1x Expand High Fidelity buffer (Roche), topped up to 50 µl with ddH_20. Thermocycling conditions for touchdown PCR were used: 5 min at 94°C, 15 cycles of 30 s denaturation at 94°C, 30 s annealing at 65-58°C and 30 s extension at 72°C, followed by 25 cycles of 30 s denaturation at 94°C, 5 s annealing at 60°C and 30 s extension at 72°C, and finally a 7 min extension at 72°C. For the amplification of genomic regions with high GC content which could not be successfully amplified under these conditions, Q5 High-Fidelity polymerase (NEB) was used. PCR products were electrophoresed on a 1.5% agarose gel and the correct-sized bands were excised and the PCR products were extracted using a QIAquick Gel Extraction Kit (Qiagen). The purified ORF and 3' UTR amplicons were then used as long forward and reverse primers respectively to amplify the eYFP gene and resistance cassette from pLENTv2 plasmid by nested fusion PCR. Each PCR reaction initially contained 50 ng of pLENTv2 plasmid, 0.2 mM final concentration dNTPs, 50 ng each of the long forward and reverse primers, 5 units of Phusion polymerase, 1x GC reaction buffer, 3% DMSO, topped up to 87 µl with ddH_20. Thermocycling conditions for the initial PCR amplification before the addition of nested primers were: 1 min at 98°C followed by 3 min at 66°C, 5 cycles of 10 s denaturation at 98°C, 1 min annealing at 66°C and 1 min 40 s extension at 72°C. The nested primers were then quickly added during a 98°C denaturation step; to each 87 µl reaction was added 13 µl containing 1 µM final concentration each of the forward and reverse nested primers, 1x GC reaction buffer, 3% DMSO, topped up with ddH_2O. Then the PCR reaction continued with 35 cycles of

10 s denaturation at 98°C, 10 s annealing at 65°C and 1 min 40 s extension at 72°C, and finally a 7 min extension at 72°C. The PCR products were ethanol precipitated and resuspended in 10 µl sterile ddH_2O ready for transfection into *L. mexicana* SMP1::mCh cells (or if strong non-specific bands were present when 1.5 µl of the PCR product were electrophoresed on a 1% agarose gel, the entire PCR product was electrophoresed and the correct-sized band was excised and gel purified before ethanol precipitation). The transfections were carried out as already described (*Section 2.2.1*), except that 10 µl of DNA construct was added to 95 µl of resuspended cells. The transfected cells were placed under drug selection in M199 medium plus blasticidin. All primers were manually designed using an online resource OligoCalc (Kibbe, 2007) to calculate annealing temperatures; the primers to amplify the 500 bp homology arms had a target annealing temperature of 62°C and the nested primers 66°C.

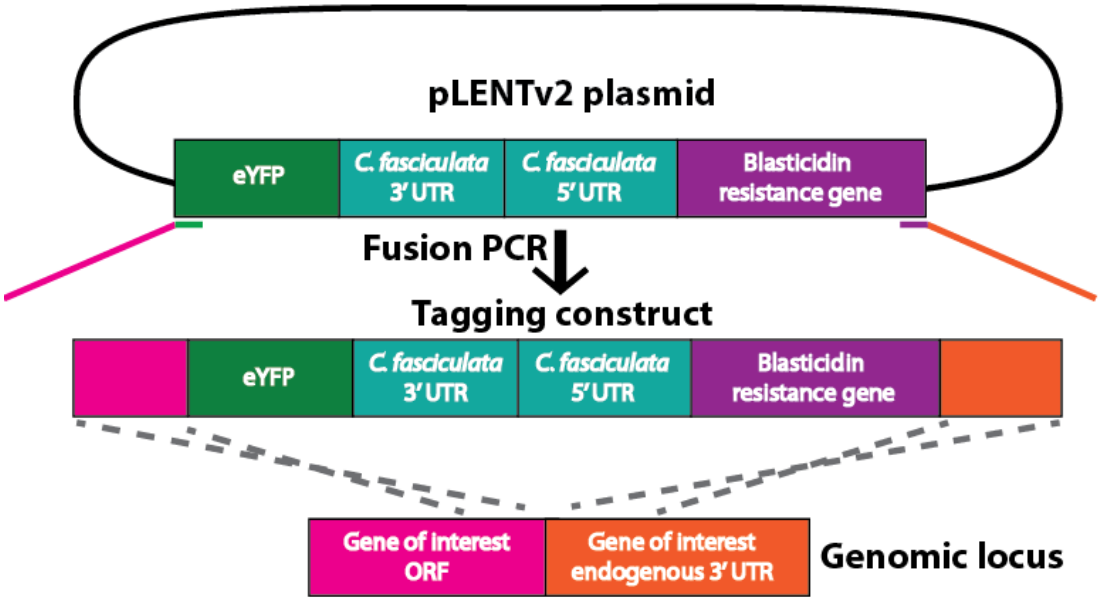

Figure 2.3. Fluorescent tagging of proteins using fusion PCR. C terminal tagging is illustrated. Sections of the locus of interest were PCR amplified to generate long primers with overhangs containing 500 bp homology to the end of the ORF of interest (pink) and the start of the 3' UTR of the gene of interest (orange); these primers were used to PCR amplify an eYFP gene and resistance gene cassette from the pLENT version 2 plasmid. The linear tagging construct was inserted into the endogenous locus by homologous recombination, introducing an in-frame eYFP gene at the 3' end of the ORF of interest followed by a resistance gene cassette.

2.3. Light microscopy imaging

2.3.1. Imaging of native fluorescence of tagged cell lines

L. mexicana cells were washed twice in phosphate-buffered saline (PBS) and settled in 50 µl PBS onto Polysine™ (VWR) slides. For live cell imaging most of the PBS was removed then a Number 1.5 coverslip was applied and cells were imaged immediately at the ambient temperature of 25–28°C. For imaging of chemically fixed cells, an equal volume of 4% paraformaldehyde (PF) was added and incubated for 5 min, then most of the liquid was removed, 10 µl of mounting medium (2.5% anti-fade agent DABCO (1,4,-diazobicycli-[2.2.2]-octane), 90% glycerol, 10% PBS) was added and the cells were imaged immediately or up to 1 day later. When Hoechst was used to stain DNA, it was incubated with live cells in medium for 30 s at 10 µg/ml. For imaging of live BMDMs, macrophages were grown in 24-well plates (Costar) on coverslips which were removed, inverted onto Polysine™ slides and imaged immediately.

Imaging of slide-mounted samples was carried out on a Leica DM5500B microscope with Leica 63x or 100x (NA 1.4) oil immersion objectives or a 40x (NA 1.25) dry objective with an Andor Neo 5.5 sCMOS camera. Alternatively, a Zeiss Axio Imager Z2 with an Orca.Flash 4.0 digital camera (Hamamatsu) using a 63x (NA 1.4) Plan-Apochromat oil immersion objective was used.

For imaging of live human iPSC-derived macrophages, cells were grown on 35 mm glass-bottom U-dishes (Greiner) or 48-well 1.5 coverslip glass-bottom plates (MatTek), Draq5™ (a far-red emitting DNA dye, BioLegend) was added at 5 µM for 5 min at 34°C, then the macrophages were washed and imaged on an inverted Zeiss Axio Observer Z1 with a Zeiss 63x LCI Plan-Neofluar (NA 1.3) water immersion objective at 34°C and 5% CO_2. Alternatively, for super-resolution microscopy live human macrophages were imaged on an inverted Zeiss LSM 880, with a Zeiss 63x (NA 1.4) Plan Apochromat oil immersion objective, and a Zeiss Airyscan 32 GaAsp PMT detector array. Airyscan processing was carried out using Zeiss Zen software. All other image processing was carried out using ImageJ software.

For imaging of isolated EVs, 10 µl of EVs resuspended in PBS were simply added to Polysine™ slides, Number 1.5 coverslips were added and imaged immediately on the Leica DM5500B microscope with a 100x (NA 1.4) oil immersion objective.

2.3.2. Immunofluorescence microscopy

For immunofluorescence experiments, cells were prepared and fixed with PF as described above then quenched for 5 min in PBS with 1% glycine followed three 5 min washes in PBS. The samples were then incubated in PBS with 10% FCS for 1 h to prevent non-specific binding. Primary and secondary antibody incubations were carried out in PBS with 10% FCS for 1 h with three 5 min PBS washes in between. Three final washes in PBS were carried out then 10 µl of mounting medium (see *Section 2.3.1*) was added and cells were imaged within 1 day. All sample incubations were carried out in a humidified, dark chamber at room temperature. Number 1.5 coverslips were used for all imaging.

Isolation of EVs and characterisation of their properties

2.4. *L. mexicana* EV isolation by ultracentrifugation or density gradient separation

EVs were always freshly prepared on the same day they were used for imaging or macrophage experiments. Crude EV samples were isolated by ultracentrifugation using a protocol based on a published method (Silverman et al., 2010a). Stationary phase *L. mexicana* promastigotes were collected by centrifugation (800 *g*, 5 min) and washed once in FCS-free medium: for PRO EV generation this was M199 medium (Life Technologies) supplemented with 2.2 g/L $NaHCO_3$, 0.005% haemin, 40 mM 4-(2-Hydroxyethyl)piperazine-1-ethanesulfonic acid pH 7.4, 10 g/L D-glucose and 0.22 g/L L-glutamine; for DIF EV generation this was Schneider's Drosophila Medium (Life Technologies) supplemented with 5.34 g/L 2-(N-morpholino)ethanesulfonic acid hydrate and 10 g/L D-glucose, adjusted with concentrated HCl to pH 5.5. The cells were resuspended in FCS-free medium at a high cell density of 4.2×10^7 cells/ml and cultured in up to six 40 ml volumes for 4 h under either promastigote or axenic amastigote conditions (see *section 2.1*) for generating PRO or DIF EVs respectively. Where necessary, a 40 ml FCS-free medium sample was included at this stage and taken through all subsequent EV isolation steps as a control for endotoxin contamination. All subsequent centrifugations were carried out at 4°C. Whole cells were removed and the conditioned medium was collected by a 30 min centrifugation at 800 *g* followed by a 30 min centrifugation at 2000 *g,* carried out in disposable 50 ml polypropylene tubes (Falcon). Filtration of the conditioned medium through a 0.22 µm pore filter was included at this stage to produce sterile EV samples for cryo-EM

imaging. Cell debris was removed by a 45 min centrifugation at 15,000 *g* in reusable 50 ml polycarbonate tubes (VWR). EVs were collected by an overnight centrifugation at 100,000 g in 70 ml polycarbonate tubes (Beckman Coulter), with additional sterile PBS added to fill the tubes. The EV pellet (usually invisible) was resuspended in cold sterile PBS by pipetting up and down for at least 1 min. At this stage the resuspended pellets from up to six tubes were pooled if necessary and transferred to either disposable 8 ml Quick-Seal polypropylene tubes (Beckman Coulter) or disposable 1.5 ml Eppendorf tubes (Beckman Coulter) and EV samples were collected by centrifugation for 1 h at 100,000 *g* followed by resuspension in cold sterile PBS. Between uses the reusable tubes were thoroughly washed using a very small amount (<1 ml) of washing up liquid (Fairy) then rinsed at least ten times with deionised water and the air-dried tubes were kept exclusively for EV isolation to reduce the risk of endotoxin contamination.

For isolation of purer EV samples by density gradient separation using a protocol based on a published method (Cvjetkovic et al., 2016), a higher density of stationary phase promastigotes of 1×10^8 cells/ml was used to produce conditioned medium to improve the EV yield. The EV isolation steps described above were carried out up to and including the overnight centrifugation at 100,000 *g,* the EV pellets were resuspended in cold sterile PBS, pooled and topped up to a final volume of 0.5 ml. This was then mixed with 1.5 ml 60% iodixanol (OptiPrep™, Sigma-Aldrich) at the bottom of an 8 ml Quick-Seal tube (Beckman Coulter). 0.75 ml fractions containing 0.25M sucrose, 10mM Tris and 1mM EDTA were then carefully layered on top of the EV sample using a 19G needle against the wall of the tube at the following iodixanol

percentages: 35, 30, 28, 26, 24, 22, 20. The remaining volume of the tube was filled with sterile PBS and the tube was centrifuged at 178,000 *g* for 16 h. To collect the fractions (fraction 1 is the top PBS fraction and fractions 9 and 10 are the bottom fraction where the EV sample was initially added), a 19G needle was inserted into fraction 1 as an air outlet, and 19G needles were used to sequentially remove the 0.75 ml fractions (except fractions 9 and 10 which were 1 ml each) from the top to the bottom. The fractions were then centrifuged for 1 h at 100,000 *g* and the final EV pellets were resuspended in cold sterile PBS (fractions 9 and 10 were pooled).

2.5. Nanoparticle tracking analysis

Isolated EV samples (see *Section 2.6*) resuspended in PBS were diluted in PBS (usually 1:100) to a final volume of 1 ml and loaded in a 1 ml syringe to allow sample loading onto the NanoSight machine LM10 (Malvern). Three 60 s data collections using the total scatter setting (i.e. no filters) were carried out for each sample and if one set of data was obviously very different to the other two for a known technical reason (i.e. there was an air bubble disrupting the particle flow) this dataset was excluded from the analysis. A flow rate of 50 (arbitrary units) was used to reduce photobleaching. The data analysis settings, most importantly camera level and detection threshold level, were kept the same for all samples measured on the same day. The NanoSight was cleaned with 0.22 µm-filtered PBS between each sample. NTA 3.1 software was used for data collection and analysis. A schematic showing how NTA works is shown in Figure 2.4.

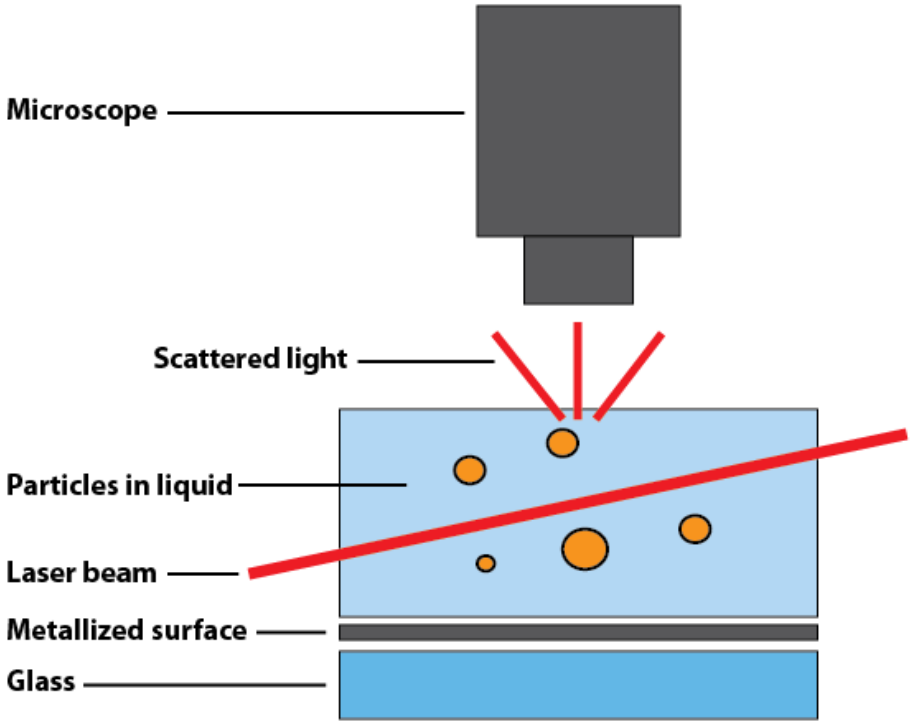

Figure 2.4. Nanoparticle tracking analysis. Particles (EVs, for example) suspended in liquid in a glass chamber are illuminated from the side by a laser beam. The light scattered by the particles is detected by the microscope allowing the movement of each particle to be individually tracked. The size of each particle is calculated based on the speed of its Brownian motion in the liquid using the Stokes-Einstein equation.

2.6. Electron microscopy sample preparation and imaging

2.6.1. Whole-mount negative staining of EVs

For negative staining EM of whole mount EVs, isolated EVs were resuspended in PBS with 4% PF and a 10 µl drop was incubated for 1 or 10 min on the carbon coated side of a 100 mesh copper grid (TAAB) which had been subjected to glow discharge at 15 mA for 20 s. For regular negative staining, grids were either subjected to 3 washes with ddH_2O over 5 min or the grids were taken straight to the next step. Grids were then incubated for 10 s with 2% uranyl acetate (UA), blotted and allowed to air dry for at least 1 day before viewing at ~30,000x magnification on the FEI Tecnai 12 TEM

with a 4 megapixel Gatan Ultrascan^{TM} 1000 CCD camera using Gatan Digital Micrograph software for image acquisition and analysis. For immuno-gold sample preparation extra steps were added between the 10 min sample incubation and UA staining: grids were incubated in PBS with 5% FCS for 5 min to prevent non-specific binding; primary and secondary antibody incubations were carried out for 1 h in PBS with 0.2% gelatine from cold water fish skin with 5 washes in the same incubation buffer in between; finally, 3 washes in PBS and 1 in ddH_2O were carried out before UA staining as already described.

2.6.2. Scanning electron microscopy of *L. mexicana* cells

For scanning EM sample preparation, EM-grade glutaraldehyde (TAAB) was added directly to cells in culture to a final concentration of 2.5% and left on a shaking platform for 2 h at ambient temperature. Cells were collected by centrifugation for 10 min at 500 g and resuspended in 10 ml PBS, at which point the cells were left in the fridge for up to 4 days. Cells were then resuspended in PBS again at a cell density of ~4.10^7 cells/ml. 0.5 ml of this cell suspension was added per well of a 24-well plate with a poly-L-lysine-coated coverslip at the bottom of each well and left to settle for 10 min. 12 mm coverslips were coated with poly-L-lysine by washing in 1M HCl for 10 min then carrying out 5x 5 min washes with ddH_2O before incubating with 0.1% poly-L-lysine in ddH_2O for 15 min then drying overnight. Coverslips with adsorbed cells were subjected to a series of solution changes to dehydrate the cells: three washes with ddH_2O, then a series of 5 min incubations with 30%, 50%, 70%, 90% and finally three 5 min incubations with dehydrated 100% ethanol. Importantly, the coverslips were never allowed to dry out. The samples were then subjected to critical point drying to replace the ethanol with liquid CO_2 using a Tousimis autosamdri-815 with a

purge time of 10 min. Sputter coating with a thin layer of gold for 60 s was performed before loading coverslips onto stubs and storing in a dehumidified chamber until imaging. Samples were imaged at ~20,000-30,000x on a JEOL JSM-6390 SEM with an Everhart-Thornley secondary electron detector using an EHT target of 2 kV and a 20 µm aperture.

2.6.3. Cryo-electron microscopy of EVs

For cryo-EM imaging of isolated EVs, 4 µl of EVs resuspended in PBS were applied to either a freshly glow-discharged Quantifoil R2/2 200 mesh copper grid (Agar Scientific) or a graphene oxide lacey carbon 300 mesh copper grid (EM Resolutions), then blotted (with either 1.5s or 3s blot time and a force/offset of -10) and vitrified in liquid ethane using an FEI Mark IV Vitrobot operated at 100% humidity and at 21 C. The grids were stored in liquid nitrogen before being loaded into a Gatan cryo-holder and imaged under low dose conditions on an FEI Talos 200 kV cryo-TEM using an FEI Ceta camera.

2.7. Western blotting and Sypro Ruby staining

L. mexicana whole cell lysates (WCLs) were prepared by washing PRO or DIF cells once in PBS then adding Laemmli buffer to a final concentration of 1x. EV sample lysates were prepared by resuspending isolated EV pellets in PBS with 1x protease inhibitors (*Section 2.7*), then Laemmli buffer was added to a final concentration of 2x. The lysates were then heated for either 10 min at 60°C (for GT2::eGFP:TY detection) or 3 min at 100°C (for all other proteins). 4×10^6 cell equivalents of WCLs or 2×10^9 cell equivalents of EV sample were loaded and subjected to electrophoresis on 10% SDS-polyacrylamide gels and transferred to nitrocellulose membranes (GE Healthcare). Macrophage WCLs were prepared as described below (*Section 2.10*) and 2.4×10^4 (Figure 5.15) or 7.5×10^4 (Figure 5.14) cell equivalents of each sample was loaded. The

membranes were incubated in blocking buffer for 1 h then probed for 1 h with primary antibody in dilution buffer, washed in Tris-buffered saline with 0.05% (w/v) Tween 20 (TBST), incubated for 1 h with secondary horseradish peroxidase (HRP)-conjugated antibody in dilution buffer, washed in TBST and visualized by addition of the ECL chemiluminescent detection system (PerkinElmer) and exposure to autoradiography film (Carestream). Details of primary and secondary antibodies and blocking conditions are shown in Table 2.2.

For Sypro Ruby staining, the same steps for Western blotting described above were carried out up to and including gel electrophoresis, then the gel was washed with ddH_20 and incubated in 40 ml Sypro Ruby protein stain (Thermo Fisher) overnight on a rocker at room temperature with a foil cover. The Sypro Ruby was then removed and two 1 h incubations in de-staining solution containing 10% methanol and 7% acetic acid were performed before washing with ddH_20 and visualising the protein banding patterns by trans-illumination with UV light (~300 nm wavelength).

Table 2.2. Antibody details. Details of primary (**A**) and secondary (**B**) antibodies used for Western blots, immuno-gold and immunofluorescence.

A)

Target protein/glycoconjugate, target species	**Expected band size (kDa)**	**Antibodies used (name, species, dilution, supplier/reference)**	**Blocking/dilution buffer**
BiP, *T. brucei*	71.5	Anti-BiP, rabbit polyclonal, 1:1000, (Bangs *et al*., 1993)	TBS, 5% non-fat dry milk
PFR1, *T. brucei*	69	L13D6, mouse monoclonal, 1:20, (Kohl, Sherwin and Gull, 1999)	TBS, 0.05% Tween 20, 1% non-fat dry milk
Alpha tubulin, *T. brucei* (also detects human protein)	49.7	TAT1, mouse monoclonal, 1:500, (Woods *et al*., JCS 1989)	TBS, 0.05% Tween 20, 1% non-fat dry milk
GT2::eGFP:TY	88	Anti-GFP, mouse monoclonal, 1:500, Roche / 10521400	TBS, 5% non-fat dry milk
SMP-1::mCh	43	Anti-RFP, rat monoclonal, 1:1000, ChromoTek / 5F8	TBS, 5% non-fat dry milk
Histone H3, *T. brucei*	15	Anti-histone H3, rabbit polyclonal, 1:500, (Gluenz and Gull, unpublished)	TBS, 5% non-fat dry milk
Phosphoglycan repeats in LPG, PPGs and SAPs, *Leishmania*	~25-60 (LPG)	LT22, mouse monoclonal, 1:1000 for WB, 1:500 for IF, 1:50 for immuno-gold, (Ilg et al., 1993); a gift from Stephen Beverley	TBS, 0.05% Tween 20, 5% non-fat dry milk
STAT3, human	95	AF4607-SP, rabbit polyclonal, 1:740, R&D	TBS, 0.1% Tween 20, 5% BSA
STAT1, human	94	AF2894-SP, rabbit polyclonal, 1:2000, R&D	TBS, 0.1% Tween 20, 5% BSA
STAT4, human	81	5267S, rabbit polyclonal, 1:1000, Cell Signaling Technology	TBS, 0.1% Tween 20, 5% BSA
Erk1/2, human	42/44	AF1018-SP, rabbit polyclonal, 1:10,000, R&D	TBS, 0.1% Tween 20, 5% BSA
p38, human	43	9211S, rabbit polyclonal, 1:1000, Cell Signaling Technology	TBS, 0.1% Tween 20, 5% BSA

B)

Species specificity	Species of origin	Antibodies used (name, conjugation, dilution, supplier/reference)
Mouse	Rabbit	A9044, HRP, 1:20,000, Sigma-Aldrich
Rat	Rabbit	Star11B, HRP, 1:1000 (Bio-Rad)
Rabbit	Goat	P0448, HRP, 1:5000, Dako
Mouse	Goat	F0257, FITC, 1:250, Sigma
Mouse	Goat	5 nm gold, 1:40, Abcam

2.8. Protein mass spectrometry

The protein concentration of EV samples in PBS was measured using a Bradford assay adjusted for small sample volumes: 10 µl of bovine serum albumin (BSA) standard, 1:2 diluted EV sample in PBs, or PBS as a blank was added to UVette cuvettes (Eppendorf). 200 µl of Bradford reagent diluted 1:5 in ddH_2O was added to each sample and mixed before measuring the absorbance at 590 nm on a spectrophotometer. Protein concentrations were interpolated from the standard curve using GraphPad Prism 7 software. To prepare for MS, EV samples in 2x Laemmli buffer and 1x protease inhibitors (50 µM leupeptin hemisulphate (Sigma), 7.5 µM pepstatin A (Sigma), 500 µM phenylmethylsulfonyl fluoride (Roche), 5 µM (2S,3S)-trans-Epoxysuccinyl-L-leucylamido-3-methylbutane ethyl ester (E-64d) (Biomol)) were electrophoresed 1 cm into a 10% gradient SDS-PAGE gel (Bio-Rad). The entire sample was excised, in-gel tryptic digest was carried out and the samples were submitted to the Advanced

Proteomics Facility (http://www.proteomics.ox.ac.uk) for label-free MS using a Thermo QExactive Orbitrap LC/MS/MS machine (Thermo Fisher). The following parameters were used: carbamidomethylation of cysteine residues was set as a fixed modification; oxidation of methionine residues was set as a variable modification; the mass values were set as monoisotropic; the peptide mass tolerance was 20 ppm; the fragment mass tolerance was 0.1 Da and the maximum number of missed cleavages was 2. An MS/MS ion search of a recently re-annotated reference *L. mexicana* genome (Fiebig et al., 2015) was carried out using Mascot software.

Testing the effects of *L. mexicana* promastigotes and EVs on macrophages

2.9. Macrophage production and cell culture

Bone marrow cells were harvested by flushing the femora, humeri and tibiae of female C57BL/6 mice, followed by erythrocyte lysis and incubation of the harvested cells in vented flasks in high glucose DMEM with L-glutamine (Sigma) plus 10% FCS, 100 U/mL penicillin and 100 µg/mL streptomycin (Invitrogen) and 10 ng/ml recombinant human M-CSF (R&D) at 37°C and 5% CO_2 to induce macrophage differentiation. The macrophages were fully differentiated and ready to use after 6 days. A different batch of BMDMs, prepared in the same way by Theodoros Kapellos in David Greaves's lab at the Dunn School, was also used for a cytokine experiment (Figure 5.11).

Human induced pluripotent stem cells (iPSC)-derived macrophages were generated as previously published (van Wilgenburg et al., 2013) in collaboration with Sally Cowley at the James Martin Stem Cell Facility. Briefly, iPSCs from three different

healthy human donors were expanded for one week, formed into spherical embryoid bodies and differentiated along the haematopoietic lineage for four weeks. The embryoid bodies were then treated with 100 ng/ml M-CSF and 25 ng/ml IL-3 to induce the production of monocytes which were harvested weekly from the culture medium for up to 6 months by passing through a 40 µm cell strainer to exclude cell aggregates or embryoid bodies. The monocytes were then cultured in the experimental format of choice (usually 96-well plates, Costar) in RPMI medium (Sigma) plus 10% FCS, 1x GlutaMax, 100 U/mL penicillin and 100 µg/mL streptomycin (Invitrogen) and 100 ng/ml M-CSF for 7 days at 37°C and 5% CO_2 with medium changes every 3-4 days to induce differentiation to ready-to-use adherent macrophages.

2.10. Macrophage infection and EV treatment

For infection of macrophages for imaging, stationary phase promastigotes (*Section 2.1*) were resuspended in macrophage culture medium, added to the macrophages and incubated at 34°C and 5% CO_2. Where indicated, macrophages were washed by replacing the medium twice to remove extracellular parasites post-infection. Where specified, macrophages were stimulated by the addition of 100 U/ml IFNγ (R&D) and 100 ng/ml LPS (Sigma). For imaging of macrophage infection with the LPG-deficient *ΔLPG1* cell line, 10^5 macrophages per well of a glass-bottom 1.5 coverslip 48-well plate (MatTek) were incubated at 34°C for 24 h prior to infection to acclimatise the cells. For cytokine secretion analysis, 10 µl of EV samples, negative control or stationary phase promastigotes resuspended in sterile PBS were added per well containing 60,000 differentiated macrophages in 200 µl in a 96-well plate (Costar). Nothing was added to the medium only controls. After 18 h at 34°C the 96-well plate was

centrifuged for 5 min at 800 *g* to remove any extracellular parasites or floating macrophages from the supernatant, then the supernatants from each well were transferred to a new 96-well plate using a multichannel pipette and stored at -20°C until cytokine analysis.

The same experimental conditions used for cytokine analysis were used to treat macrophages for phosphoprotein WB analysis with one exception: a 24-well format with 2×10^5 macrophages per well was used. To collect macrophage WCLs the macrophages were washed once with PBS, 50 µl of ice-cold RIPA buffer (Sigma, R0278) containing phosphatase and protease inhibitors (Pierce, 88668) was added and the macrophages were scraped with a cell scraper, transferred to Eppendorf tubes on ice for 30 min, pipetted up and down twice with a 26G needle to shear genomic DNA, centrifuged at 12,000 rpm for 4 min, transferred to new Eppendorf tubes and stored at -80°C until use. The WCLs were prepared for SDS-PAGE electrophoresis by adding an equal volume of 2x Laemmli buffer and heating at 100°C for 5 min.

2.11. Macrophage cytokine analysis

For initial cytokine screening, 200 µl of human iPSC-derived macrophage supernatants were used to probe a membrane with 36 dots containing anti-cytokine antibodies using a Proteome Profiler Human Cytokine Array Kit (R&D). After membrane treatment similar to Western blotting (Figure 2.5) the amount of each cytokine was visualized by addition of a chemiluminescent detection system (provided by the manufacturer) and exposure to autoradiography film (Carestream). The amount of each cytokine present was measured in a semi-quantitative way by measuring the

integrated pixel density (IntDen, the product of the area and mean grey value) of equal-sized areas surrounding each cytokine dot using ImageJ software.

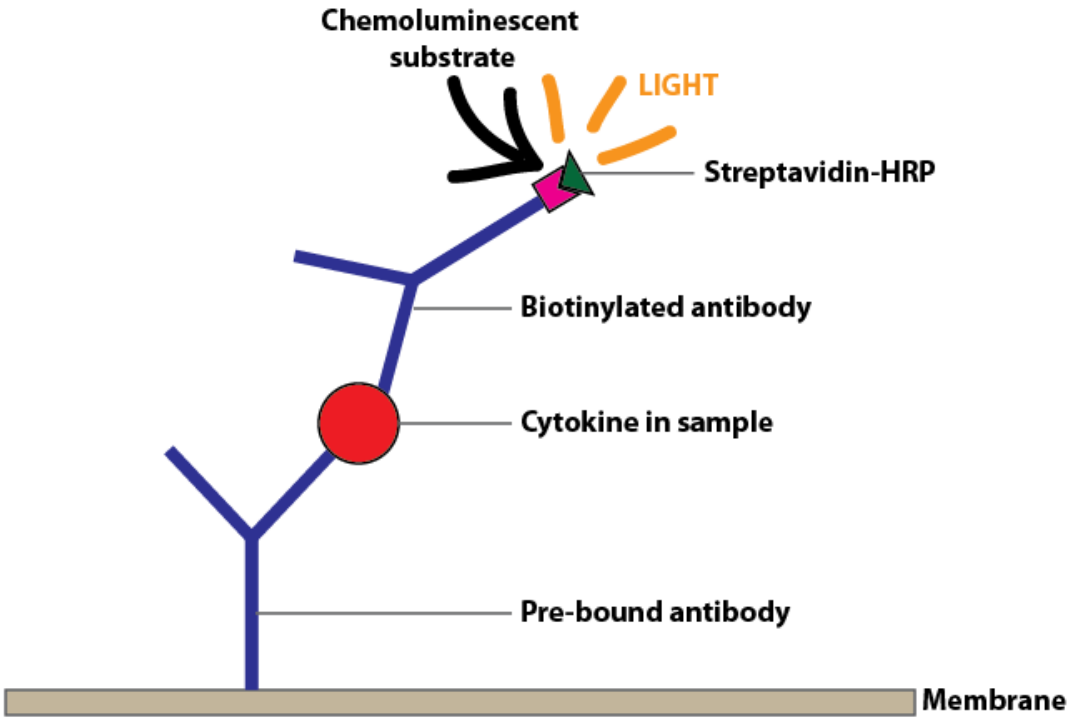

Figure 2.5. Proteome Profiler cytokine analysis. Pre-bound antibodies in spots on the membrane bind specifically to cytokines in the macrophage sample supernatant before the excess supernatant is washed away. Biotinylated antibodies then bind the same cytokine before excess antibody is washed away. Finally, streptavidin-HRP is added and binds the biotin on the secondary antibodies. When a chemiluminescent substrate is added light is produced which can be detected using autoradiography film.

For further cytokine analysis, 75 µl of each macrophage sample supernatant was used for multiplexed quantitative ELISA to measure the absolute concentrations of multiple cytokines at once using either human or murine Premixed Magnetic Luminex Screening Assays (R&D) (Figure 2.6). The cytokine concentrations were measured

using a Bio-Plex analyser (Bio-Rad). All statistical tests were carried out using GraphPad Prism 7 software.

A)

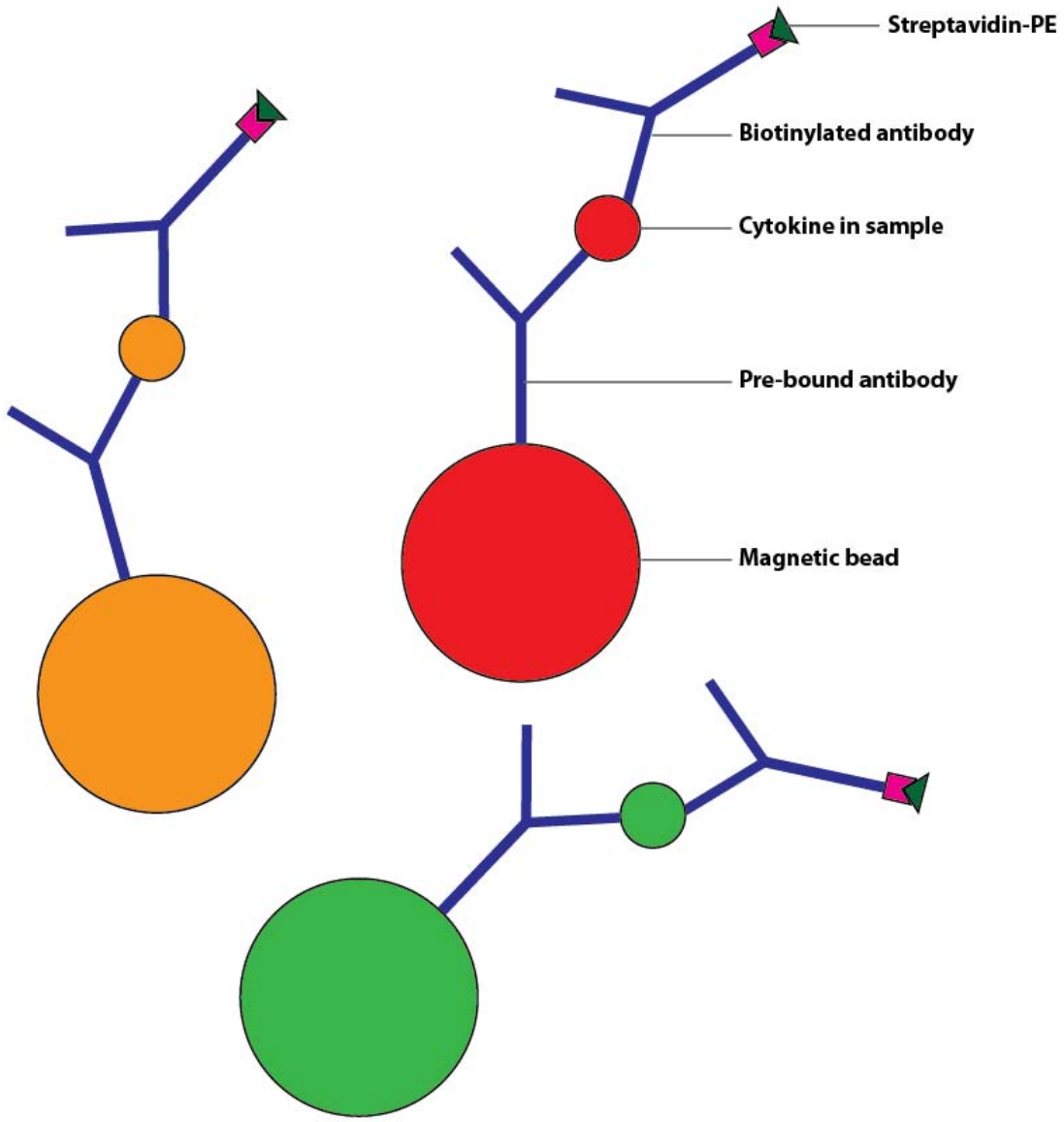

B)

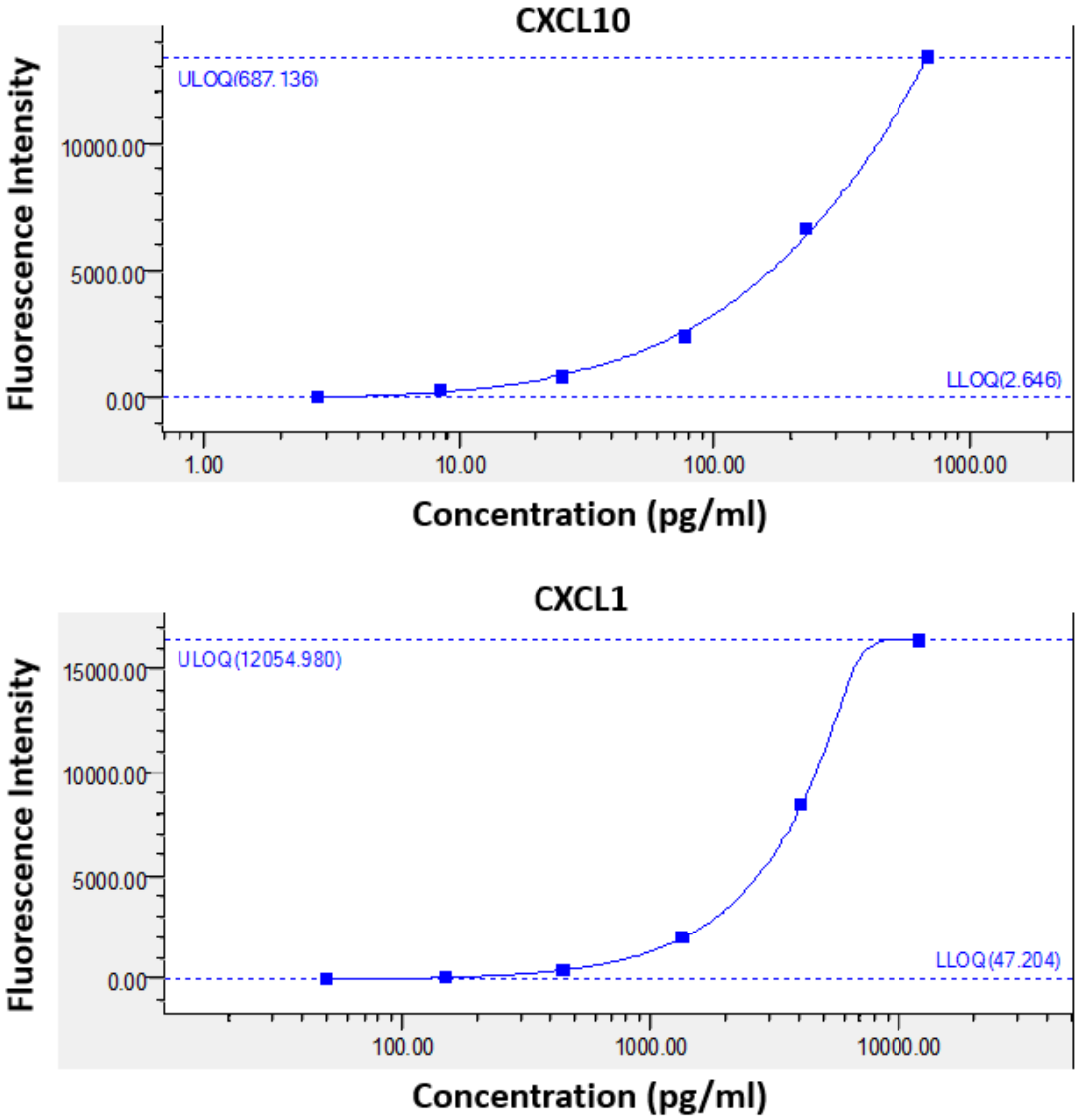

Figure 2.6. Luminex cytokine analysis. A) Cytokines specific to a particular antibody are pre-bound to magnetic beads which are colour-coded according to their cytokine specificity. The antibodies bind to cytokines in the macrophage sample supernatant before the excess supernatant is washed away. Biotinylated antibodies then bind the same cytokine before excess antibody is washed away. Finally, streptavidin-PE (phycoerythrin) is added and binds the biotin on the secondary antibodies. The beads are then illuminated in a monolayer in a

Bio-Plex analyser; one light emitting diode (LED) detects which cytokine is being measured by identifying the bead colour, another LED measured the amount of PE which is associated with that bead, which is directly proportional to the amount of cytokine bound to that bead. Standard beads with known amounts of pre-bound cytokines are used to calibrate the measurements to allow quantification of cytokine concentration in the samples. **B)** Typical examples of calibration curves used to interpolate cytokine concentrations from the Fluorescence Intensity (FI).

2.12. Blue^{TM} NFκB/AP-1 reporter cell line culture and assays

RAW-Blue cells (InvivoGen, a gift from the Quentin Sattentau lab) are derived from RAW 264.7 murine macrophages. The cells express secreted embryonic alkaline phosphatase (SEAP) on a chromosomally integrated plasmid which is under the transcriptional control of the transcription factors NFκB and AP-1, and can be used to quantify the activity of these transcription factors (Figure 2.7). The cells were cultured in vented flasks at 37°C and 5% CO_2 in high glucose DMEM (Sigma), 1x GlutaMax, 10% FCS and 200 µg/ml Zeocin (InvivoGen) to maintain selection pressure for the retention of the SEAP construct and were sub-cultured using a cell scraper every 2-3 days. For transcription factor assays, 20 µl of *L. mexicana* EV samples or stationary phase promastigotes resuspended in sterile PBS were added to the bottom of wells of a 96-well plate (Costar) prior to the addition of 180 µl of RAW-Blue cells suspended in culture medium at 100,000 cells per well. Sterile PBS was used as a negative control and 100 ng/ml LPS (Sigma) as a positive control. After 18 h at 37°C, unless otherwise specified, the plate was centrifuged for 5 min at 800 *g* to remove extracellular

parasites or floating macrophages from the supernatant, then 50 µl of supernatant was added to 150 µl of pre-warmed QuantiBlue reagent (InvivoGen) and incubated at 37°C for between 30 min and 24 h to allow blue colouration to develop, then absorbance at 630 nm was measured using a Spectramax M5 and SoftMax Pro version 5 software.

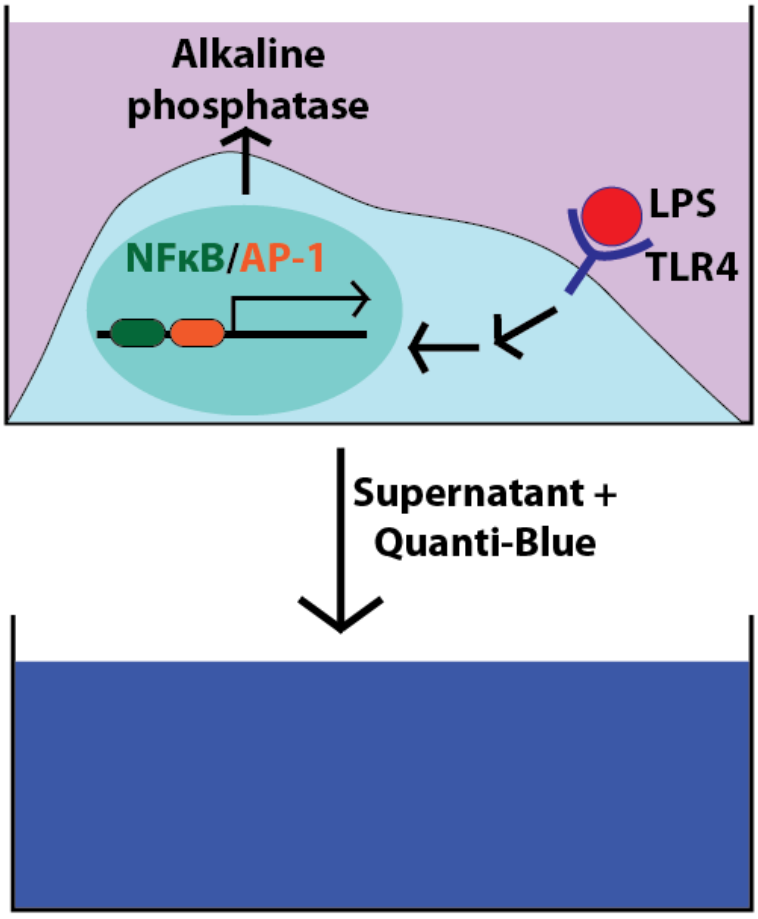

Figure 2.7. Quantification of NFκB and AP-1 activity using RAW-Blue cells. RAW-Blue cells express all TLRs (except TLR5) and several other PRRs including NOD1, NOD2 and RIG-1. When a PRR such as TLR4 is bound by its cognate agonist, i.e. LPS, a signalling cascade occurs leading to the activation of transcription factors which may include NFκB and/or AP-1. Once activated, NFκB and/or AP-1 bind to promoters upstream of the SEAP gene and initiate transcription. SEAP protein is then secreted into the culture medium and when QuantiBlue reagent is added

to the supernatant the alkaline phosphatase activity of SEAP turns the reagent from pink to blue. The intensity of the blue colouration is directly proportional to the amount of alkaline phosphatase present and therefore the level of NFκB and/or AP-1 activity.

---

3. Subcellular origin and structure of *L. mexicana* EVs

3.1. Introduction

3.1.1. Flagella as secretory organelles involved in sending cellular messages

An emerging field of research has shown that, in addition to their motility and sensory functions, eukaryotic flagella have a secretory role. Initial evidence for this came from studies of the green algae *C. reinhardtii:* flagellar-derived EVs deliver subtilase-like serine proteases required for cell wall breakdown, allowing hatching of daughter cells following cell division (Wood et al., 2013). *C. reinhardtii* is a valuable model organism to study flagellar EVs since their cell body is encased in a cell wall leaving only the flagellar membrane (FM) exposed. It is therefore assumed that only flagellar-derived EVs are isolated from *C. reinhardtii*-conditioned medium; supporting this, EVs are not found in conditioned medium from flagella-less mutants (Wood and Rosenbaum, 2015). Flagellar-derived EVs modulate mating behaviour in *C. elegans* (Wang et al., 2014) and photoreceptor cilia renewal in mammals (Young, 1971). Outside *C. reinhardtii* research, studying a sub-population of flagellar EVs in a heterogeneous pool of exosomes and microvesicles from various surface membranes is challenging. Isolating flagellar-derived EVs to study protein composition, for example, would likely require immunoprecipitation. This requires specific markers for flagellar-derived EVs and that epitopes are presented on the outer face of the membrane. This is especially challenging for the study of non-mammalian organisms, including *Leishmania* spp.

with >40% of their genes unannotated (based on TriTrypDB data) and only a small number (<10) of known FM proteins (Landfear et al., 2015).

3.1.2. Evidence for flagellar EV release

FM budding has been observed by transmission electron microscopy (EM) of *L. donovani* flagella (Silverman et al., 2010a) and by scanning EM of mammalian inner medullar collecting duct (IMCD3) kidney cells (Nager et al., 2016). While these EM studies give insight into the detailed structure of FM elaborations, they cannot give us information about dynamics: do the blebs originate from the FM to which they are adjoined, and if so will they undergo scission and be released; are they in the process of fusing to rather than budding from the flagellum? Live time-lapse imaging and imaging of tagged proteins with specific subcellular localisations can help address this. The most convincing demonstration that EVs are released directly from FMs was carried out in IMCD3 cells; time-lapse imaging of the fluorescently labelled ciliary membrane-localised G-protein coupled receptor (GPCR) somatostatin receptor 3 (SSTR3) clearly showed rounding and scission of the ciliary tip, leaving behind a shorter cilium (Nager et al., 2016). DIC time-lapse imaging showed EV release from the flagellar tip of *C. reinhardtii* (Wood et al., 2013), and in *T. brucei* appeared to show the scission of FM nanotubes followed by vesicularisation (Szempruch et al., 2016b). However, whether the *T. brucei* nanotubes were truly flagellar-derived was unclear due to low image resolution and lack of a specific FM marker. The importance of the flagellum in *T. brucei* EV release is supported by the fact that flagellar surface proteins are 4-fold enriched in the *T. brucei* EV proteome compared to the whole cell proteome (Szempruch et al., 2016b).

3.1.9. Flagellar EV cargo sorting and biogenesis

The mechanisms of microvesicle release from the flagellum are poorly understood. Ciliary EV release from murine IMCD3 cells was shown using inhibitors to be dependent on actin, myosin 6 and drebrin (Nager et al., 2016), providing the first evidence that ciliary EVs may be generated using the same actin-dependent mechanisms described for general microvesicle release (Muralidharan-Chari et al., 2009). Another study provided mechanistic insight into flagellar EV cargo selection and release; proteomic comparison of *C. reinhardtii* flagellar EVs versus FMs showed enrichment of a subset of proteins, including ESCRT-related proteins, ubiquitinated proteins and glycoproteins, in the EV fraction, suggesting selective cargo loading rather than non-specific membrane shedding (Long et al., 2016). The authors propose a model whereby ubiquitinated proteins are selected by ESCRT-related chaperones and packaged into membrane buds which are released from the FM in an ESCRT machinery-dependent manner. Both actin polymerisation (Romer et al., 2010) and ESCRT machinery (reviewed in (Schoneberg et al., 2017)) are well known to mediate membrane scission, a process required for EV biogenesis. It is unclear whether these proposed ESCRT- and actin- dependent mechanisms could function together.

3.1.10. The link between EV release and flagellar shortening

A concept has emerged very recently in *C. reinhardtii* research, proposing that release of flagellar EVs contributes to flagellar length regulation. In some cases, including *C. reinhardtii* (Rasi et al., 2009), mammalian cells with primary cilia (Pan and Snell, 2007) and *Leishmania* spp. (Wheeler et al., 2015), flagellar shortening occurs during the life cycle. Our understanding of axonemal disassembly has made significant progress in recent years (reviewed in (Pan and Snell, 2007, Ran et al., 2015)): in summary, Aurora

kinase activates deacetylase HDAC6 which deacetylates alpha-tubulin and cortactin leading to axonemal disassembly and FP actin polymerisation, driving ciliary resorption. A recent study on mammalian RPE-1 cells showed that actin polymerisation at the ciliary pocket leading to increased clathrin-mediated endocytosis initiates ciliary disassembly (Saito et al., 2017). However, the authors argue that this clathrin-mediated endocytosis is not a mechanism for FM removal since it appears to be required only at the early stages of ciliary shortening (i.e. in the first hour; ciliary resorption in RPE-1 cells takes place biphasically, in the 1-2 h and 18-24 h following serum re-addition (Pugacheva et al., 2007)), rather it helps initiate a signalling cascade to trigger ciliary shortening. Therefore, how excess FM is removed during flagellar shortening remains an open question (reviewed in (Hsu et al., 2017)).

Steady-state *C. reinhardtii* flagella shed EV quantities equivalent to an entire FM every 6 hours (Dentler, 2013). Maintaining a steady-state flagellum appears to rely on the balance between Golgi-derived vesicle fusion to surface membranes and EV release from the flagellum. This model is supported by the fact that inhibiting the delivery of Golgi-derived vesicles with Brefeldin A leads to flagellar disassembly, presumably through continued release of flagellar EVs (Dentler, 2013). During flagellar disassembly induced by sodium pyrophosphate, which chelates calcium ions creating a low calcium environment conducive to flagellar shortening (Lefebvre et al., 1978, Quader et al., 1978), the shedding of EVs increases three-fold (Dentler, 2013). Increased EV release during flagellar shortening was reported in another study of *C. reinhardtii* (Long et al., 2016). FM release was tracked during flagellar shortening by measuring the fluorescence intensity in the medium of cells stained with a lipid dye;

the majority of shed membrane appeared to be flagellar-derived since a control flagella-less intraflagellar transport *(ift)-88* mutant showed drastically reduced fluorescence intensity. Flagellar protein release was also tracked by isolating EVs from the medium of cells with a luciferase-tagged EV-enriched protein, PDCD6, and measuring luciferase activity (Long et al., 2016). These data both support increased flagellar EV release during shortening. Knockdown of either of the ESCRT-related proteins PDCD6 and Vps4 leads to reduced EV release during flagellar shortening and reduced rate of shortening (Long et al., 2016).

Together, these data from *C. reinhardtii* (Long et al., 2016, Dentler, 2013) and mammalian kidney cell studies (Nager et al., 2016) show that flagellar EV release is temporally linked to flagellar shortening. The emerging hypothesis is that flagellar EV release drives FM loss and shortening. Both flagellar EV release and shortening are inhibited upon knockdown or inhibition of certain proteins (Long et al., 2016, Nager et al., 2016), suggesting that the two processes are mechanistically linked and do not occur passively. However, the current data cannot rule out that flagellar EV release is a consequence rather than a cause of flagellar shortening. The relationship between axonemal disassembly and FM loss in terms of signalling (is one process triggered first which then drives the other or could a common pathway such as ubiquitination govern both?) remains to be elucidated. Finally, whether flagellar EV release is the primary mechanism of FM loss during shortening and how widespread it is among eukaryotes remains to be discovered.

3.1.11. Known regulators of *Leishmania* flagellar length control

While the exact mechanisms contributing to flagellar shortening in *Leishmania* are unknown, several proteins have been proposed as regulators of flagellar length.

Mitogen-activated protein kinase 3 (MPK3) (Erdmann et al., 2006) and mitogen-activated protein kinase kinase (MKK) (Wiese et al., 2003) KO *L. mexicana* cells have shorter flagella than WT cells, with the average length of KO flagella being ~2 µm compared to ~12 µm in WT cells. In line with their highly similar phenotypes, MPK3 and MKK are thought to belong to the same signalling pathway, since MKK has been shown to phosphorylate MPK3 (Erdmann et al., 2006). Protein kinase 4 (PK4), like MKK and MPK3, is a MAPKK homolog (Kuhn and Wiese, 2005) which is specifically expressed in the promastigote stage and may therefore also play a role in flagellar length control, although this is yet to be tested. Overexpression of Arl3A in *L. donovani* also induced shorter flagella, and interestingly these cells secreted lower levels of SAP, suggesting a role for Arl3A in trafficking (Cuvillier et al., 2000). Overexpression of the katanin-like protein Kat60b in *L. major* (Casanova et al., 2009) also led to cells with shorter flagella and in line with a role in flagellar regulation, Kat60b was found to localise to the flagellum. Katanins are microtubule severing proteins; Kat60b may promote flagellar shortening via severing of axonemal microtubules. Kinesin-13 knockdown in *L. major* induced longer flagella; this kinesin localises to the flagellum and is thought to depolymerise axonemal microtubules from the tip, providing a possible mechanism for flagellar length regulation (Blaineau et al., 2007). Manipulation of these proteins could provide valuable insight into the relationship between flagellar shortening, FM nanotubes and EV release.

3.1.12. Aims

In previous experiments performed by Richard Wheeler (unpublished observations), it was noticed that flagella of *L. mexicana* undergoing flagellar shortening during differentiation appeared to shed membrane. FM nanotubes, similar to those

described in *T. brucei* (Szempruch et al., 2016b), have also been observed on *L. mexicana* promastigotes. The aims here are (i) to quantify these observations and determine whether differentiating cells release more membrane than promastigotes and (ii) to isolate these membrane vesicles from cell culture supernatants and characterise their subcellular origin and structure. In addition, (iii) we aim to generate KO cell lines in the search for essential proteins involved in EV biogenesis; these cells will be screened for their ability to generate FM nanotubes and to undergo flagellar shortening. These cell lines will be used to investigate putative links between FM nanotube formation, flagellar EV release and flagellar shortening.

3.2. Results

3.2.1. FM nanotube formation increases during promastigote to amastigote differentiation

Evidence for FM shedding by light microscopy

We aimed to characterise the formation and dynamics of *L. mexicana* FM elaborations during differentiation. For the purposes of this study, FM elaborations were classified as blebs (spherical bud-like formations, Figure 3.1A, B) or nanotubes (thin streamer-like projections, Figure 3.1C, D). Flagellar shortening during axenic promastigote to amastigote differentiation is fully complete after 16 h, with the majority of cells having an amastigote-like flagellum after 8 h (Wheeler et al., 2015). The formation of FM elaborations was quantified using fluorescence microscopy at 0, 4, 8 and 32 h post-induction of axenic differentiation (Figure 3.2A, B). The proportion of flagella with no FM elaborations fell significantly from a mean of 74 to 48% between 0 and 4 h time points then rose again slightly to 55% by 32 h (Figure 3.2B). These data were highly reproducible. The level of FM elaborations at the flagellar tip rose throughout differentiation while the level of lateral FM elaborations rose between the 0 and 4 h time points then fell to 0.7% by 32 h, reflecting the fact that by this time point only the tip is exposed (Figure 3.2B) (Wheeler et al., 2015).

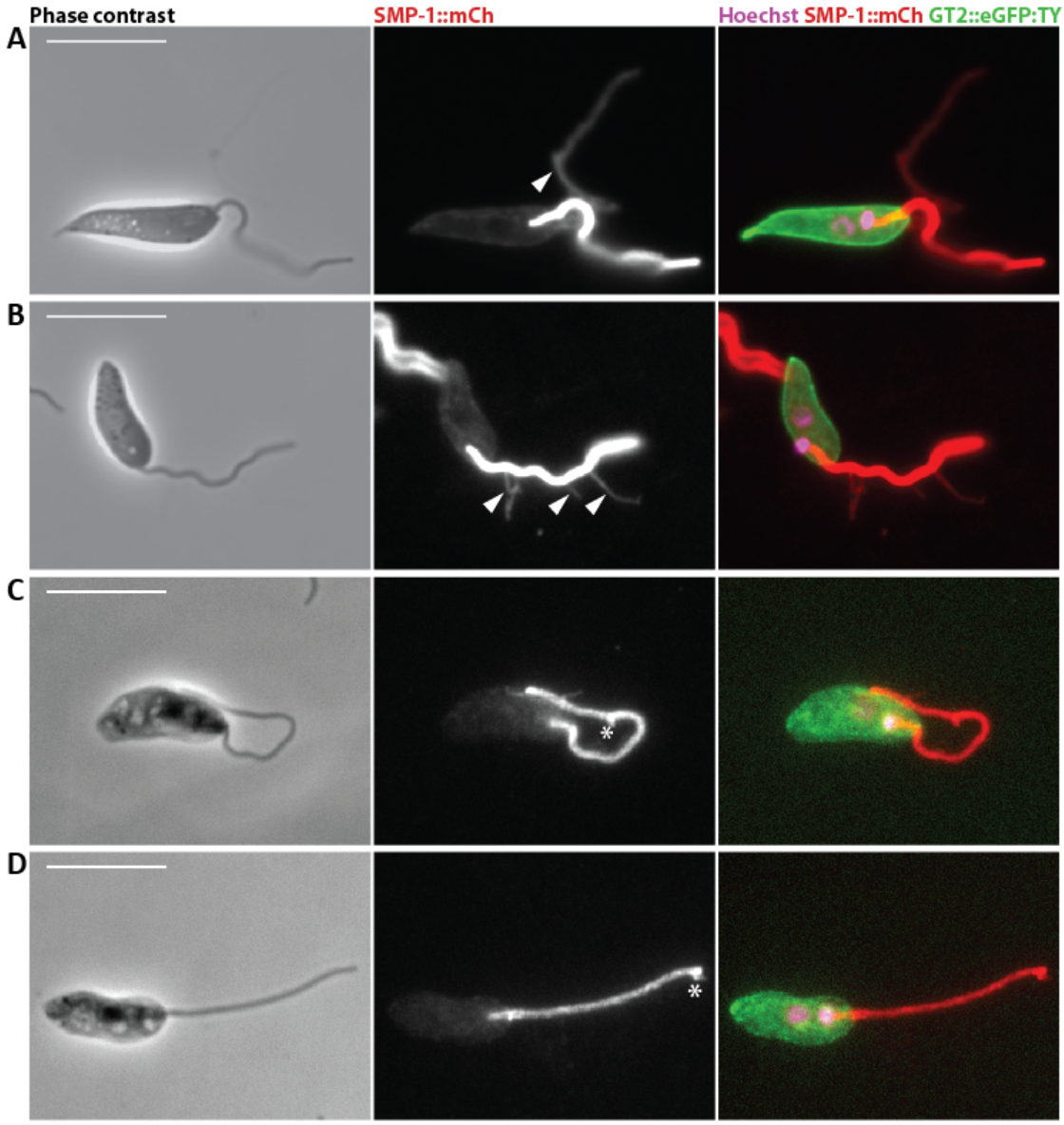

Figure 3.1. Examples of FM nanotubes and blebs. Example images of *L. mexicana* Clone 3 promastigotes displaying FM blebs (asterisks) or nanotubes (arrowheads). In the Clone 3 cell line, endogenous alleles of small myristoylated protein (SMP)-1, an FM marker, and glucose transporter (GT)-2, a cell body membrane marker, are tagged with mCh and eGFP genes respectively. Scale bars 10 μm.

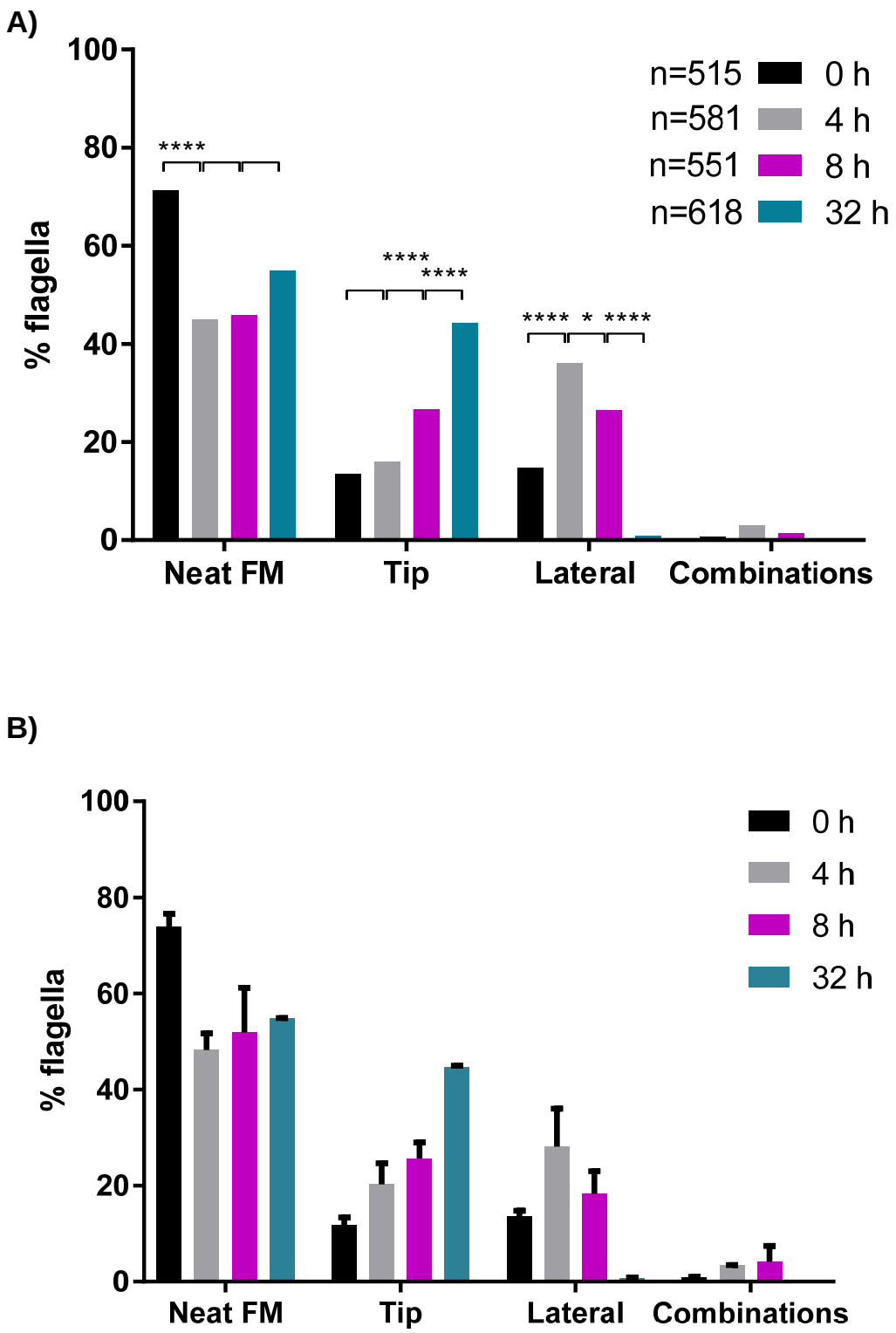

Figure 3.2. FM nanotube formation increases during promastigote to amastigote differentiation. **A)** Log phase *L. mexicana* Clone 3 promastigotes were incubated in SM5.5, pH 5.5 at 34°C, to induce axenic differentiation and samples were collected, washed and observed by

fluorescence microscopy on Polysine™ slides at 0, 4, 8 and 32 h. More than 500 cells were counted for each sample and each in focus flagellum was categorised as having either a neat FM or blebbing either laterally, from the tip or both (combinations). Asterisks show significant differences between time-points using a Fisher's exact test with p values as follows: * p≤0.05; ** p≤ 0.01; *** p≤0.001; **** p≤0.0001. This dataset is representative of three biological repeats. **B)** Combined data of three repeats of the experiment shown in Fig. 3.2A. The error bars show the mean ± SEM. Values are percentages of the total flagella (in focus) counted.

Evidence for FM shedding by scanning EM

Scanning EM was used to examine FM nanotubes and blebs in more detail. The levels of FM elaborations seemed higher on DIF (Figure 3.3B) compared to PRO (Figure 3.3A) flagella (not quantified). FM blebs were present on the majority of flagella while FM nanotubes (Figure 3.3Ba, f, h) were more difficult to find. The diameter of FM blebs ranged from ~50-500 nm while FM nanotubes were ~50 nm across, consistent with the size range of EVs being ~40-1000 nm across (Raposo and Stoorvogel, 2013). In some cases, elaborate clusters of FM blebs along 1 µm or more of FM were observed (Figure 3.3Bd, e, j, k).

A) PRO

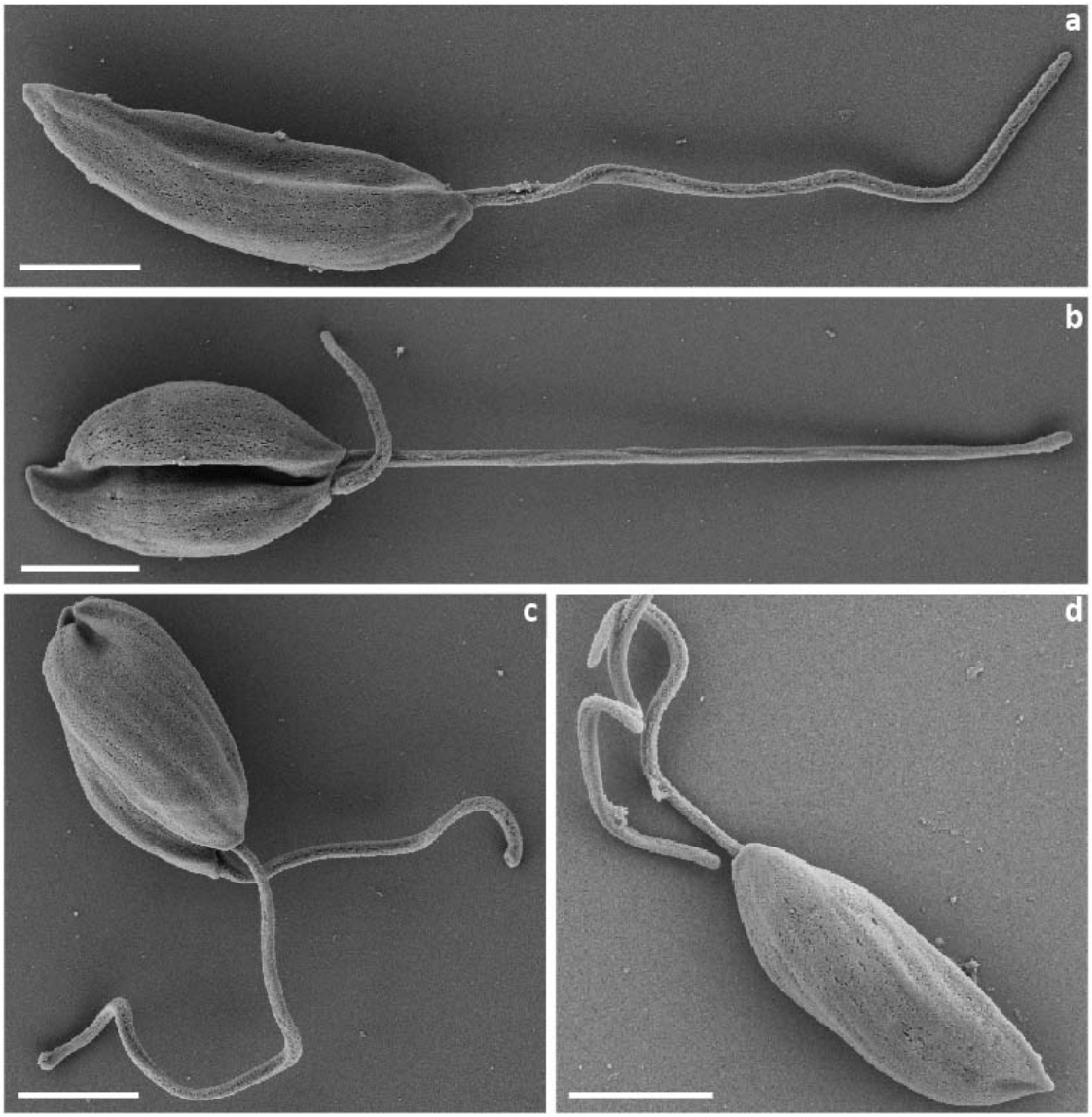

B) DIF

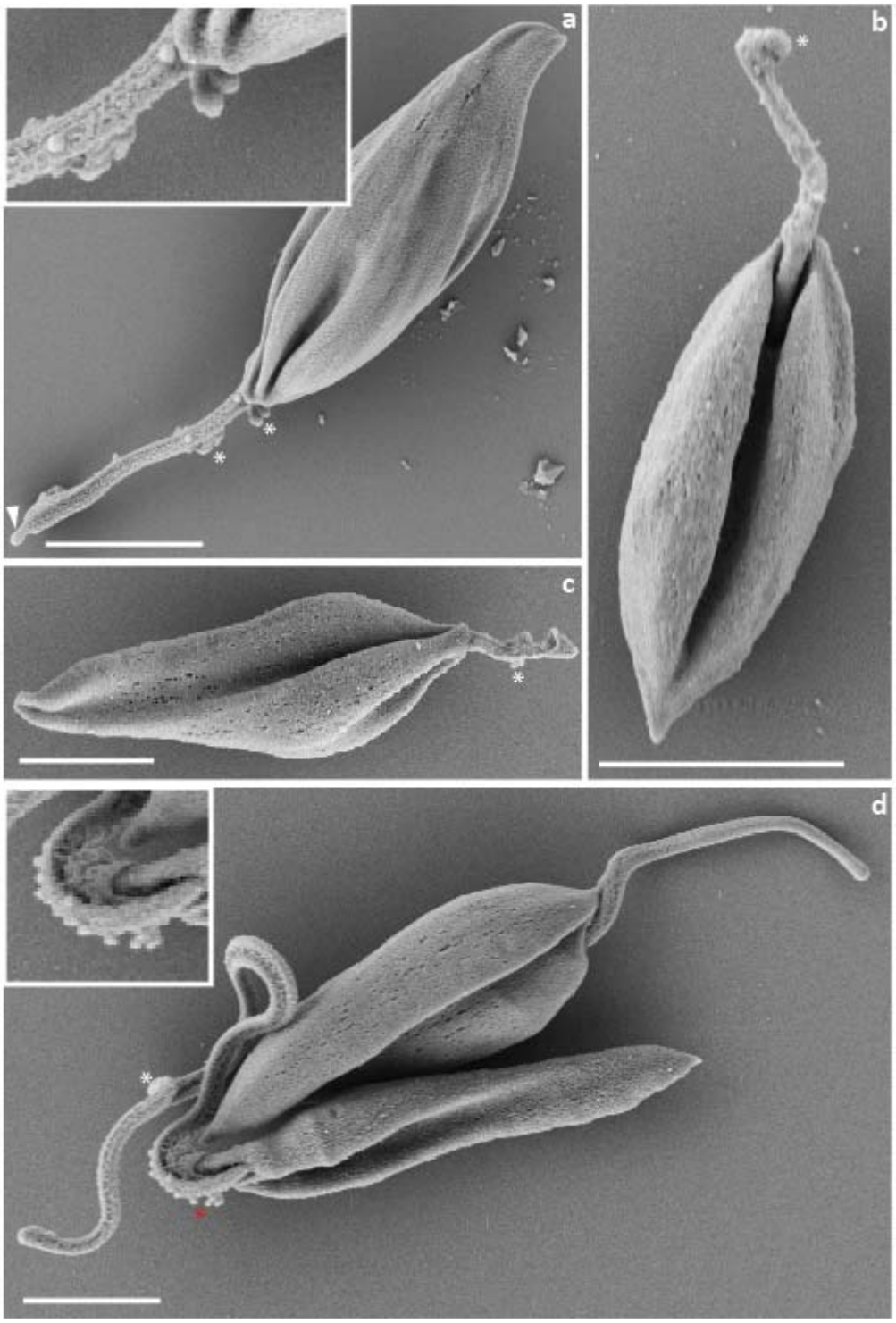

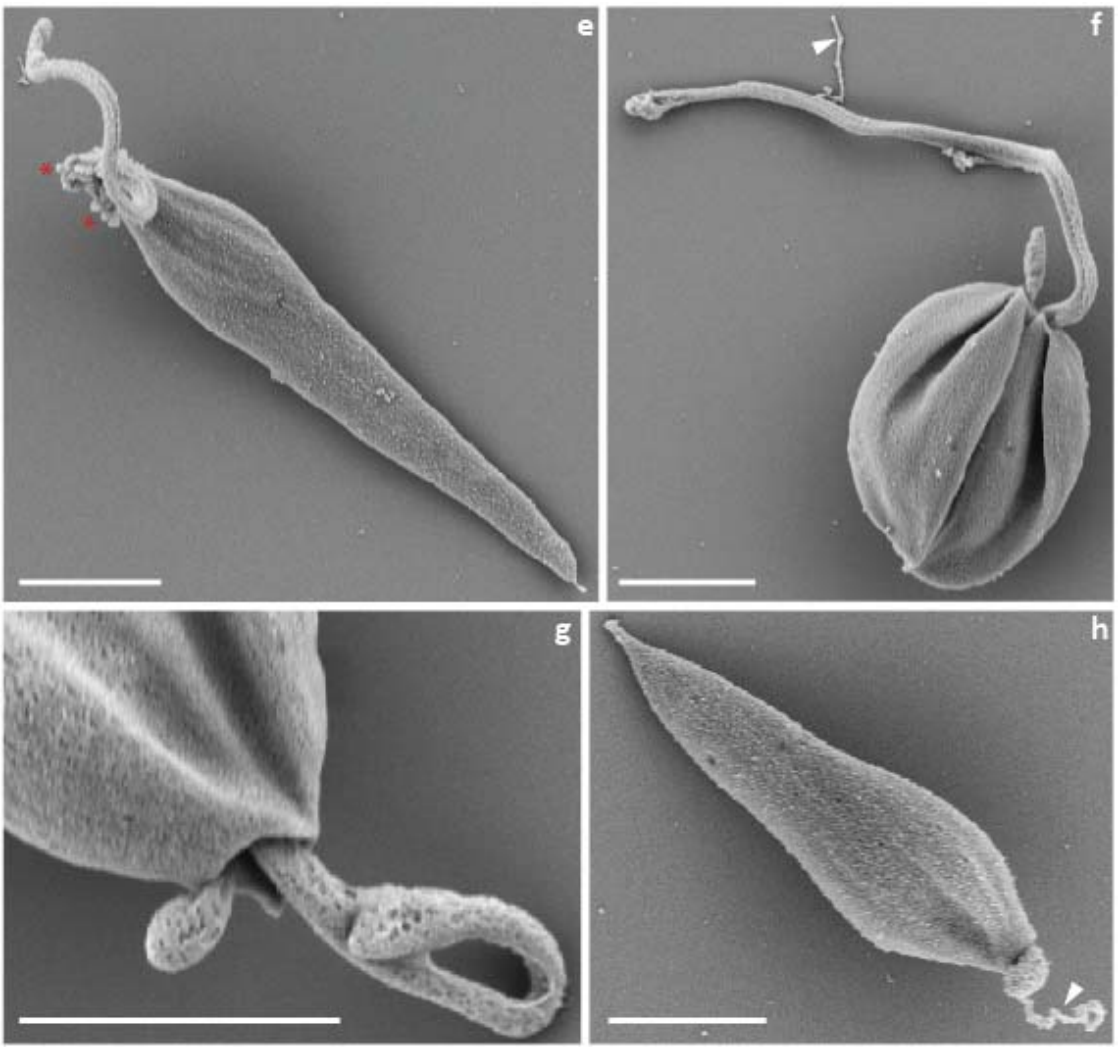
e
f
g
h


i
j
k
l

C) Temperature shock

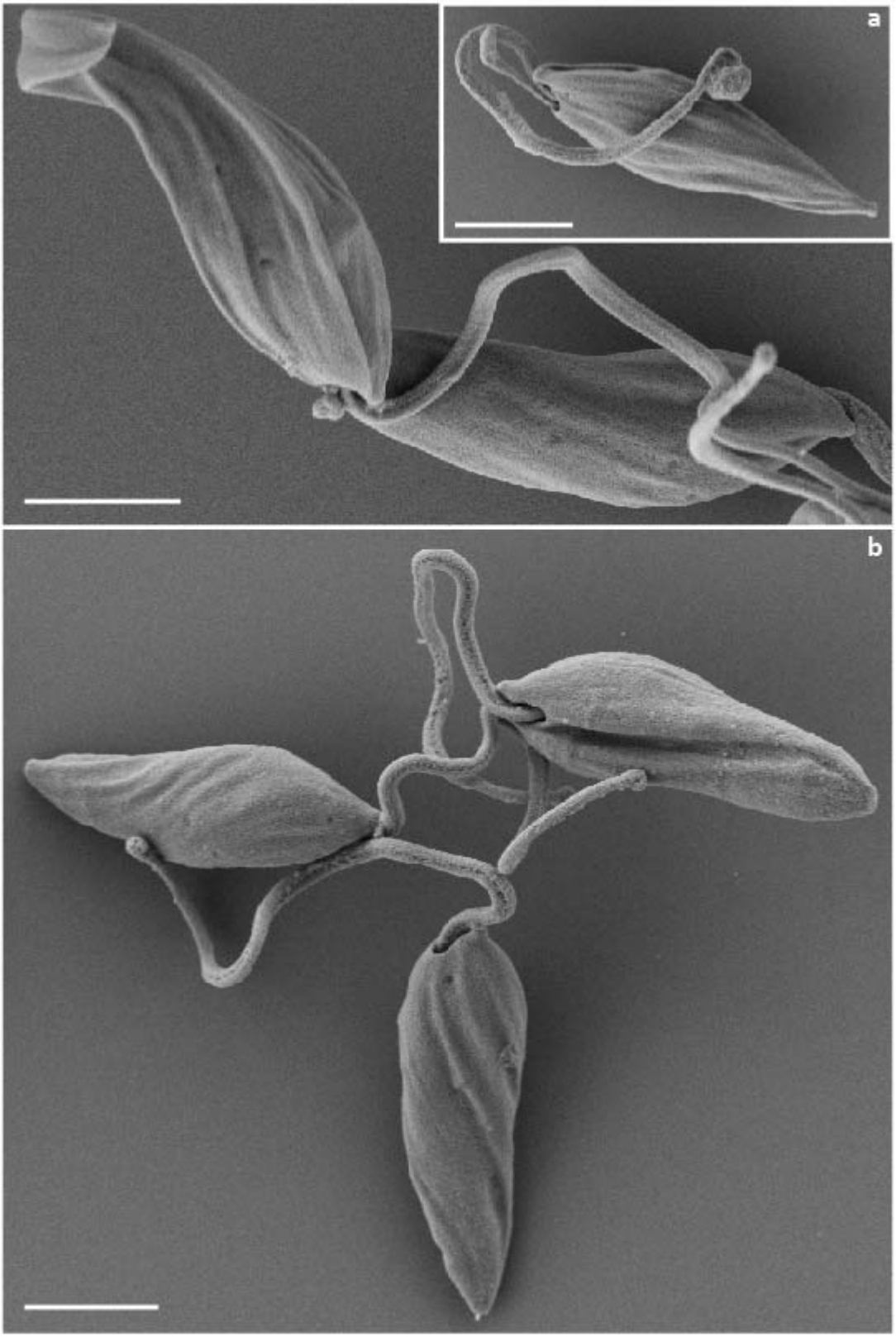

Figure 3.3. Scanning EM of PRO, DIF and temperature-shocked *Leishmania* cells. Log phase *L. mexicana* Clone 3 promastigotes were seeded into three parallel cultures in FCS-free medium for 4 h: **A)** PRO cells in M199 at 28°C **B)** DIF cells in SM5.5 at 34°C **C)** temperature-shocked cells in M199 at 37°C. The cells were fixed in 2.5% glutaraldehyde, prepared on glass slides and sputter coated with gold before imaging on the scanning EM. The DIF images are representative of two independent experiments. White asterisks: blebs; red asterisks: bleb clusters; white arrowheads: nanotubes. All scale bars 2 µm.

Formation of FM elaborations under different conditions: protein synthesis

We investigated the formation of FM elaborations under different conditions.

We wondered whether *de novo* protein synthesis was required for FM elaborations. While there was a 6% increase in the proportion of flagella with no FM elaborations after a 30 minute 100 µg/ml cycloheximide incubation, this difference was not significant (Figure 5A). However, a longer 4 h incubation of promastigotes with 10 or 100 µg/ml (100 µg/ml cycloheximide reported to inhibit 100% of protein synthesis in *L. infantum* (Cloutier et al., 2012, Kamau et al., 2001, Wilson et al., 1993)) of the protein synthesis inhibitor cycloheximide led to significant increases in the proportion of flagella with no FM elaborations from 43% in the no drug control to 66% and 65% respectively (Figure 5B). To see whether cycloheximide had any effect on differentiation itself, drug was added, or not as a control, at 0, 4 and 8 h during axenic promastigote to amastigote differentiation and the cells were imaged at 0, 4, 8 and 30 h to monitor their morphological differentiation. In summary, by comparing cells with drug added to control cells it is evident that cells did not differentiate morphologically any further after the addition of cycloheximide (Figure 3.5).

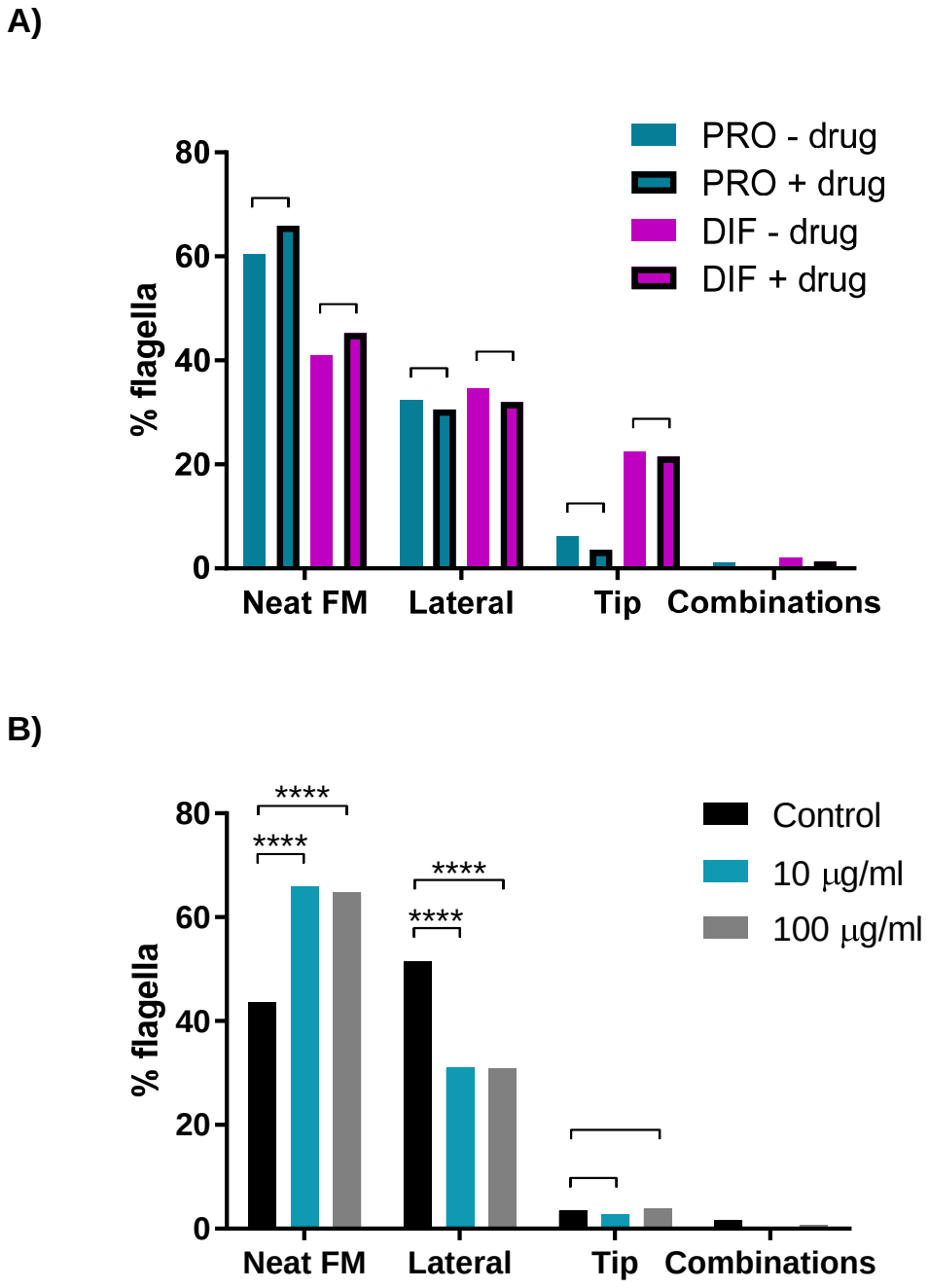

Figure 3.4. Prolonged protein synthesis inhibition reduces the level of FM nanotube formation. **A)** Graph shows effect of a 30 min cycloheximide incubation on FM nanotube formation. Log phase Clone 3 promastigotes were incubated either in M199 at 28°C (PRO) or in SM5.5, pH 5.5 at 34°C to induce axenic differentiation (DIF). The cells were incubated either with nothing (- drug) or with 100 μg/ml cycloheximide (+ drug). After 30 min samples were collected,

washed and observed by fluorescence microscopy on Polysine™ slides. Each in focus flagellum was categorised as having either a neat FM or blebbing either laterally, from the tip or both (combinations). **B)** Graph shows effect of a 4 h cycloheximide incubation on FM nanotube formation. Log phase *L. mexicana* Clone 3 promastigotes were incubated in M199 at 28°C either with nothing as a control, or with 10 or 100 µg/ml cycloheximide. After 4 h samples were collected and analysed as above. Asterisks show significant differences between time-points using a Fisher's exact test with p values as follows: * $p \leq 0.05$; ** $p \leq 0.01$; *** $p \leq 0.001$; **** $p \leq 0.0001$.

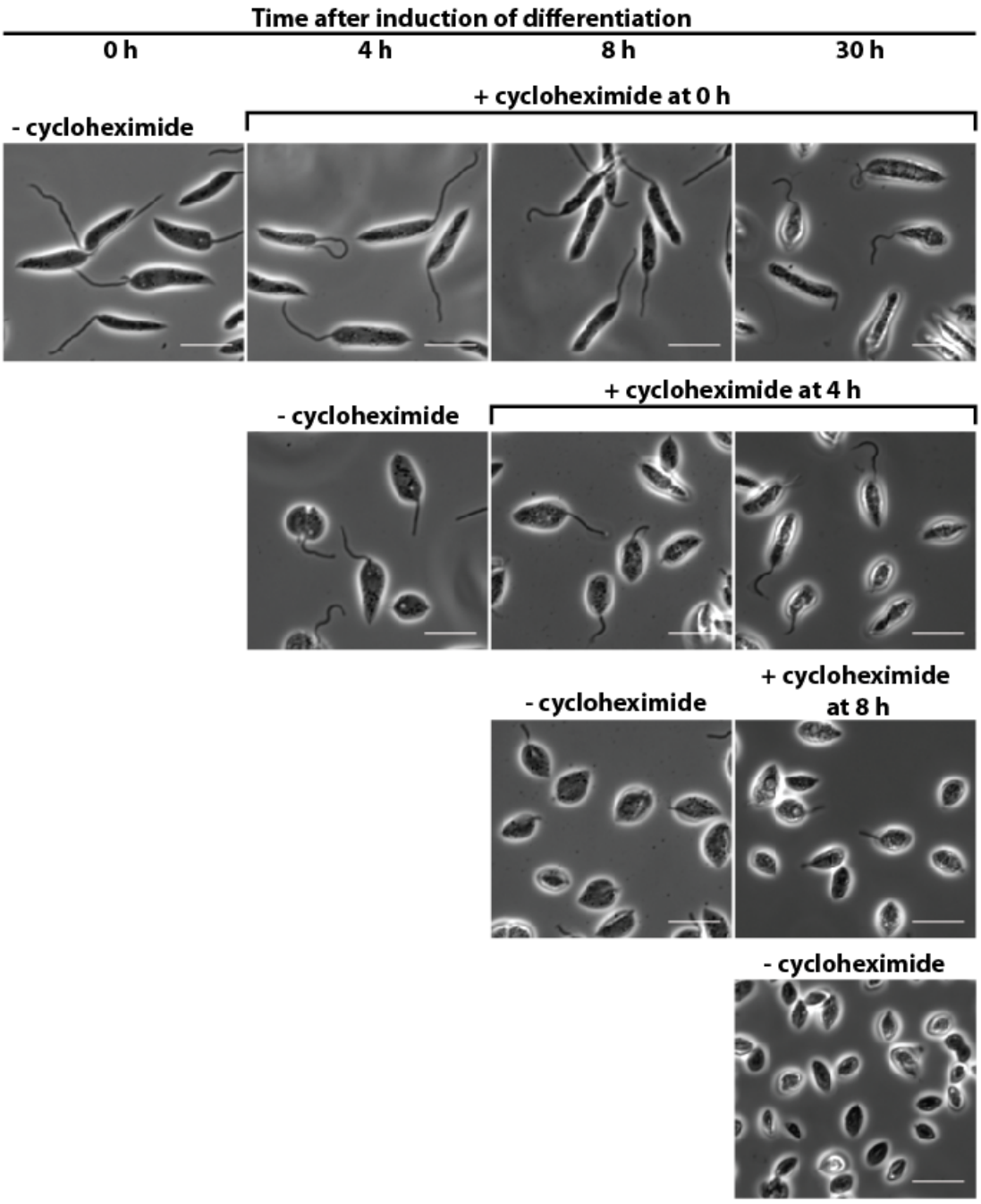

Figure 3.5. Protein synthesis inhibition stalls morphological axenic differentiation. Four cultures of log phase *L. mexicana* Clone 3 promastigotes were incubated in SM5.5, pH 5.5 at 34°C to induce axenic differentiation at the same time. A control culture with no added cycloheximide (- cycloheximide) was imaged by phase contrast microscopy at 0 h, 4 h, 8 h and 30 h. 100 ug/ml cycloheximide was added to the remaining cultures at either 0 h, 4 h or 8 h post-

induction of differentiation and the cells were imaged alongside the control cells at the subsequent time points. Scale bars 10 µm.

Formation of FM elaborations under different conditions: fixation

We addressed the possibility that FM elaborations could be an artefact of sample preparation for microscopy by comparing the level of FM elaborations in cells which were chemically fixed either before or after washing with PBS and settling onto microscopy slides. The proportion of flagella with no FM elaborations was 70% when fixed before and 79% when fixed after sample preparation (Figure 3.6) and this difference was significant. Therefore, cell washing and settling onto slides slightly decreases FM elaborations rather than causing them.

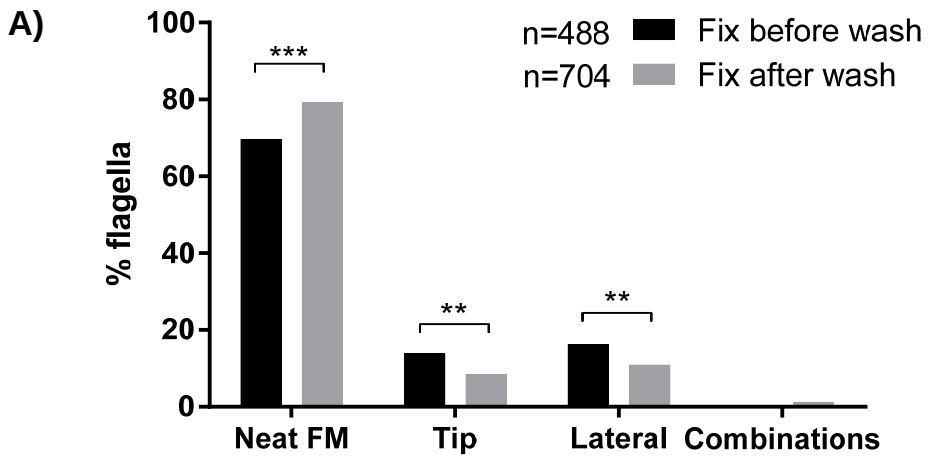

Figure 3.6. Effect of sample preparation for microscopy on FM nanotube formation. Log phase *L. mexicana* SMP1::eYFP promastigotes were collected and either fixed in 3% PF and then washed once with PBS before settling onto Polysine^{TM} slides, or the cells were washed twice with PBS and settled onto Polysine^{TM} slides first before being fixed in 2% PF. The cells were then observed by fluorescence microscopy. More than 400 cells were counted for each

sample and each in focus flagellum was categorised as having either a neat FM or blebbing either laterally, from the tip or both (combinations). Asterisks show significant differences between time-points using a Fisher's exact test with p values as follows: * p≤0.05; ** p≤ 0.01; *** p≤0.001; **** p≤0.0001.

Formation of FM elaborations under different conditions: macrophage infection

To explore further whether formation of FM elaborations was an artefact of *in vitro* culture, parasites were imaged live inside macrophages. FM elaborations were also visible within infected macrophages, both murine (Figure 3.7) and human (Figure 3.8) by imaging of flagella with a fluorescently tagged FM protein marker, SMP1. Figure 3.8 shows FM nanotubes and blebs formed 3-5 h post-infection and time-lapse imaging showed that in several cases parts of these structures appeared to undergo scission and floated away inside the macrophage (Figure 3.8A-D) on a timescale of minutes. In one case the distal 2-3 µm of a flagellum grew narrower before becoming classified as a nanotube after around 6 minutes (Figure 3.8E).

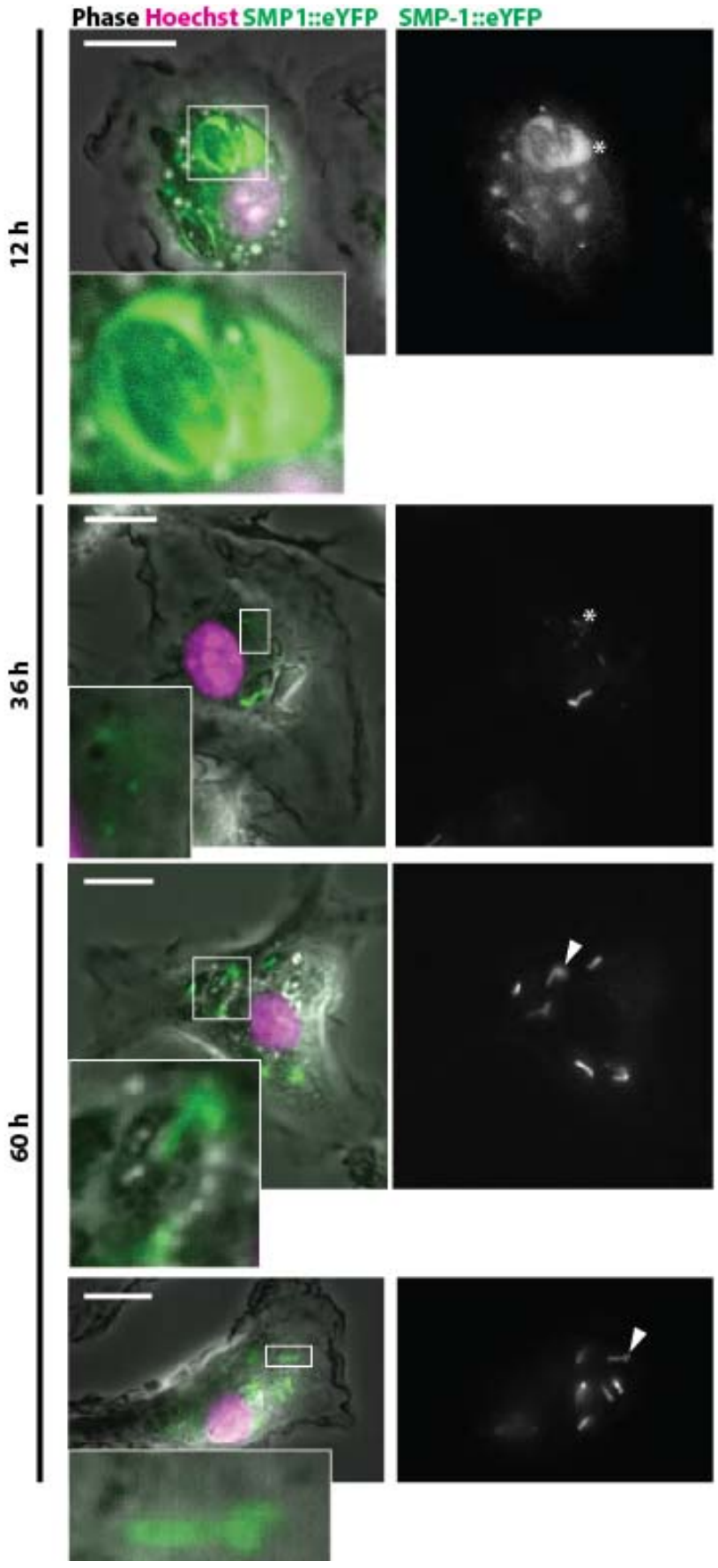
Phase Hoechst SMP1::eYFP
SMP-1::eYFP
12 h
36 h
60 h

Figure 3.7. FM nanotubes and SMP1::eYFP shedding in infected macrophages. Murine BMDMs were infected at an MOI of 5 with stationary phase *L. mexicana* SMP1::eYFP promastigotes. After 2 h the macrophages were washed to remove extracellular parasites and stained with the DNA dye Hoechst and imaged live by phase contrast (phase) and fluorescence microscopy at the indicated time points post-infection. Non parasite-associated eYFP-bright foci within macrophages are indicated with asterisks. FM nanotubes are indicated with arrowheads. Scale bars 10 μm.

A)

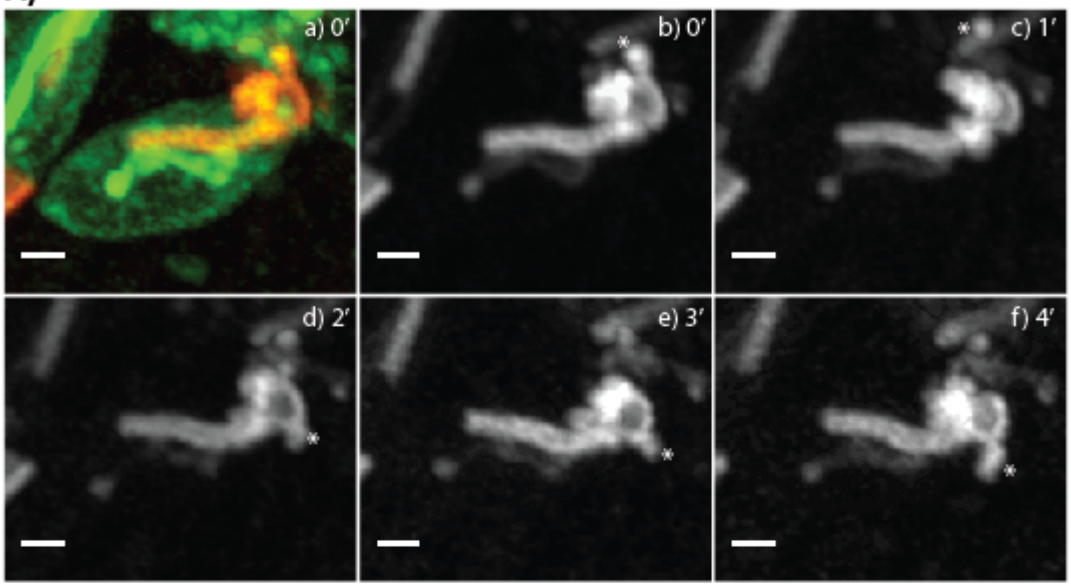

B)

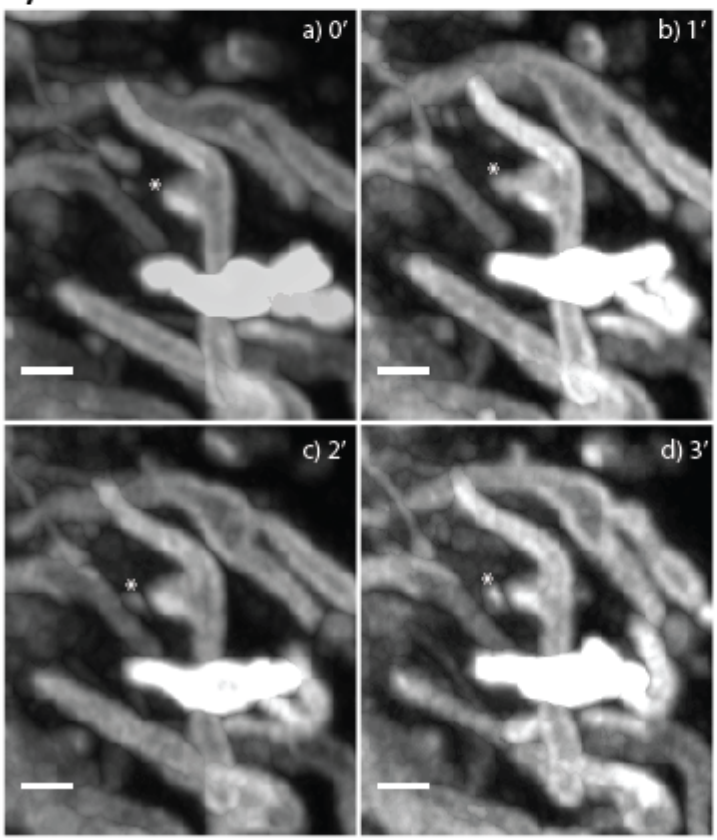

C)

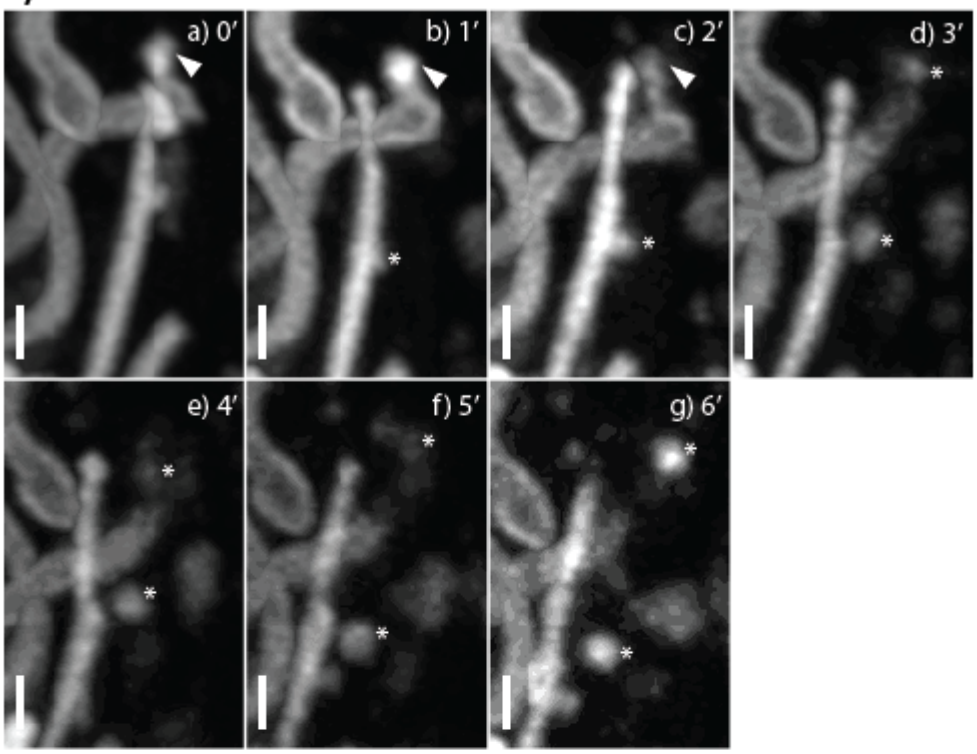

D)

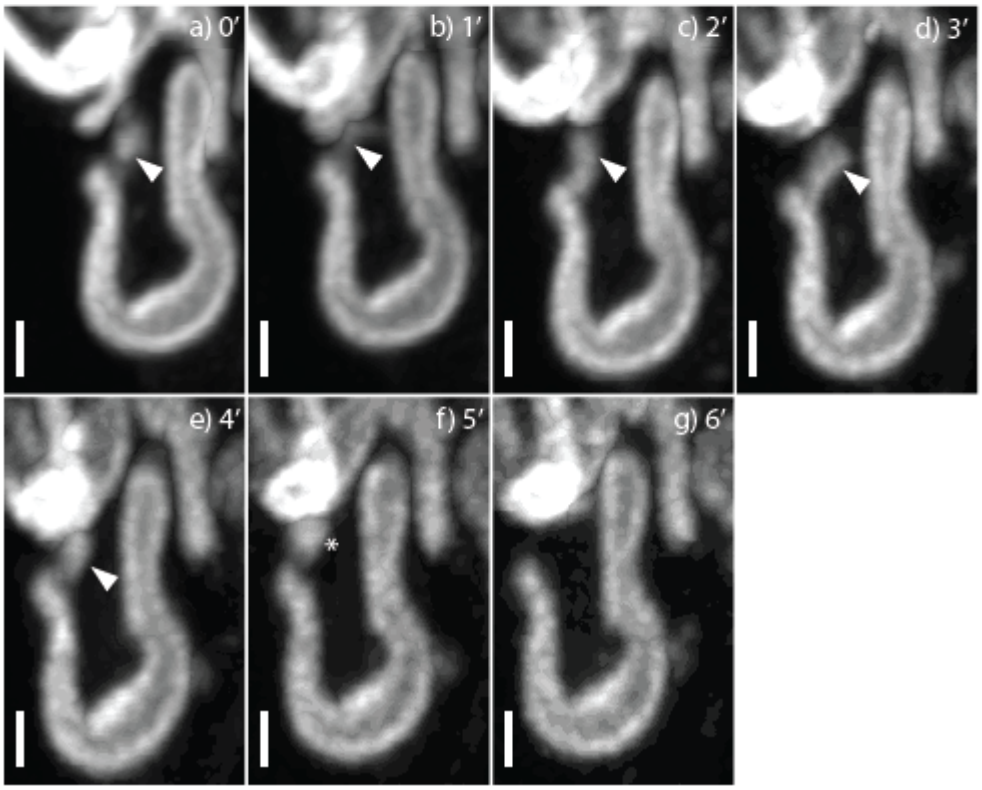

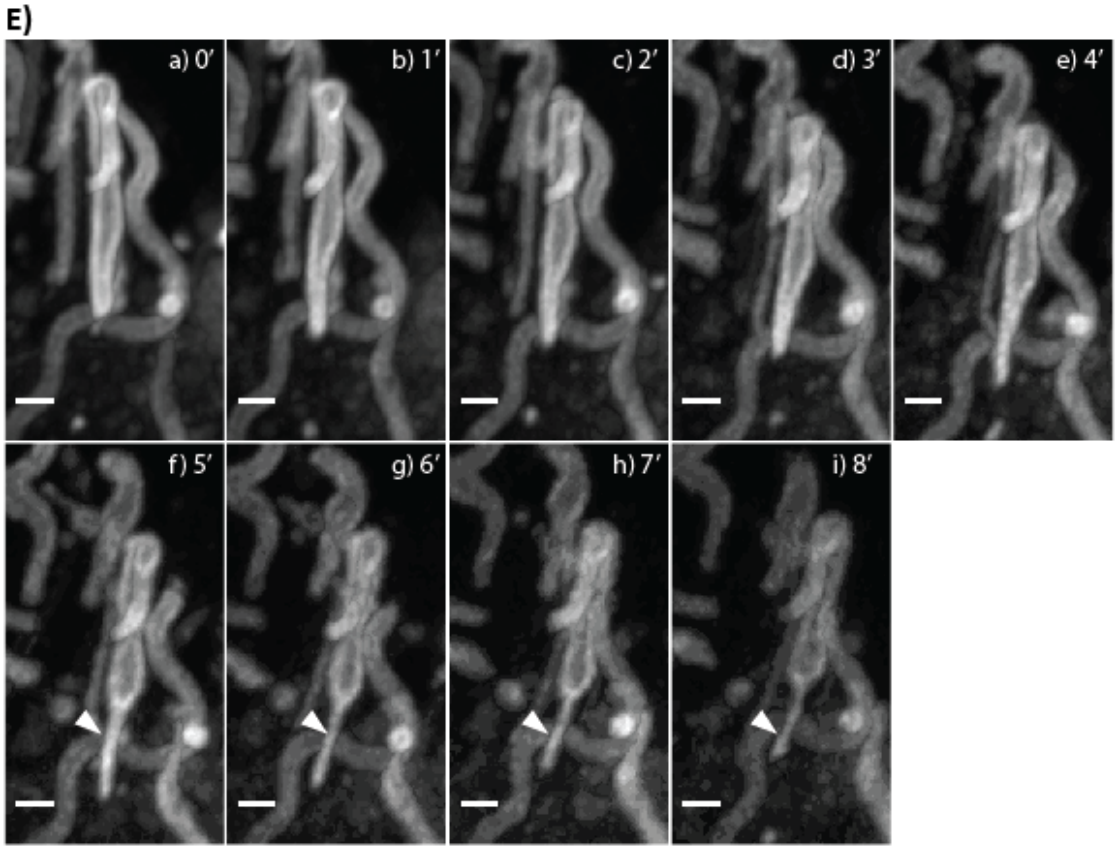

Figure 3.8. FM nanotube dynamics and shedding in infected macrophages. Human iPSC-derived macrophages were infected at an MOI of ~20 with stationary phase *L. mexicana* Clone 3 promastigotes. After 2 h the macrophages were washed to remove extracellular parasites and imaged live over time on an Airyscan microscope. **A-E)** Each figure shows a time-lapse series of the same field of view. Numbers 1′-8′ indicate the time since the start of imaging in minutes. Panel **a)** in **A)** shows the SMP1::mCh and GT2::eGFP channels merged. All other panels show the SMP1::mCh channel. FM blebs (asterisks) or nanotubes (arrowheads) are indicated. All fields of view shown were checked in the brightfield channel to ensure no extracellular parasites were visible. Scale bars 1 µm.

Formation of FM elaborations under different conditions: FCS-free culture

Since FCS-free conditions are necessary for EV isolation studies because FCS contains abundant EVs (Shelke et al., 2014), we investigated whether the absence of FCS led to changes in morphological differentiation or levels of FM elaborations. Cells in FCS-free medium were morphologically indistinguishable (not quantified) by microscopy from control cells at 4, 8, and 32 h post-induction of axenic promastigote to amastigote differentiation (Figure 3.9). The proportion of cells with no FM elaborations were not significantly different before and after a 4 h incubation of promastigotes in FCS-free medium, while DIF cells showed the expected significant increase in FM elaborations after 4 h of axenic promastigote to amastigote differentiation in FCS-free medium (Figure 3.10).

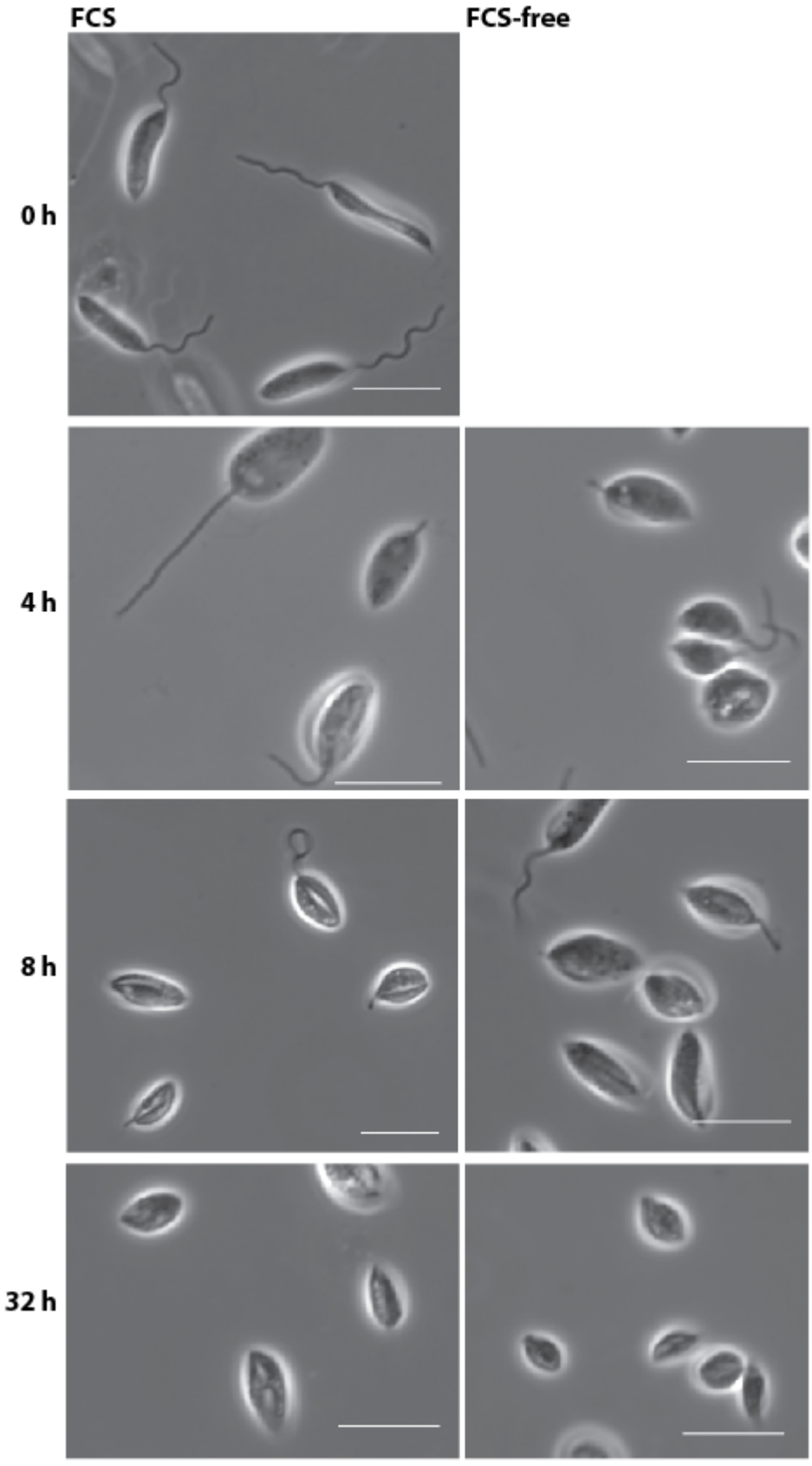
FCS
FCS-free
0 h
4 h
8 h
32 h

Figure 3.9. Absence of FCS has no effect on morphological axenic differentiation. Log phase *L. mexicana* Clone 3 promastigotes were incubated in SM5.5, with or without 10% FCS, at pH 5.5 and 34°C to induce axenic differentiation. Both cultures were imaged by phase contrast microscopy at 0 h, 4 h, 8 h and 32 h. Scale bars 10 µm.

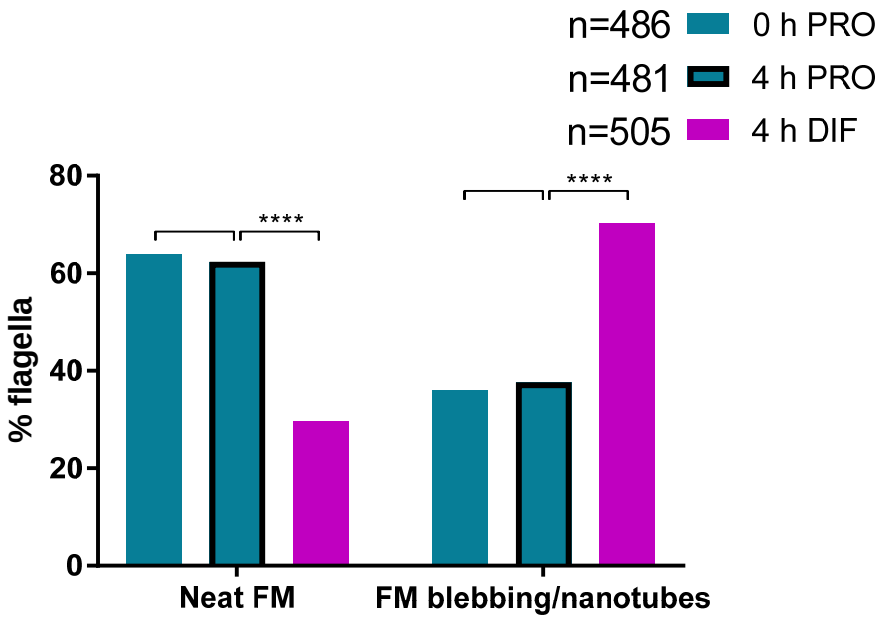

Figure 3.10. FCS has no significant effect on the level of FM nanotube formation. Log phase Clone 3 *L. mexicana* promastigotes in M199 with 10% FCS at 28°C (0 h PRO) were seeded without FCS into M199 at 28°C (4 h PRO) or SM5.5 at 34°C (4 h DIF) and incubated for 4 h. The samples were collected, washed, fixed in 2% PF and observed by fluorescence microscopy on Polysine™ slides. Each in focus flagellum was categorised as having either a neat FM or blebbing either laterally, from the tip or both (combinations). Asterisks show significant differences between time-points using a Fisher's exact test with p values as follows: * p≤0.05; ** p≤ 0.01; *** p≤0.001; **** p≤0.0001.

Formation of FM elaborations under different conditions: heat shock

Temperature-shocked parasites were also imaged by scanning EM since this treatment had been previously reported to induce excessive formation of surface membrane blebs (Hassani et al., 2011). However, while the surface membrane of temperature-shocked parasites had a more shrunken appearance (Figure 3.3C) consistent with the published data (Hassani et al., 2011), we did not observe more surface membrane blebbing compared to the PRO parasites (Figure 3.3A).

Formation of FM elaborations under different conditions: SMP1 tagging

Since cell lines with the FM protein SMP1 tagged with either mCh or eYFP were used for the majority of these studies, validation of the cell line and its use in FM dynamics studies were necessary. A growth curve of Clone 3 compared to WT cells showed that the tagged cell line grew slightly slower (Figure 3.11). In addition, the level of FM elaborations observed in the Clone 3 cell line were not significantly different to WT cells (Figure 3.12).

These data show that membrane is shed from the flagellum of *L. mexicana* promastigotes, axenic differentiating cells and cells differentiating inside macrophages. The amount of shed membrane appears to increase during differentiation. We next sought to investigate the biogenesis mechanisms behind the formation of FM elaborations.

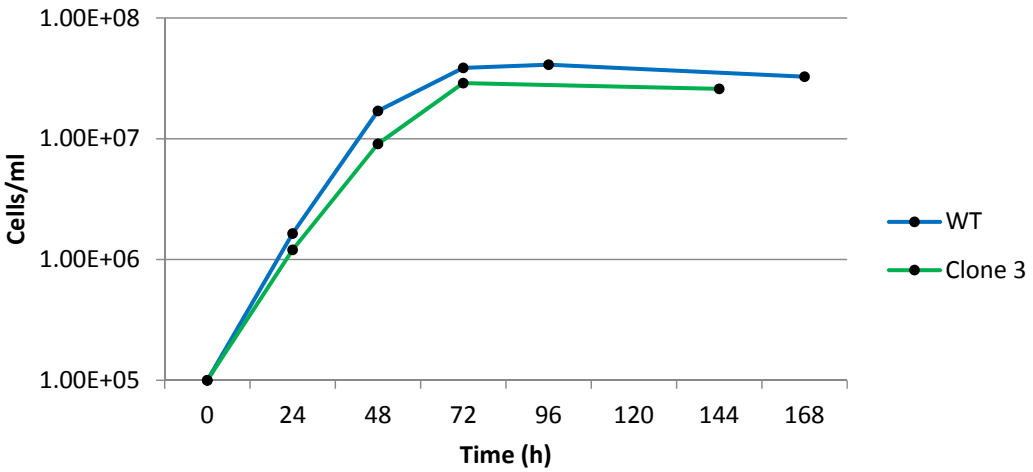

Figure 3.11. Growth curve of Clone 3 cell line. Log phase *L. mexicana* Clone 3 promastigotes were seeded at ~1.10^5 cell/ml at 0 h then their cell densities were measured. Cell densities were measured again at the indicated time points.

A)

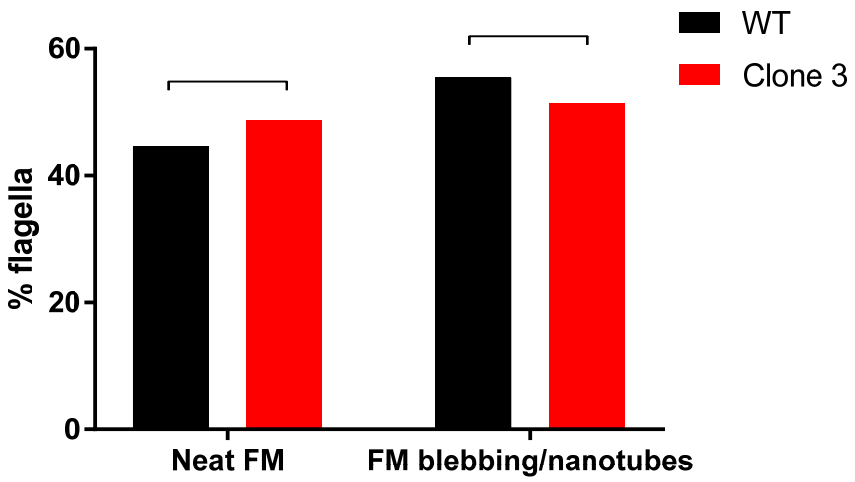

B)

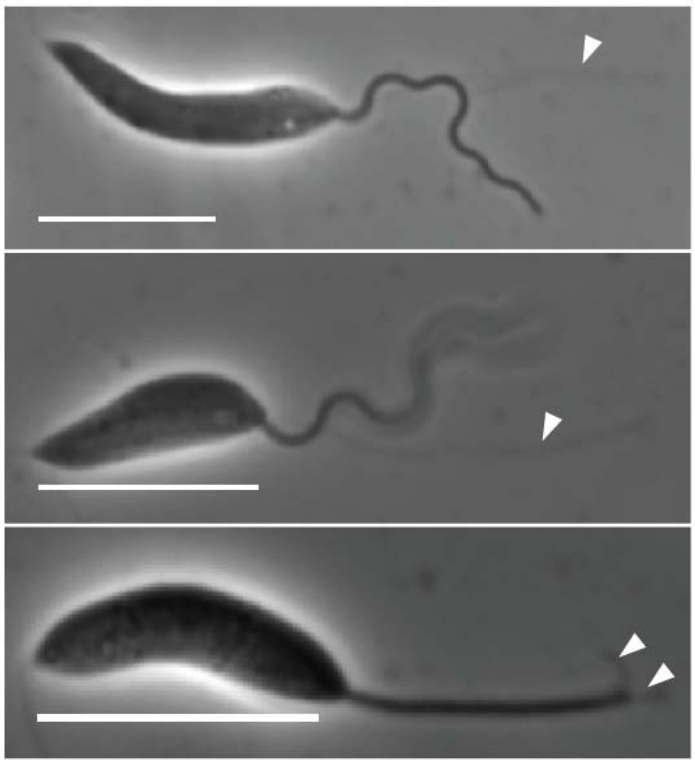

Figure 3.12. FM nanotubes form at the same rate in WT and Clone 3 cells. *L. mexicana* WT and Clone 3 promastigotes were collected from exponentially growing cultures of similar densities, washed and observed by phase contrast microscopy on Polysine™ slides. **A)** More than 200 cells were counted for each sample and each flagellum was categorised as having either a neat FM or FM blebbing/nanotube formation. Bars show non-significant differences between the cell lines with p values of more than 0.05 using a Fisher's exact test. This data is representative of two biological repeats. **B)** Representative phase contrast images of WT cells displaying FM nanotubes (arrowheads). Scale bars 10 μm.

3.2.2. Selection and KO of candidate EV biogenesis proteins

Proteins were selected based on the literature which may be involved in EV biogenesis. We aimed to see whether these proteins are essential for FM nanotube formation by targeting these proteins for KO (Table 2). The list included ESCRT proteins (putative Tsg101 homolog and Vps4) and accessory proteins (putative Alix homolog), and proteins of the exocyst complex (putative Sec8, Sec10 and Sec15 homologs). Our interest in the link between flagellar length and EV release also led us to select proteins for KO which are involved in flagellar length control based on *Leishmania* spp. literature (Table 2); if a mutant was generated which either produced no flagellum at all or a flagellum which did not undergo shortening during differentiation these would be useful control cell lines for studying flagellar EV release. For 10 out of the 17 genes, both alleles were successfully deleted using Crispr-Cas9 (Beneke et al., 2017), as demonstrated by PCR showing absence of ORF and correct integration of drug resistance genes for 10 out of the 12 cell lines which survived transfection (Figure 3.13). One PCR checking for correct blasticidin integration (LmxM.32.1380) and two PCRs checking puromycin integration (LmxM.24.2320 and LmxM.33.3120) did not yield the correct product; this is likely to be due to technical PCR problems, which is supported by the fact that two of the failed PCRs had strong primer dimers (Figure 3.13). Two cell lines had integrated both drug resistance genes but retained the ORF and were not therefore null mutants (Figure 3.13).

TriTrypDB accession	Protein description	Reason for knockout	Successful knockout?	Blasticidin PCR amplicon length	Puromycin PCR amplicon length	ORF PCR amplicon
LmxM.04.1230	Actin	EV biogenesis components	Yes	667	752	116
LmxM.32.1380	Erk1		Yes	825	910	171
LmxM.32.0170	Tetraspanin		Yes	683	768	205
LmxM.08_29.2500	VPS4		No			
LmxM.31.0985	TSG101, putative		No	739	824	307
LmxM.27.1640	Alix, putative		No			
LmxM.08.0200	ISCL		No			
LmxM.21.1540	Sec8, putative		No			
LmxM.23.0960	Sec10, putative		No			
LmxM.11.0160	Sec15, putative		No	815	900	169
LmxM.08_29.0880	Arl3A	Flagellar length regulators	Yes	688	773	221
LmxM.13.0130	Kinesin-13		Yes	742	827	211
LmxM.10.0490	MPK3		Yes	764	849	117
LmxM.08_29.2320	MKK		Yes	623	708	171
LmxM.24.2320	PK4		Yes	658	743	290
LmxM.13.0960	KAT60b		Yes	625	710	108
LmxM.33.3120	LPG2	Positive control for knockout method	Yes	690	775	316

Table 3.2. Summary of EV biogenesis and flagellar length control proteins targeted for knockout. Replacement of both alleles of the genes for these proteins with blasticidin and puromycin resistance cassettes was attempted in a single transfection using Crispr-Cas9. The parental cell line expressed SMP1::mCh as a FM marker. The cell lines which successfully survived transfection and were resistant to both selection drugs are indicated in the 'Successful knockout?' column. Protein descriptions and the reason for the knockout are shown. The amplicon lengths (number of nucleotides) of the PCRs to verify the successful loss of ORF and gain of resistance genes in the transfected cell lines are shown. Two cell lines which survived transfection were shown by PCR (Fig. 3.13) to have retained the ORF of the target gene (TSG101 and Sec15) and were therefore not successful knockouts.

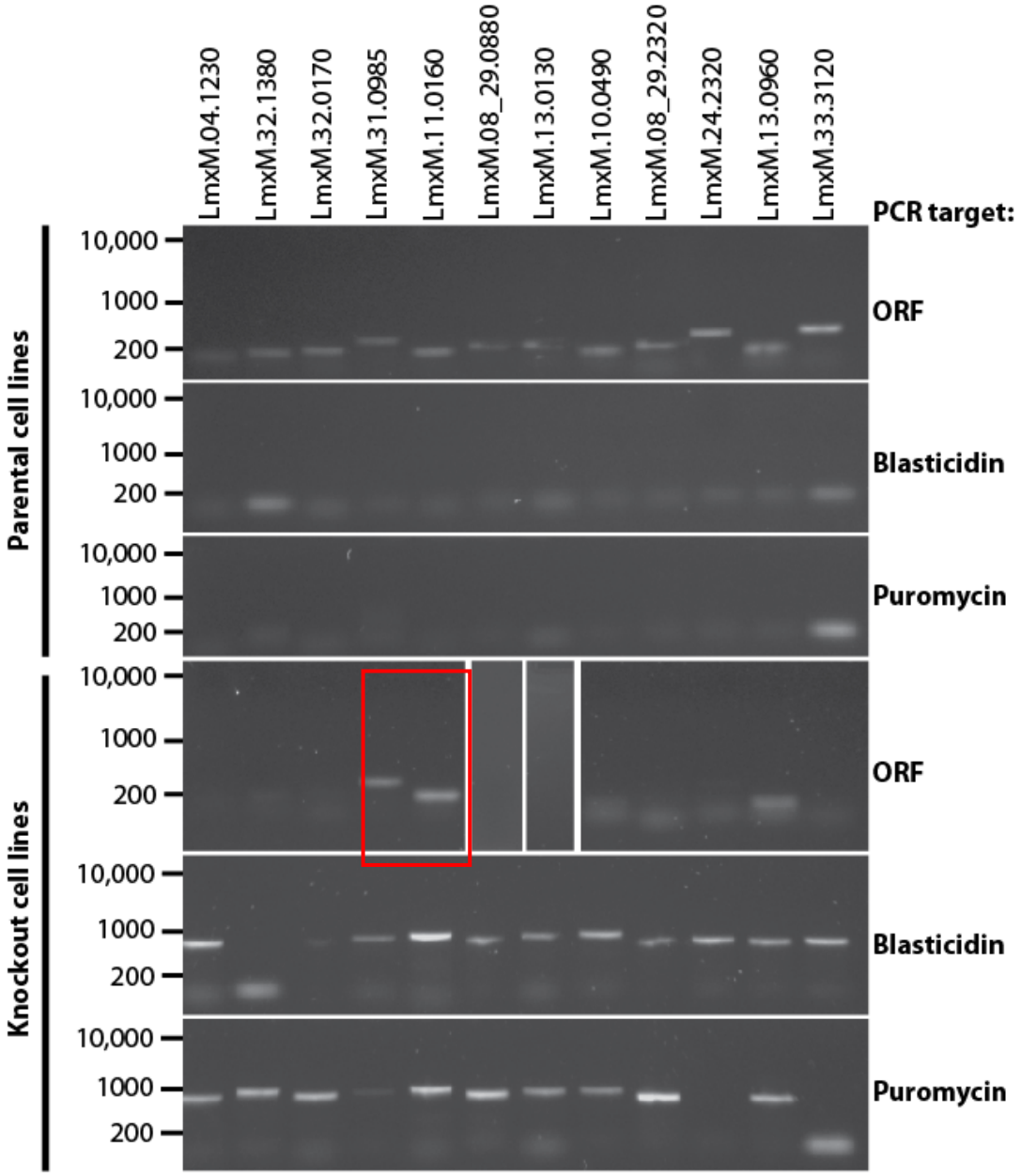

Figure 3.13. Verification of EV biogenesis and flagellar length control protein knockouts by PCR. PCRs were carried out on genomic DNA from the parental cell line (Cas9 T7 SMP1::mCh) and from each transfected knockout cell line shown in Table 3.2. For each cell line and parental control three PCRs were carried out: ORF) amplifies a region within the ORF, Blasticidin) amplifies between a forward primer in the endogenous 5' UTR and a reverse primer in the blasticidin ORF, Puromycin) amplifies between a forward primer in the endogenous 5' UTR and a reverse primer in the puromycin ORF. PCRs showing that the attempted LmxM.31.0985

and LmxM.11.0160 knockout cell lines have retained the ORF are highlighted in red. The 2 inserts in the ORF panel show products from a different gel. Amplicon sizes in base pairs are indicated by the numbers on the left hand side.

3.2.3. Phenotypes of candidate EV biogenesis KOs

All null mutant cell lines were imaged by fluorescence microscopy to observe changes in flagellar length compared to the parental cell line. Actin, Erk1, tetraspanin, kinesin-13, PK4 and Kat60b null mutants showed no changes in flagellar length (not quantified) (Figure 3.14). Arl3A null mutant cells displayed varying flagellar lengths; some cells had no discernible flagellum, some appeared to have normal length flagella and some had an intermediate phenotype (Figure 3.14). Strikingly, the SMP1::mCh localisation of Arl3A null mutant cells was cell body and FM instead of the expected FM-enriched localisation (Figure 3.14). Arl3A KO cell lines have been independently generated twice more resulting in the same SMP1 mislocalisation phenotype (Gluenz lab, unpublished data). As expected (Erdmann et al., 2006), MPK3 and MKK null mutants had short flagella extending up to ~2 µm beyond the cell body compared to ~10 µm in the parental cell line, and in addition their cell bodies were more rounded than the parental cell line (Figure 3.14). Observation of SMP1::mCh signal showed that all cell lines were able to produce FM nanotubes (Figure 3.14), showing that none of the genes which were deleted are essential for this process. All null mutant cell lines grew into stationary phase at similar rates to the parental cell line, except the actin null mutant which grew slower (Figure 3.15).

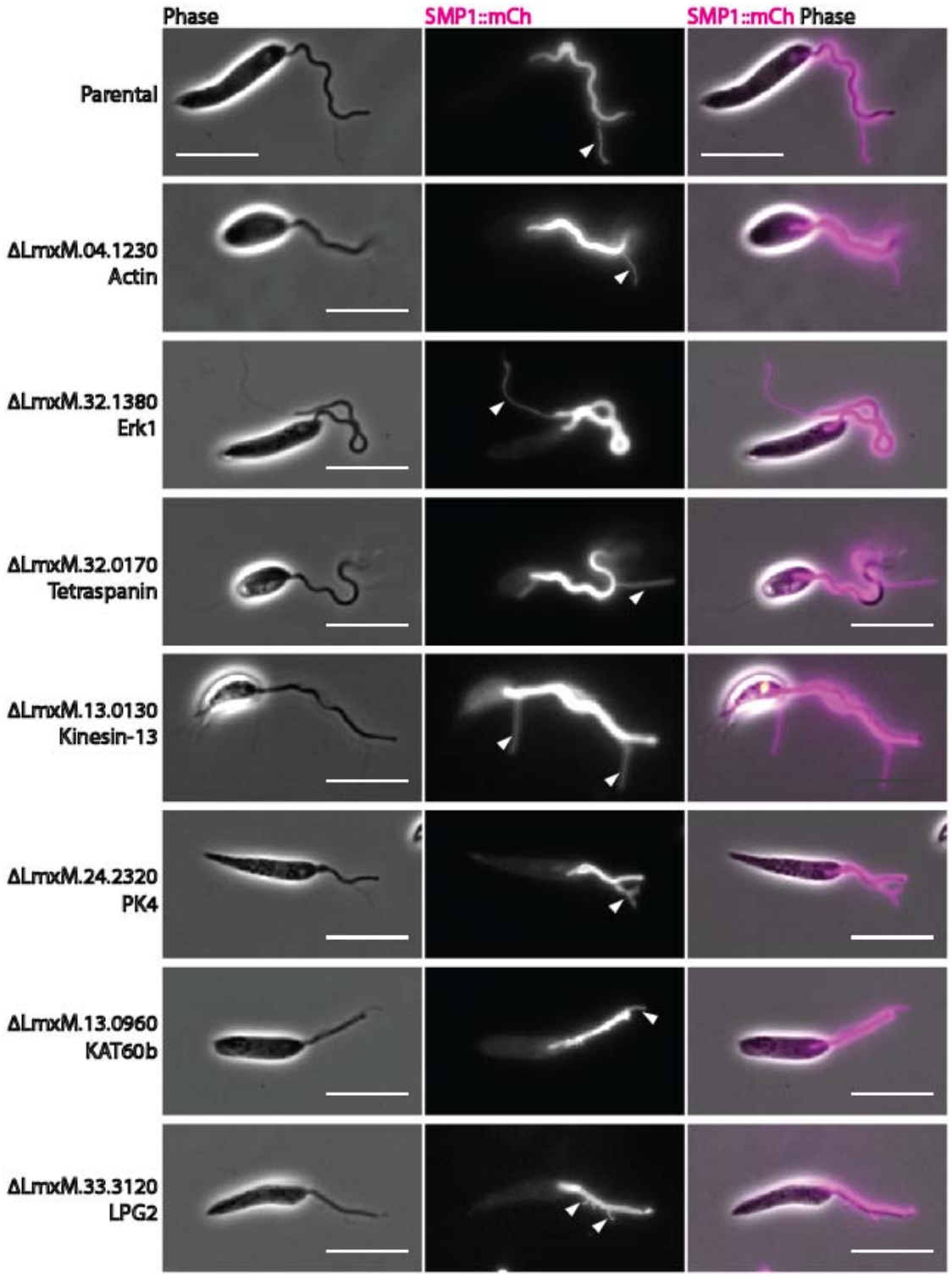
Phase
SMP1::mCh
SMP1::mCh Phase
Parental
ΔLmxM.04.1230
Actin
ΔLmxM.32.1380
Erk1
ΔLmxM.32.0170
Tetraspanin
ΔLmxM.13.0130
Kinesin-13
ΔLmxM.24.2320
PK4
ΔLmxM.13.0960
KAT60b
ΔLmxM.33.3120
LPG2

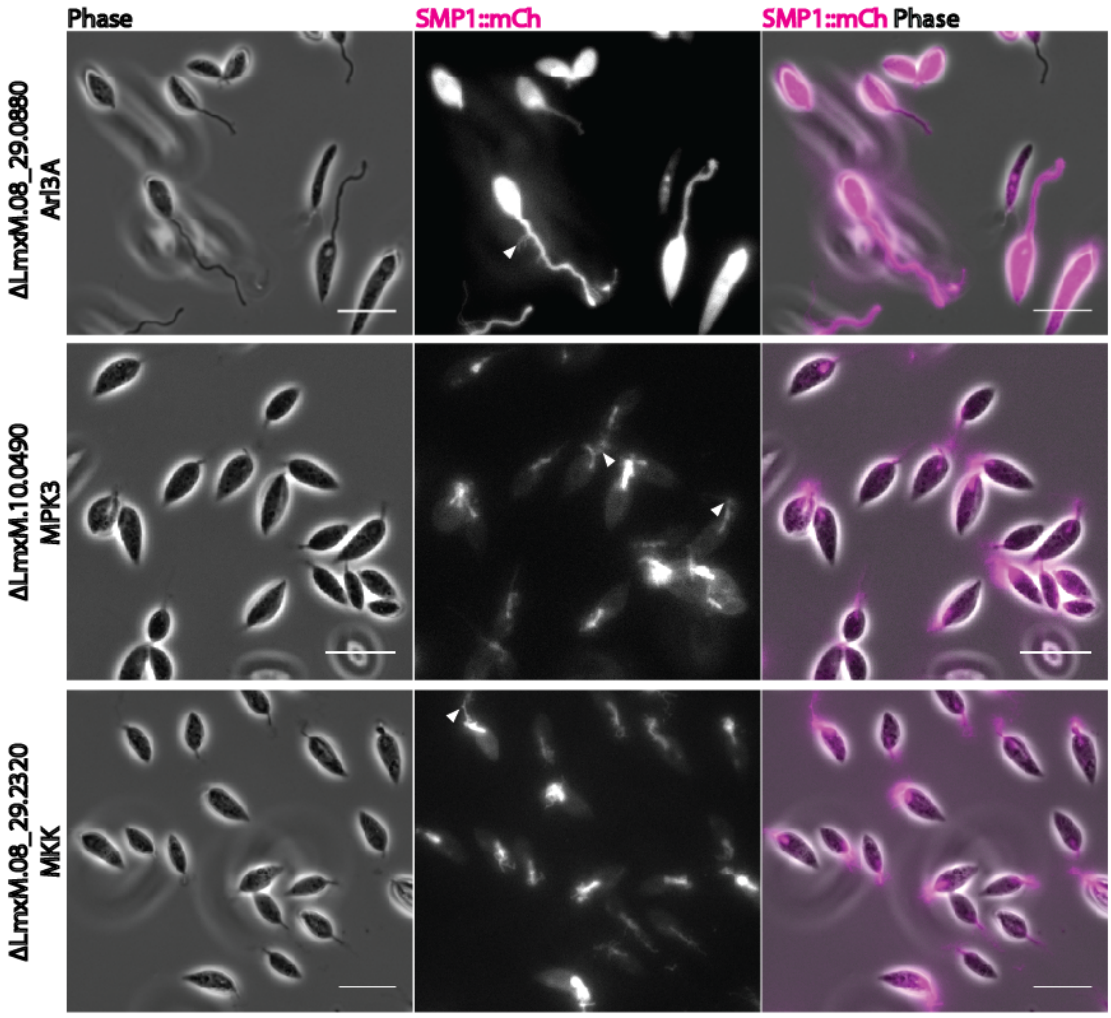

Figure 3.14. Imaging of EV biogenesis and flagellar length control knockout cell lines. The parental cell line (Cas9 T7 SMP1::mCh) expresses SMP1::mCh as a FM marker. The confirmed null mutant cell lines from Table 3.2 and Fig. 3.13 as well as the parental cell line were imaged on a fluorescence microscope. The panels are phase contrast (phase), and merged SMP1::mCh and phase contrast. At least one example of a cell displaying FM nanotubes is indicated by white arrowheads for each cell line. Fields of view of the flagellar length mutants ΔLmxM.08_29.0880, ΔLmxM.08_29.2320 and ΔLmxM.10.0490 are shown. All scale bars are 10 µm.

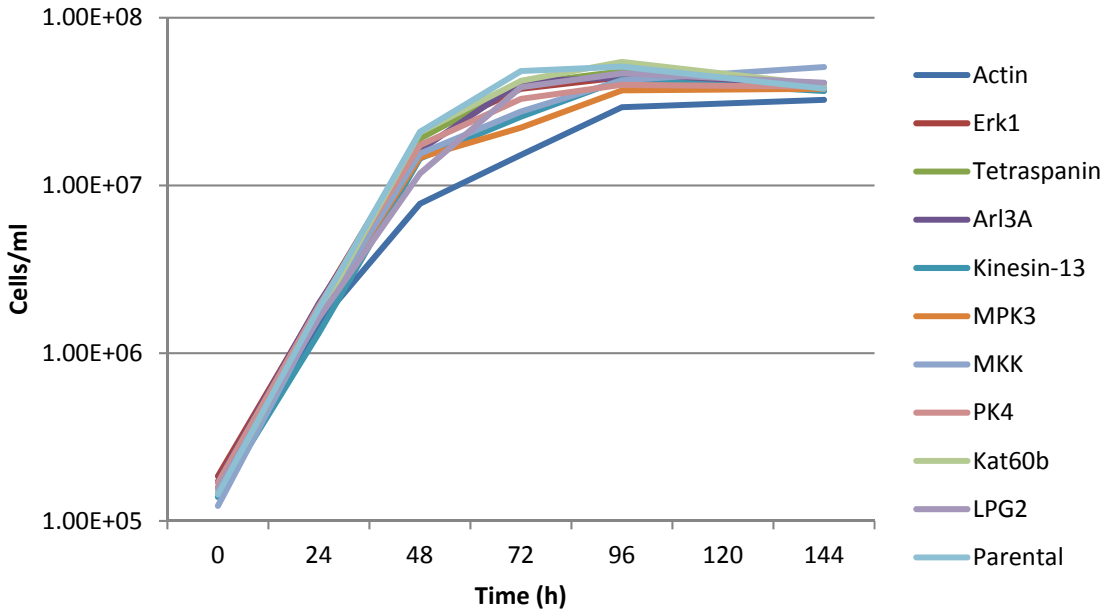

Figure 3.15. Growth curves of EV biogenesis and flagellar length control knockout cell lines. All knockout cell lines from Fig. 3.14 and the parental cell line (Cas9 T7 SMP1::mCh) were seeded at ~1.10^5 cells/ml at 0 h, their cell densities were measured and then measured again at 24, 48, 72, 96 and 144 h.

3.2.4. EM shows successful isolation of EVs from *Leishmania* cultures

To allow subcellular origin and structural studies, EVs were isolated by differential centrifugation from FCS-free medium conditioned with *L. mexicana* promastigotes (PRO) or cells which had undergone axenic promastigote to amastigote differentiation (DIF) for 4 h. A 4 h incubation was chosen because cells at that time point are undergoing flagellar shortening, few cells have fully shortened amastigote-like flagella (Wheeler et al., 2015), and the levels of FM elaborations are the highest of the time points measured in this study (Figure 3.2A, B). While a longer incubation may have improved EV yield, we aimed to maximise cell health by minimising the time cells spend in FCS-free medium, and also to maximise DIF sample homogeneity by isolating

EVs from a population where the majority of cells are undergoing flagellar shortening (Wheeler et al., 2015).

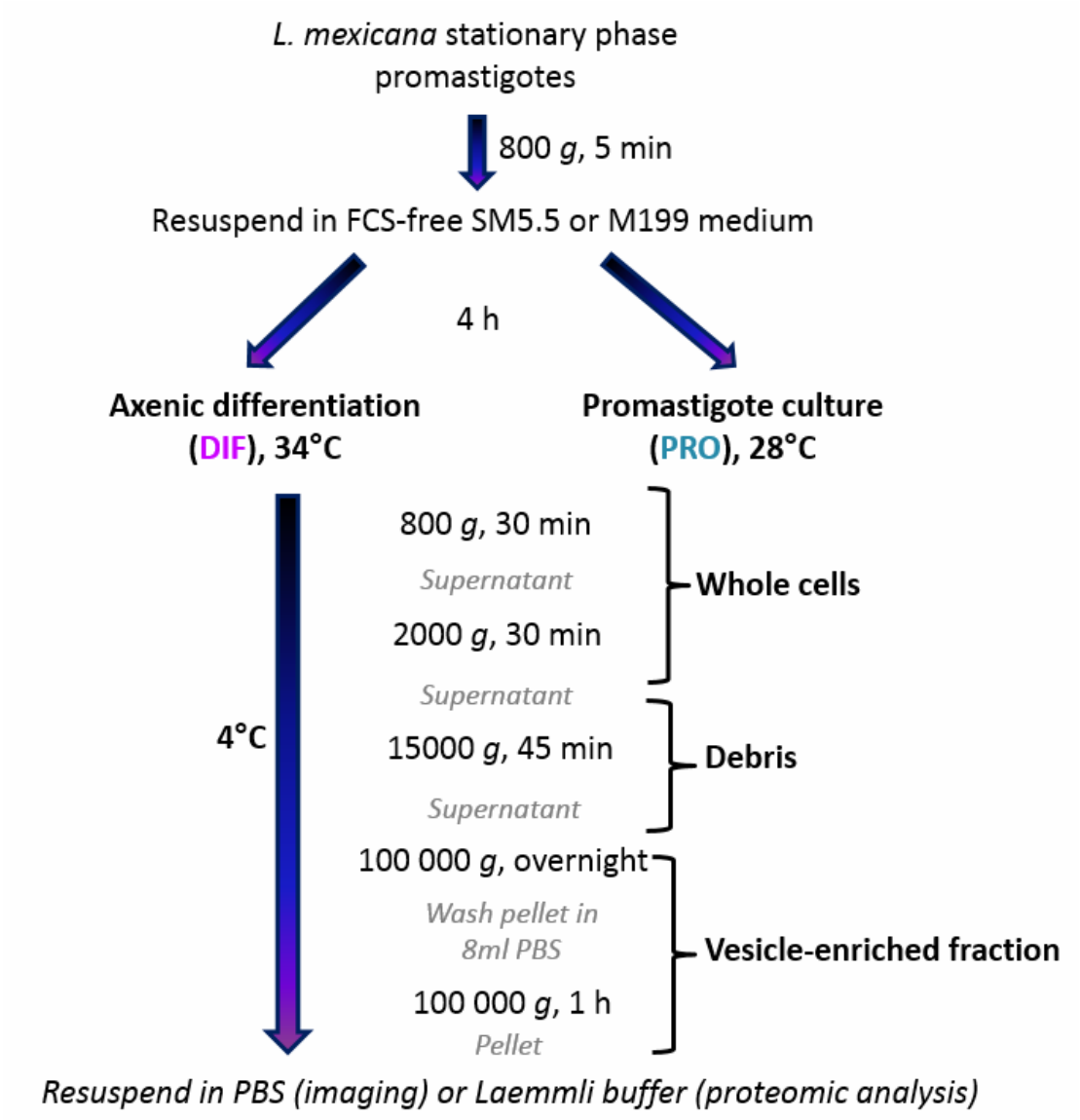

Isolated PRO (Figure 3.16A) and DIF (Figure 3.16B) EVs with diameters of ~100 nm were visible by negative staining EM and none were visible in the FCS-free medium only control (Figure 3.16C). What appeared to be filamentous extracellular proteins were also visible (Figure 3.16A). Using this EM sample preparation method, however,

EVs were very scarce making it difficult to obtain an accurate idea of the range of EV sizes. Figure 3.17 shows the same EV sample prepared for negative staining EM with a 1 minute sample incubation and 3 ddH_2O washes (Figure 3.17A) compared to a 10 minute incubation and no ddH_2O washes (Figure 3.17B). Using the former method, EVs were abundant in only 1 square of the EM grid (Figure 3.17A), whereas the latter method led to more uniform EV abundance across the grid (Figure 3.17B) as well as the increased abundance of small EVs (< 40 nm in diameter). In both cases, EVs with diameters between 30 and 200 nm as well as filamentous proteins were visible (Figure 3.17A and B). Negative staining EM gives a good idea of the abundance and size distribution of isolated particles but does not prove that the objects of interest are true vesicles, with a lipid bilayer. Cryo-EM was used to image a DIF EV sample with an EV concentration 2-fold higher than the sample shown in Figure 3.17. Only two vesicles were observed which were around 150 nm across (Figure 3.18); this low abundance could be due to the fact that cryo-EM requires high sample concentrations (Cabra and Samso, 2015, Fernandez-Leiro and Scheres, 2016). The lipid bilayer was clearly visible as a double line showing that these are membrane-bound vesicles.

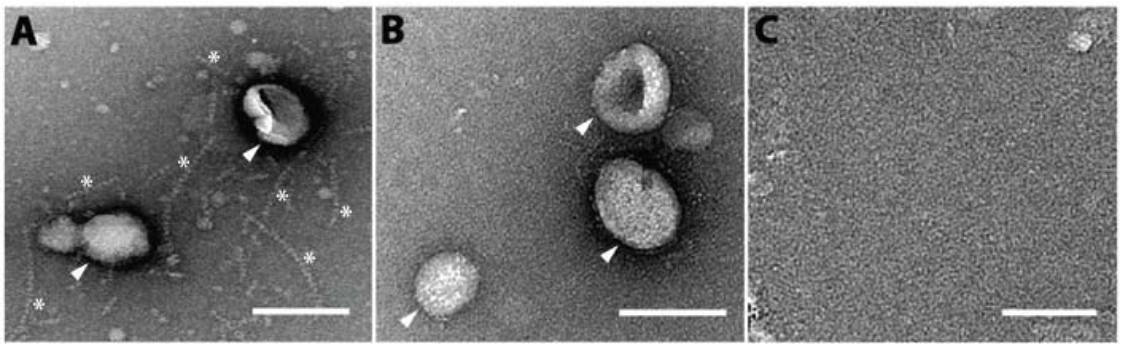

Figure 3.16. Isolated EVs from *Leishmania* cultures imaged by negative staining EM. EVs were isolated from Clone 3 cells by differential centrifugation; either from promastigotes in FCS-free M199 (**A**), cells which had been differentiating in FCS-free SM5.5 for 4 h (**B**), or an FCS-free SM5.5 medium control. The isolated EVs were resuspended in PBS with 4% PF, prepared for negative staining on carbon coated grids with UA staining and imaged by transmission EM. Arrowheads: vesicles; asterisks: protein filaments. Scale bars 100 nm.

A)

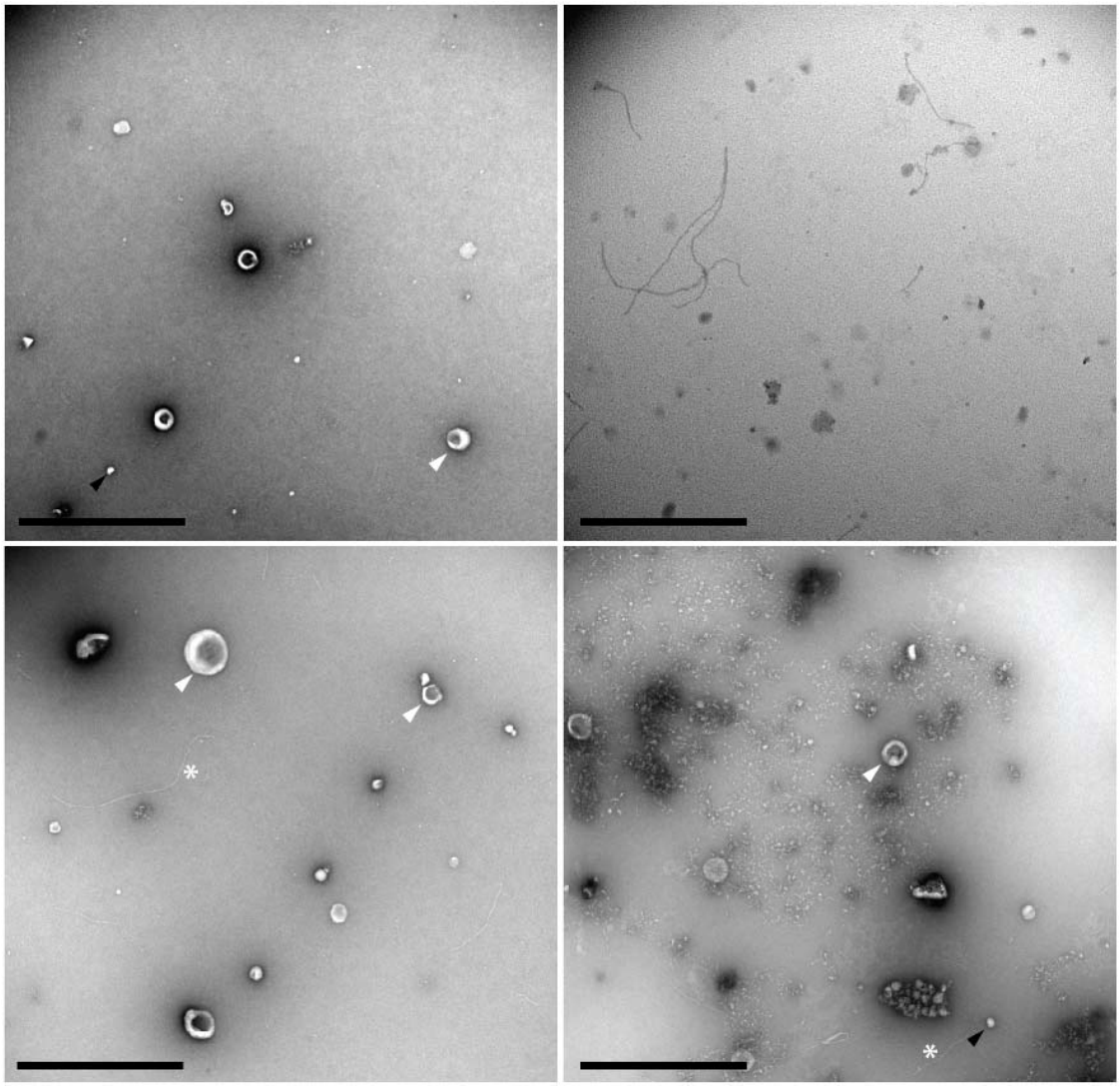

B)

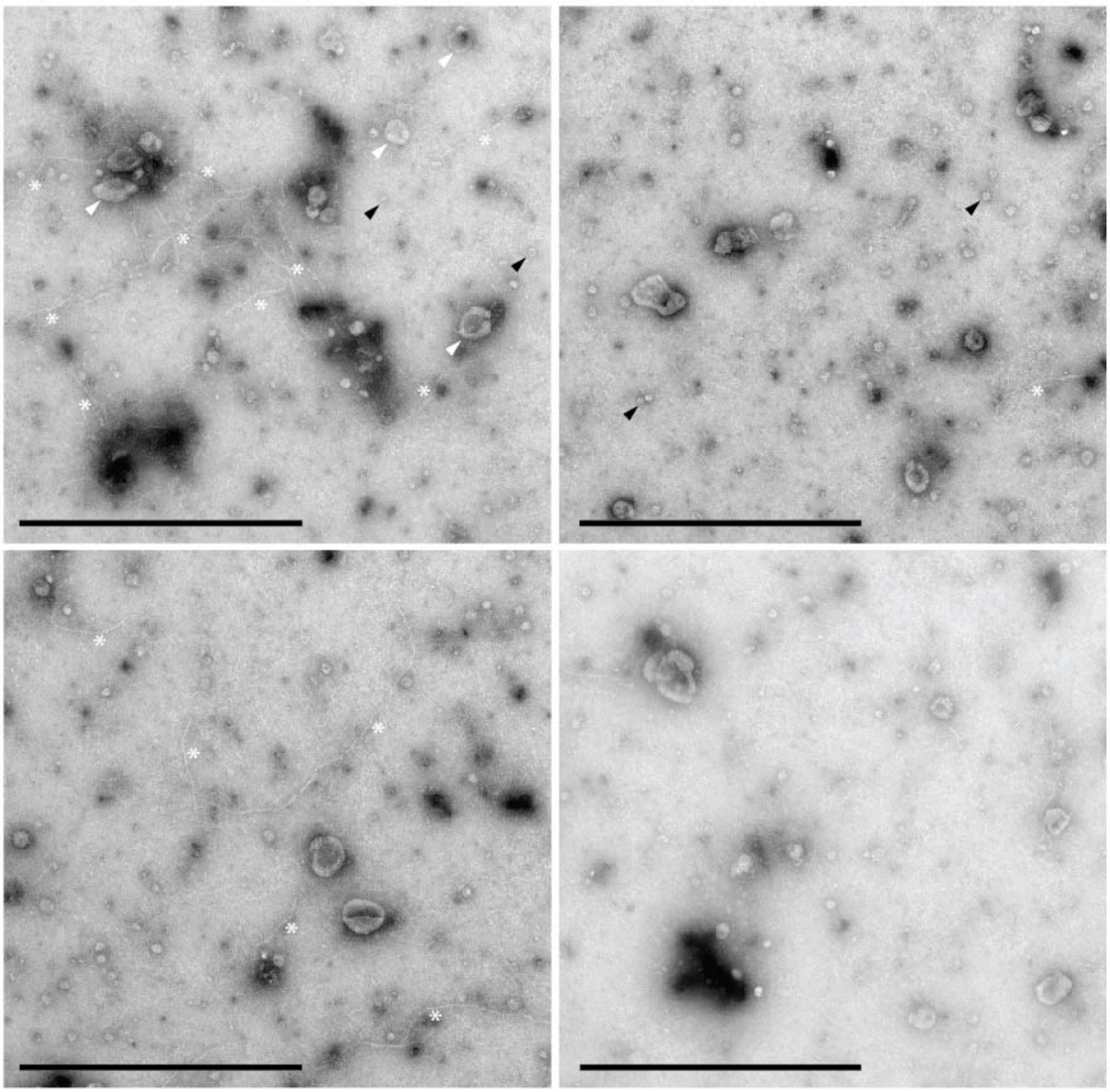

Figure 3.17. Improvement of negative staining EM of isolated EVs. EVs were isolated by differential centrifugation from *L. mexicana* Cas9 T7 cells which had been differentiating in FCS-free SM5.5 for 4 h. Isolated EVs were resuspended in PBS + 2% PF. The EVs were prepared on carbon coated grids with either **A)** standard sample preparation of 1 min sample incubation with 3 ddH_2O washes or **B)** a 10 min sample incubation with no ddH_2O washes. Panels show 4 representative images of EVs isolated by both methods. Both samples were stained with UA. Black arrowheads indicate some of the EVs in the <40 nm diameter size range

and white arrowheads some of the EVs in the >40 nm diameter size range. Asterisks indicate protein filaments. All scale bars 1 µm.

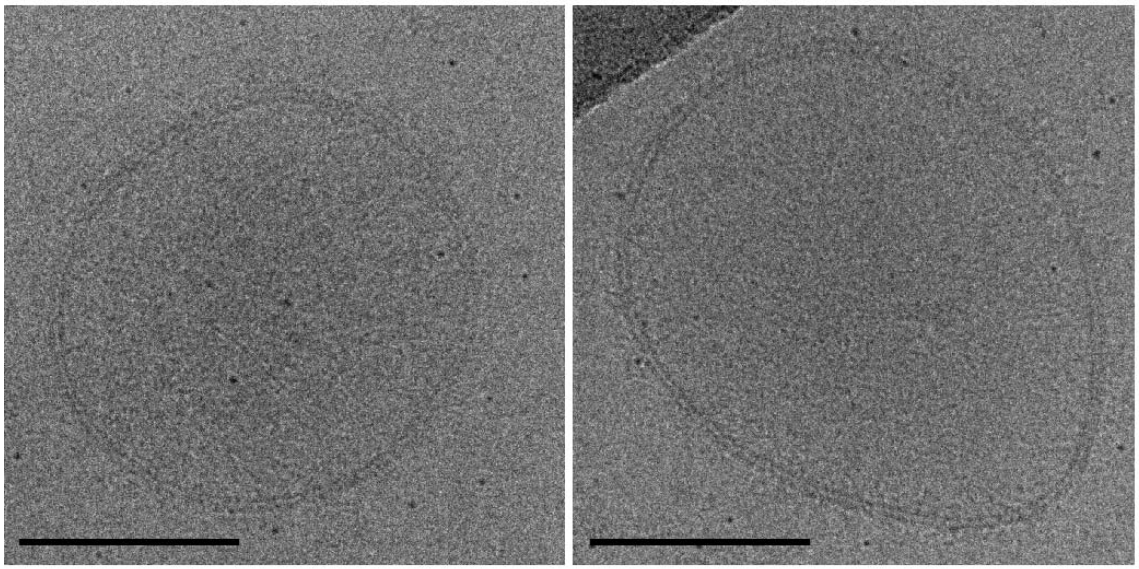

Figure 3.18. Cryo-electron imaging of isolated EVs showing lipid bilayer. EVs were isolated from *L. mexicana* Clone 3 cells by differential centrifugation from cells which had been differentiating in FCS-free SM5.5 for 4 h. The EVs were resuspended in PBS and prepared for cryo-electron imaging. Scale bars 100 nm.

3.2.5. Density gradient separation of vesicle fractions

The observation of contaminating filamentous proteins in EV samples (Figures 3.16 and 3.17) led us to attempt further purification of EVs using an iodixanol density gradient separation protocol based on a published method for isolation of EVs of a similar size range (Cvjetkovic et al., 2016). DIF EVs were isolated by differential centrifugation followed by density gradient separation then particle concentrations of fractions 1-9 were measured by nanoparticle tracking analysis (NTA). The highest particle concentrations were consistently measured in fractions 2 and 3, which together contained a mean of 66% of the total particles in all fractions (Figure 3.19A). By calculating the sum of particles in all fractions (mean of 8.2×10^{10}) and dividing by the total number of *L. mexicana* cells used (2.2×10^{10}), the average number of particles per cell was 3.7. By comparison, the average number of particles per *L. mexicana* cell when DIF EV samples isolated by differential centrifugation were measured by NTA using the same Nanosight machine settings was 1.3 (mean of 5×10^{9} total particles divided by 4×10^{9} cells used, calculated from parental sample data used in Figure 5.12); note that the number of particles per cell described here is lower than for DIF EV samples described in *Section 3.2.7*. This is likely due to technical issues: damage to the Nanosight machine occurred between the experiments carried out in *Section 3.2.7* and this section, leading to decreased sensitivity of the camera and likely underestimation of particle counts. The average mean (Figure 3.19B) and median (Figure 3.19C) particle diameters varied among fractions 1-9 from 130 to 210 nm; these differences followed no pattern and were not large.

Fractions 1-9 were also analysed by negative staining EM (Figure 3.20). At least 1 EV was visible in all fractions. EVs were most abundant in fractions 2, 3 and 7 and were

difficult to find in the remaining fractions, consistent with NTA data. Square crystals were also abundant in fraction 3. Filamentous protein was not observed in any of the fractions, it is possible that the increased number of washes compared to differential centrifugation alone reduced non-vesicle contamination. No obvious segregation based on EV size was observed, consistent with NTA data (Figure 3.19B, C).

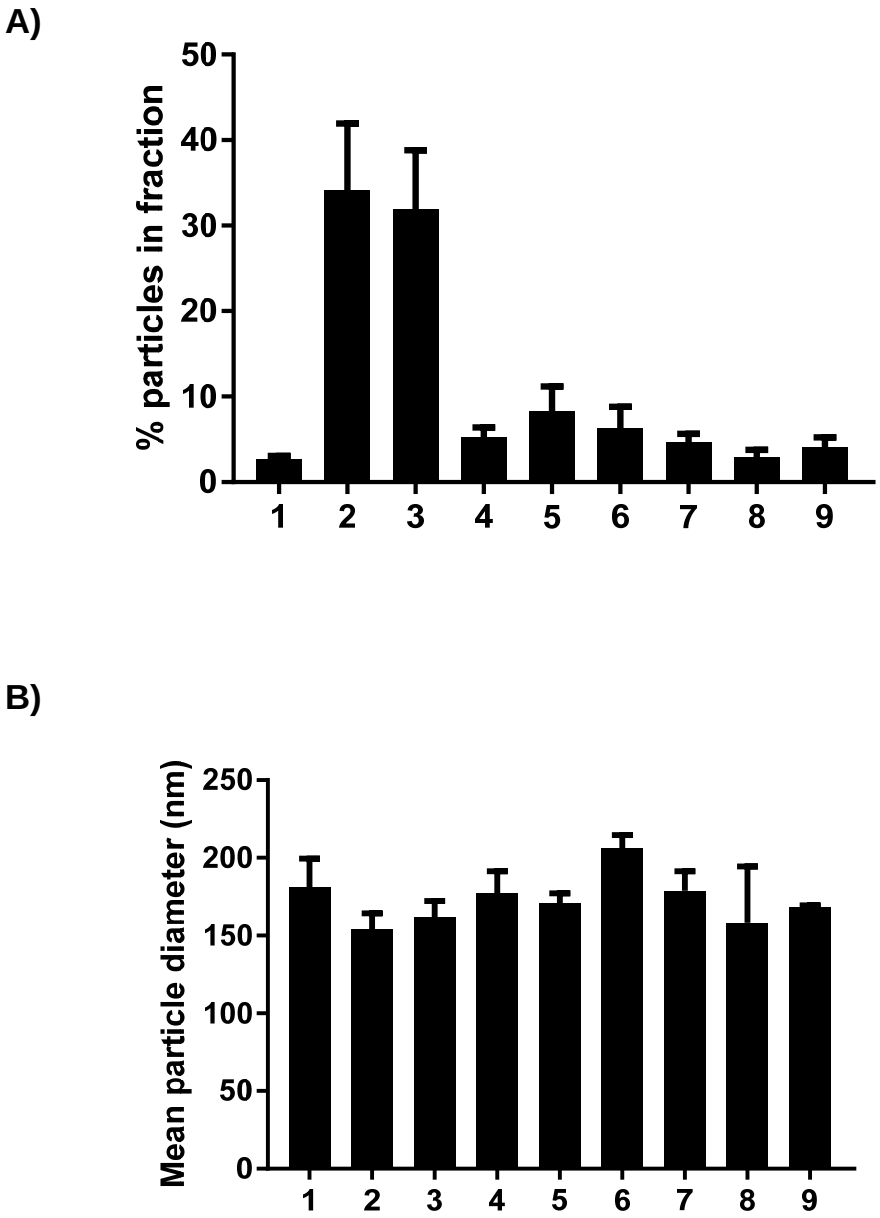

C)

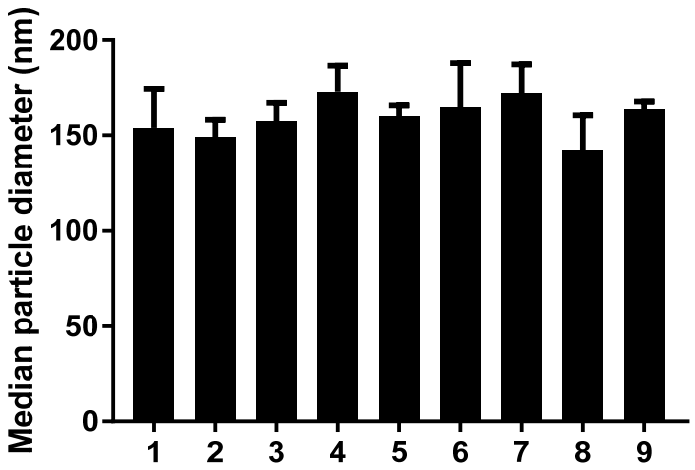

Figure 3.19. Density gradient separation of EVs measured by NTA. EVs were isolated from *L. mexicana* Clone 3 cells which had been differentiating in FCS-free SM5.5 for 4 h by differential centrifugation followed by further purification on an iodixanol (Optiprep^{TM}) density gradient. Nine equal fractions were collected (fraction 1 being taken from the top of the tube), pelleted and resuspended in PBS and the particle concentration of each fraction was measured by NTA. **A)** The graph shows the mean percentage of total particles in all fractions ± SEM in each fraction from 3 biological repeats. **B, C)** The graphs show the mean (**B**) and median (**C**) particle diameter ± SEM in each fraction from 3 biological repeats.

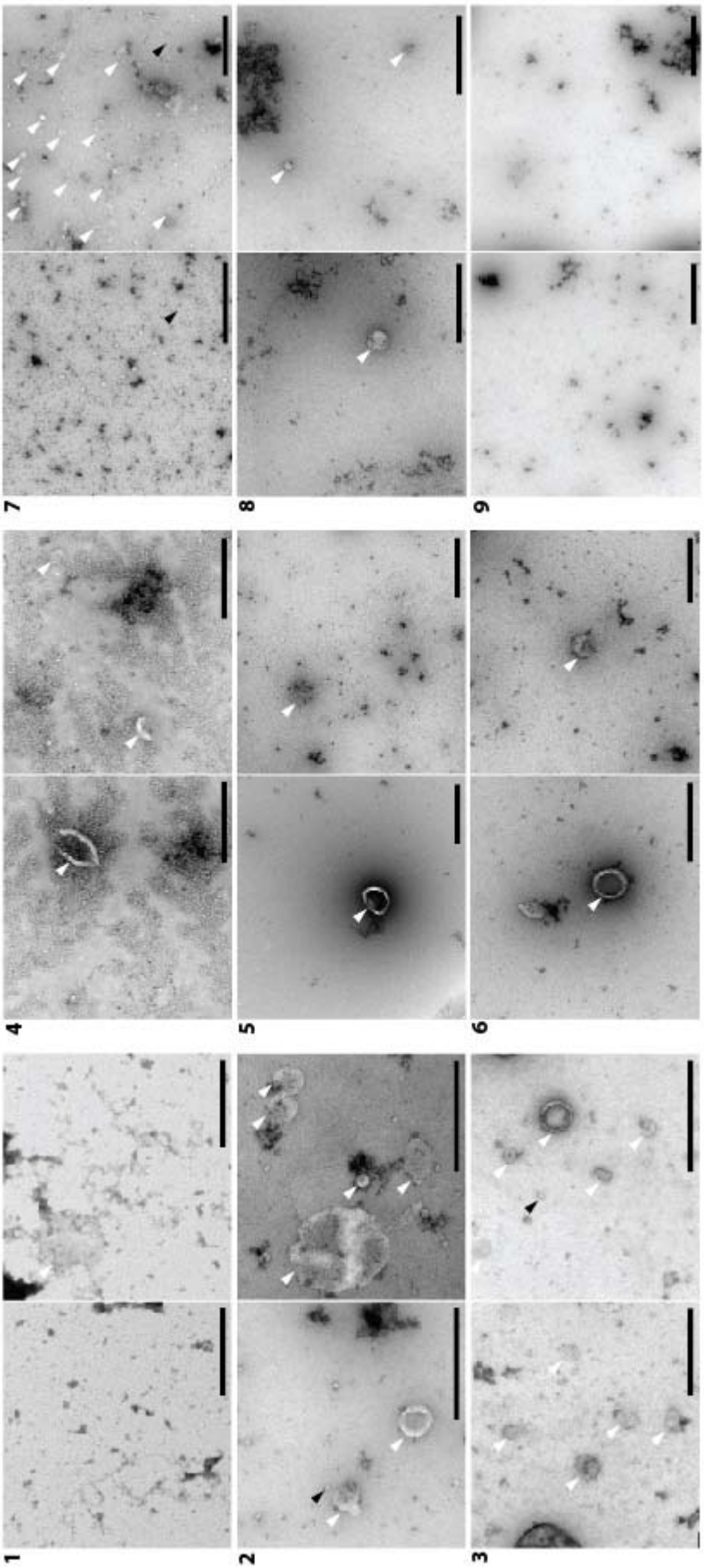
1
2
3
4
5
6
7
8
9

Figure 3.20. Density gradient separation of EVs analysed by negative staining EM. Fractions 1-9 were collected, pelleted and resuspended in PBS with 2% PF and prepared for negative staining EM on carbon coated grids with UA staining. At least three grid squares were imaged for each fraction and two representative images are shown. Black arrowheads indicate some of the EVs in the <40 nm diameter size range and white arrowheads the EVs in the >40 nm diameter size range. Scale bars 500 nm.

3.2.6. Fluorescence microscopy of EVs from SMP1::mCh-GT2::eGFP:TY cells suggests EV release from flagellum and cell body

Data from *Section 3.2.1* suggests that EVs are released from *L. mexicana* FM nanotubes and blebs. To further investigate and quantify EV subcellular origin before and during differentiation, EVs were isolated from Clone 3 (SMP1::mCh-GT2::eGFP:TY) cells. mCh- and eGFP- bright foci were observed in isolated EV samples from the tagged reporter cell line but not from WT cells (Figure 3.21A), indicating that the fluorescent foci corresponded to SMP1::mCh and GT2::eGFP. Foci which were both mCh- and eGFP- bright were not observed (Figure 3.21A). The foci were in the size range of EVs (<1 μm) but their exact sizes could not be determined due to the diffraction limit of light. In both PRO and DIF EV samples the number of mCh-bright foci was higher than eGFP-bright foci (Figure 3.21B): 5-fold higher in the PRO and 206-fold higher in the DIF. The absolute number of mCh-bright foci was 2.5-fold higher in the DIF sample, whereas the absolute number of eGFP-bright foci was 16-fold higher in the PRO.

A)

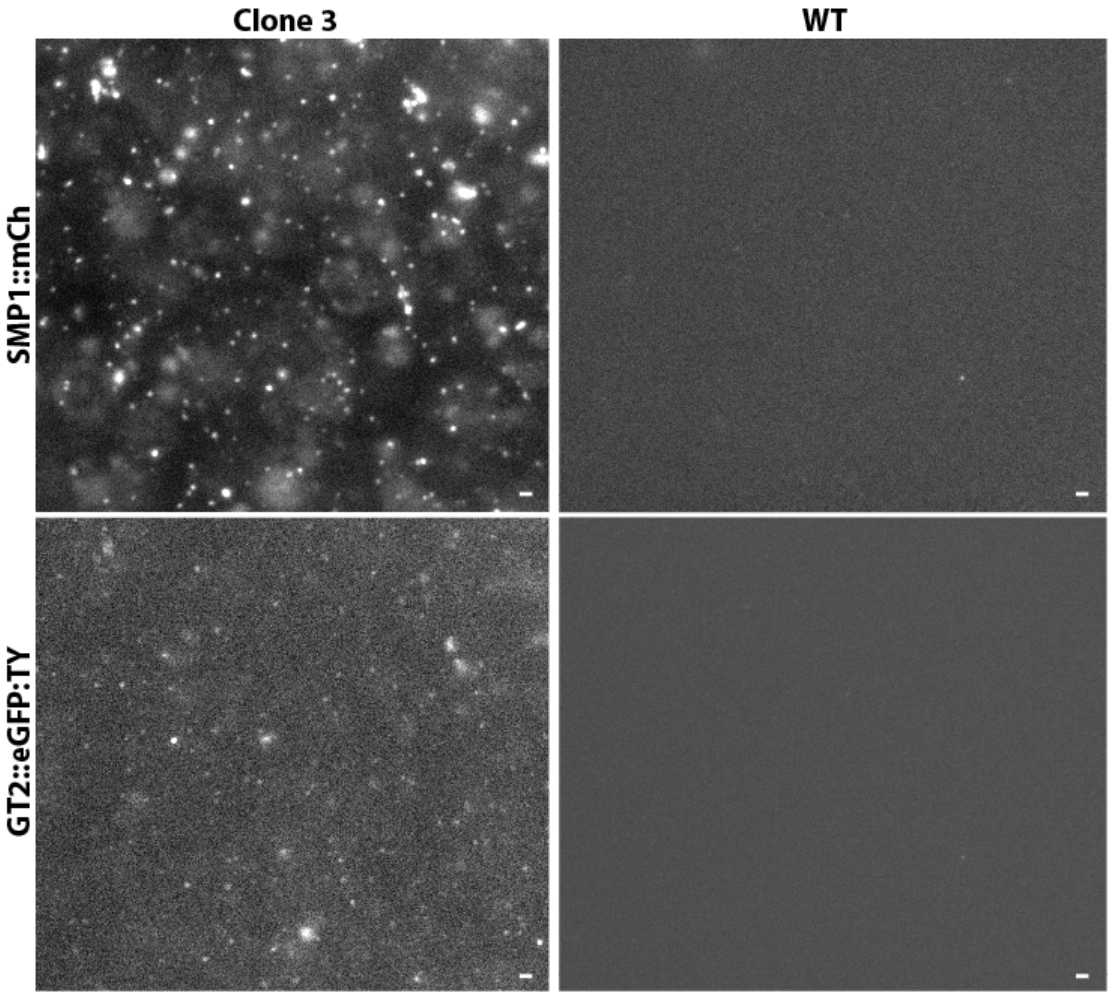

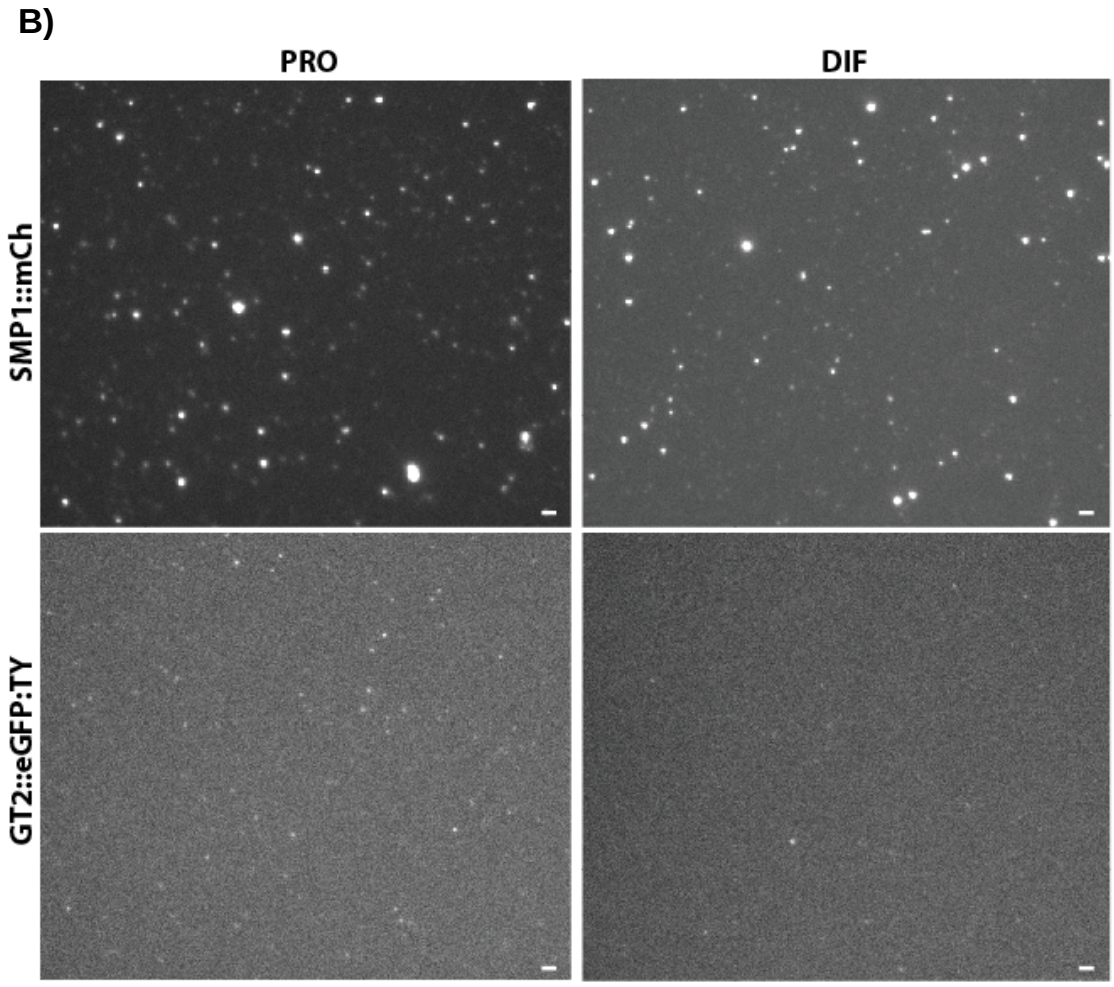

Figure 3.21. Fluorescence microscopy of EVs from Clone 3 cells suggests EV release from the flagellum. **A)** EVs were isolated from *L. mexicana* Clone 3 or wild type cells which had been incubated in FCS-free M199 at 28°C for 4 h. Isolated EVs were resuspended in PBS and observed by fluorescence microscopy. These images are representative of three independent experiments. **B)** EVs were isolated from Clone 3 cells which had been incubated in FCS-free M199 at 28°C (PRO) or in FCS-free SM5.5 at 34°C (DIF) for 4 h. Pelleted EVs were resuspended in PBS and observed by fluorescence microscopy. Scale bars 1 µm.

3.2.7. Nanoparticle tracking analysis suggests increased EV release during differentiation

NTA showed that both PRO and DIF EV samples have a particle size distribution ranging from ~50-300 nm with very similar mean diameters of 140 and 147 nm respectively (Figure 3.22A). Particles <50 nm in diameter were not detected by NTA under the conditions of this study. The commonly used methods for EV isolation (reviewed in (Szatanek et al., 2015)) are differential ultracentrifugation with or without a density gradient step, immuno-affinity isolation, size exclusion chromatography, and commercially available kits including qEV size exclusion columns (Vogel et al., 2016). Differential ultracentrifugation is the most commonly used method (Livshits et al., 2015) and has the advantage of not relying on unknown reagents and methods of commercial kits. However, the protocol takes at least one day to carry out, therefore alternative isolation methods are worth investigating to determine whether they can reduce isolation time and also improve yield. For qEV column isolation, I carried out 800 *g* and 2,000 *g* centrifugation steps, as for the differential ultracentrifugation protocol, then applied the supernatant to the qEV column; the protocol lasted a few hours compared to 1.5 days for differential ultracentrifugation. Higher concentrations of DIF compared to PRO particles were isolated by both differential centrifugation (Figure 3.22B) and qEV size exclusion columns (Figure 3.22C). However, particle yield was higher using differential ultracentrifugation (mean of 5.7 PRO and 8.3 DIF EVs per *L. mexicana* cell) compared to qEV columns (mean of 3.7 PRO and 5.0 DIF EVs per *L. mexicana* cell), therefore differential ultracentrifugation continued to be used for all experiments. The increase in mean EV concentration between PRO and DIF EV samples was 44% and this difference was significant (Figure 3.22D). A FCS-free medium control which had

undergone all steps of EV isolation was also analysed (data not shown) and measured particle concentrations were >40-fold lower than for isolated EV samples.

In conclusion, FM elaborations were observed on axenic promastigotes and differentiating cells both in axenic culture and inside macrophages. The frequency of FM elaborations was unaffected by SMP1 being fluorescently tagged and FCS-free conditions, but was decreased by protein synthesis inhibition and increased 2-fold during promastigote to amastigote differentiation. These structures appeared to be linked to flagellar EV release since time lapse imaging showed EV release from FM nanotubes and blebs. EVs were successfully isolated from *L. mexicana*-conditioned medium by differential ultracentrifugation and imaged by negative staining EM, which showed a heterogeneous population of EVs ~30-300 nm in diameter suggestive of both exosomes and microvesicles. Non-vesicle-associated filamentous protein contamination was observed by EM. Further purification of EVs using density gradient separation successfully enriched 66% of total particles (assumed to be EVs) in 2 out of 9 fractions, and appeared to remove filamentous protein contamination. Supporting the observation of increased FM elaborations during differentiation, ~44% more particles (assumed to be EVs) in the >50 nm size range were released from differentiating cells compared to promastigotes. Due to technical restrictions, particles in the <50 nm size range could not be measured. Fluorescence microscopy of EVs isolated from a tagged cell line suggests that the FM is a major source of EVs and that the proportion of FM-derived EVs increases during differentiation.

A

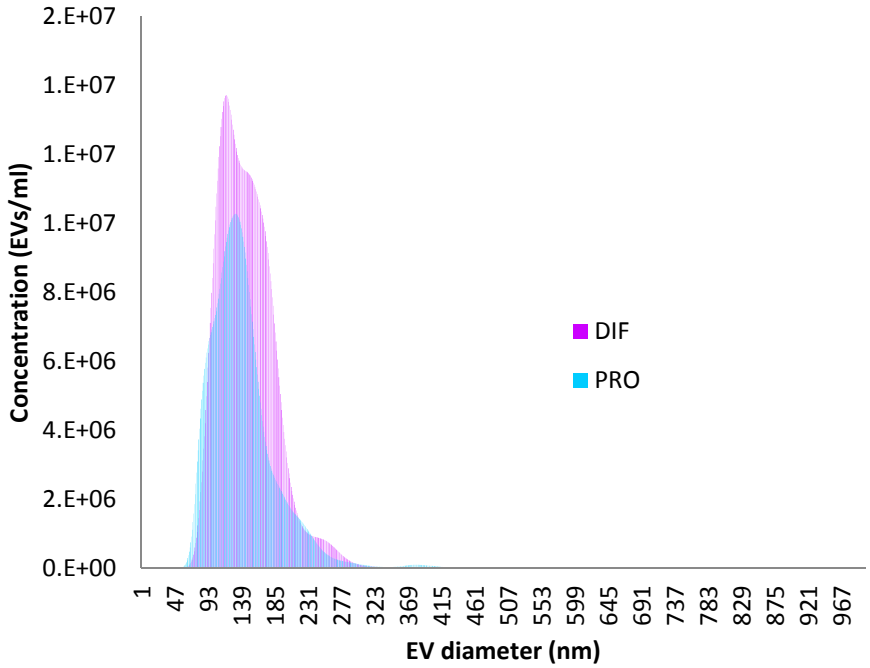
2.E+07
1.E+07
1.E+07
1.E+07
8.E+06
6.E+06
4.E+06
2.E+06
0.E+00
Concentration (EVs/ml)
1
47
93
139
185
231
277
323
369
415
461
507
553
599
645
691
737
783
829
875
921
967
EV diameter (nm)
DIF
PRO

B

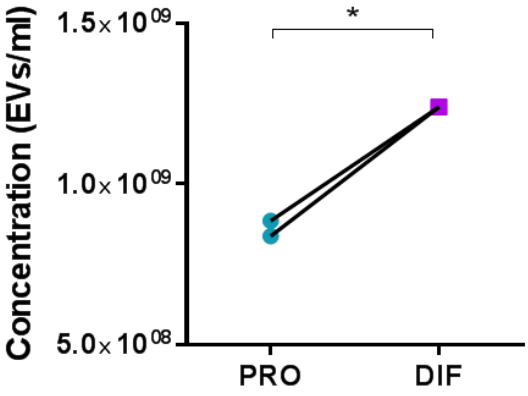
1.5×10^09
1.0×10^09
5.0×10^08
Concentration (EVs/ml)
*
PRO
DIF

C

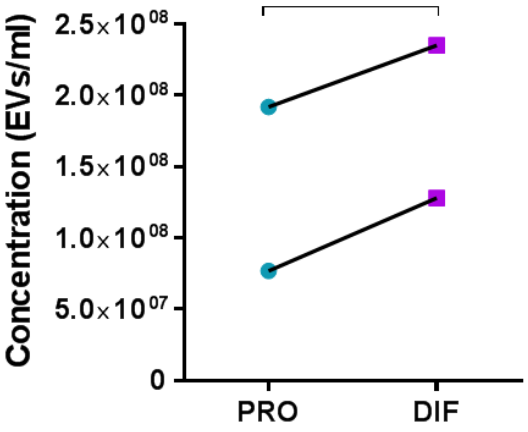
2.5×10^08
2.0×10^08
1.5×10^08
1.0×10^08
5.0×10^07
0
Concentration (EVs/ml)
PRO
DIF

D

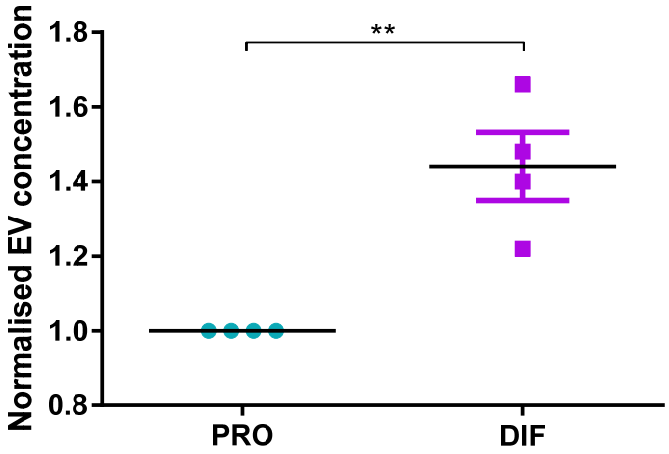

Figure 3.22. NTA of EVs shows increased EV release during *Leishmania* differentiation. PRO and DIF EVs were isolated and measured by NTA using total scatter mode. **A)** The histogram shows the size distributions of PRO and DIF EVs from SMP1::eYFP cells isolated by differential centrifugation. **B)** EVs were isolated from SMP1::eYFP cells by differential centrifugation. The graph shows the EV concentrations of PRO versus DIF samples from two independent experiments. **C)** EVs were isolated from SMP1::mCh cells using Izon qEV columns. The graph shows the EV concentrations of PRO versus DIF samples from two independent experiments. **D)** The graph show the normalised EV concentrations ± SEM from the four independent experiments shown in Fig.s 23B and 23C. Asterisks show significant differences as tested by paired (**B** and **C**) or unpaired (**D**) t-tests with p values as follows: * p≤0.05; ** p≤ 0.01; *** p≤0.001; **** p≤0.0001.

3.3. Discussion

3.3.1. EV release and flagellar shortening are linked

As discussed in *Section 3.1.1*, there is mounting and convincing evidence that FMs are a functionally important source of EVs in *C. reinhardtii* (Dentler, 2013), *C. elegans* (Wang et al., 2014) and mammalian cells (Nager et al., 2016). This field of research has only recently started to be explored in trypanosomatids (Szempruch et al., 2016b), however, and there is not yet convincing published data on flagellar EVs from *Leishmania* spp.. We find that *L. mexicana* forms FM elaborations in the form of blebs and nanotubes (Figure 3.1) and time-lapse imaging suggests these structures are sites for EV release (Figure 3.8). The frequency of these structures approximately doubles during the flagellar shortening phase of promastigote to amastigote differentiation (Figure 3.2). Supporting these observations of whole cells, analysis of cell supernatants demonstrated the presence of EVs (Figures 3.16 and 3.17) and showed that the total number of EVs released (Figure 3.22) as well as the ratio of flagellar-derived EVs (Figure 3.21) increases during differentiation. These data suggest a link between flagellar shortening and EV release, as has been shown in other organisms (Dentler, 2013, Nager et al., 2016, Long et al., 2016).

Based on the length of an average promastigote flagellum being ~10 µm (Wheeler et al., 2011) and the diameter ~300 nm (Gluenz et al., 2015), the approximate surface area of the FM is ~9.6 μm^2. Taking the average DIF particle diameter of 147 nm and therefore membrane surface area of 0.3 μm^2, 35.4 DIF particles equal the same surface area as 1 FM. After 16 h of axenic promastigote to amastigote differentiation,

flagellar shortening of all cells is complete (Wheeler et al., 2015). Therefore, assuming a model where flagellar EV release drives shortening and a constant rate of flagellar EV release, after the 4 h of differentiation which is used to prepare our DIF EVs we can predict that a quarter of 35.4, 8.9, EVs would be released per flagellum. This rough prediction is close to the measured value of 8.3 DIF particles per *L. mexicana* cell (*Section 3.2.5*), which is surprising given the expected loss of EVs during isolation. While it is encouraging that the measured data is in the same range as the prediction, there is reason to doubt the accuracy of the measured 8.3 particles per cell. A problem with NTA is the inability to distinguish vesicles from non-vesicle particles such as aggregated protein and inorganic crystals present in the medium or PBS, although the fact that medium only controls have >40-fold lower particle concentrations than EV samples (*Section 3.2.7*) suggests that the majority of particles measured in EV samples are *L. mexicana*-derived. The Nanosight used in this study is able to measure green fluorescent particles which would, in theory, allow the use of specific markers. However, the fluorescent signal of isolated EVs from the SMP1::eYFP cell line was below the detection limit of the camera. It would be advisable in future experiments to use a cell membrane dye to stain isolated EVs for NTA in order to measure only membranous particles.

Our data show a clear temporal correlation between flagellar shortening and EV numbers. What is missing to show a causal relationship between flagellar EV release and flagellar shortening are control experiments using either mutant flagella-less cell lines or a cell line which does not undergo flagellar shortening during differentiation to show whether increased EV release and FM elaborations are still observed.

Unfortunately, we were unable to find a flagella-less control cell line; existing 'flagella-less' mutant cell lines, including IFT protein KOs, possess a flagellar transition zone and still synthesize and shed FM (unpublished data from our lab), and we have been unable to generate mutant cell lines which do not undergo flagellar shortening upon differentiation (*Section 3.2.3*). However, live time-lapse imaging provides some evidence that flagellar EV release can cause shortening, since these images seem to show flagellar EV release and nanotube formation at the tip leaving behind a shorter flagellum (Figure 3.8C, E).

3.3.2. Insights into flagellar EV biogenesis

Studies in other organisms have shown dependency of flagellar EV release on active actin (Nager et al., 2016) or ESCRT-related (Long et al., 2016) proteins; we show that protein synthesis inhibition leads to a reduction in FM elaboration (Figure 3.4), supporting the dependency of this process on *de novo* protein synthesis. Although, since protein synthesis inhibition has global effects on cellular function, it is likely that differentiation itself is inhibited. This is supported by our observations of differentiating cells in the presence of cycloheximide showing that morphological differentiation, including flagellar shortening, is stalled (Figure 3.5), therefore reductions in FM elaboration may be a secondary effect. Interestingly, while global translation is attenuated by ~20% during differentiation via eukaryotic initiation factor 2α phosphorylation (Cloutier et al., 2012), it is likely that increased translation of a subset of proteins is necessary to drive differentiation: the translation of certain developmentally regulated proteins such as A2 (Cloutier et al., 2012) and HSP83 (Larreta et al., 2004) is upregulated during differentiation, although whether this is necessary to drive differentiation was not addressed in these studies. To our

knowledge, we provide the first published evidence that *de novo* protein synthesis is required for morphological differentiation of *L. mexicana*. KO of specific proteins, such as Vps4 which was knocked down in *C. reinhardtii* leading to reduced EV release and flagellar shortening, could be carried out to learn more about the mechanisms underlying these processes in *L. mexicana*.

We show that both blebs and nanotubes can release EVs (Figure 3.8), but whether these structures form and release EVs by distinct mechanisms requiring different protein machinery and/or membrane domains is not clear. Intriguingly, the dynamics of EV release from the FM (Figure 3.8) resemble the phenomenon known as pearling (Jelercic and Gov, 2015). It would be interesting to carry out high resolution time-lapse imaging of *L. mexicana* FM nanotubes in cells with stained or tagged actin to establish whether this process is analogous to pearling. The fact that both FM blebs and nanotubes are formed within infected macrophages reassures us that the FM elaboration analyses carried out on cells in culture have some relevance. These in-culture studies are highly reproducible under different conditions and in different cell lines, i.e. with and without FCS and in cell lines with tagged or untagged SMP1. Whether the absolute levels of FM elaborations are the same in culture and within macrophages remains an open question, which could be easily addressed by quantifying FM elaborations at the same time points as were used for the axenic experiment (0, 4, 8 and 32 h) in z-stack images of macrophages infected with *L. mexicana* stationary phase Clone 3 promastigotes.

Previous published data has shown a massive increase in surface membrane blebbing and EV production of *L. mexicana* following a 4 h heat shock at 37°C (Hassani et al.,

2011). It was not clear whether the surface blebs were the source of the EVs, however. Furthermore, the biological significance of this effect is open for discussion, since these temperature-shocked cells arguably did not look healthy and *L. mexicana* would usually replicate in skin-resident macrophages where the temperature would be lower than 37°C. We were unable to reproduce these results (Figure 3.3C); it is possible that additional conditions such as particular medium supplements are needed to induce this effect. Based on our data, though, it seems obvious that heat-shock alone is not sufficient to cause a massive increase in membrane blebbing.

3.3.3. Generation of KO cell lines for FM nanotube and EV biogenesis studies

KO cell lines for three EV biogenesis proteins Actin, Erk1 and tetraspanin, and six flagellar length control proteins were generated in the search for a protein which is essential for FM nanotube formation. In addition, these cell lines will be useful as tools for future studies on *L. mexicana* EV biogenesis and flagellar EV release. To our knowledge, this is the first time an actin null mutant cell line has been generated; in mammalian cells, KOs of one actin isoform have been achieved but other isoforms remained present (Bunnell et al., 2011, Tondeleir et al., 2012). *L. mexicana* has only one encoded protein with very high sequence homology (70% identity) to mammalian actin which is annotated as actin (LmxM.04.1230), however several actin-like proteins with actin domains are also encoded. Further research into the identity and function of these actin-like proteins is necessary before we could confirm our generation of an actin null mutant. If a null mutant has indeed been generated, this may indicate the relative unimportance of actin in *Leishmania* spp., which rely largely on a microtubule-based rather than actin-based cortical cytoskeleton for cell shape and movement (Sahasrabuddhe et al., 2004, Gull, 1999). *L. mexicana* actin may not be essential but

the KO was the only cell line in this study which grew substantially slower than the parental (Figure 3.15), suggesting actin may have important functions which are currently poorly understood (Sahasrabuddhe et al., 2004). Despite two attempts, KO of three ESCRT-related proteins which would have been valuable cell lines for the study of EV biogenesis, given the widespread importance of ESCRT in vesicle formation (Obita et al., 2007, Colombo et al., 2013), was unsuccessful. The development of a conditional KO system in *L. mexicana* (which does not possess siRNA machinery (Lye et al., 2010)) would be invaluable for this line of study. All KO cell lines were able to form FM nanotubes (Figure 3.14), showing that none of the deleted genes are essential in this process. However, it would be interesting to quantify the frequency of FM nanotubes in these KO cell lines to capture any subtle effects. It would also be worthwhile to directly measure the level of EV release (by NTA, for example) from the KO cell lines to see if any are likely to be involved in EV biogenesis. In addition, all KO cell lines were able to fully morphologically differentiate to amastigotes with short flagella within 24 h (data not shown), suggesting they have no obvious defects in flagellar shortening, although the detailed kinetics of shortening were not quantified.

3.3.4. Arl3A plays a role in the FM localisation of SMP1

The only other KO cell line with obvious changes in flagellar length was the Arl3A null mutant which has flagella ranging from residual to normal length, similar to the phenotype observed under conditions of constitutively active Arl3A overexpression (Cuvillier et al., 2000). Interestingly, the FM-enriched localisation of N-terminally myristoylated protein SMP1 is disrupted in this cell line, with SMP1 distributed across the cell body and FM (Figure 3.14). An *Arl3A* add-back (AB) cell line would have to be

generated to prove that this phenotype is due to the absence of Arl3A. This mislocalisation phenotype is consistent with the known role of mammalian Arl3, which mediates the ciliary localisation of myristoylated proteins by triggering their release from Protein Unc-119 Homolog A which targets them to the cilium (Ismail et al., 2012). Arl3 is widely conserved in ciliated organisms (Avidor-Reiss et al., 2004). Arl3A has been previously implicated in *Leishmania* flagellar function since Arl3A mutant cells had short flagella (Cuvillier et al., 2000), but it was not clear whether this phenotype was related to its known function in mammalian cilia; our result suggests that the role of Arl3 in flagellar protein localisation may be conserved between *Leishmania* spp. and mammals.

3.3.5. The FM as a source of EVs

Fluorescence imaging and quantification of isolated *L. mexicana* EVs from a cell line with fluorescently tagged FM and cell body membrane proteins suggests that the majority of EVs observed are flagellar-derived (Figure 3.21). This simple method is, to the best of our knowledge, a novel approach which is not widely used for studying the subcellular origin of EVs. One problem, however, is that we cannot conclude that the fluorescent foci observed are EVs, they may be aggregated protein or other cellular debris. This could be addressed using high pressure freezing to preserve native fluorescence of whole-mount or thin-section EVs isolated from Clone 3 cells, followed by correlative fluorescence and electron microscopy to see whether fluorescent foci correspond to EVs. This approach would also address another issue: non-fluorescent EVs may come from cellular compartments other than surface membranes (exosomes for example) and are not visible by fluorescence microscopy. It is therefore possible that a large number of other EVs are present and unaccounted for in our analysis and

that flagellar-derived EVs could constitute a much smaller fraction of total EVs. Another issue is that we assume EVs labelled with the fluorescently tagged FM protein SMP1::mCh are therefore FM-derived. This may not be true; surface membrane proteins inevitably spend some of their time being trafficked in intracellular vesicles which could either be released as exosomes or by lysed cells and isolated alongside EVs. As far as we know, cell body membrane and FM proteins are not trafficked by distinct subsets of intracellular vesicles, therefore the fact that isolated vesicles labelled with both tagged FM and cell body membrane proteins are not observed argues to some extent against this possibility. Despite these caveats, these data support the hypothesis that the FM is a source of EVs and that FM shedding increases during differentiation.

3.3.6. Analysing a heterogeneous population of EVs and contaminants

We show that EVs isolated from *L. mexicana*-conditioned medium range in size from ~30-300 nm (Figure 3.17). This size range leaves open the possibility that both exosomes (~40-100 nm) and microvesicles (~50-1000 nm) are present. Negative staining EM relies on the adsorption of objects in suspension to grids which is likely to vary depending on object size and charge, therefore we cannot be sure that the distribution of size ranges observed by this technique reflect the true distribution. By negative staining EM, the most abundant EVs are in the <40 nm size range (Figure 3.17) therefore they would not be classified as EVs according to most published sources (Reviewed in (Raposo and Stoorvogel, 2013)). EVs as small as 20 nm have also been observed in other studies (Huebner et al., 2015, Akers et al., 2016) but the functional importance of these smaller vesicles is unknown. Indeed, whether or not they are true membrane-bound vesicles is hard to tell from negative staining EM

images, it is possible they are non-vesicle aggregates. Vesicles with ~150 nm diameters were observed by cryo-EM and confirmed to be bona fide vesicles surrounded by a lipid bilayer (Figure 3.18); <40 nm diameter vesicles were not visible by cryo-EM in our hands therefore we were unable to confirm whether they are true vesicles. A major limitation of this study is that these smaller 'vesicles' are below the detection limit of our nanoparticle tracking analyses (Figure 3.22A), therefore we do not know whether they are produced at higher levels during differentiation like the larger EVs.

We observe filamentous protein contamination in crude isolated EV samples (Figures 3.16 and 3.17), confirming that these samples are impure and therefore any effects observed in experiments using these samples may be due to non-vesicle-associated material rather than EVs themselves. Based on the facts that SAP is known to be a secreted filamentous protein in *L. mexicana* which looks very similar by negative staining EM in published data to our observations (Stierhof et al., 1998, Ilg et al., 1991) and that SAP is the top hit in MS analysis of our EV samples (Table 4.2, Chapter 4), it is likely that SAP is the contaminating filamentous protein. Further purification of EVs using density gradient separation goes some way to addressing this problem and we successfully enrich for EVs in two of the less dense fractions (Figure 3.19A); these results are similar to those in previously published EV density gradient analyses (Cvjetkovic et al., 2016). Our result that particle yield is higher using differential centrifugation followed by density gradient separation compared to differential centrifugation alone (*Section 3.2.5*) is unexpected, since the former method includes more wash steps which are likely to reduce yield. The most likely explanation for this

result is that particle concentrations of Optiprep fractions excluding 2 and 3 were below the optimal minimum concentration, which increases the standard deviation and therefore the error of these measurements (Malvern, 2015, Liu and Zhang, 2012) (it was not possible to increase the concentrations of these fractions due to the Nanosight requirement for a large sample volume of 1 ml). While these density gradient separated fractions are undoubtedly purer than EVs isolated by differential centrifugation alone, no clear segregation based on EV size is observed and the non-vesicle-associated material content of each fraction is unknown, meaning that more analysis would have to be done to be confident that any effects induced by these fractions are not due to non-vesicle contamination. These analyses could involve comparing the effects of EVs which have been either treated or untreated with membrane impermeable proteases.

3.3.7. Conclusions and outlook

To conclude, we show that in *L. mexicana,* EVs are released from FM blebs and nanotubes (Figure 3.8) and that this process is likely to play a role in shortening of the flagellar membrane during promastigote to amastigote differentiation. Both FM elaborations (Figure 3.2) and EV release increase significantly during differentiation (Figure 3.22). Whether EV release is the only mechanism contributing to FM shortening cannot be answered from this study. Our data suggest that the flagellum is the major source of EVs in *L. mexicana* (Figure 3.21), but more experiments which take into account all EV sub-populations are needed to show this conclusively. The mechanisms governing FM bleb and nanotube formation and EV release are a potentially very interesting area of future study, being poorly understood in all other model organisms as well as *Leishmania* spp., and systematic KO screens could address

this. The KO cell lines already generated here would be useful in such studies (Figure 3.13).

KO cell lines of candidate EV biogenesis proteins and proteins involved in flagellar length control were generated (Figure 3.13), including an actin null mutant which we believe may be the first in any species. None of these proteins appear to be essential for FM nanotube formation (Figure 3.14) or flagellar shortening, but the ability of these cell lines to release EVs remains an interesting open question. We were unable to KO any ESCRT or excocyst proteins, which could highlight their importance in *L. mexicana* cell function. We show that SMP1 is mislocalised in Arl3A KO cells (Figure 3.14), suggesting that *L. mexicana* Arl3A may be involved in a conserved mechanism of myristoylated FM protein targeting which has been described in mammalian cells.

4. Biochemical and molecular characterisation of *L. mexicana* EVs

4.1. Introduction

4.1.1. Protein cargo of *Leishmania* EVs

Studies of EV composition have mostly focussed on protein and RNA content with a small number of lipidomic studies (proteomic and lipidomic research is reviewed in (Kreimer et al., 2015); RNA studies reviewed in (Lefebvre and Lecuyer, 2017)). This study has focussed mainly on EV protein composition. The EV proteomes of diverse species, cell types and bodily fluids have been studied: from porcine mesenchymal stem/stromal cells (Eirin et al., 2016), bovine milk (Samuel et al., 2017a), human plasma and urine (Welton et al., 2016), human colorectal cancer cells (Choi et al., 2012) to *C. reinhardtii* (Long et al., 2016). Proteins commonly identified as EV cargo include ESCRT-related proteins such as Alix and Tsg101, tetraspanins including CD9, CD63 and CD81, lipid raft associated proteins such as flotillin, and HSPs (Kowal et al., 2016, Raposo and Stoorvogel, 2013). In addition to these common markers, the composition of EVs has been found to reflect that of the cells of origin (Corbetta et al., 2015, Minciacchi et al., 2017). Therefore, the proteomic study of EVs in biofluids has been intensive due to the potential benefits of finding biomarkers for disease (reviewed in (Yokoi et al., 2015)).

Several proteomic MS studies have been carried out on *Leishmania* EVs: EVs isolated from stationary phase *L. donovani* promastigotes (Silverman et al., 2010a, Silverman et al., 2010b), WT and GP63 KO *L. major* promastigotes (Hassani et al., 2014) and EVs secreted by *L. major* and *L. infantum* within the sand fly midgut (Atayde et al., 2015). Furthermore, entire *Leishmania* exoproteomes have been analysed (containing all

secreted proteins including EV-associated proteins): from *L. donovani* stationary phase promastigotes (Silverman et al., 2008), *L. braziliensis* promastigotes (Cuervo et al., 2009), and *L. mexicana* promastigotes under temperature-shock conditions (Hassani et al., 2011). There is considerable overlap between exoproteomes and EV proteomes: one study found that 52% of 358 proteins identified in an *L. donovani* exoproteome (Silverman et al., 2008) were also found in an *L. donovani* EV proteome containing 329 proteins (Silverman et al., 2010a). There is likely to be considerably more sample loss in the preparation of EVs compared to supernatants for exoproteome analysis, which may result in the identification of fewer proteins; supernatants are prepared by removing whole cells by relatively low-speed centrifugation (Hassani et al., 2011, Cuervo et al., 2009, Silverman et al., 2008), while the majority of EV studies prepare samples using either ultracentrifugation (Silverman et al., 2010a, Hassani et al., 2014, Atayde et al., 2015) or ultrafiltration (Silverman et al., 2010b) followed by sucrose density gradient separation.

The protein banding patterns of *Leishmania* EVs were found to be less complex and distinct from those of whole cells (Silverman et al., 2010a), supporting the idea that there is enrichment of specific proteins within EVs and that isolated EVs are not simply whole cell debris. The total number of proteins identified by MS in *Leishmania* EV proteomes ranges from 61 in a study on *L. major* EVs isolated from sand fly midguts (Atayde et al., 2015) to 424 proteins identified in EVs isolated from 7 day *L. major*-conditioned medium (Hassani et al., 2014). This compares to 3999 proteins identified in a recent proteomic analysis of whole *L. donovani* cells (Nirujogi et al., 2014), showing the relative lack of protein complexity in EVs. The comparison of whole cell

and EV proteomes to find EV-specific proteins may yield promising candidate EV markers in the future.

Proteins commonly identified in *in vitro Leishmania* EV and exoproteome studies include SAP, EF-1α, enolase, HSPs, surface antigens, GP63, histones, calpain-like cysteine peptidases, P-type ATPases, tubulin, and proteasomal and ribosomal proteins (Atayde et al., 2015, Silverman et al., 2010a, Silverman et al., 2010b, Hassani et al., 2014, Cuervo et al., 2009, Hassani et al., 2011, Silverman et al., 2008). Similar proteins were identified in *Leishmania* EVs isolated from sand fly midguts and inocula (Atayde et al., 2015) to those isolated from promastigotes *in vitro* (Silverman et al., 2010a), suggesting that results from *in vitro* isolated EVs may be applicable to the *in vivo* situation. Among these proteins, SAP is a known secreted, non EV-associated, filamentous protein (Stierhof et al., 1998) and enolase is a known secreted protein in *Leishmania* spp. (reviewed in (Avilan et al., 2011)). EF-1α (Momen-Heravi et al., 2013) and HSPs, particularly HSP70 and HSP90 (Faught et al., 2017, Vega et al., 2008, Yoshioka et al., 2013), are known EV-associated proteins across diverse mammalian cell types which are often used as EV markers. In addition, secreted EF-1α is likely to be a *Leishmania* virulence factor (see Introduction) (Nandan et al., 2002). In the EV field, the search is ongoing for better EV markers since current ones, such as EF-1α and HSPs, are also abundant in whole cells and therefore their presence in EVs does not exclude the possibility of whole cell contamination. Ideally, good EV markers would also distinguish between exosomes and microvesicles. Some mammalian EV markers such as tetraspanins CD63, CD9 and CD81 (Kowal et al., 2016), seem to be significantly enriched in EVs, particularly exosomes, compared to whole cells, but

these proteins are not present in *L. mexicana* which encodes only 1 tetraspanin (LmxM.32.0170) with no significant homology to any mammalian tetraspanins.

Currently there are no good negative control proteins which are known to be absent in EVs. Histones, proteasomal and ribosomal proteins localise to large complexes present in the nucleus, cytosol/nucleus and cytosol respectively which would not be expected to be secreted, yet they are commonly identified in *Leishmania* EV proteomes (Atayde et al., 2015, Silverman et al., 2010a, Silverman et al., 2010b, Hassani et al., 2014). They are all abundant proteins in whole cells which may mean that even low level whole cell lysis could lead to contamination of EV samples, but it is also possible that these housekeeping proteins have novel functions outside the cell, as has been described for *Leishmania* EF-1α in host macrophages (Nandan et al., 2002); indeed, one study has shown the release of a specific histone H1 variant, thought to be involved in tumorigenesis, in EVs specifically from mammalian oligodendroglioma cells but not astrocytes (Schiera et al., 2013). One way of confirming that a protein of interest is contained within vesicles rather than being a non-vesicle-associated contaminant is to show by WB that it is not degraded in EV samples by a protease such as trypsin. This approach was used on *Leishmania* EVs to confirm that HSP70, HSP90 and EF-1α were present inside vesicles (Silverman et al., 2010a). However, this approach is only useful for non-transmembrane proteins and proteins not associated with the outer vesicle membrane.

4.1.2. Effect of culture conditions on protein secretion

Total promastigote *L. mexicana* secreted protein was shown to increase after 4 h at 37°C compared to 25°C and WBs showed that the secretion of EV-associated proteins GP63 and HSP70, but not control glycosomal protein (Hypoxanthine

phosphoribosyltransferase 1, HGPRT), increased (Hassani et al., 2011). Similarly in *L. donovani*, the presence of HSP70, HSP90 and alpha and beta tubulin in isolated EVs increased after 24 h at 37°C compared to 26°C, as measured by MS (Silverman et al., 2010a). This result was interpreted to mean that the number of EVs released also increased at 37°C since equal loading of HSPs and tubulin in EVs was assumed. The same study also compared EV protein content by MS after 24 h at pH 7 or 5.5 and found some proteins including HSP10 which were enriched at pH 5.5, but no changes in HSP70, HSP90 or alpha and beta tubulin (Silverman et al., 2010a); therefore it was concluded that a drop in pH did not change the level of EV release but may modulate EV cargo. However, conclusions about the level of EV release under these different conditions cannot be drawn with certainty since they were inferred from the levels of HSPs and tubulin rather than quantified directly.

4.1.3. Aims

Several proteomic studies of *Leishmania* EVs from promastigotes or differentiating promastigotes have been published, but a detailed comparison of the EV proteomes of these two life cycle stages has not yet been performed (Atayde et al., 2015, Silverman et al., 2010a, Silverman et al., 2010b, Hassani et al., 2014). We aim to address this open question in a novel MS approach by comparing EVs from PRO and DIF cells and selecting DIF-enriched proteins for further analysis, since we hypothesise that proteins released during flagellar shortening and virulence factors important for the early stages of infection could be enriched in this sample. Once identified, DIF-enriched proteins will be investigated further through a large-scale fluorescent tagging screen. These studies will help to determine the subcellular sources of *Leishmania* EVs, which are currently unknown, and whether the flagellum could be an

important source of EVs (as suggested by our existing data discussed in Chapter 3). To further address this question we will use Western blotting to confirm the presence or absence of a subset of proteins with known cellular localisations in our EV samples. Another reason for wide-scale fluorescent tagging of candidate EV proteins is to find a transmembrane protein with an exclusive FM localisation which is also present in isolated EVs to use as bait for an FM-derived EV pull-down. This would allow us to quantify the proportion of flagellar-derived EVs and to carry out MS analysis of EV subsets.

4.2. Results

4.2.1. Cell body and flagellar markers are detected in whole cell and EV samples

To investigate the composition of *L. mexicana* EVs, PRO whole cell and EV lysates were probed by WBs for a range of proteins as well as the glycoconjugates LPG, SAP and proteophosphoglycans (PPGs) (Figure 4.1A-G), which all have known subcellular localisations. For a subset of proteins, DIF whole cell and EV lysates were also probed (Figure 4.1D-G). Alpha tubulin and binding immunoglobulin protein (BiP) are abundant proteins which localise to the cortical cytoskeleton and flagellar axoneme (Gull, 1999) or ER (Bangs et al., 1993) respectively; both proteins were present in PRO EV as well as PRO WCL samples (Figure 4.1A, B). Paraflagellar rod (PFR)-1, which localises to the flagellar extra-axonemal PFR structure (Santrich et al., 1997), was detected as expected in the PRO WCL sample, but not the PRO EV sample (Figure 4.1C). GT2 and SMP1 are surface membrane proteins localised to the cell body (Rodriguez-Contreras et al., 2015) and flagellum (Tull et al., 2010) respectively; fluorescently tagged copies of both proteins were detectable in PRO and DIF WCL samples from Clone 3 (see Figure 3.1) cells, as expected, as well as in PRO EV samples, but only SMP1 was detectable in the DIF EV sample (Figure 4.1D, E). Histone H3, a nuclear-localised protein (Postberg et al., 2010), was detectable in PRO and DIF WCL but not PRO or DIF EV samples (Figure 4.1F). Antibody LT22 detects *L. mexicana* linear phosphoglycan repeats which are present in the glycoconjugate LPG (see Figure 5.1) as well as the glycosylated proteins PPGs and SAPs (Ilg et al., 1993, Stierhof et al., 1999); these phosphoglycan repeat-containing structures are predominantly cell surface-localised (Ilg, 2000). LPG-positive bands were detected in PRO and DIF WCL

samples between ~35-50 kDa and in PRO and DIF EV samples between ~30-40 kDa; high molecular weight bands corresponding to PPGs and SAPs (Ilg et al., 1993) were also present in all samples and the bands were stronger in the EV samples (Figure 4.1G).

These WBs show that both the cell body membrane marker GT2 and the FM marker SMP1 are present in EV samples, in addition to the ER marker BiP and the cytoskeletal protein alpha tubulin. Absence of the abundant flagellar axonemal protein PFR2 and nuclear histone H3 suggests there is selective loading of cargo into EVs, and that the EV samples are not significantly contaminated with whole cells.

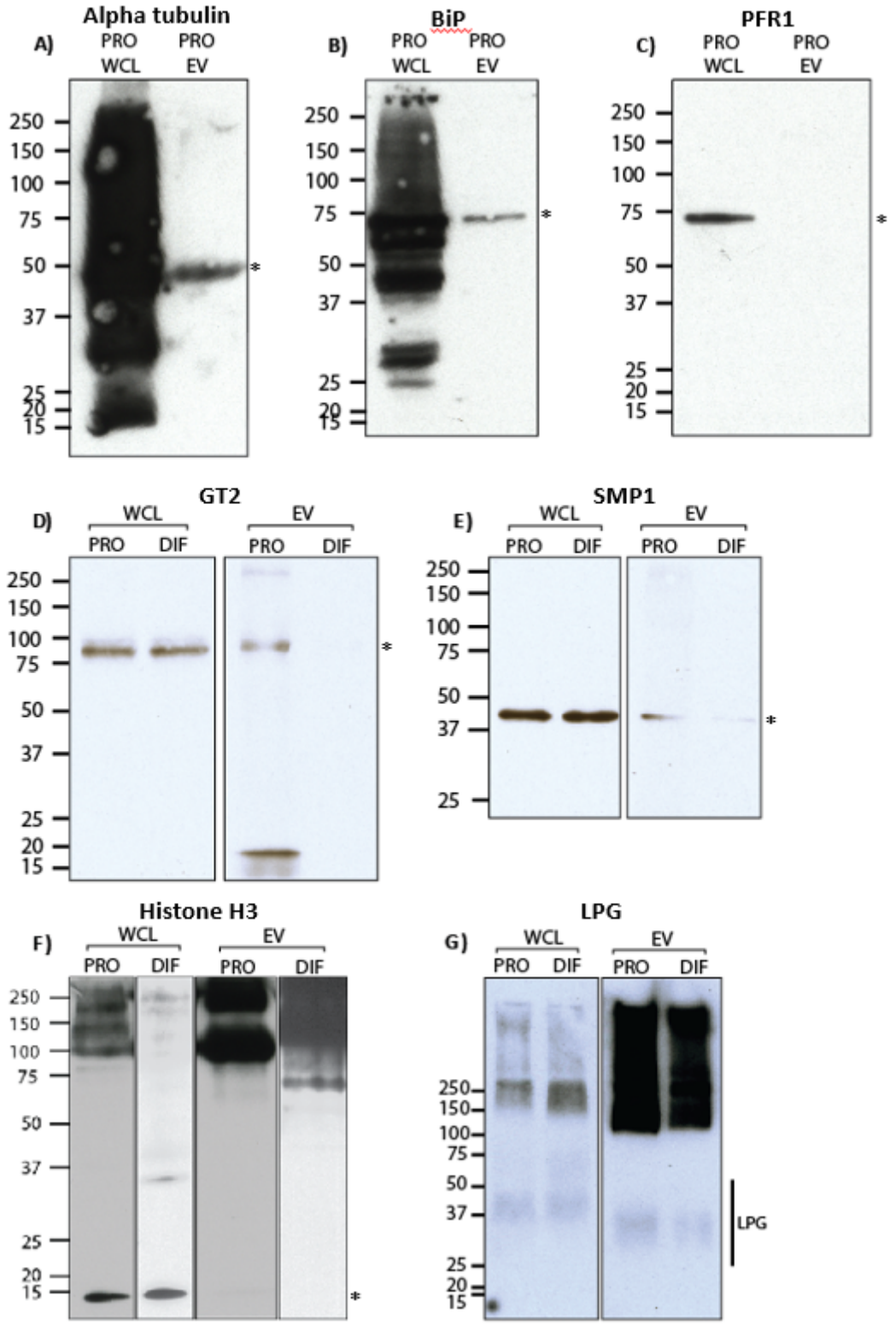

Figure 4.1. Western blotting of *L. mexicana* whole cells and EVs for a range of proteins and glycoconjugates. WCLs or EV lysates were made from PRO or DIF Clone 3 cells, electrophoresed on a SDS-PAGE gel, transferred to nitrocellulose membranes and probed for

A) alpha tubulin **B)** BiP **C)** PFR1 **D)** GT2::eGFP:TY **E)** SMP1::mCh **F)** histone H3 or **G)** LPG, PPGs and SAPs. The expected size range of LPG is indicated on the blot and the higher molecular weight bands correspond to PPGs and SAPs. 4.10^6 cell equivalents of WCL and 2.10^9 of EV lysate were loaded per lane. Many non-specific bands are present and obscure the expected specific band in the anti -alpha tubulin and -BiP PRO WCL samples although the shortest possible membrane exposure time was used. The expected sizes of the proteins and all blotting conditions are shown in Table 2.2 in Materials and Methods and are indicated by asterisks (*). Numbers to the left of the panels indicate molecular weights in kDa.

4.2.2. Protein mass spectrometry of EVs identifies known virulence factors, known EV-associated proteins and unannotated proteins

WBs give us a valuable but very limited view of EV composition and our aim was to use MS to probe the proteomic composition of EVs more fully. First, the overall proteomic complexity of PRO and DIF WCL and EV samples was compared using Sypro Ruby staining to reveal protein banding patterns (Figure 4.2). As expected, the WCL samples displayed complex banding patterns with proteins of all sizes present from 25-250 kDa and strong bands present at ~50 kDa (corresponding to alpha and beta tubulin), with no obvious differences between the PRO and DIF samples. The PRO and DIF EV samples displayed 7 visible bands in common and the DIF sample displayed 1 additional band at ~60 kDa; no distinct bands were visible with molecular weights below 40 kDa. Given that GP63 (LmxM.10.0470) was found to be more abundant in DIF than PRO EV samples by MS analysis (Table 4.2) and that its molecular weight is 63.7 kDa, it is possible that this is the identity of the additional band. Three of the strongest bands in both samples were identified by MS as SAP, HSP70 and beta tubulin (Figure 4.2). Given that SAP is a known secreted filamentous protein (Stierhof et al.,

1998) and HPS70 and tubulin are commonly detected in *Leishmania* EVs (Silverman et al., 2010b), this data confirms our EM studies of EV samples which show that secreted proteins and EVs are present in EV samples (Figure 3.16 and Figure 3.17).

In preparation for MS sample analysis, the protein concentrations of PRO and DIF EV samples were measured by Bradford assay (Figure 4.3) and the mean masses of protein per 10^9 cell equivalents of EV sample were 2.25 µg and 0.59 µg respectively (Figure 4.4). 3 PRO and 3 DIF EV samples with total protein contents between 1.5-20 µg (Table 4.1) were submitted to in-gel tryptic digest followed by label-free MS (see Materials and Methods).

In total, 901 proteins were identified in PRO EV samples and 978 in DIF EV samples with 605 in common (Figure 4.5A). Lists of all proteins identified in all samples by a MS/MS ion search using Mascot software against a recently re-annotated *L. mexicana* genome (Fiebig et al., 2015) are given in Appendix 1. GO term enrichment analysis of proteins present in every PRO repeat and every DIF repeat are given in Appendix 2. There was significant variation between the triplicate samples with only 144 of 901 proteins found in every PRO EV triplicate sample (Figure 4.5B, C) and 238 of 978 proteins found in every DIF EV triplicate sample (Figure 4.5B, D). A quality control cut-off Mascot score of >60 was applied to aid the selection of candidate EV proteins for further study (Figure 4.5E-I). Of the 56 proteins present in every PRO EV triplicate sample (Figure 4.5G) and the 127 in every DIF EV triplicate sample (Figure 4.5H), 37 were in common, 19 were unique to PRO EV samples and 90 were unique to DIF EV samples (Figure 4.5F); this latter group of 90 proteins were consistently present in DIF but not PRO EV samples. Since we were interested in identifying proteins enriched in EVs during differentiation and flagellar shortening, these 90 proteins were used as the

list from which the majority of candidate EV proteins of interest for fluorescent tagging were selected ('Enriched in DIF (by manual comparison)' dataset, Table 4.5). We compared our EV MS data to a published *L. major* exosome proteome containing a total of 321 proteins (Silverman et al., 2010b). 205 of these proteins were also identified in at least one of our EV samples and the remaining 116 proteins were found only in the *L. major* exosome proteome (Figure 4.5I). Lists of the 127 proteins found in all DIF EV triplicate samples, the 56 proteins in all PRO triplicate samples, and the 37 proteins in all six samples are shown in Appendix 3.

Many proteins commonly found in previously published *Leishmania* EV proteomes (Atayde et al., 2015, Silverman et al., 2010a, Silverman et al., 2010b, Hassani et al., 2014) and exoproteomes (Cuervo et al., 2009, Hassani et al., 2011, Silverman et al., 2008) were identified, including HSPs, GP63, EF-1α, surface antigens, calpain-like cysteine peptidases, enolase, P-type ATPases, histones, and ribosomal and proteasomal proteins. Of these, all were found in all six EV samples suggesting they are consistent and abundant EV sample-associated proteins, except histones, surface antigens and proteasomal proteins which were found in all DIF EV triplicate samples (Appendix 3).

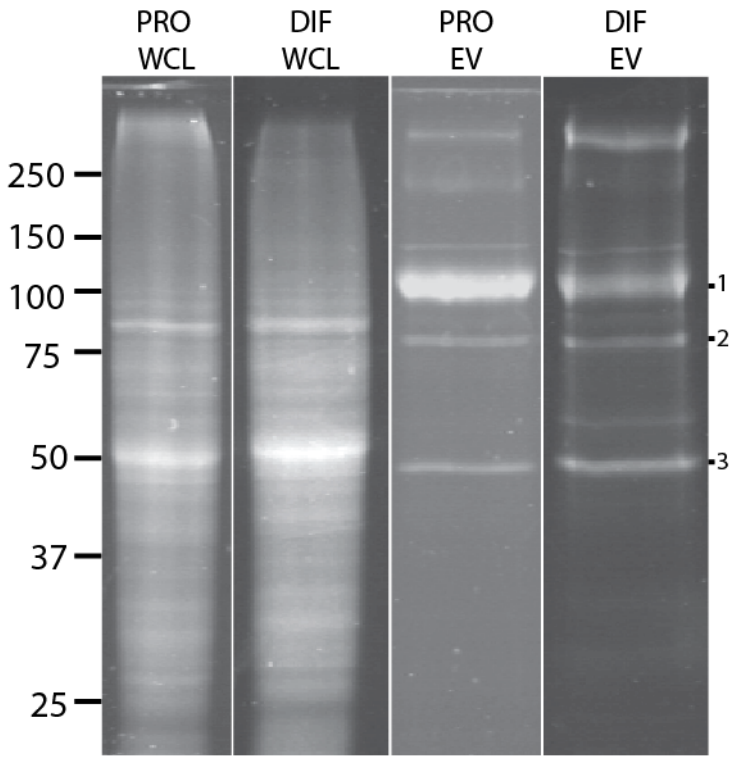

Figure 4.2. Protein banding patterns of representative EV samples submitted for MS. WCLs (4.10^6 cell equivalents per sample) and isolated EV (2.10^9 cell equivalents per sample) lysates from PRO and DIF Clone 3 cells were run on a 10% SDS-PAGE gel and stained with Sypro Ruby. Bands 1, 2 and 3 were submitted for label free MS and identified: 1) histidine secretory acid phosphatase (SAP, LmxM.36.6480) 2) heat shock protein 70 (hsp70, LmxM.28.2770) 3) beta tubulin (LmxM.08.1230). Numbers to the left of the panels indicate molecular weights in kDa.

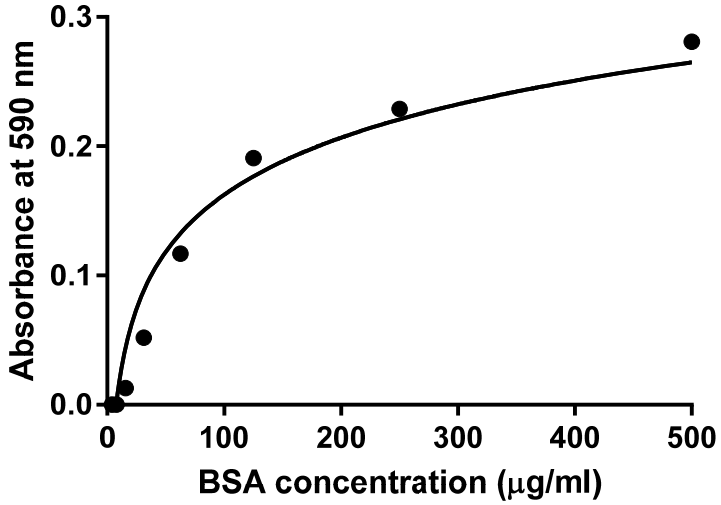

Figure 4.3. BSA standard curve used for Bradford assay protein concentration measurements. A representative standard curve of BSA concentrations ranging from 3.9 to 500 μg/ml used to interpolate protein concentrations of EV samples. The absorbance was measured by spectrophotometer at 590 nm.

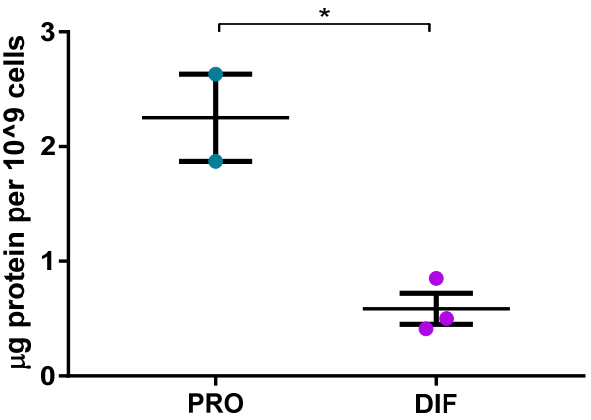

Figure 4.4. Protein content of EV samples submitted for MS is higher in PRO versus DIF samples. PRO and DIF EV samples from Clone 3 cells were resuspended in PBS and their protein content was measured by Bradford assay. Repeat 2 of the PRO EV samples was not measured. The error bars are ± SEM. The asterisk shows significant difference as tested by unpaired t-test with a p value of less than 0.05.

	Protein content of sample (µg)		
	Repeat 1	**Repeat 2**	**Repeat 3**
PRO	9	Not measured	20
DIF	6	1.5	5

Table 4.1. Submission of EV samples for MS. The total protein content of biological triplicates of PRO and DIF EV samples from Clone 3 cells was calculated from Bradford assay measurements (the interpolated values were within the protein concentration range of the standard curve shown in Fig. 4.3). The 6 samples were submitted for label-free MS.

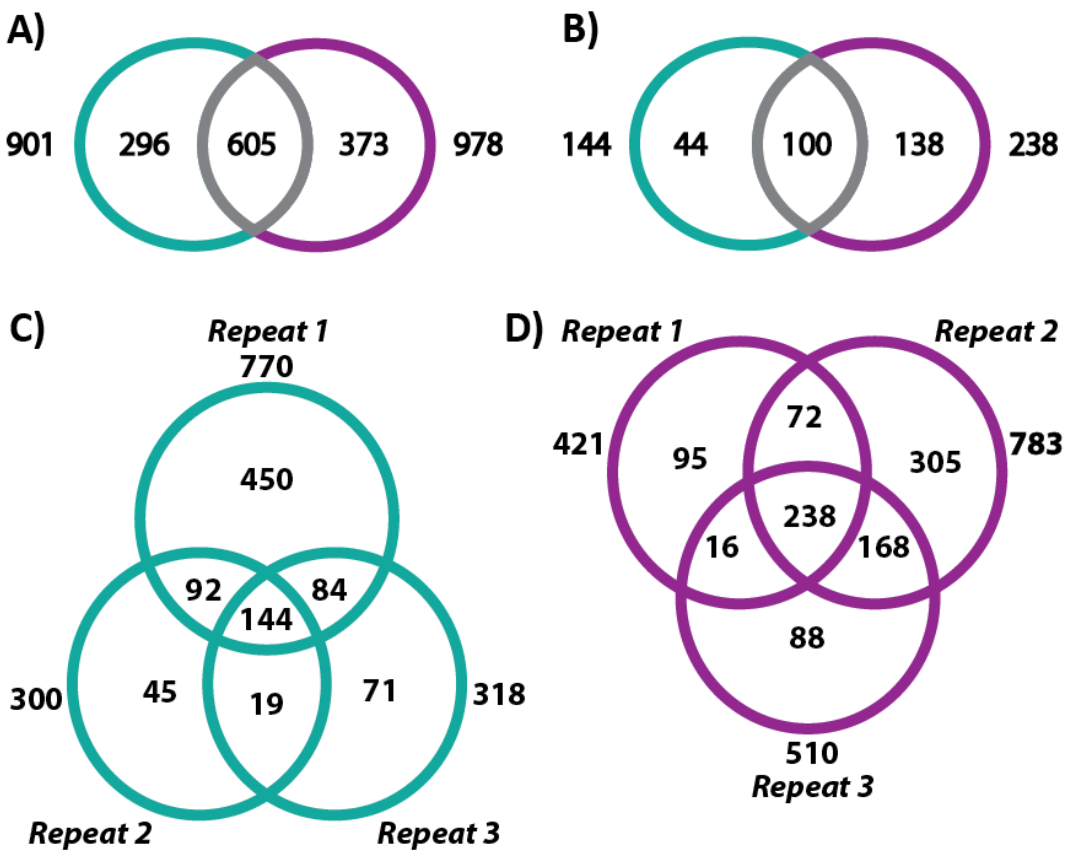

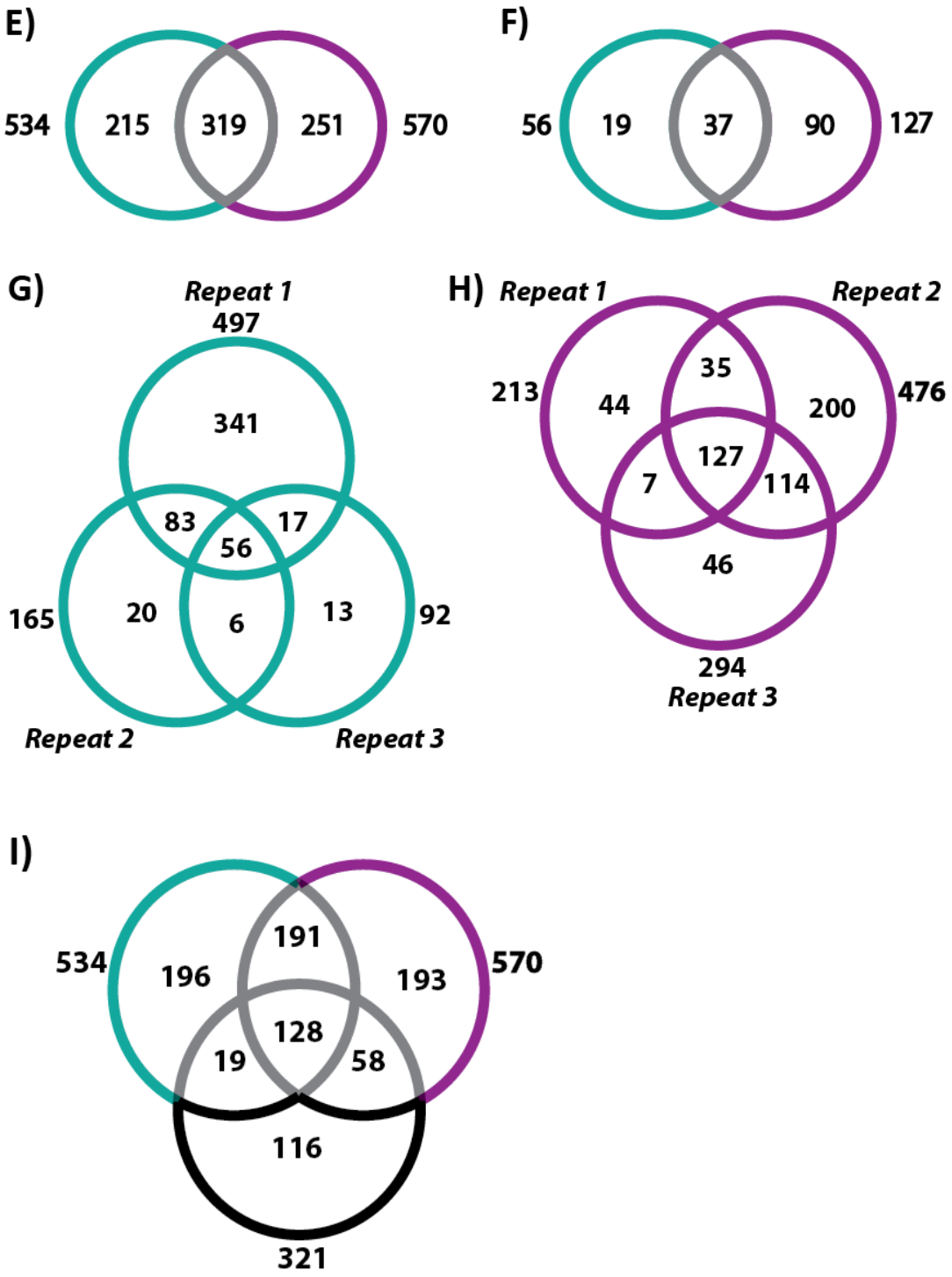

Figure 4.5. Summary of MS data from PRO and DIF EV samples. Unfiltered data (**A-D**) or data with a quality control cut-off of a Mascot score (the higher this score the less likely that this protein was identified by chance) of >60 (**E-I**) is shown. PRO data is shown in turquoise, DIF in purple and data from a published *L. major* exosome proteome in black (Silverman et al., 2010b). **A** and **E)** Turquoise circle: proteins detected in at least one PRO repeat (901 and 534);

purple circle: proteins detected in at least one DIF repeat (978 and 570). **B** and **F)** Turquoise circle: proteins detected in all three PRO repeats (144 and 56); purple circle: proteins detected in all three DIF repeats (238 and 127). **C, D, G** and **H)** these diagrams show the overlaps between the three biological repeats for the PRO **(C** and **G**) and DIF (**D** and **H**) repeats. **I)** Turquoise and purple circles: same as for **E**; black circle: *L. major* exosome proteome proteins (321).

The top ten PRO and DIF EV proteins by Mascot score ranking were identified; neither list contained abundant tubulin or ribosomal proteins which are common MS contaminants. This is surprising given that one of the prominent Sypro Ruby-stained protein bands in the EV samples was identified as beta tubulin (Figure 4.2). Six proteins were found in both lists, including SAP which was the top protein in both cases and known *Leishmania* EV-associated protein and virulence factor EF1-α, (Silverman et al., 2010a) (Nandan et al., 2002) (Table 4.2). HSPs 70 and 83-1 were also found in both lists (Table 4.2), which supports the identification of HSP70 as one of the prominent Sypro Ruby-stained protein bands in the EV samples (Figure 4.2). Four hypothetical or unspecified proteins were among the top ten PRO EV proteins and one was present among the top ten DIF EV proteins (Table 4.2). Three proteins of interest were present in the top ten DIF EV proteins but not the PRO: known virulence factor GP63 (Contreras et al., 2010, Gomez et al., 2009, Halle et al., 2009) and two similar (by protein sequence) but non-identical surface antigen-like proteins which have unknown functions (Table 4.2). GP63 was present in all PRO and DIF EV samples but ranked 17th by Mascot score in PRO EV samples compared to 3rd in the DIF. The two surface antigen-like proteins were only present in one PRO triplicate sample (Appendix 1).

PRO top 10 proteins	
TriTrypDB accession	**Protein description**
LmxM.36.6480	histidine secretory acid phosphatase
LmxM.30.0440	unspecified product
LmxM.17.0080	elongation factor 1-α
LmxM.27.0500	calpain-like cysteine peptidase
LmxM.32.0312	hsp 83-1
LmxM.18.1520	P-type H+-ATPase
LmxM.30.0680	hypothetical protein
LmxM.08.1171	unspecified product
LmxM.08_29.0110	hypothetical protein
LmxM.28.2770	hsp70
DIF top 10 proteins	
TriTrypDB accession	**Protein description**
LmxM.36.6480	histidine secretory acid phosphatase
LmxM.18.1520	P-type H+-ATPase
LmxM.10.0470	GP63, leishmanolysin
LmxM.32.0312	hsp 83-1
LmxM.30.0440	unspecified product
LmxM.28.2770	hsp70
LmxM.04.0190	surface antigen-like protein
LmxM.04.0180	surface antigen-like protein
LmxM.36.0180	elongation factor 2
LmxM.17.0080	elongation factor 1-α

Table 4.2. The top proteins from EV MS analyses. Table showing the 'top 10' proteins present in all PRO (turquoise) or all DIF (purple) repeats ordered by rank. The top proteins were defined by their average ranking across the 3 repeats by highest to lowest Mascot scores. High Mascot scores indicate low probability that the identification was made due to chance (MatrixScience); therefore, the proteins with the highest Mascot scores are likely to be abundant.

In conclusion, 1274 proteins were identified in total in PRO and DIF EV samples. Among the most consistent and abundant proteins identified were proteins commonly found in *Leishmania* EV proteomes, including GP63, EF-1α and cysteine peptidases. A group of 90 proteins of interest were identified which are present in all DIF EV triplicate samples but not all PRO samples, to be further investigated for their potential flagellar association and importance for the establishment of infection.

4.2.3. Analysis of mass spectrometry data and selection of proteins to fluorescently tag

We wanted to check whether our PRO and DIF EV proteome data could inform us about the likely subcellular origin of the EVs by comparing our data to existing proteomic analysis of *L. mexicana* cell fractions (Gluenz lab, unpublished data / Beneke et al., *manuscript in preparation*). For this existing dataset, the proteomes of isolated promastigote *L. mexicana* cell bodies and flagella were analysed and the relative enrichment of each protein in the cell body versus flagellar fractions were calculated and displayed on a scatter plot. PRO (Figure 4.6A) and DIF (Figure 4.6B) EV proteins which were also detected in this existing dataset of ~2500 proteins were overlaid onto the scatter plots showing cell body versus flagellar enrichment. Many PRO and DIF EV proteins were present in both the flagellar- and cell body- enriched fractions with no obvious over-representation in either fraction (Figure 4.6A, B), suggesting that the EVs are likely to be of both flagellar and cell body origin. Surprisingly, only 73% of PRO and 58% of DIF EV proteins were present in the whole promastigote dataset (Table 4.3). The proportion of flagellar-enriched proteins was not significantly different from the expected value in either the PRO or DIF EV datasets (Table 4.3).

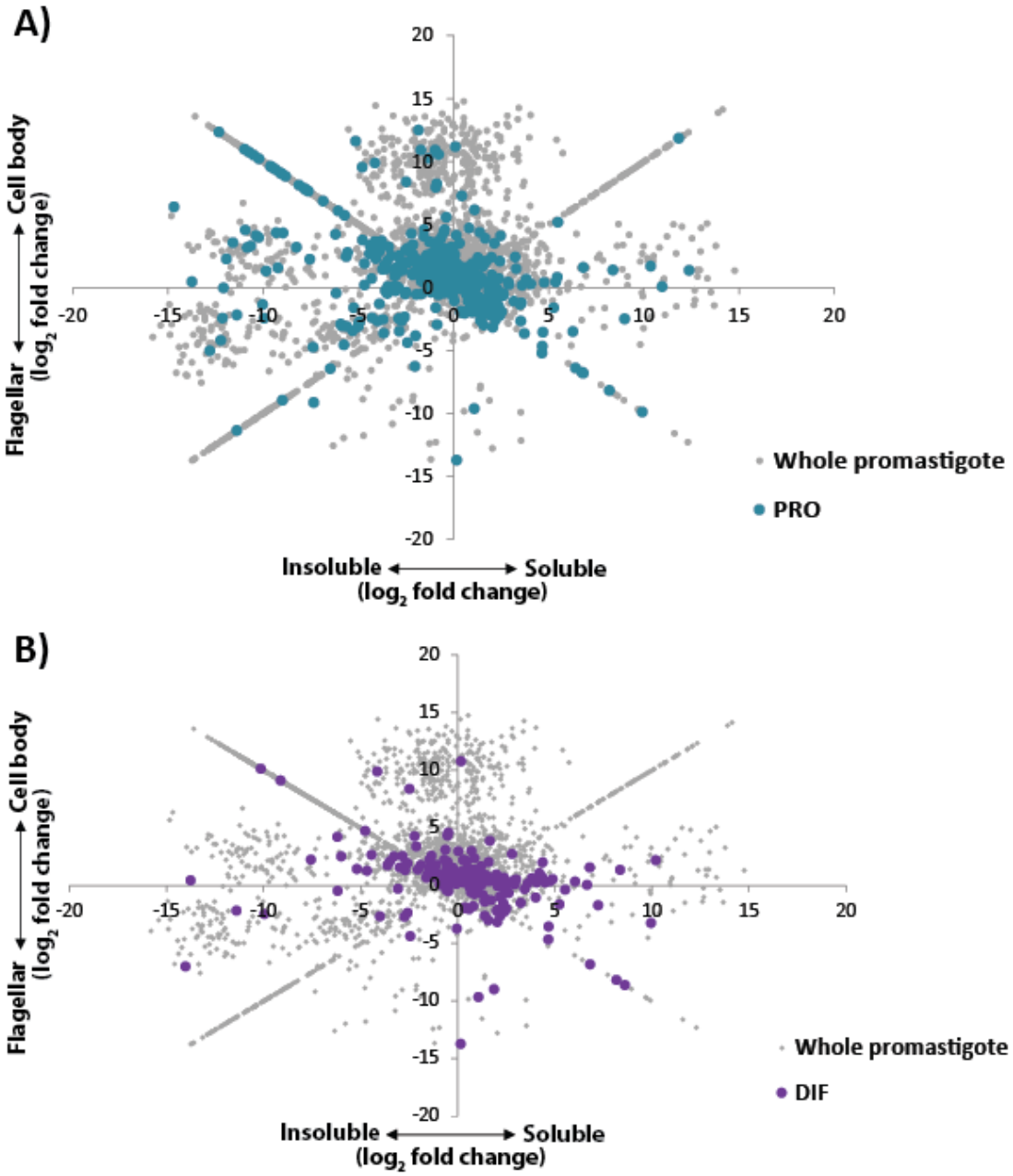

Figure 4.6. Comparison of EV MS data with existing subcellular compartment enrichment data. Previous MS analysis (Gluenz lab, unpublished data / Beneke et al., *manuscript in preparation*) identified ~2500 proteins in cell fractions of *L. mexicana* promastigotes (isolated flagella and cell bodies, each separated into detergent soluble and insoluble pools). Label-free quantification (SINQ, (Trudgian et al., 2011)) was used to determine relative enrichment in flagellar vs. cell body and soluble vs. insoluble fractions (plotted in grey in **A** and **B**). This list was used to search for protein ID matches in PRO and DIF datasets with a threshold Mascot

score of >50 (these are defined as good protein identifications; a slightly lower threshold was used than for previous figures in order to include more proteins). **A)** Turquoise dots: proteins also found in the PRO EV dataset; **B)** purple dots: proteins also found in the DIF EV dataset. Data is shown from one randomly selected biological repeat of PRO (repeat 1) and DIF (repeat 3) EV samples.

	Proportion of proteins present in whole promastigote dataset (%)	Proportion of proteins present in whole promastigote dataset that are flagellar-enriched (%)
PRO repeat 1	73	13
DIF repeat 3	58	14

Table 4.3. Comparison of EV MS data with whole promastigote data. Table showing the proportion of proteins from the EV datasets which were present in the whole promastigote dataset (described in Fig. 4.6), and the proportion of those proteins which were more than 4-fold enriched in the flagellar fraction in the whole promastigote dataset. The proportion of proteins in the whole promastigote dataset which were more than 4-fold enriched in the flagellar fraction was 15%; the proportions of flagellar-enriched proteins in the PRO (13%) and DIF (14%) EV datasets were not statistically significantly different from this expected proportion by Chi-square test.

We then carried out an analysis of the PRO and DIF EV MS datasets of PRO versus DIF enrichment using Proteome Discoverer software (Figure 4.7); proteins which were significantly enriched in either sample formed a list from which candidate EV proteins were selected for fluorescent tagging with a preference for DIF-enriched proteins (Table 4.4, 'Enriched in PRO/DIF (Proteome Discoverer)' dataset Table 4.5). A final list of 43 candidate EV proteins were selected based on the following criteria: absence in

the whole promastigote dataset, suggesting that the bulk of these proteins might be secreted; absence in all PRO replicates, suggesting these proteins are DIF EV-specific; highly abundant proteins as determined by Mascot score, including beta-fructofuranosidase and a P-type ATPase which have been previously identified in *Leishmania* EV proteomes (Atayde et al., 2015), since it would be valuable to learn more about these proteins; enrichment in DIF EV samples since these proteins may be involved in macrophage infection, differentiation and/or flagellar shortening; one protein, an ATP-dependent RNA helicase which has been previously identified in an *L. major* EV proteome (Atayde et al., 2015), which was the most significantly PRO EV-enriched protein was selected; flagellar enrichment, since we are interested in the release of flagellar EVs during differentiation; known components of vesicle secretion pathways since these could be useful controls and it would be valuable to know their localisation in *L. mexicana* (Table 4.5). In addition, preference was given to transmembrane proteins since these could be EV membrane components, and unannotated proteins with unknown functions. Likely contaminating proteins such as ribosomal components were excluded. Additional information about the selected proteins is shown in Appendix 4.

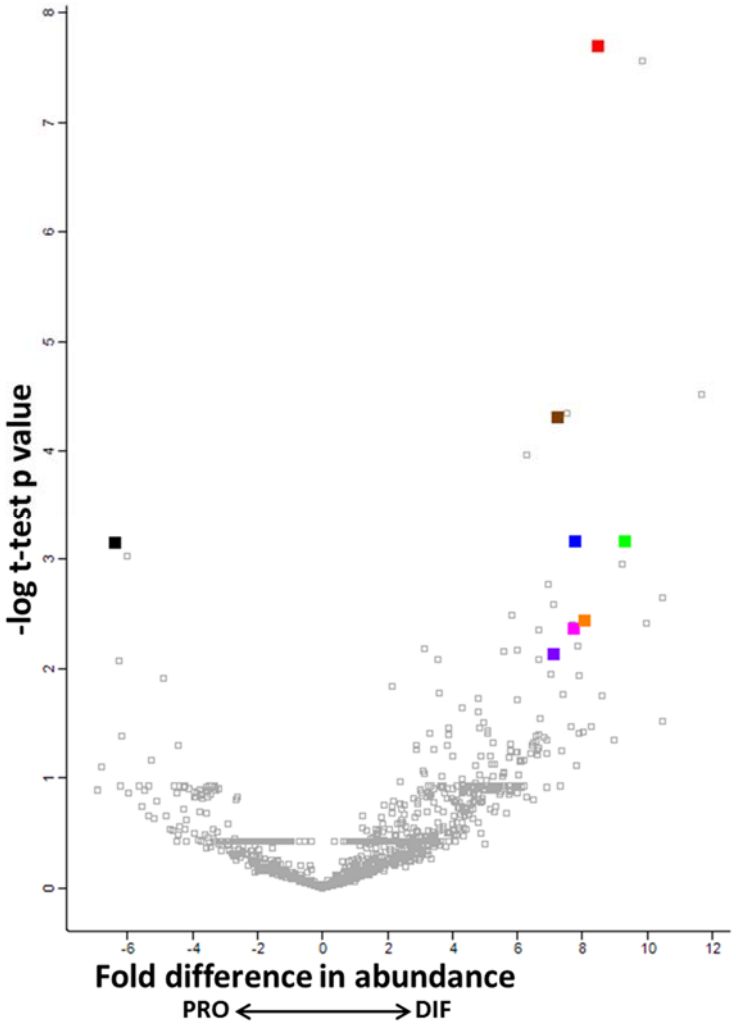

Figure 4.7. Protein enrichment analysis of PRO versus DIF EV MS data. Proteins from the triplicate unfiltered data of PRO and DIF EV samples were analysed by Proteome Discover software (David M. Horn et al.) to measure the enrichment of each protein (indicated by a square) in either sample. Proteins above 2 on the y axis have a t-test p value of less than 0.05 therefore proteins above this cut-off are considered to be significantly enriched in either the PRO or DIF samples. Significantly enriched proteins which were selected for fluorescent tagging based on this analysis are indicated with filled coloured boxes.

	TriTrypDB accession	Description
	LmxM.34.1590	hypothetical protein, conserved
	LmxM.14.0190	hypothetical protein, conserved
	LmxM.19.0570	hypothetical protein, conserved
	LmxM.21.1700	proteasome alpha 2 subunit, putative
	LmxM.23.0200	endoribonuclease L-PSP (pb5), putative
	LmxM.25.1580	casein kinase I, putative
	LmxM.32.2300	udp-glc 4'-epimerase, putative
	LmxM.34.3100	ATP-dependent RNA helicase, putative

Table 4.4. Subset of proteins selected for fluorescent tagging based on enrichment in PRO or DIF EV MS datasets. Table showing the identities of proteins selected for fluorescent tagging based on significant enrichment in PRO or DIF EV samples as described in Fig. 4.7. The coloured squares on the graph in Fig. 4.7 correspond to the colours next to each protein in this table.

TriTrypDB accession	Annotation in TriTrypDB	Reason for fluorescent tagging
LmxM.30.1445	hypothetical protein	Absence in whole promastigote lysates (TB's datset)
LmxM.20.1270	hypothetical protein	
LmxM.24.1410	hypothetical predicted transmembrane protein	
LmxM.26.2680	hypothetical protein	
LmxM.30.0960	unspecified product	
LmxM.34.0040	phosphatidylinositol-specific phospholipase-like protein	
LmxM.10.0630	flagellar glycoprotein-like protein	Absent in PRO
LmxM.04.0310	beta-fructofuranosidase, putative	Abundant in all replicates
LmxM.34.2080	calcium motive p-type ATPase, putative	
LmxM.30.0440	unspecified product	
LmxM.36.5620	isoleucyl-tRNA synthetase, putative	Enriched in DIF (by manual comparison)
LmxM.06.0030	hypothetical protein, conserved	
LmxM.10.0290	isocitrate dehydrogenase [NADP], mitochondrial precursor, putative	
LmxM.10.0380	unspecified product	
LmxM.11.0630	aminopeptidase, putative, metallo-peptidase, Clan MF, Family M17	
LmxM.16.1005	hypothetical protein, unknown function	
LmxM.18.1510	P-type H+-ATPase, putative	
LmxM.20.1280	calpain-like cysteine peptidase, putative, calpain-like cysteine peptidase, Clan CA, family C2	
LmxM.22.0010	hypothetical protein, conserved	
LmxM.24.0761	malic enzyme	
LmxM.25.0910	cyclophilin type peptidyl-prolyl cis-trans isomerase, cyclophilin a, putative (CYPA)	
LmxM.26.1570	thimet oligopeptidase, putative, metallo-peptidase, Clan MA(E), Family M3	
LmxM.27.0190	proteasome alpha 7 subunit, putative	
LmxM.30.0010	5-methyltetrahydropteroyltriglutamate--homocyst ei nemethyltransferase, putative	
LmxM.30.2790	ADP-ribosylation factor, putative	
LmxM.34.1590	hypothetical protein, conserved	
LmxM.36.2020	chaperonin HSP60, mitochondrial precursor	
LmxM.36.3910	S-adenosylhomocysteine hydrolase	
LmxM.14.0190	hypothetical protein, conserved	Enriched in DIF (Proteome Discoverer)
LmxM.23.0200	endoribonuclease L-PSP (pb5), putative	
LmxM.25.1580	casein kinase I, putative	
LmxM.32.2300	udp-glc 4'-epimerase, putative	
LmxM.21.1700	proteasome alpha 2 subunit, putative	
LmxM.19.0570	hypothetical protein, conserved	Enriched in DIF (Proteome Discoverer) and absence in TB's dataset
LmxM.27.1640	hypothetical protein, conserved	Enriched in DIF, known vesicle-associated protein in mammalian cells
LmxM.34.3100	ATP-dependent RNA helicase, putative	Enriched in PRO (Proteome Discoverer)
LmxM.23.1490	hypothetical protein, unknown function	Flagellar-enriched
LmxM.17.0080	elongation factor 1-alpha	Known secreted protein, abundant in all replicates
LmxM.36.6480	histidine secretory acid phosphatase, putative	Most abundant protein, marker for free protein contamination
LmxM.10.0470	GP63, leishmanolysin	Transmembrane version of GP63
LmxM.04.1230	actin	Vesicle secretion pathway
LmxM.32.0170	hypothetical protein, conserved	Vesicle secretion pathway
LmxM.09.0891	polyubiquitin, putative	Vesicle secretion pathway, enriched in DIF

Table 4.5. Proteins selected for fluorescent tagging based on PRO and DIF EV MS analysis. Table showing the accession numbers and descriptions of the 43 where fluorescent tagging was attempted and the reason they were chosen.

4.2.4. Most fluorescently tagged candidate EV-associated proteins do not have a distinct localisation or strong fluorescent signal

We attempted to fluorescently tag 43 candidate EV proteins using either fusion PCR (Dean et al., 2015) or Crispr-Cas9 (Beneke et al., 2017). 36 drug-resistant tagged cell lines were successfully generated, although the presence of fusion proteins of the correct size was not confirmed by Western blot. All cell lines were imaged by

fluorescence microscopy to determine the subcellular localisations of the tagged proteins (Figure 4.8A-I). Four proteins had a cell body membrane localisation (Figure 4.8A), 14 diffuse cytoplasmic localisation (Figure 4.8B) two cell body reticulated (Figure 4.8C), and 11 had no detectable localisation (Figure 4.8D). The remaining localisations were diverse: one nucleolar (Figure 4.8E), one cell body and flagellar neck (Figure 4.8F), one distinct foci (Figure 4.8G), one endosomal (Figure 4.8H) and one FM (Figure 4.8I).

Fields of view displaying several cells were shown to illustrate the localisations of two of the most interesting tagged proteins, LmxM.27.1640 (Figure 4.9A) and LmxM.27.0190 (Figure 4.9B), in more detail. LmxM.27.1640 shares homology and the same domain architecture with ESCRT-associated protein Programmed Cell Death 6-Interacting protein (PDCD6IP), possessing an N-terminal Bro1 domain and C-terminal ALIX V-shaped domain. PDCD6IP, also known as Alix, binds ESCRT proteins Tsg101 and CHMP4 and is thought to help mediate cargo sorting and membrane budding and abscission processes involved in ILV formation and viral release (Odorizzi, 2006). These processes are also essential for EV release, and PDCD6IP has been described as a common EV marker across several species (Gallart-Palau et al., 2015, Buck et al., 2014, Willms et al., 2016) and in human breast cancer cells depletion of PDCD6IP by RNAi led to a 50% reduction in EV production, suggesting a possible role in EV biogenesis (Baietti et al., 2012). In addition, a syntenic homolog of LmxM.27.1640 was also identified in a previously published *L. donovani* EV proteome (Silverman et al., 2010a). Tagged LmxM.27.1640 localised to distinct foci which appeared to localise within the cell body (although it is not possible to tell from these images whether the foci were inside or outside the cell) and on the cell surface including the flagellum and

the number of foci per cell varied (Figure 4.9A). LmxM.27.0190 is annotated as a proteasome subunit (alpha 7) which has been previously identified in *L. mexicana* (Hassani et al., 2011) and *L. braziliensis* exoproteomes (Cuervo et al., 2009). A proteasomal protein would be expected to localise to the cytoplasm and nucleus but not the flagellum (Brooks et al., 2000). Our images showed that tagged LmxM.27.0190 localised to the cell body and flagellum and colocalised with FM nanotubes which were also visualised with SMP1::mCh; this colocalisation was present for all FM nanotubes in the DIF sample and a subset in the PRO sample (Figure 4.9B).

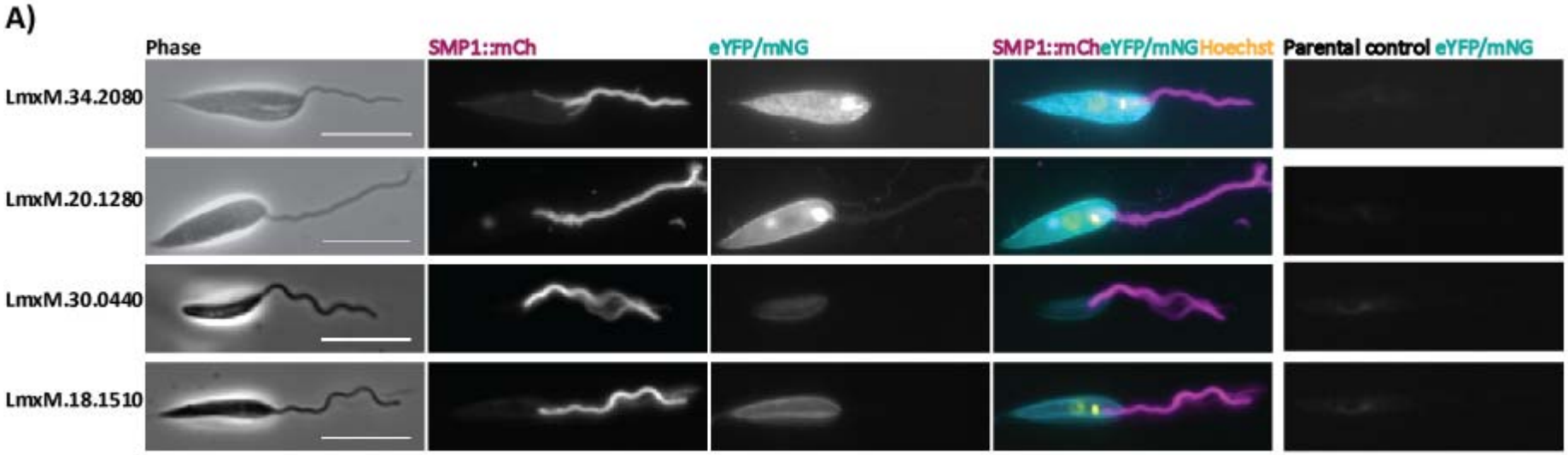
A)
Phase
SMP1::mCh
eYFP/mNG
SMP1::mCheYFP/mNGHoechst
Parental control eYFP/mNG
LmxM.34.2080
LmxM.20.1280
LmxM.30.0440
LmxM.18.1510

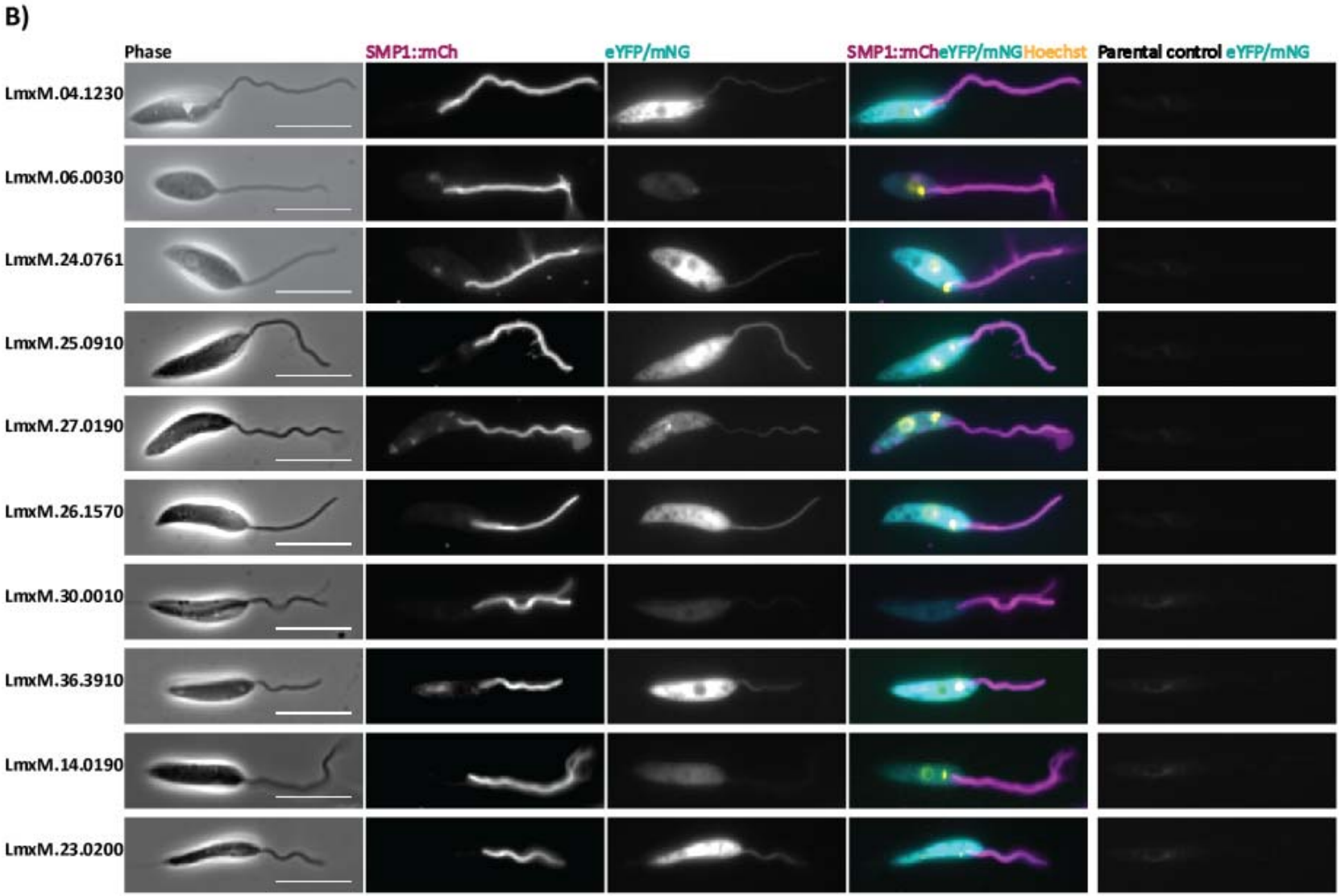
B)
Phase
SMP1::mCh
eYFP/mNG
SMP1::mCheYFP/mNGHoechst
Parental control eYFP/mNG
LmxM.04.1230
LmxM.06.0030
LmxM.24.0761
LmxM.25.0910
LmxM.27.0190
LmxM.26.1570
LmxM.30.0010
LmxM.36.3910
LmxM.14.0190
LmxM.23.0200

B continued)

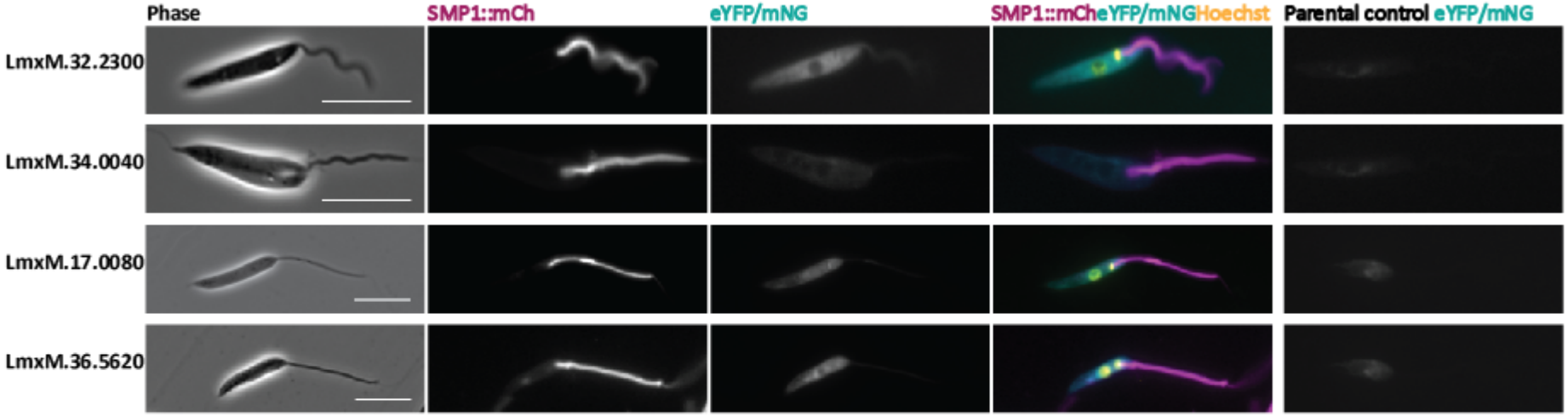

C)

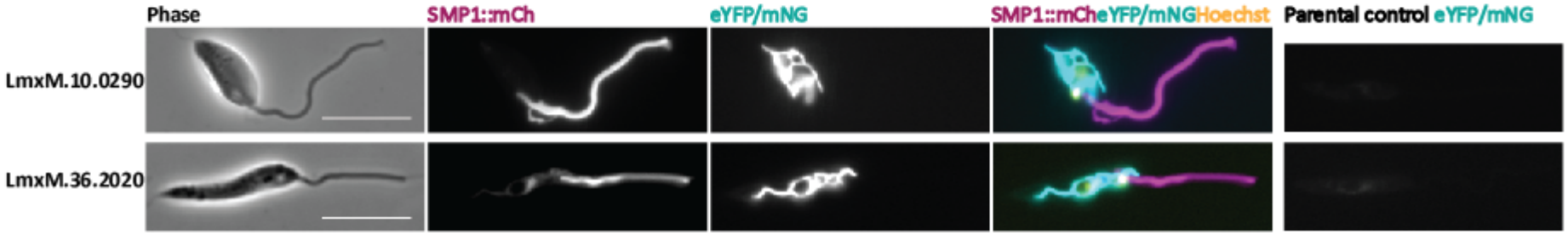

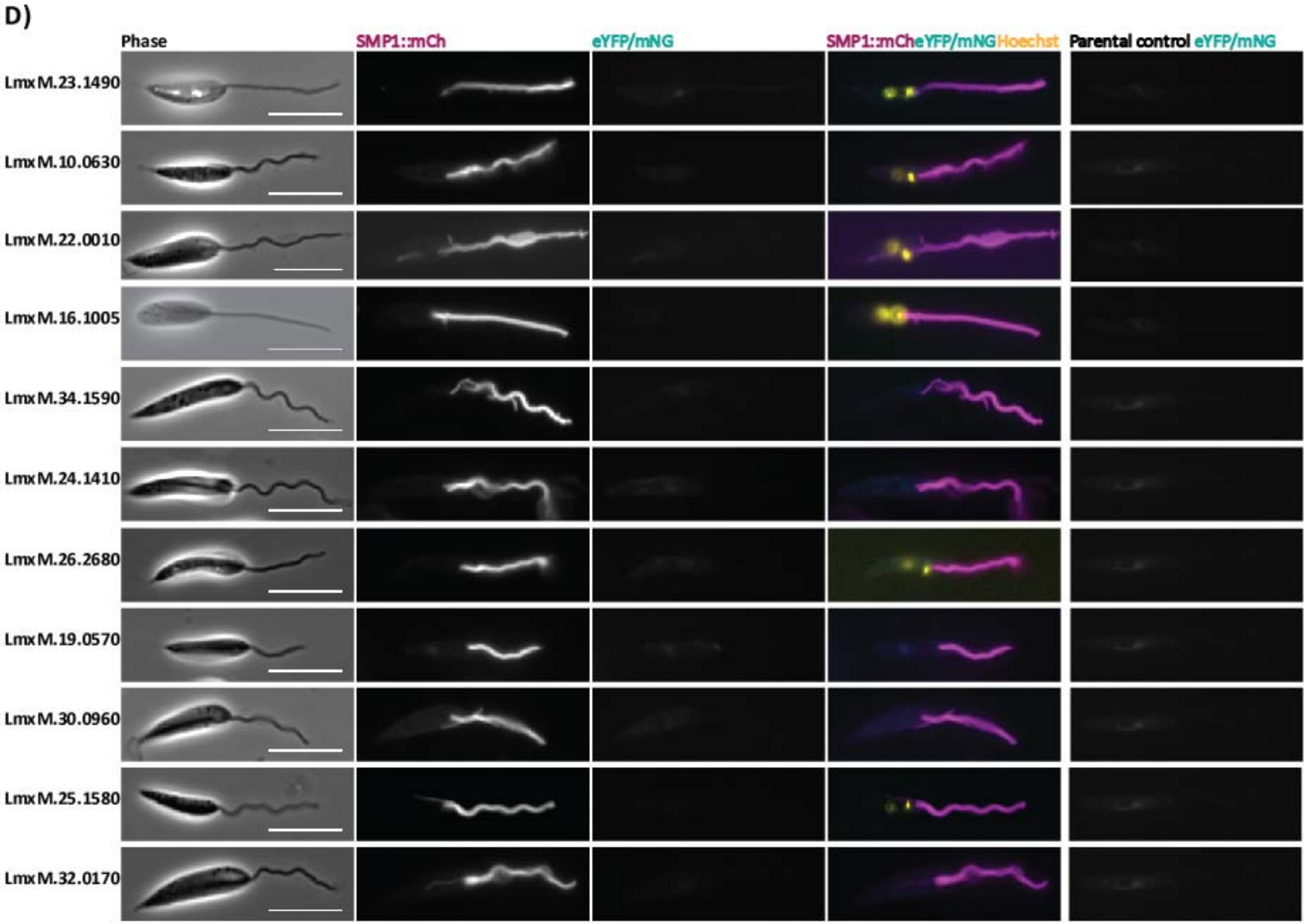
D)
Phase
SMP1::mCh
eYFP/mNG
SMP1::mCheYFP/mNGHoechst
Parental control eYFP/mNG
LmxM.23.1490
LmxM.10.0630
LmxM.22.0010
LmxM.16.1005
LmxM.34.1590
LmxM.24.1410
LmxM.26.2680
LmxM.19.0570
LmxM.30.0960
LmxM.25.1580
LmxM.32.0170

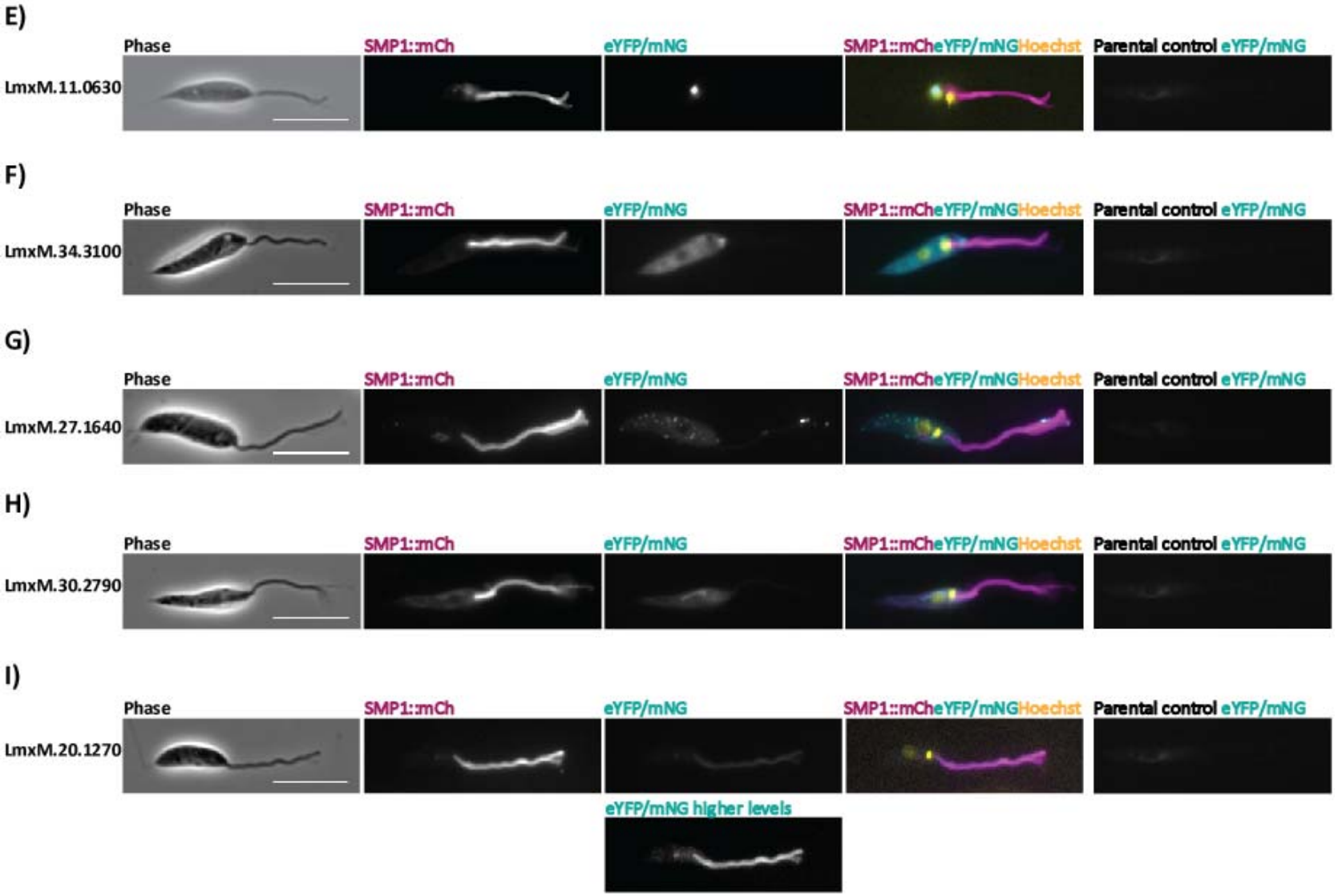
E)
Phase
SMP1::mCh
eYFP/mNG
SMP1::mCheYFP/mNGHoechst
Parental control eYFP/mNG
LmxM.11.0630
F)
Phase
SMP1::mCh
eYFP/mNG
SMP1::mCheYFP/mNGHoechst
Parental control eYFP/mNG
LmxM.34.3100
G)
Phase
SMP1::mCh
eYFP/mNG
SMP1::mCheYFP/mNGHoechst
Parental control eYFP/mNG
LmxM.27.1640
H)
Phase
SMP1::mCh
eYFP/mNG
SMP1::mCheYFP/mNGHoechst
Parental control eYFP/mNG
LmxM.30.2790
I)
Phase
SMP1::mCh
eYFP/mNG
SMP1::mCheYFP/mNGHoechst
Parental control eYFP/mNG
LmxM.20.1270
eYFP/mNG higher levels

Figure 4.8. Fluorescent tagging of candidate EV-associated proteins shows that most have a weak or no fluorescent signal. A fluorescent protein gene was inserted at the 3' end of the endogenous locus of genes encoding candidate EV-associated proteins from Table 4.5. 36 out of 43 attempted proteins were successfully fluorescently tagged. Cells were stained with the DNA dye Hoechst and imaged on a fluorescence microscope. The parental cell line was imaged and processed using the same exposure times and contrast levels as each tagged cell line and the eYFP/mNG panel is shown in every case. Phase contrast (phase), SMP1::mCh, eYFP/mNG and merged eYFP/mNG, SMP1::mCh and Hoechst (Hoechst staining not present for every cell line) panels are shown. Proteins were either tagged at the N terminus using Crispr-Cas9 with mNG in the parental cell line Cas9 T7 SMP1::mCh (cell lines LmxM.17.0080::mNG and LmxM.36.5620::mNG), or at the C terminus by fusion PCR with eYFP in the parental cell line SMP1::mCh (all other cell lines). **A-I)** Fluorescent localisations were grouped as follows with the number of cell lines in each group in brackets: **A)** Cell body membrane (4); **B)** Diffuse cytoplasmic (14); **C)** Cell body reticulated structures, likely to be ER-localised or mitochondrial (2); **D)** No fluorescent signal above parental control levels (11); **E)** Nucleolar (1); **F)** Cell body and flagellar neck (1); **G)** Distinct foci (1); **H)** endosomal, likely to be multivesicular tubule-localised (1) (Mullin et al., 2001); **I)** FM (1). All scale bars are 10 µm.

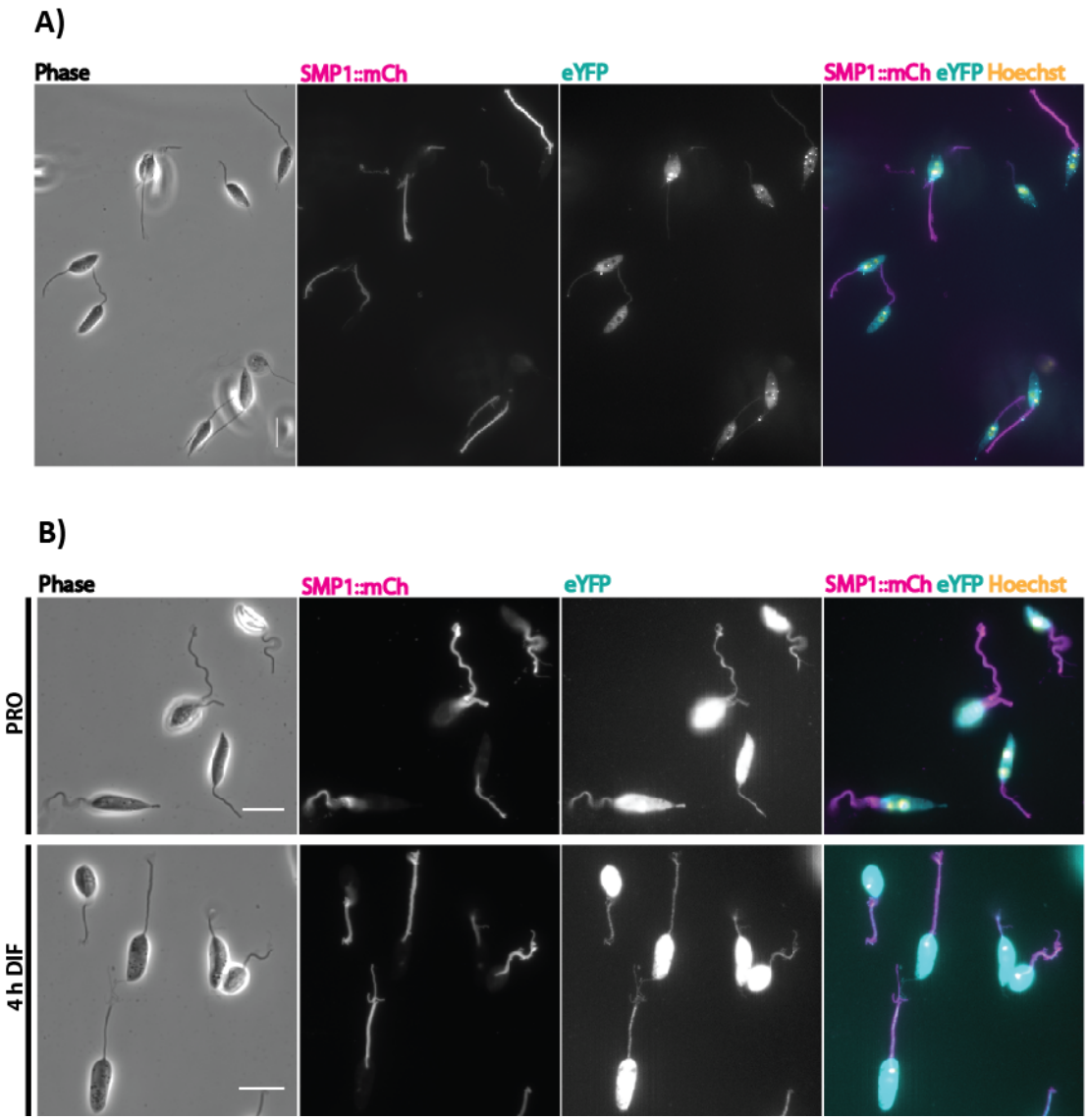

Figure 4.9. Further imaging of tagged EV candidate proteins LmxM.27.1640 and LmxM.27.0190. The cell lines were stained with the DNA dye Hoechst and imaged on a fluorescence microscope. Images show larger representative fields of view of two of the fluorescently tagged cell lines shown in Fig. 4.8: **A)** PRO LmxM.27.1640 and **B)** PRO and 4 h DIF LmxM.27.0190. Scale bars are 10 µm.

The majority of tagged candidate EV proteins had a weak or no fluorescent signal in whole *L. mexicana* cells, but this information cannot help us determine whether they

are released outside the cell as EV cargo. Since we hypothesise that EVs are released from *L. mexicana* during the early stages of host cell infection inside the PV, we wanted to see whether accumulation of tagged protein could be observed inside RAW macrophages infected for 2 h with our tagged cell lines. Unfortunately, imaging of macrophages infected with the parental cell line showed high background in the green channel (Figure 4.10), therefore it was impossible to distinguish signal from tagged cell lines from background signal.

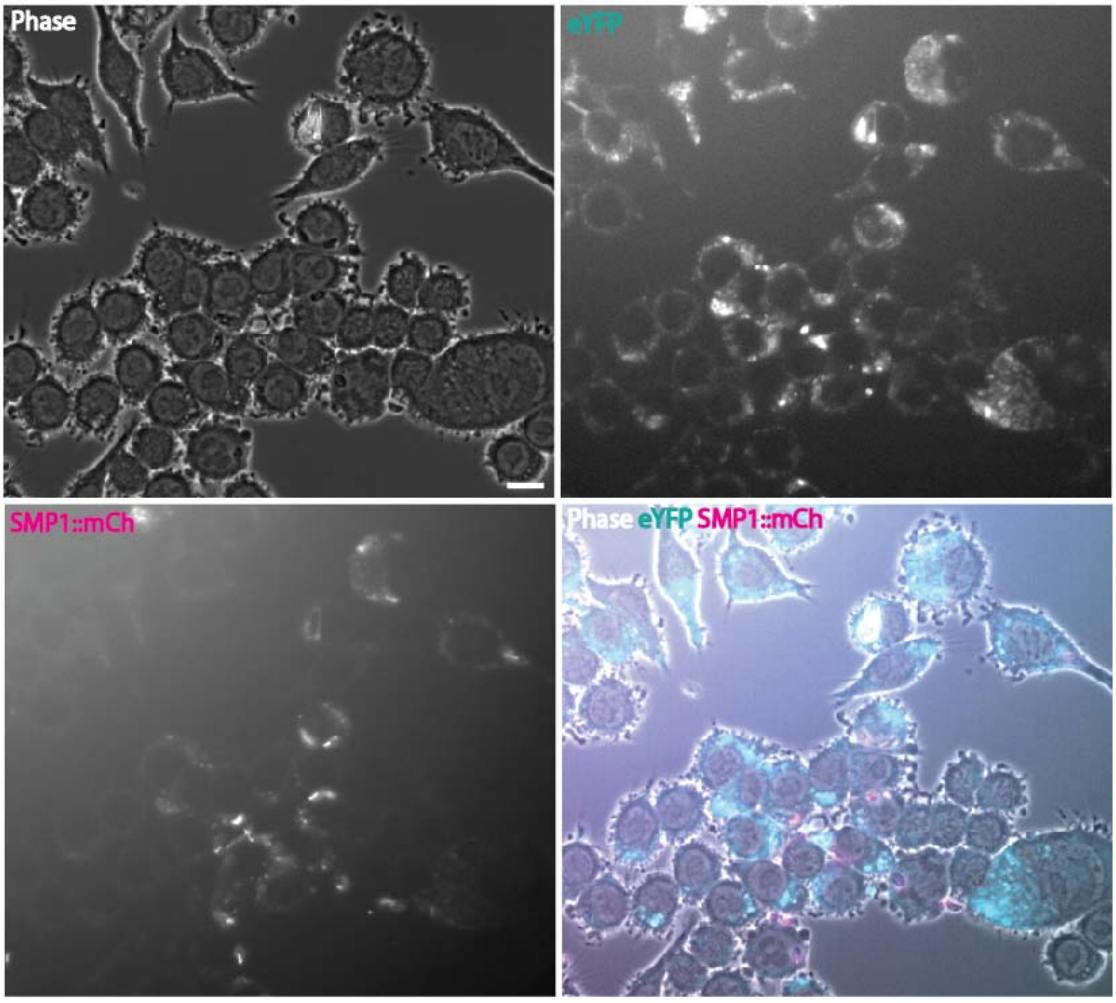

Figure 4.10. Imaging of SMP1::mCh-infected RAW macrophages shows high background fluorescence in the eYFP channel. RAW macrophages were infected at an MOI of 10 with stationary phase *L. mexicana* SMP1::mCh (the parental cell line used for EV candidate tagging)

promastigotes. At 2 h post-infection the macrophages were washed and at 2 days they were imaged on the fluorescence microscope. Scale bar 10 μm.

Overall, the majority of tagged candidate EV-associated proteins had either a diffuse cytoplasmic localisation or no detectable localisation. This makes it difficult to draw conclusions about the likely subcellular origins of the isolated EVs which were analysed to select these candidate proteins. This data does not directly support our hypothesis that the flagellum is a major source of EVs, since only one flagellar protein was identified using this approach. Given that the majority of tagged proteins were identified as abundant hits in our MS analysis of EVs but do not appear to be abundant in whole *L. mexicana* cells based on fluorescent tagging, it is possible that these proteins have important functions outside the cell.

4.2.5. Fluorescent tagging of adenylyl cyclases as candidate targets for pull-down of flagellar EVs

In trypanosomatids, adenylyl cyclases (ACs) are single transmembrane domain proteins with a large predicted extracellular N-terminal domain which may play a role in signal transduction (Makin and Gluenz, 2015). Interestingly, many of the trypanosomatid ACs studied have been FM-localised (D'Angelo et al., 2002, Paindavoine et al., 1992). Four ACs were identified in our MS analysis of PRO and DIF EV samples; we decided to fluorescently tag these proteins to see whether they could be useful transmembrane markers for flagellar EVs since we do not currently have a suitable marker protein with epitopes on the outer leaflet of the FM (to facilitate pull-

down experiments, for example). All the tagged ACs had a FM signal which colocalised with FM marker SMP1::mCh (Figure 4.11). However, all the tagged ACs also had strong fluorescent signal in the cell body (most likely in the endosomal system) (Figure 4.11) and would not therefore be a specific candidate marker for flagellar EVs.

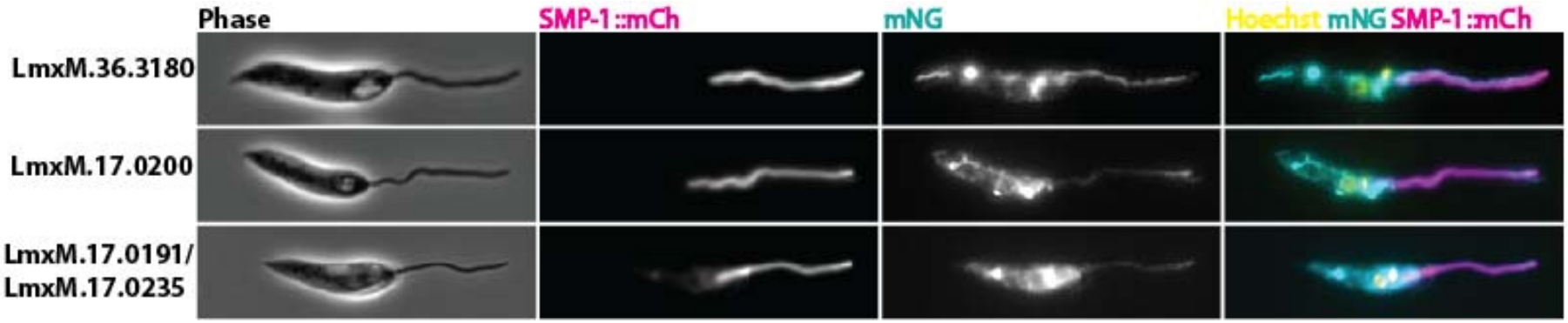
Phase
SMP-1::mCh
mNG
Hoechst mNG SMP-1::mCh
LmxM.36.3180
LmxM.17.0200
LmxM.17.0191/
LmxM.17.0235

Figure 4.11. Fluorescent tagging of adenylate cyclases. A mNG fluorescent protein gene was inserted at the 3' end of the endogenous locus of genes encoding adenylate cyclase proteins. The 3' ends of the genes and 3' UTRs of LxmM.17.0191 and LmxM.17.0235 are indistinguishable therefore both or one of the proteins may be tagged. The genomic insertions were carried out using Crispr-Cas9. The parental cell line (Cas9 T7 SMP1::mCh) expressed SMP1::mCh as a FM marker. The cell lines were stained with the DNA dye Hoechst and imaged on a fluorescence microscope. Phase contrast (phase), SMP1::mCh, mNG and merged Hoechst, SMP1::mCh and mNG panels are shown.

4.2.6. Generation of *ΔLPG1* cell line

Having characterised the proteomic content of isolated EVs, we turned our attention to non-protein factors which could be present in EVs. Since LPG is an abundant surface glycoconjugate (see *Section 5.1.1*) which is likely to be included on vesicles budding from surface membranes (indeed, we detected LPG in isolated EV samples (Figure 4.1G)) and it is a well-studied virulence factor with many known effects on macrophages (Ilg, 2001, Lodge and Descoteaux, 2005), we decided to generate a *ΔLPG1* cell line by knocking out the synthetic enzyme LPG1 (Ilg, 2000) using Crispr-Cas9 (Beneke et al., 2017). We also generated an AB cell line to show whether any effects of the null mutant are specifically due to loss of *LPG1*. Loss (Figure 4.12A, B) and regain (Figure 4.12B) of the *LPG1* ORF and correct integration of drug resistance genes (Figure 4.12C, D) was demonstrated by PCR and loss and regain of LPG itself was shown by Western blot (Figure 4.12E). In both the *ΔLPG1* and AB cell lines the abundance of high molecular weight PPGs and/or SAPs was increased, as shown previously (Ilg, 2000) (Figure 4.12E). *ΔLPG1* clone F3 was used for all subsequent experiments unless otherwise stated. *ΔLPG1* cell lines reached slightly lower

stationary phase cell densities (Figure 4.13A) and grew slightly slower in logarithmic phase (Figure 4.13B) than the parental cell line. Immunofluorescence of unpermeabilised parental cells, which should not therefore allow antibodies to cross the PM, using antibody LT22, which detects LPG as well as PPGs and SAPs (Ilg et al., 1993, Stierhof et al., 1999), showed a strong signal across the cell body and flagellar surfaces (Figure 4.14). The fluorescent signal was greatly reduced in the *ΔLPG1* cell line and almost completely disappeared from the flagellum (Figure 4.14).

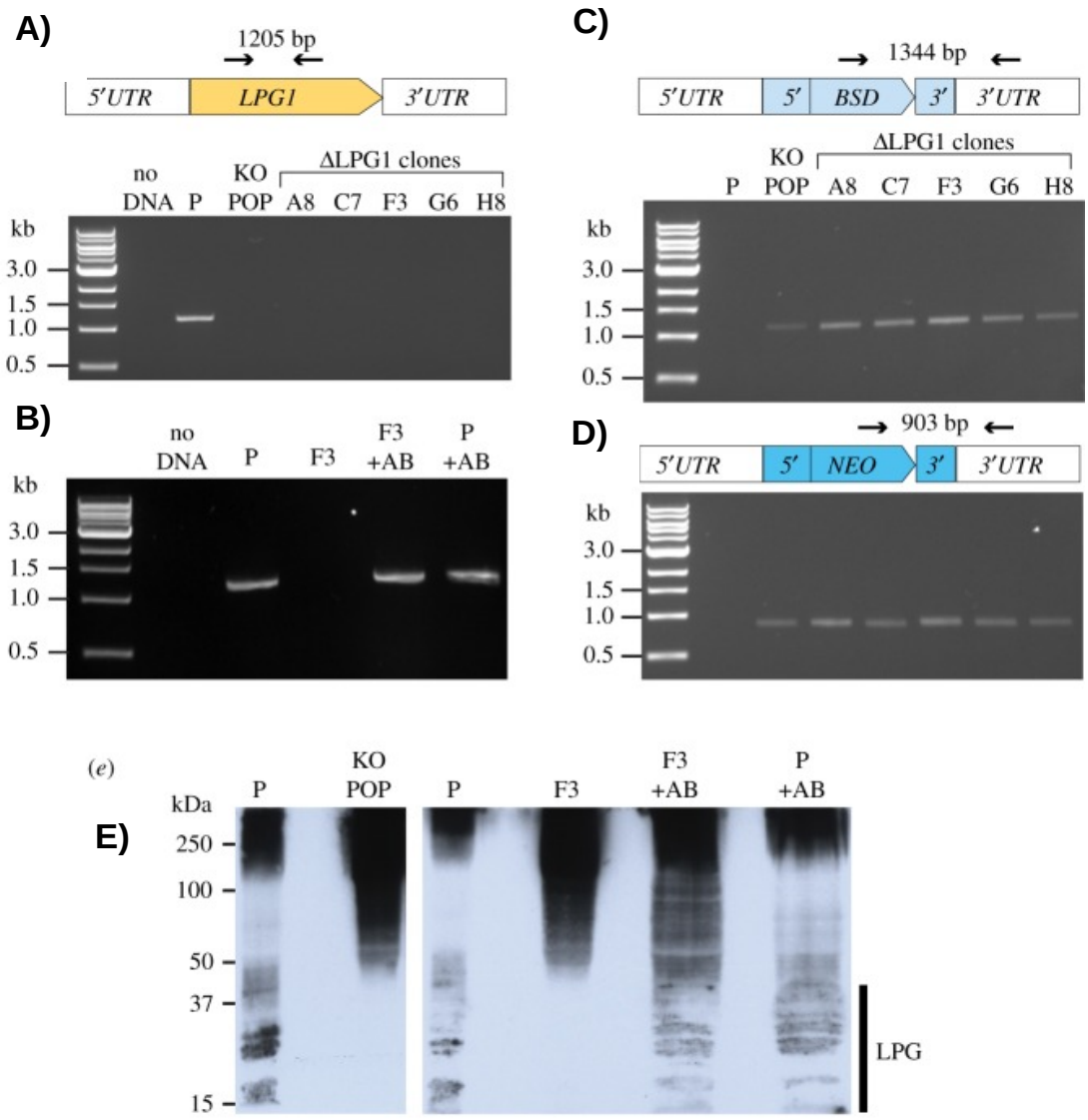

Figure 4.12. Knockout verification of *ΔLPG1* cell line by WB and PCR. **A-D)** PCR analysis of *ΔLPG1* cell lines. 3 PCRs were carried out as shown in the diagrams: **A, B)** PCR to test for the presence of the *LPG1* ORF, **C)** PCR to test for the presence of the blasticidin resistance gene, **D)** PCR to test for the presence of the neomycin resistance gene. **E)** WB of WCLs probed with anti-LPG antibody LT22 (antibody details in Table 2.2 in Materials and Methods). The expected size range of LPG is shown. P: parental cell line Cas9 T7 (p); KO pop: *ΔLPG1* population; A8/C7/F3/G6/H8: clonal *ΔLPG1* cell lines; +AB: cell lines expressing an ectopic copy of *LPG1* (Beneke et al., 2017).

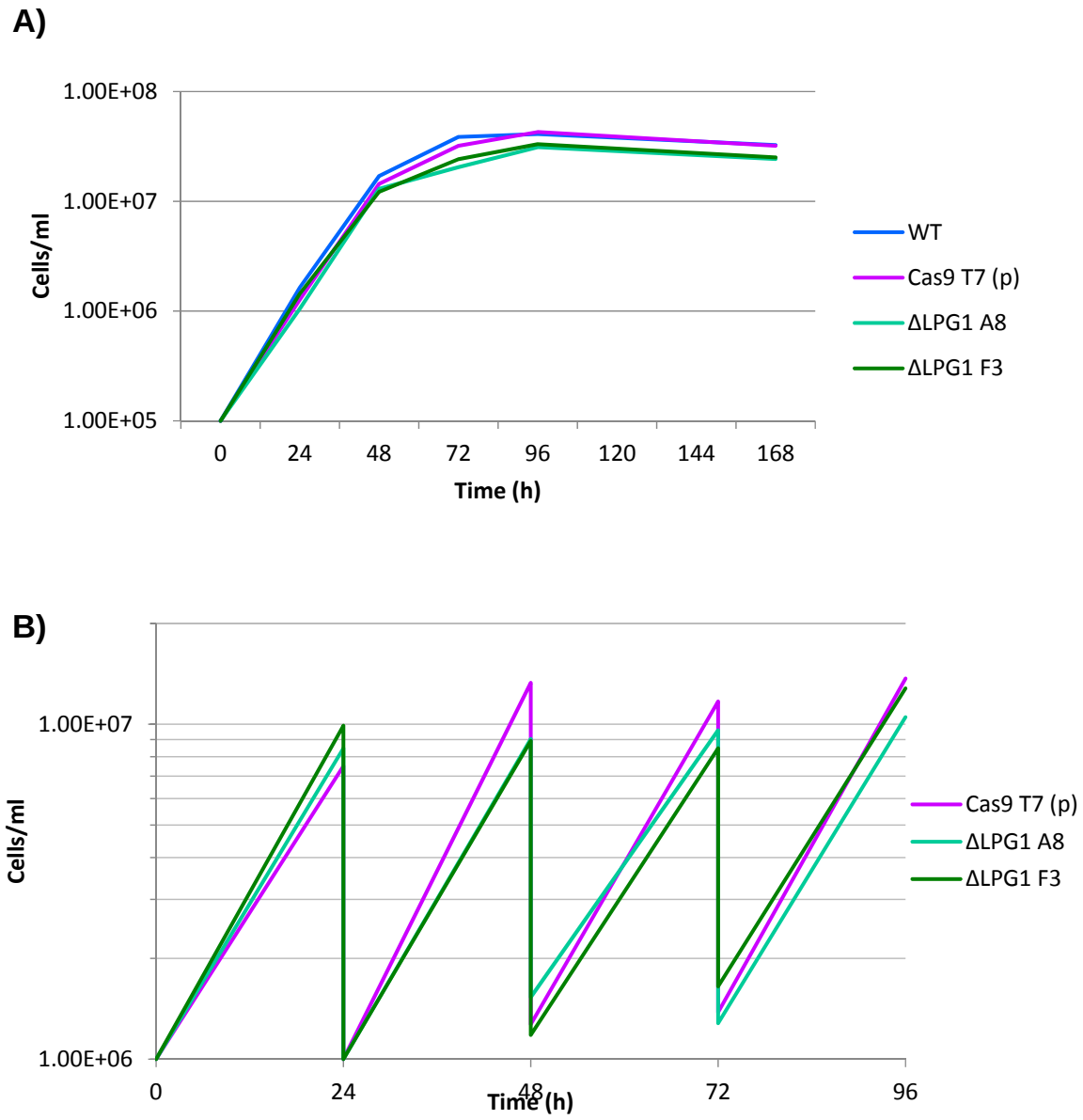

Figure 4.13. Growth curves of *ΔLPG1* cell lines. Growth curves of clonal *ΔLPG1* cell lines compared to the parental cell line. **A)** Log phase promastigotes were seeded at ~1.10^5 cells/ml at 0 h, their cell densities were measured and then measured again at 24, 48, 72, 96 and 168 h. **B)** Log phase promastigotes were seeded at ~1.10^6 cells/ml, their cell densities were measured and then measured again 24 h later before being diluted back to ~1.10^6 cells/ml.

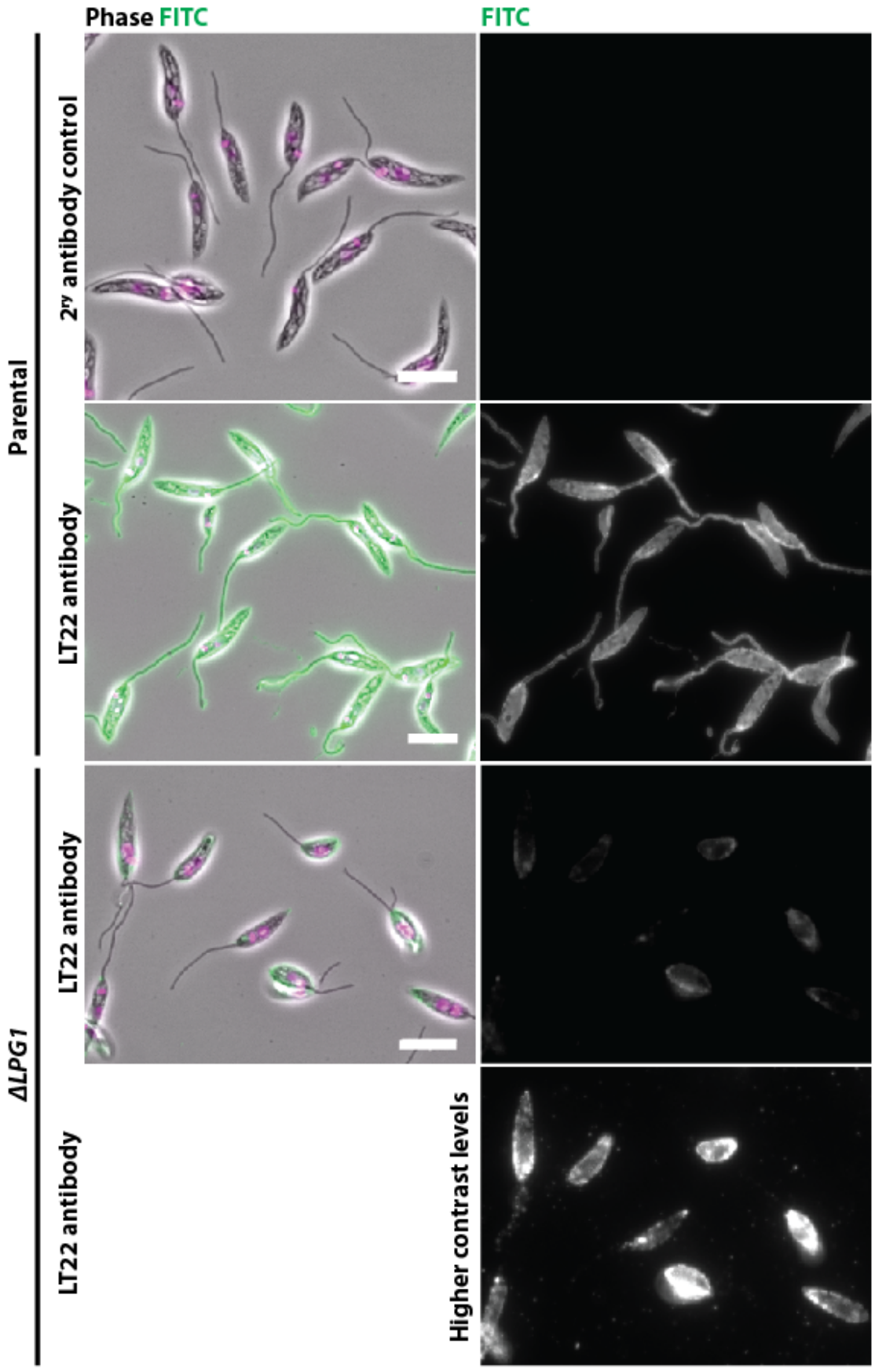
Phase FITC
FITC
Parental
ΔLPG1
2ry antibody control
LT22 antibody
LT22 antibody
LT22 antibody
Higher contrast levels

Figure 4.14. Anti-LPG immunofluorescence of *ΔLPG1* cells. *ΔLPG1* clone F3 and parental Cas9 T7 (p) cells were fixed with 2% PF and stained with LT22 primary and FITC-conjugated secondary antibodies. All images were taken with the same exposure times. The first three rows of images were processed using the same contrast levels, and the 4th row was processed using higher contrast levels to show the fluorescent localisation of the remaining PPG signal in more detail. All scale bars 10 µm.

4.2.7. Immuno-gold analysis of LPG localisation in EV samples

Although LPG was detected in isolated PRO and DIF EV samples (Figure 4.1G), we cannot conclude from these data whether LPG is EV-associated or if it is a non EV-associated contaminant. To address this question we employed immuno-gold EM using antibody LT22 against DIF EV samples. Since LT22 is not specific for only LPG, it was essential to compare EVs isolated from the parental and *ΔLPG1* cell lines in order to deduce the likely localisation of LPG. Both EV- and non EV-associated gold particles were visible and there were far fewer gold particles in the *ΔLPG1* sample (Figure 4.15B) than the parental (Figure 4.15A) or AB samples (Figure 4.15C), reflecting the reduction observed in immunofluorescence labelling in the *ΔLPG1* sample using LT22 antibody (Figure 4.14). The size distribution of vesicles from all three cell lines was similar with vesicles ranging from ~30-150 nm in diameter (Figure 4.15A-C). The number of EV- and non EV-associated gold particles were quantified (Figure 4.15D), showing that the *ΔLPG1* sample contained 25-fold fewer EV-associated and 5-fold fewer non EV-associated gold particles than the parental (Figure 4.16A). In summary, the fraction of EV-associated gold particles was 49% in the parental sample, compared to 17% in the *ΔLPG1* and 42% in the AB (Figure 4.16B).

The abundance of LPG present on *L. mexicana* cell surface membranes (Figure 4.14) suggests that LPG is also likely to be present on the surface of secreted microvesicles. Immuno-gold experiments to investigate this (Figure 4.15) were difficult to interpret due to the unspecific nature of the antibody used and the difficulty in accurately determining whether a gold particle is vesicle-associated based on our images. It seems likely, though, based on this data that at least a fraction of the LPG present in EV samples is EV-associated.

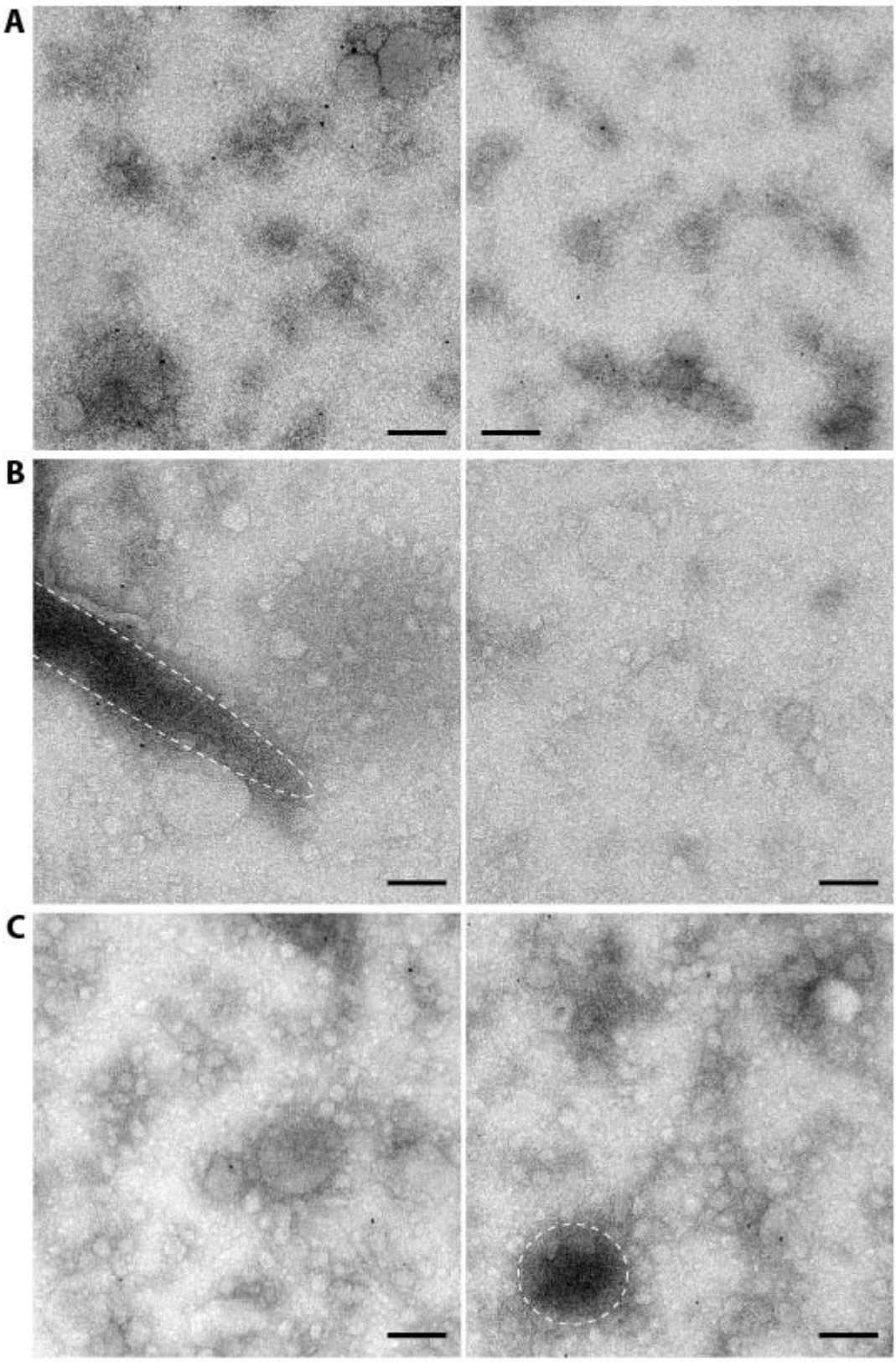
A
B
C

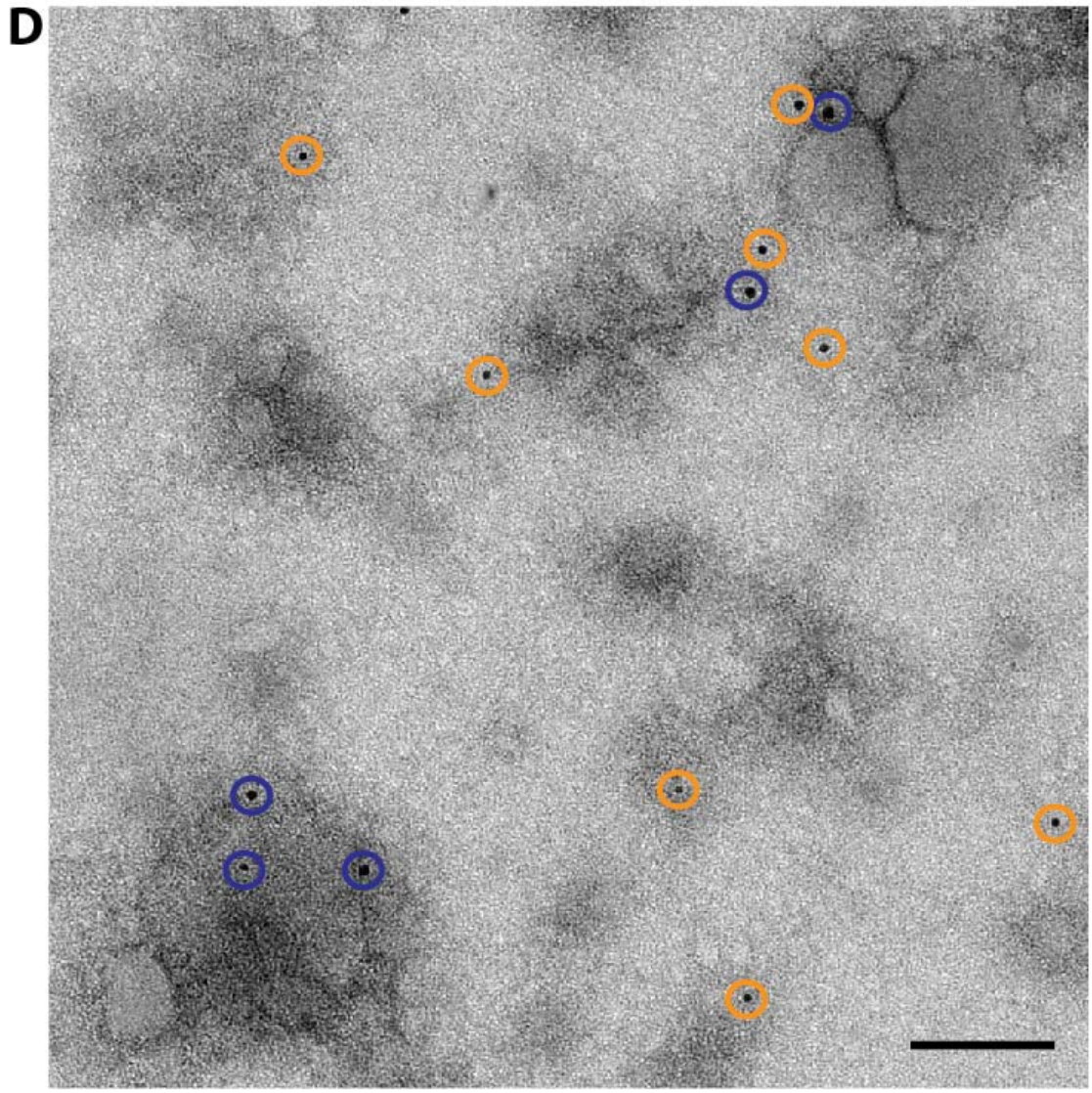

Figure 4.15. Anti-LPG immuno-gold EM of EVs from parental, *ΔLPG1* and AB cell-lines. Isolated DIF EVs from parental (**A**), *ΔLPG1* (**B**) and *LPG1* AB (**C**) cell-lines were resuspended in PBS with 2% PF and prepared on carbon coated grids for immuno-gold negative staining EM. Two fields of view which are representative of the images used for quantification are shown for each sample. Primary anti-LPG antibody LT22 and secondary antibody conjugated to 5nm gold particles were used to visualise the presence of LPG. Dark areas of intense staining (outlined with dashed lines) are likely to be gelatine deposits and were not included in the quantification. **D)** An example of gold particle assignment: blue circles indicate vesicle-associated particles and orange non-vesicle-associated. Scale bars 100 nm.

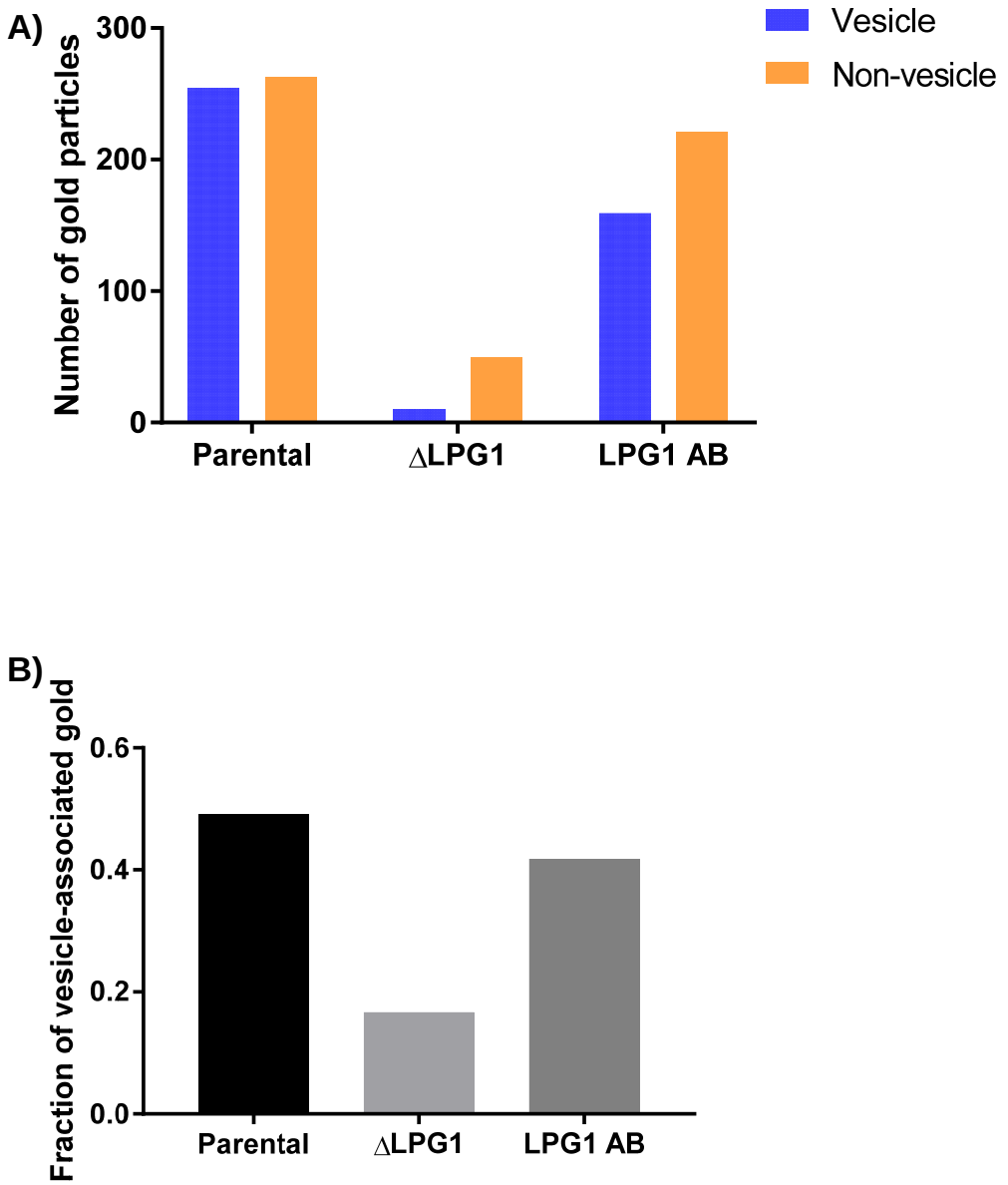

Figure 4.16. Quantification of anti-LPG immuno-gold EM. Gold particles were counted and assigned as either vesicle-associated or non-vesicle-associated. Dark areas of intense staining were not included in the quantification. **A)** Gold particles in 19 fields of view at the same magnification for each sample were counted and assigned as either vesicle-associated (blue) or non-vesicle-associated (orange). **B)** Graph showing the fraction of vesicle-associated gold particles which is lower for the *ΔLPG1* cell line than the parental or AB.

4.3. Discussion

4.3.1. Identification of novel markers in *L. mexicana* EV samples including SMP1, GT2 and LPG

Our study of *L. mexicana* EV composition using WB adds BiP, alpha tubulin, GT2 and SMP1 to the list of proteins confirmed to be present in EV samples (Figure 4.1), alongside EF-1α, GP63 and HSPs (Silverman et al., 2010a, Atayde et al., 2015). However, we cannot exclude the possibility that BiP and alpha tubulin, as abundant proteins, are detected in EV samples as a result of whole cell contamination. Indeed, we cannot conclude that any of the factors detected by WB or MS in our EV samples are vesicle-associated, merely that they are present in vesicle-enriched fractions. Trypsin digestion experiments alongside Western blotting would help to determine whether proteins detected in EV samples are protected from digestion and therefore likely to be EV cargo.

We show that histone H3 and PFR2 may be useful negative controls for *Leishmania* EV studies, since these are abundant proteins in whole cells which are not detected in *L. mexicana* EV samples (Figure 4.1). The absence of histone H3 and PFR2 in our EV samples is reassuring, suggesting that whole cell debris or lysed cells are not major contaminants. This result reflects our EV MS data which shows that histone H3 and PFR2 are among the 'bottom hits' as determined by Mascot score ranking (Appendix 1). Distinct protein banding patterns between EV and whole cell samples also supports the idea that there is minimal whole cell contamination in EV samples (Figure 4.2). Both FM and cell body membrane proteins SMP1 and GT2 are detected in *L. mexicana* EV samples, providing the first WB-based evidence that both the flagellum and cell

body are likely to be sources of EVs. An alternative explanation is that flagellar proteins are translated and trafficked in the cell body and could be incorporated into EVs via that route, but the fact that another flagellar protein, PFR2, was not detected in EV samples argues to some extent against this possibility. FM protein SMP1 is detected in both PRO and DIF EV samples but cell body membrane protein GT2 is only detected in the PRO sample, supporting our previous observations suggesting that the ratio of SMP1- to GT2- positive EVs increases during differentiation (Figure 3.21B).

While the presence of LPG in EVs has been postulated based on the presence of the LPG synthetic enzyme LPG2 (Silverman et al., 2010b), we show for the first time that LPG is present in EV samples (Figure 4.1). Intriguingly, LPG in EV samples is present at a slightly lower range of molecular weights than in whole cells. A secreted form of LPG has been described (see Chapter 5 Introduction) which has a slightly different structure to the surface-bound form (Ilg et al., 1994), but it is expected to have more phosphoglycan repeats and therefore higher molecular weights than the surface-bound form. SAPs and PPGs, which are secreted non-vesicle-associated proteins (Stierhof et al., 1998, Stierhof et al., 1999), are also detected at high levels in our EV samples, supporting our previous EM observations of the presence of non-vesicle contaminants (Figure 3.16 and Figure 3.17).

4.3.2. MS approach to enrich for flagellar proteins and virulence factors

The novelty of our MS approach was in comparing EVs from PRO and 4 h DIF cells and selecting DIF-enriched proteins for further analysis in the hope of finding flagellar-derived EV proteins and virulence factors important for the early stages of infection. A previous MS study separately compared EVs released from cells at 37 versus 26°C and pH 7 versus 5.5, but in contrast to our study, the effects of increased temperature

and lowered pH (to mimic differentiation conditions) were not studied together and a longer incubation time of 24 h was used (Silverman et al., 2010a).

A total of 901 PRO and 978 DIF EV proteins were identified (Figure 4.5A), which is strikingly more than other *Leishmania* EV studies where the highest number of identified proteins was 424 (Hassani et al., 2014). However, the number of proteins identified in individual replicates varied between 300 and 783, with up to 450 unique proteins in one out of three replicates in the PRO EV samples (Figure 4.5C, D). These figures indicate that the data is not of the high quality based on reproducibility which would allow reliable enrichment analyses to be carried out. However, there was a high degree of reproducibility among the more abundant proteins (as determined by Mascot score, Appendix 1). For MS analysis of complex samples, ideally at least 10 µg should be analysed (EMBL et al.), therefore it is likely that the low (~1.5-20 µg) and variable protein content of our EV samples (Table 4.1) limited the quality of the MS output data.

Overall, the proteins identified are in good agreement with previously published data, including SAP, EF-1α, enolase, HSPs, surface antigens, GP63, histones, calpain-like cysteine peptidases, P-type ATPases, tubulin, and proteasomal and ribosomal proteins (Appendix 1). GP63 (Contreras et al., 2010, Gomez et al., 2009, Halle et al., 2009), surface antigen-like proteins, proteasomal subunits, several hypothetical proteins and metabolic enzymes seem to be enriched in the DIF EV sample (Table 4.2, Table 4.5). Several proteins identified are involved in known vesicle secretion pathways including an Alix-like protein, actin and ubiquitin (Table 4.5). PRO and DIF EVs contain a range of cell body and flagellar-enriched proteins with no skew towards

either cellular compartment, supporting our hypothesis that *L. mexicana* EVs are both cell body and flagellar-derived (Figure 4.2, Table 4.3). It is notable, given the fact that the whole cell proteome contains many more proteins that our EV proteomes (Figure 4.6), that only 73% of PRO and 58% of DIF EV proteins are also present in a whole promastigote *L. mexicana* proteome (Table 4.3). Many of the proteins only found in the EV proteomes are hypothetical proteins (Table 4.5) and we can speculate that their primary functions lie outside of *L. mexicana* cells as secreted factors.

4.3.3. Majority of tagged candidate EV proteins have no signal or a diffuse localisation

Based on our MS analysis, 36 candidate EV proteins were successfully fluorescently tagged and localised (Figure 4.8), giving us valuable information about a group of poorly studied *L. mexicana* proteins. The majority (25 out of 36) of tagged candidate EV proteins either localise in a diffuse cytoplasmic pattern or have no detectable localisation in whole *L. mexicana* promastigotes (Figure 4.8B, D). Perhaps it is not surprising that proteins identified based on MS analysis of secreted products have a weak or no detectable localisation in whole cells, but these results mean it is difficult to draw conclusions about the likely functions of these proteins. Unfortunately, we were unable to confirm whether any of the tagged proteins indeed localise to EVs despite attempts to visualise secretion of tagged protein into macrophage PVs (Figure 4.10) and to carry out WBs on acetone-precipitated *L. mexicana* conditioned medium (data not shown). Other localisations of tagged proteins include the nucleolus, cell body membrane and cell body reticulated structures (Figure 4.8). To investigate if any of these candidate EV proteins are important for early infection of macrophages, a KO screen could be carried to see if any null mutants are unable to survive in macrophages. The most interesting localisation was of a homolog to the known

ESCRT-related and EV-associated protein PDCD6IP (also called Alix) (Odorizzi, 2006), which was enriched in vesicle-like foci in the cell and on cell body and flagellar surfaces (Figure 4.9A). It would be interesting to carry out live time-lapse imaging of this cell line to see whether the foci are blebbing from or adsorbing to these surfaces.

4.3.4. The search for an FM-derived EV marker

One aim of this study was to identify a transmembrane protein with an exclusive FM localisation which is also present in isolated EVs. Tagging such a protein on the outer membrane side would allow us to perform FM-derived EV pull-downs which would be highly useful for the future in-depth analysis of EV subsets from different subcellular sources. Unfortunately, none of the tagged candidate EV proteins (Figure 4.8) nor ACs (Figure 4.11) fit the criteria.

4.3.5. Analysis of LPG localisation in EV samples

LPG has a strong cell body and flagellar surface localisation (Figure 4.14), suggesting it is likely to be included on both cell body- and flagellar- derived microvesicles unless there is a mechanism to exclude LPG from vesicular cargo. Immuno-gold experiments suggest that at least a fraction (up to 50%) of LPG is vesicle-associated (Figure 4.15, Figure 4.16), however this interpretation is limited by our lack of an LPG-specific antibody and our ability to confidently assign gold particles as vesicle- or non-vesicle-associated (Figure 4.15D) due to the abundance of small, indistinct vesicles. Immuno-gold labelling using an LPG-specific antibody or WBs of EVs which have been further purified by density gradient separation would be necessary to determine with confidence whether LPG is EV-associated.

4.3.6. Conclusions and outlook

We show that *L. mexicana* EV samples contain cell body membrane and FM markers GT2 and SMP1, suggesting that both the cell body and flagellum may be a source of EVs. MS analysis of PRO and DIF EV samples confirmed the presence of proteins identified in other *Leishmania* EV studies, including virulence factors and known EV-associated proteins GP63 and EF-1α. Analysis of MS datasets led to the selection of DIF-enriched candidate EV proteins, with the aim of identifying flagellar proteins and proteins involved in the early stages of macrophage infection. 36 candidate EV proteins were fluorescently tagged and localised: the majority had either a diffuse cytoplasmic or no localisation and only one exclusive flagellar localisation was identified, therefore it is hard to draw conclusions about the likely function of these proteins or their presence in EVs. A homolog of PDCD6IP, a known EV marker in mammalian cells, localises to distinct foci resembling vesicles. This protein is therefore a good candidate for involvement in EV biogenesis in *Leishmania* spp. and merits further study; unfortunately attempts to KO the protein in this study were unsuccessful, suggesting that it may be essential (Chapter 3). A major limitation of this study is the need to carry out further analysis of the candidate EV-associated proteins in tagged whole cells, rather than on the EVs they release which are the focus of this study, since high-throughput isolation of EVs from many cell lines is not currently feasible (due to technical restrictions such as low EV yields and the number of samples which fit in an ultracentrifuge rotor). Perhaps the best approach to circumvent this issue would be a high-throughput KO screen of the candidate EV proteins to see whether any are required for infection or flagellar shortening, which would allow the selection of a smaller yet promising subset of proteins for detailed EV studies.

LPG is a very well-studied virulence factor but how it is delivered to the host and whether it is carried by EVs remains unknown. Our data show for the first time that LPG is present in EV samples and that it is likely to be at least partially EV-associated, although further study is needed to confirm this. We generated a *ΔLPG1* cell line to use in the study of LPG in the context of EVs.

While we have a lot of data concerning the composition of *Leishmania* EVs, several open questions remain. There are many unannotated proteins found in *Leishmania* EVs whose functions remain unknown. Some of these proteins are not detected in whole cells and it is possible their main function is as a secreted product; they therefore deserve further study as potential virulence factors which could modulate host function. The consistent identification of ribosomal, proteasomal and histone proteins in *Leishmania* EV samples should be addressed to determine whether these proteins have novel functions as secreted factors.

5. Biological effects of *L. mexicana* promastigotes and EVs on macrophages

5.1. Introduction

5.1.1. LPG: structure and importance as a virulence factor

LPG has been extensively studied as a *Leishmania* virulence factor and has many known effects on macrophage biology (Ilg, 2001, Lodge and Descoteaux, 2005, Spath et al., 2000), particularly during the early stages of infection when promastigotes are phagocytosed by macrophages and undergo differentiation to amastigotes. During this process, the *Leishmania*-containing phagosome is resistant to fusion with lysosomes and late endosomes (Scianimanico et al., 1999), and this is postulated to be important to allow promastigote to amastigote differentiation in a conducive environment. Studies showing that *Leishmania* LPG-deficient mutants are unable to inhibit phagolysosomal maturation (Desjardins and Descoteaux, 1997, Scianimanico et al., 1999) suggest that LPG is responsible, although the underlying mechanisms are unclear.

Despite the many published biological effects of LPG, whether LPG is a virulence factor at all seems to depend on the *Leishmania* species. Research to address this question has used both *LPG1* knockout parasites (Ilg, 2000) (Spath et al., 2000), which are specifically unable to synthesis LPG, and *LPG2* knockouts, which are unable to synthesise any phosphoglycan repeat-containing molecules (Ilg et al., 2001). While *L. major LPG1* knockout promastigotes have greatly impaired ability to infect sand flies, macrophages and mice (Spath et al., 2000), another similar study showed that *L. mexicana LPG1* knockouts replicate normally in macrophages and mice (Ilg, 2000).

Both studies used a Balb/c murine model, with footpad lesion size as the only measure of infection level. As discussed in *Section 1.2.2*, this output is not ideal as a measurement of parasite survival since lesion size and parasite load do not always correlate (Vargas-Inchaustegui et al., 2009). Therefore, conclusions about lesion severity, not parasite load, can be drawn from these two studies. As for parasite survival in macrophages, the *L. major* study clearly shows a dramatic reduction in *ΔLPG1* parasite load within 2 days post-infection (Spath et al., 2000), whereas the *L. mexicana* study shows the percentages of *ΔLPG1*- versus WT- infected macrophages are similar (Ilg, 2000). The percentage of infected macrophages tells us about infection dynamics but is not a direct measure of parasite load, since a variable number of parasites can infect one macrophage. Therefore, *ΔLPG1 L. major* parasite survival in macrophages is clearly attenuated under the conditions tested, but we cannot draw conclusions about the ability of *ΔLPG1 L. mexicana* to survive in macrophages. Therefore, LPG seems to be important for *L. major* virulence and may not be needed at all for *L. mexicana* virulence. Furthermore, *LPG2* knockout *L. mexicana* are virulent in macrophages and mice (Ilg et al., 2001), suggesting that phosphoglycan repeats in general are not necessary for virulence in this species. *LPG2* knockout *L. donovani* (Gaur et al., 2009) and *L. major* (Spath et al., 2003), on the other hand, display even more severely attenuated virulence than the *LPG1* knockouts. *L. mexicana* LPG, as discussed in *Section 1.2*, does undoubtedly exert effects on macrophages, including cytokine production and signalling pathways, but whether these effects are relevant to infection given that LPG itself is not required is difficult to say. One point to note is that the LPG virulence studies were carried out in mice, and it is possible that the extent to which the parasite relies on LPG may vary between host species. This idea is

supported by the fact that the immune responses to leishmaniasis in mice and humans are different (Sharma and Singh, 2009), as discussed in *Section 1.1.2*.

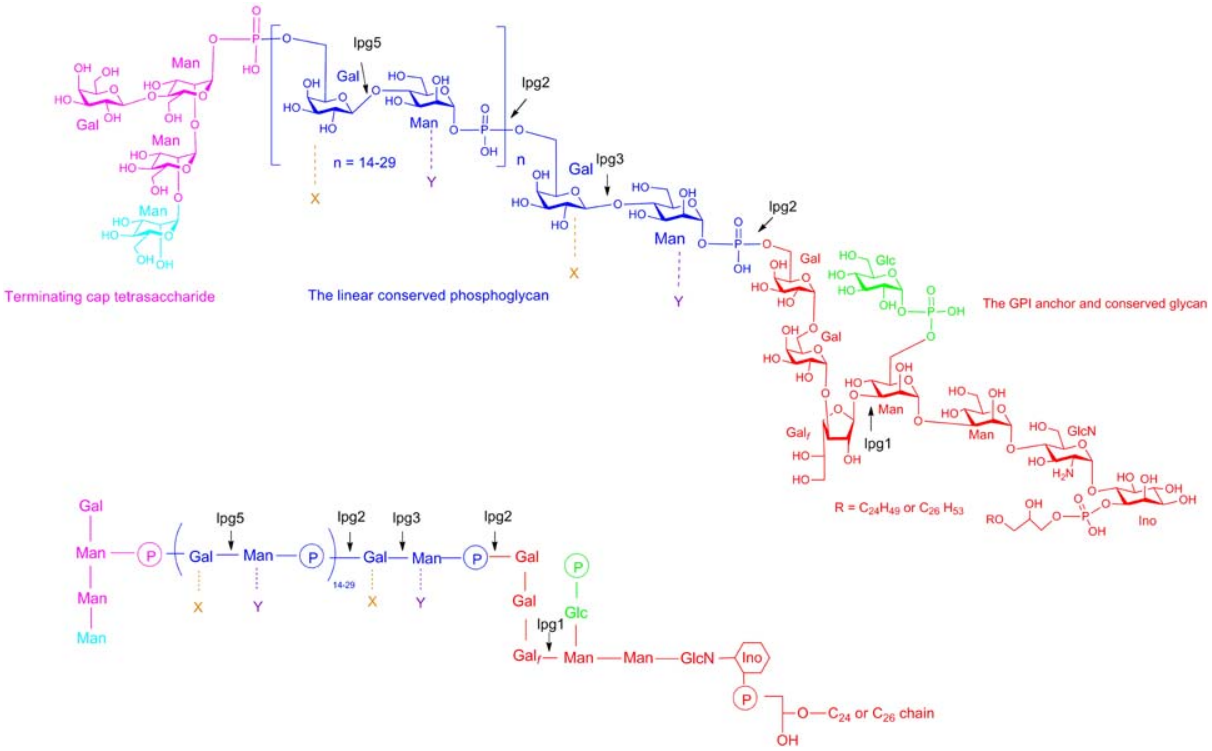

Figure 5.1. Structure of lipophosphoglycan. Figure taken from (Forestier et al., 2014). Two representations of the chemical structure of LPG are shown. The four domains are colour-coded: GPI anchor and glycan core (red); linear phosphoglycan repeats (blue); oligosaccharide cap (pink). The residue shown in green is present in some *Leishmania* species including *L. mexicana*. X represents glycosylation present on the LPG of some *Leishmania* species including *L. mexicana*. *Leishmania* species have variable sugar residues branching off the phosphoglycan chain, variable numbers of phosphoglycan repeats and variable di- tri- or tetra- saccharide cap structures (Forestier et al., 2014). The promastigote surface LPG of *L. mexicana* has on average 20 phosphoglycan repeats, around 20% of the galactose groups are β-glycosylated, and the terminal cap has three possible structures: Manα1-2Man, Manα1-

2Manαl-2Man or Manαl-2(Galβl-4)Man (Ilg et al., 1992). Gal, galactose; Man, Mannose; Glc, glucose; Galf, galactofuranose; GlcN, glucosamine; Ino, inositol.

While the structure of *L. mexicana* LPG in other life cycle stages is unknown, there are changes in the cap (Sacks et al., 1995) and phosphoglycan structures of LPG in other species. For example, the number of phosphoglycan repeats in *L. major* LPG increases from around 19 to 34 following the procyclic to metacyclic transition (Barron and Turco, 2006) and the number of the phosphoglycan repeats of *L. donovani* (Sacks et al., 1995) and *L. chagasi* (Barron and Turco, 2006) LPG increases following metacyclogenesis. These structural changes probably reflect the different roles LPG performs in different life cycle stages: LPG is required for attachment to epithelial cells in the sand fly midgut (Sacks et al., 2000), therefore it is possible that structural epitopes present in promastigote LPG mediate this interaction.

Two studies carried out over twenty years ago identified a distinct form of LPG in *L. major* amastigotes (Glaser et al., 1991, Moody et al., 1993). This LPG is recognised by different antibodies from those which identify promastigote LPG (Glaser et al., 1991), has 36 phosphoglycan repeats and has a different set of phosphoglycan side chain residues (Moody et al., 1993). Amastigote LPG is present at about 6.10^4 (Moody et al., 1993) copies per cell compared to around 6.10^6 copies per promastigote (Moradin and Descoteaux, 2012), and its functional importance is unknown. While *LPG1* knockout *L. major* promastigotes are quickly degraded by macrophages, knockout amastigotes are able to replicate normally (Spath et al., 2000), suggesting a less important role for LPG in this life cycle stage.

In addition to the surface membrane-bound form, LPG is also secreted into cell culture supernatants of *L. mexicana, L. donovani* and *L. major* (Ilg et al., 1994). This secreted form has a slightly different structure, for example *L. mexicana* has 20 phosphoglycan repeats in the surface-bound form and 28 in the secreted form (Ilg et al., 1994). Secreted LPG can be enriched for in culture supernatants by ultrafiltration (Ilg et al., 1994), therefore it is possible that *Leishmania* EV studies which use this method could also enrich for secreted LPG. It is intriguing that the GPI anchor remains present in the secreted form of LPG, and it is not clear whether LPG is freely secreted or secreted as EV cargo.

5.1.2. Known effects of LPG on cytokine production

The majority of research carried out on the immunomodulatory effects of LPG has been done using purified LPG (Becker et al., 2003, Favila et al., 2015, Srivastava et al., 2013, Passero et al., 2015, Rojas-Bernabe et al., 2014, Argueta-Donohue et al., 2008). Whether or not this approach gives an accurate idea of the role of LPG in vivo is debatable (see Introduction), and it has been suggested that a major role for LPG may be its expression on the parasite surface where it can shield immunogenic surface molecules. Further complication is added by the fact that studies are carried out in different host cell types, species and *Leishmania* species. Furthermore, the structure of LPG changes during the *Leishmania* life cycle, and different forms can have have different effects on cytokine production; metacyclic LPG induces a stronger increase in IFNγ production from NK cells than procyclic LPG (Becker et al., 2003).

While LPG is generally considered to have immunosuppressive effects (Spath et al., 2000, Frankenburg et al., 1990), several reports have also shown increases in pro-inflammatory cytokines in response to LPG. Purified LPG from *L. major* increases pro-

inflammatory IFNγ and TNFα production when incubated with human NK cells (Becker et al., 2003) and IL-12 production in human DCs (Favila et al., 2015). The fact that LPG induces IL-12 production in human DCs was further supported by the same study which compared the IL-12 levels induced by live WT and *LPG1* knockout *L. major* parasites (Favila et al., 2015). While in murine macrophages LPG from *L. major* induces increases in anti-inflammatory cytokines IL-10 and TGFβ production (Srivastava et al., 2013), another study also observed an increase in TNFα, as well as IL-10, in response to purified LPG from *L. shawi* (Passero et al., 2015). Similarly, IL-10, IL-12 and TNFα were increased in human DCs and monocytes, and in macrophages IL-1β was also increased (Rojas-Bernabe et al., 2014), in response to purified LPG from *L. mexicana* (Argueta-Donohue et al., 2008). Overall, the response to LPG appears to be more complex than simply pro or anti-inflammatory and several studies show LPG-induced increases in both pro- and anti-inflammatory cytokines (Passero et al., 2015, Rojas-Bernabe et al., 2014, Argueta-Donohue et al., 2008).

LPG has been linked to reductions in chemotactic activity. Purified LPG from *L. donovani* reduces expression of the chemokine MCP-1 in human endothelial cells and transendothelial migration of monocytes (Lo et al., 1998). However, to date there are no reports of LPG affecting production of any of the CXCL chemokines, perhaps because these chemokines are not commonly measured and the use of unbiased cytokine screening panels has only been adopted fairly recently (Sampey et al., 2016, Paggetti et al., 2015, Civini et al., 2013).

5.1.3. Role of CXCL- chemokines in *Leishmania* infection

The chemokine CXCL10 is produced in response to IFNγ by several cell types including monocytes, endothelial cells and macrophages, and recruits various immune cells

including T cells, NK cells, monocytes and macrophages (Carter et al., 2007). The importance of CXCL10 in Th1-driven responses was shown in CXCL10 knockout mice which have reduced T cell proliferation and IFNγ production in response to antigenic stimulation (Dufour et al., 2002). CXCL9, 10 and 11 are all recognised by the common receptor CXCR3, which is up-regulated on Th1-type T cells, and appear to have overlapping but non-redundant roles (Carter et al., 2007). The fact that CXCL10 is associated with the promotion of a Th1 immune response is important since a Th1 response is thought to be protective in *Leishmania* infection (Gaafar et al., 1995).

CXCL10 has been shown to have direct cytotoxic activity on *L. mexicana* promastigotes *in vitro* (Sobirk et al., 2013), as shown by a substantial increase in PM permeability and decrease in mitochondrial function. This result should be interpreted with caution, however, since the concentrations of CXCL10 used in the study were in the micromolar range, which is much higher than the nanomolar concentrations which would usually be found *in vivo* (Wolf and Moser, 2012).

There is mounting evidence that CXCL10 treatment reduces *Leishmania* infection *in vivo*. Both pre-treatment of macrophages *in vitro* and injection into lesion sites with CXCL10 results in significantly lower parasite burdens during *L. amazonensis* infection (Vasquez and Soong, 2006). In *L. donovani* murine infection, CXCL10 treatment at days 1, 3 and 7 post-infection leads to a drastic >90% decrease in parasite load by day 28 (Gupta et al., 2009). Consistent with an environment conducive to *Leishmania* infection control, splenocytes from these mice produced higher levels of Th1 type cytokines IFNγ, IL-12, TNFα, and lower levels of immunosuppressive cytokines IL-10, IL-4 and TGF-β (Gupta et al., 2009, Gupta et al., 2011). *L. donovani*-infected murine

macrophages also showed these changes in cytokine secretion (except for IFNγ which was not measured) when treated with CXCL10 (Gupta et al., 2009). It was shown through the use of specific inhibitors that the ability of CXCL10 to reduce *L. donovani* parasite loads in mice is dependent on NO production, which is a primary mechanism of *Leishmania* killing in macrophages (Panaro et al., 2001, Mukbel et al., 2007), and p38 signalling (Gupta et al., 2009). CXCL10-dependent reduction in parasite load in infected macrophages and mice was also reported for *L. infantum*, and splenocytes from the infected mice secreted higher levels of IFNγ and lower levels of IL-10 and TGF-β (Figueiredo et al., 2017). CXCL10 treatment of infected mice also affected T cell function: greater proliferative capacity of isolated T cells in response to leishmanial antigen was observed (Gupta et al., 2009), as well as reduced recruitment of regulatory T cells, which are associated with non-resolving *Leishmania* infection (Rai et al., 2012, Mendez et al., 2004), to the spleen (Gupta et al., 2011).

In line with the idea that lowered CXCL10 levels are conducive to *Leishmania* infection and may therefore be down-regulated by the parasite, *L. major*-infected human macrophages *in vitro* have significantly reduced CXCL10 mRNA expression (Guerfali et al., 2008). A study of CXCL11 production by peripheral blood mononuclear cells from patients with healing or non-healing cutaneous leishmaniasis (likely to be caused by *L. major*), showed that high CXCL11 levels were associated with the self-healing form of the disease (Moafi et al., 2017), supporting the idea that CXCL11, like CXCL10, promotes the control of *Leishmania* infection. Conversely, *L. braziliensis* infection of human macrophages induced increased production of CXCL10 (Vargas-Inchaustegui et al., 2010). In a mouse model of visceral *L. donovani* infection, the mRNA levels of

several chemokines including CXCL10 were found to be elevated in the liver at three weeks post-infection (Murray et al., 2016). The importance of IFNγ in the induction of these CXCL- chemokines was confirmed by the fact that infected IFNγ knockout mice were unable to produce elevated chemokine levels (Murray et al., 2016).

Interestingly, in contrast to the documented protective roles of CXCL10 in *L. amazonensis*, *L. infantum* and *L. donovani* infection, in one study CXCL10 knockout mice had lower parasite burdens than WT mice 2-4 weeks post-infection with *L. donovani,* suggesting an infection-enhancing role for CXCL10 (Murray et al., 2016). Different mouse models are unlikely to account for this discrepancy since C57BL/6 mice were used for the CXCL10 knockout study and both C57BL/6 and BALB/C mice were used in the studies showing protective roles for CXCL10. It is possible that CXCL10 knockout mice have systemic changes in their immune system leading to enhanced parasite control. In conflict with this result, the same study showed that mice lacking CXCR3, the receptor for CXCL10, had slightly increased parasite loads for reasons that are not well understood, perhaps suggesting a CXCL10-independent protective role for CXCR3 (Murray et al., 2016).

Taken together, there is compelling evidence that CXCL10 induces control of *Leishmania* infection via both enhanced macrophage killing and T cell regulation. High CXCL10 levels in infected mice and macrophages induces a Th1 environment conducive to parasite control, with high levels of pro-inflammatory cytokines such as IL-12 and IFNγ and low levels of immunosuppressive cytokines IL-10 and TGF-β.

5.1.4. Aims

While there have been several studies on the effects of *Leishmania* on macrophage cytokine secretion, most studies of promastigotes and all studies of EVs analyse a small subset of cytokines based on previously published results. We aim here to screen a broad panel of macrophage cytokines in an unbiased fashion for regulation by *L. mexicana* promastigotes and EVs. We further hope to investigate whether EVs from promastigotes or differentiating cells have different effects on cytokine production, to help establish whether these EV samples are functionally different. Finally, our finding that LPG is present in EV samples (Chapter 4) leads us to question whether this secreted LPG exerts effects on macrophage cytokine production, as has been documented for purified and cell-associated LPG. We aim to use the *LPG1* cell line which we generated to address this question.

5.2. Results

5.2.1. Infective promastigotes and EVs induce reductions in macrophage chemokine and IFNγ secretion

Fluorescence microscopy of human iPSC-derived macrophages 3 days after infection with the doubly labelled *L. mexicana* SMP1::mCh-GT2::eGFP:TY cell line, (Clone 3, see Figure 3.1) showed the presence of amastigotes within PVs as expected (Figure 5.2A, B). As seen in infected murine BMDMs (Figure 3.7), non-parasite-associated mCherry signal was widely distributed within infected (Figure 5.2A, B), but not uninfected (Figure 5.2C), human macrophages, consistent with the possibility that flagellar membrane proteins are shed from the parasites. The presence of amastigotes three days post-infection shows that *L. mexicana* parasites are able to differentiate and survive within human iPSC-derived macrophages, establishing these cells as a good model system to study *Leishmania*-macrophage interactions.

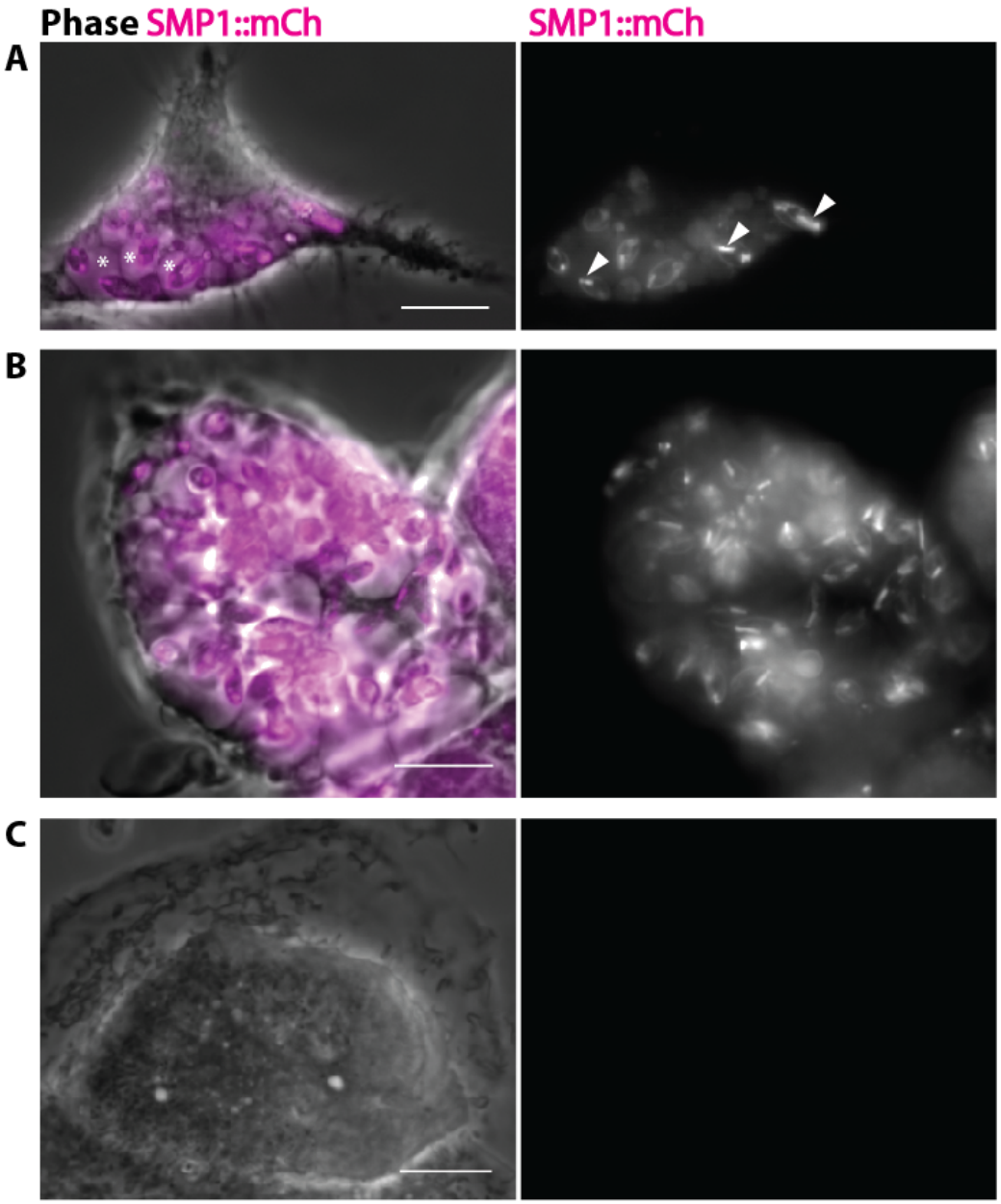

Figure 5.2. Imaging of *Leishmania*-infected human iPSC-derived macrophages. iPSC-derived macrophages were infected at an MOI of 5 with stationary phase Clone 3 promastigotes. The macrophages were washed after 18 h to remove extracellular parasites and were imaged by phase contrast and fluorescence microscopy at 3 days post-infection. Infected (**A, B**) and uninfected (**C**) macrophages are shown. **A)** Examples of PVs containing amastigotes are indicated by asterisks and examples of amastigote flagella visualised with tagged FM protein SMP1::mCh are indicated by arrowheads. All panels were imaged and processed at the same contrast levels. Scale bars 10 µm.

We investigated the effects of *L. mexicana* samples on human macrophage cytokine production. Since macrophage activation induces the secretion of many cytokines and has been shown to increase *Leishmania* killing (Green et al., 1990, Mukbel et al., 2007) we compared the effects of *L. mexicana* infection or EVs on 1) unstimulated macrophages, 2) macrophages stimulated with LPS and IFNγ *before* the addition of *Leishmania* samples, and 3) macrophages stimulated with LPS and IFNγ *after* the addition of *Leishmania* samples. To the macrophages were added either (i) nothing, (ii) medium which has been through the same EV isolation procedure as the EV samples to control for endotoxin contamination, (iii) stationary phase promastigotes (PRO live), (iv) PRO or (v) DIF EVs. After 18 h incubation the culture supernatants were assayed for cytokines. We first looked for the induction of a broad panel of 36 human cytokines using a semi-quantitative Proteome Profiler kit (using samples from macrophage conditions 1 and 2). As expected, more cytokines were induced by LPS/IFNγ-activated iPSC macrophages (van Wilgenburg et al., 2013), and in total the following 14 cytokines were detected: MCP-1, MIP-1α/MIP-1β, CXCL1, CXCL10, CXCL11, ICAM-1, IFNγ, IL-1β, IL-1ra, IL-6, IL-8, MIF, Serpin-E1 and TNFα (Figure 5.3A). The remaining 22 undetected cytokines included IL-10 and IL-12, which have been implicated in *Leishmania* infection persistence (Anderson et al., 2008, Saha et al., 2007, Salhi et al., 2008) or clearance (Ghalib et al., 1995, Strauss-Ayali et al., 2005) respectively (Figure 5.3B). Relative levels of cytokines were quantified. The untreated and medium control samples induced similar levels of cytokine production, suggesting there was minimal endotoxin contamination during EV isolation (Figure 5.3C, D). Due to the semi-quantitative nature of the Proteome Profiler assay, only three-fold or more changes in cytokine production are considered to be reliable (based on guidance

from R&D representative). Among the LPS/IFNγ-pre-stimulated macrophage samples the following decreases in cytokine secretion were induced: CXCL10 and CXCL11 by all three *L. mexicana* samples; MIP-1α/β secretion by PRO live cells; IL-1β by both PRO live cells and PRO EVs (Figure 5.3C). Among the unstimulated macrophage samples, IL-1ra and IL-8 were decreased by PRO live cells (Figure 5.3D). No substantial increases in cytokine secretion were observed in response to any *L. mexicana* samples.

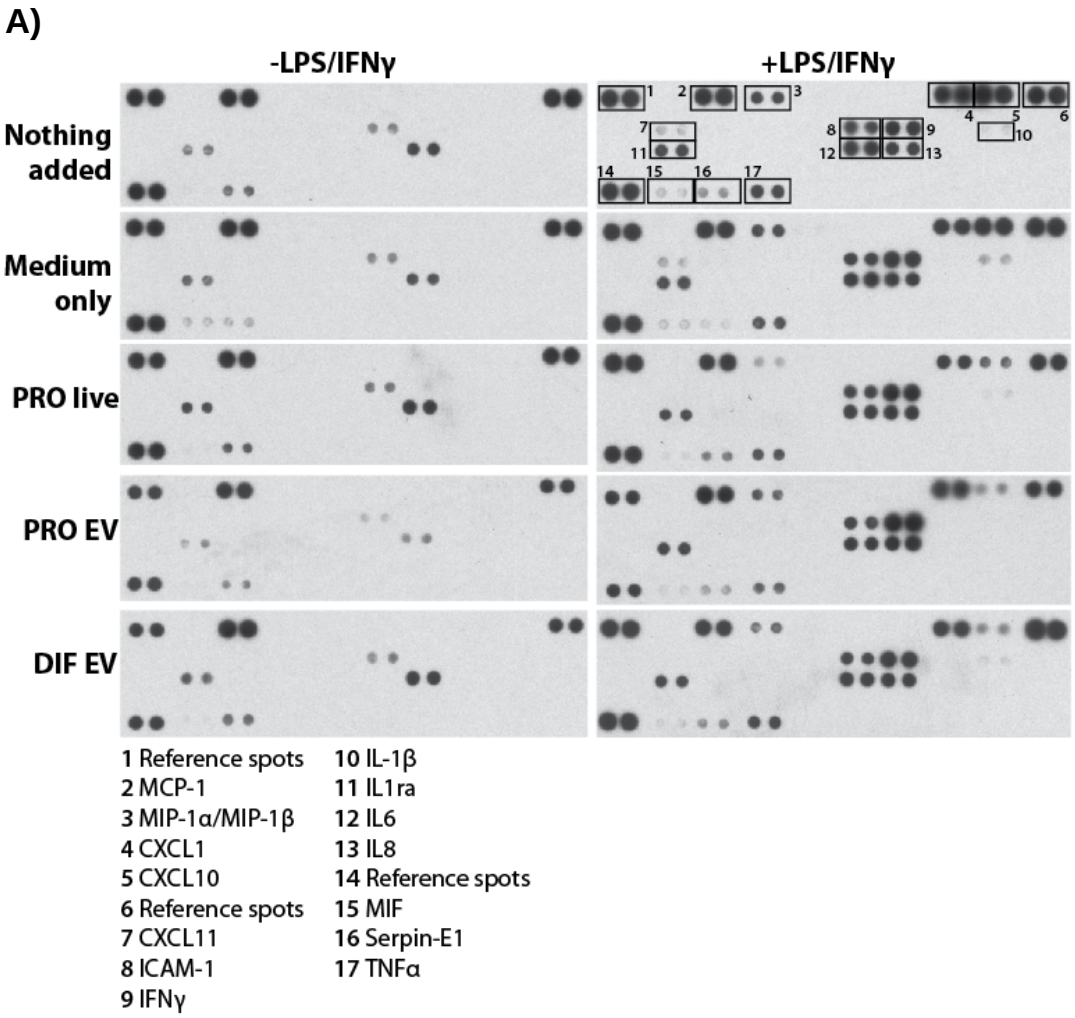

B)

CCL1	IL10
CCL5	IL12
CD40 ligand	IL13
Complement component C5/C5a	IL16
CXCL12	IL17A
G-CSF	IL17E
GM-CSF	IL18
IL-1α	IL21
IL2	IL27
IL4	IL32α
IL5	TREM-1

C)

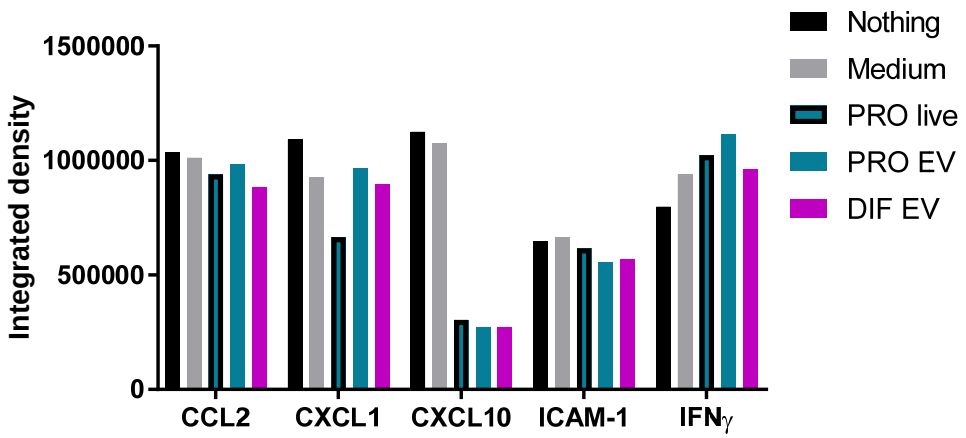

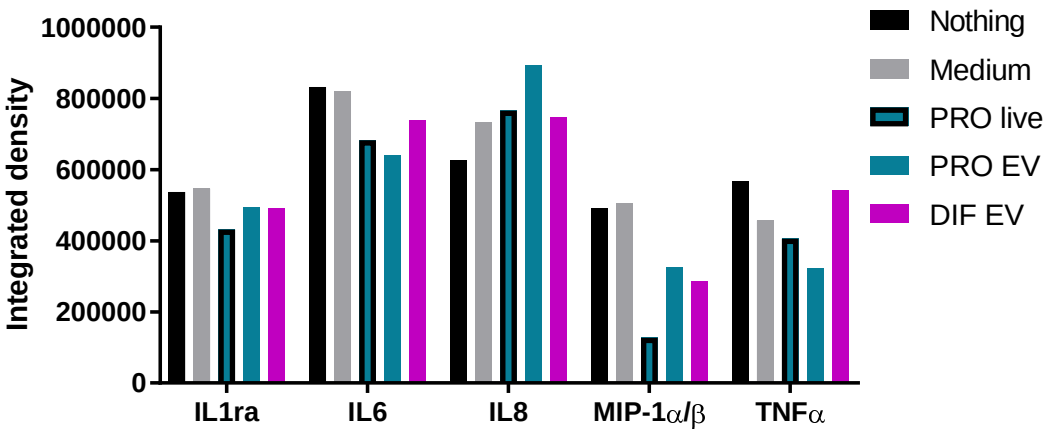
Integrated density
1000000
800000
600000
400000
200000
0
IL1ra
IL6
IL8
MIP-1α/β
TNFα
Nothing
Medium
PRO live
PRO EV
DIF EV

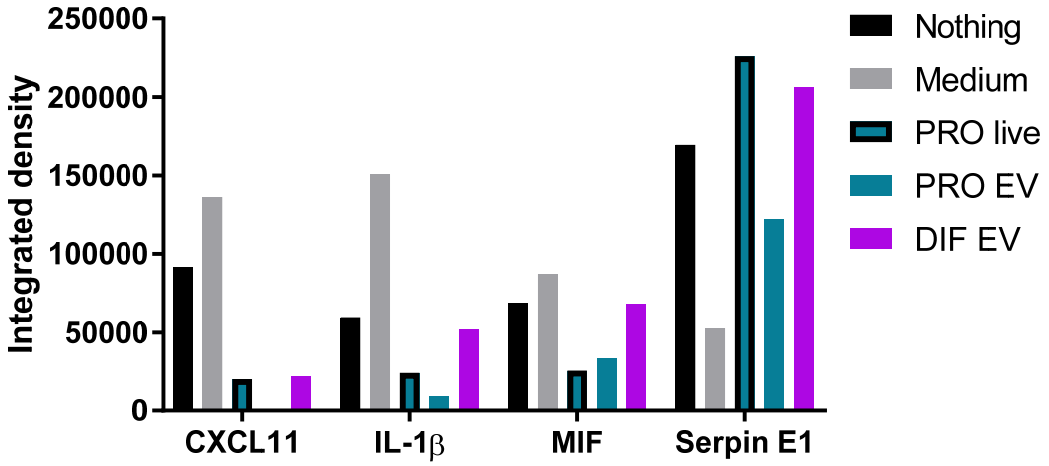
Integrated density
250000
200000
150000
100000
50000
0
CXCL11
IL-1β
MIF
Serpin E1
Nothing
Medium
PRO live
PRO EV
DIF EV

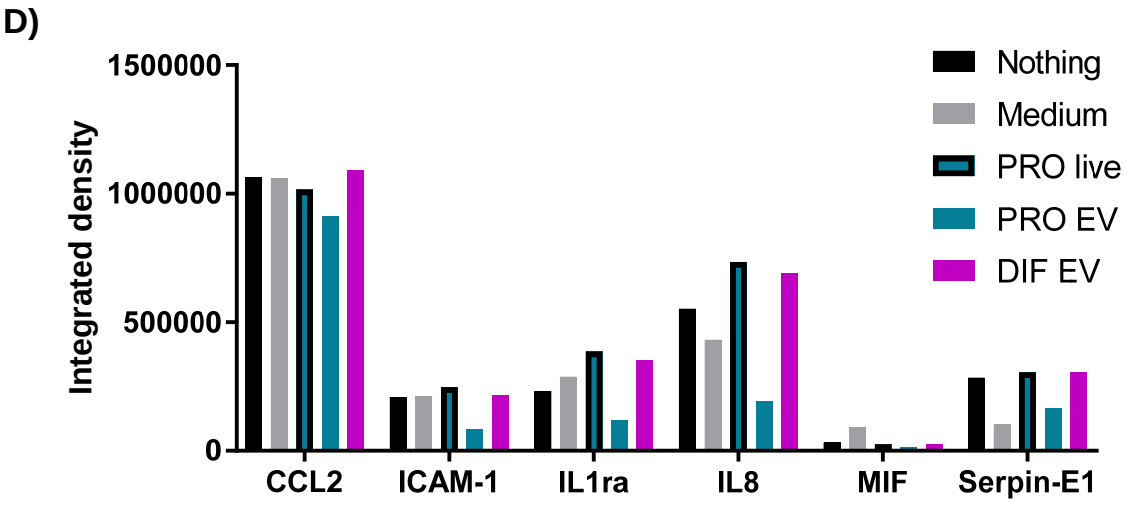

Figure 5.3. Proteome profiler cytokine screening of human macrophages incubated with live *Leishmania* or EVs. iPSC-derived human macrophages were treated for 3 days with LPS/IFNγ, or left untreated, then infected at an MOI of 10 with stationary phase *L. mexicana* Clone 3 promastigotes (PRO live) or incubated with PRO or DIF EVs from the same cell line. As negative controls either nothing or a medium control were added. After 18 h macrophage supernatants were collected and screened for a panel of 36 human cytokines using a Proteome Profiler kit. **A)** Proteome Profiler membranes showing cytokine detection (the more cytokine present the darker the spots). All the cytokine detection spots which were visible by eye are annotated and identified in the legend. The reference spots are non-specific positive controls to show that the assay was technically successful. **B)** All cytokine detection spots which were not visible by eye are identified and listed. **C** and **D**) Quantification of cytokine levels using ImageJ software. Only cytokines where the detection spots were visible by eye are shown. **C)** +LPS/IFNγ samples. **D)** –LPS/IFNγ samples.

We decided to follow these results up with quantitative ELISA analysis of samples from macrophage conditions 1, 2 and 3, measuring all 14 cytokines induced by *L. mexicana* samples, as well as IL-10, IL-12 and TGF-β1 which have been shown to be regulated by *Leishmania* infection (Anderson et al., 2008, Saha et al., 2007, Salhi et al., 2008)

((Teixeira et al., 2006, Matte and Olivier, 2002). For the quantitative ELISA, the samples were prepared under the same conditions as for the Proteome Profiler assay. Confirming the Proteome Profiler results, CXCL11 (Figure 5.4A) and CXCL10 (Figure 5.4C) secretion were significantly decreased by all three *L. mexicana* samples in LPS/IFNγ-pre-stimulated macrophages (condition 2), and the same effects were observed on CXCL1 (Figure 5.4B) and IFNγ (Figure 5.4E) secretion. These were the most consistent and substantial effects on cytokine secretion observed; CXCL1 secretion was reduced by ~50%, CXCL10 reduced by ~8-fold, CXCL11 by ~4-fold and IFNγ by ~2-fold. Smaller but significant decreases in CXCL1 (~2-fold, Figure 5.8C), CXCL10 (~3-fold, Figure 5.8B) and IFNγ (~10%, Figure 5.8D), but not CXCL11 (Figure 5.8A) secretion, were also induced by DIF EVs under macrophage condition 3 (Figure 5.4). PRO live cells also slightly decreased CXCL10 secretion but not as much as DIF EVs (Figure 5.8B). Overall, the effects of *L. mexicana* samples on cytokine production under macrophage condition 3 were different compared to condition 2 (Table 5.2A, B), and most significant changes were smaller in magnitude. Since we observed that PRO and DIF EVs induced very similar effects on cytokine secretion under macrophage conditions 1 and 2 (Figure 5.4-5.7), only DIF EVs were used for the macrophage condition 3 experiment. Under macrophage condition 1, CXCL10 secretion was also significantly decreased by all three samples (Figure 5.4D).

IL-8 (Figure 5.5A) and IL-1ra (Figure 5.5B) secretion by unstimulated macrophages were increased by PRO live cells and DIF EVs (Figure 5.5B). TNFα secretion by unstimulated macrophages was also increased by DIF EVs (Figure 5.5D), while its secretion by activated macrophages was decreased by PRO live cells and PRO EVs (Figure 5.5C). MCP-1 secretion by unstimulated macrophages was decreased by PRO

live cells (Figure 5.5E) and TGF-β1 secretion was increased by PRO and DIF EVs (Figure 5.5F). Finally, ICAM-1 secretion by activated macrophages was decreased by PRO EVs (Figure 5.6B). Other significant differences were measured but were not discernible by eye (Figure 5.6A, C, D, E). No significant changes in IL-10 (Figure 5.7A), IL-12 (Figure 5.7B), MIP-1β (Figure 5.7C) or IL-6 (Figure 5.7D) secretion were observed.

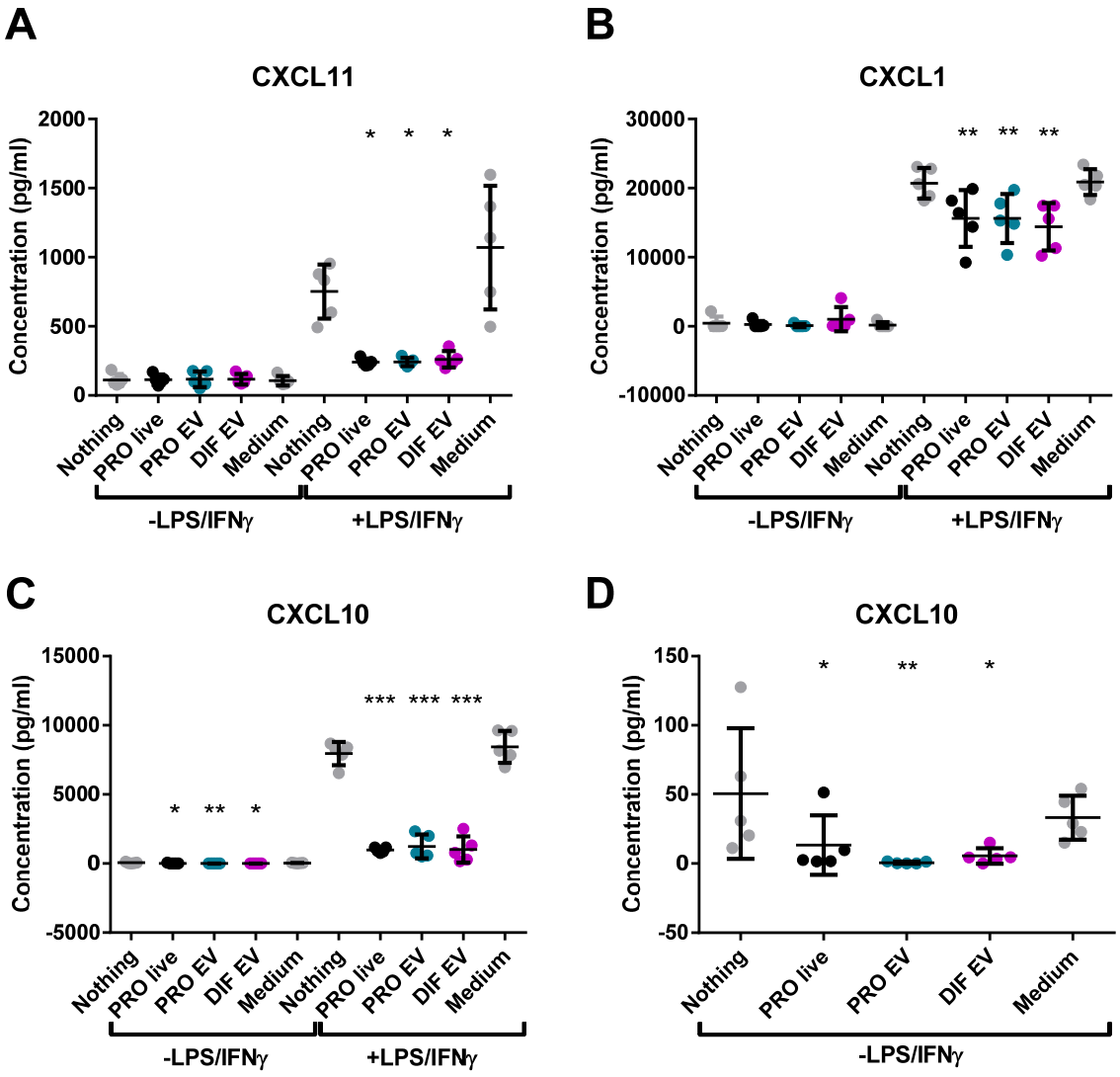

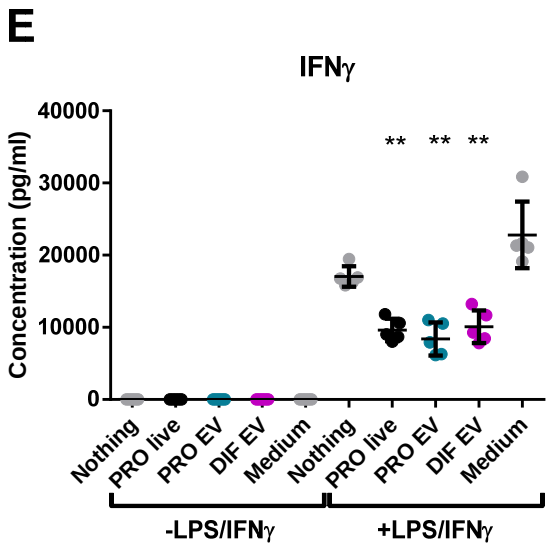

Figure 5.4. Cytokine analysis of human macrophages incubated with live *Leishmania* or EVs following LPS/IFNγ stimulation: cytokines which are strongly down-regulated in stimulated macrophages. **A-E)** Cytokines which are strongly down-regulated by *L. mexicana* PRO live cells and PRO and DIF EVs in stimulated macrophages are shown. As for Fig. 5.3, iPSC-derived human macrophages were treated or untreated for 3 days with LPS/IFNγ then infected at an MOI of 10 with stationary phase Clone 3 promastigotes (PRO live) or incubated with PRO or DIF EVs (MOI equivalent of 2500) from the same cell line. As negative controls either nothing or a medium control were added. After 18 h macrophage supernatants were collected and the 14 cytokines which were detected by Proteome Profiler analysis as shown in Fig. 5.3 plus IL-12, IL-10 and TGF-β1 were quantified by multiplexed Luminex ELISA. 5 replicates from two biological repeats are shown, error bars show the mean ± 1 standard deviation. Asterisks show significant differences compared to the medium control as tested by paired t-tests with p values as follows: * p≤0.05; ** p≤ 0.01; *** p≤0.001; **** p≤0.0001.

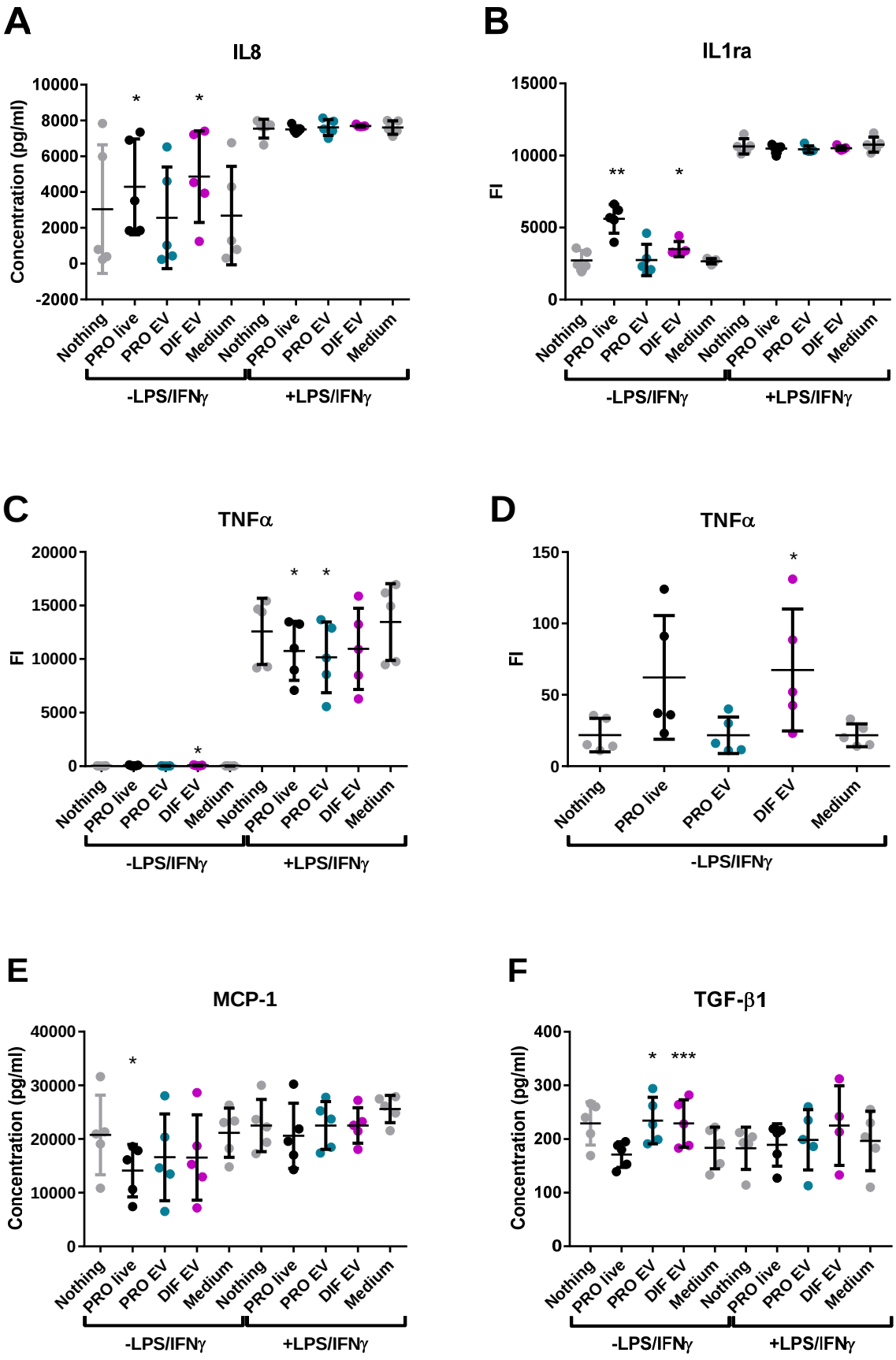
A
IL8
Concentration (pg/ml)
10000
8000
6000
4000
2000
0
-2000
*
*
Nothing
PRO live
PRO EV
DIF EV
Medium
Nothing
PRO live
PRO EV
DIF EV
Medium
-LPS/IFNγ
+LPS/IFNγ
B
IL1ra
FI
15000
10000
5000
0
**
*
Nothing
PRO live
PRO EV
DIF EV
Medium
Nothing
PRO live
PRO EV
DIF EV
Medium
-LPS/IFNγ
+LPS/IFNγ
C
TNFα
FI
20000
15000
10000
5000
0
*
*
*
Nothing
PRO live
PRO EV
DIF EV
Medium
Nothing
PRO live
PRO EV
DIF EV
Medium
-LPS/IFNγ
+LPS/IFNγ
D
TNFα
FI
150
100
50
0
*
Nothing
PRO live
PRO EV
DIF EV
Medium
-LPS/IFNγ
E
MCP-1
Concentration (pg/ml)
40000
30000
20000
10000
0
*
Nothing
PRO live
PRO EV
DIF EV
Medium
Nothing
PRO live
PRO EV
DIF EV
Medium
-LPS/IFNγ
+LPS/IFNγ
F
TGF-β1
Concentration (pg/ml)
400
300
200
100
0
*
***
Nothing
PRO live
PRO EV
DIF EV
Medium
Nothing
PRO live
PRO EV
DIF EV
Medium
-LPS/IFNγ
+LPS/IFNγ

Figure 5.5. Cytokine analysis of human macrophages incubated with live *Leishmania* or EVs following LPS/IFNγ stimulation: cytokines which are regulated in unstimulated macrophages. **A-F)** Cytokines which are weakly regulated by *L. mexicana* samples in unstimulated macrophages (and in stimulated macrophages in the case of TNFα (**C**)) are shown. **D)** The unstimulated samples shown in **(C)** are shown in more detail with a different y-axis scale. Experimental details are the same as for Fig. 5.4.

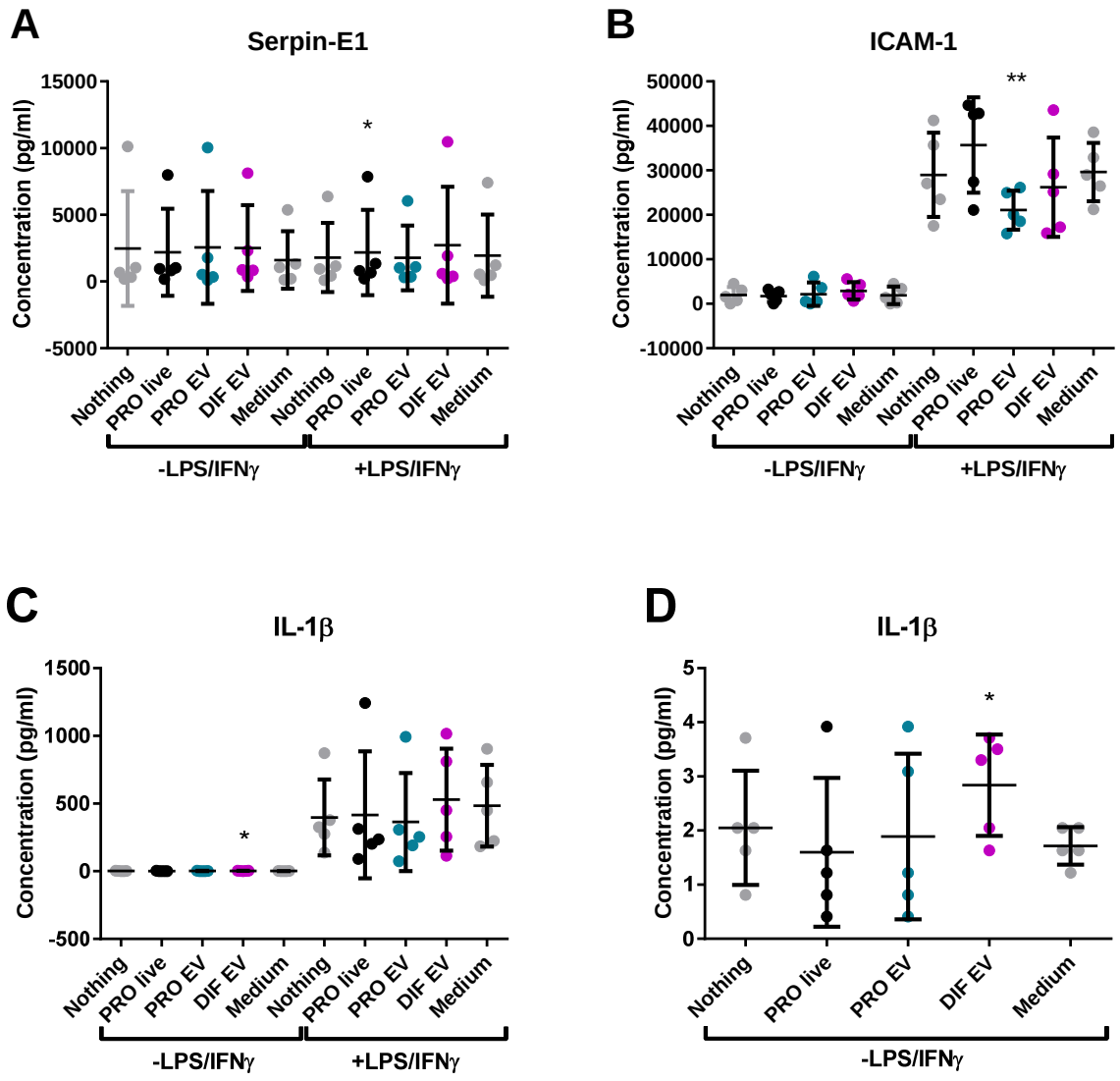

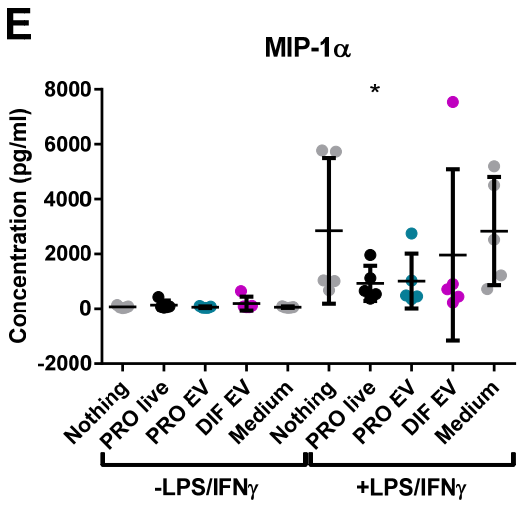

Figure 5.6. Cytokine analysis of human macrophages incubated with live *Leishmania* or EVs following LPS/IFNγ stimulation: cytokines which are very weakly regulated. **A-E)** Cytokines which are significantly but very weakly regulated by *L. mexicana* samples in stimulated macrophages (and in unstimulated macrophages in the case of IL-1β (**C**)) are shown. **D)** The unstimulated samples shown in **C)** are shown in more detail with a different y-axis scale. Experimental details are the same as for Fig. 5.4.

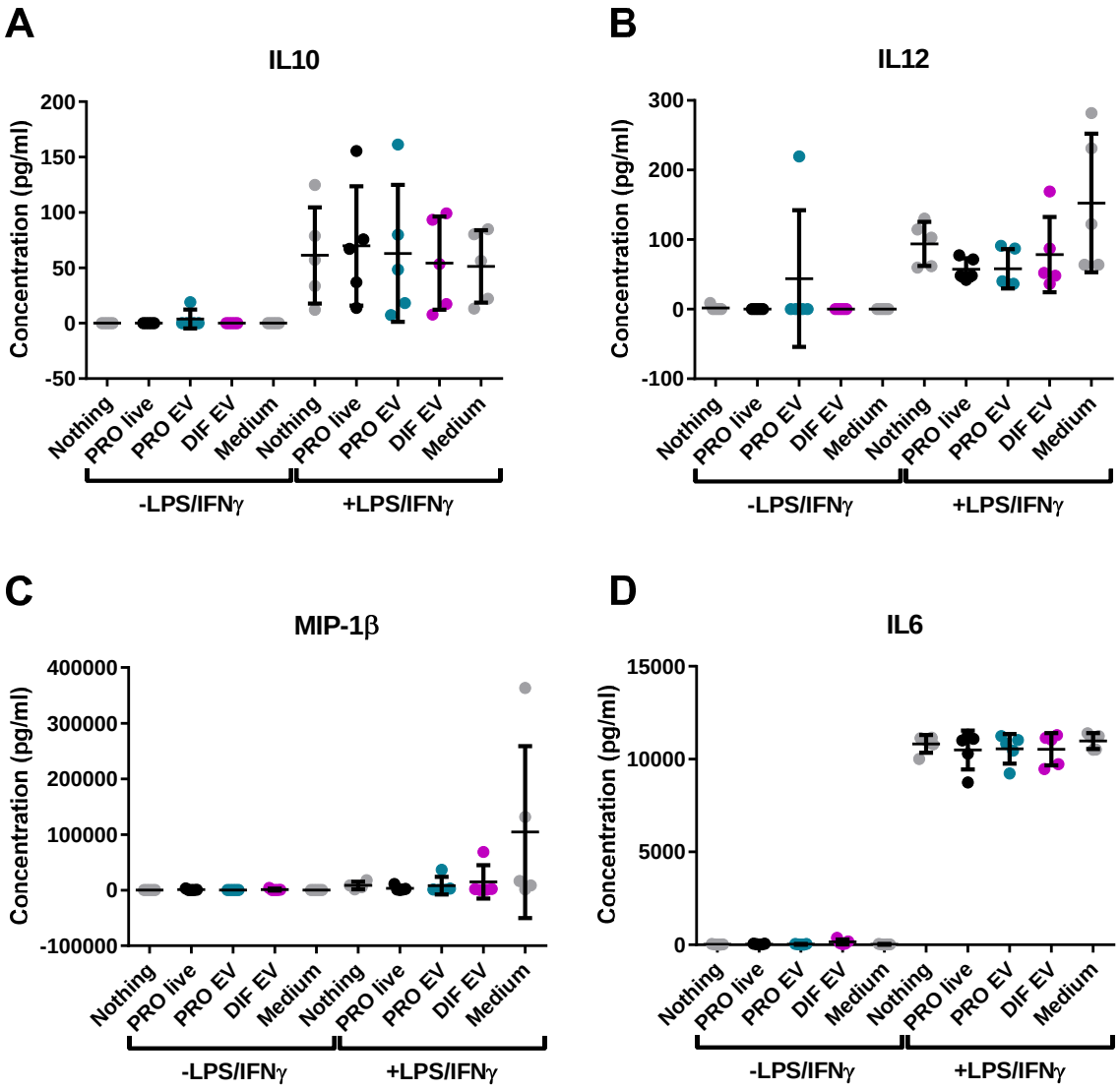

Figure 5.7. Cytokine analysis of human macrophages incubated with live *Leishmania* or EVs following LPS/IFNγ stimulation: cytokines which are not significantly regulated. **A-D)** Cytokines which do not differ significantly from the medium control in response to *L. mexicana* samples in stimulated or unstimulated macrophages are shown. Experimental details are the same as for Fig. 5.4.

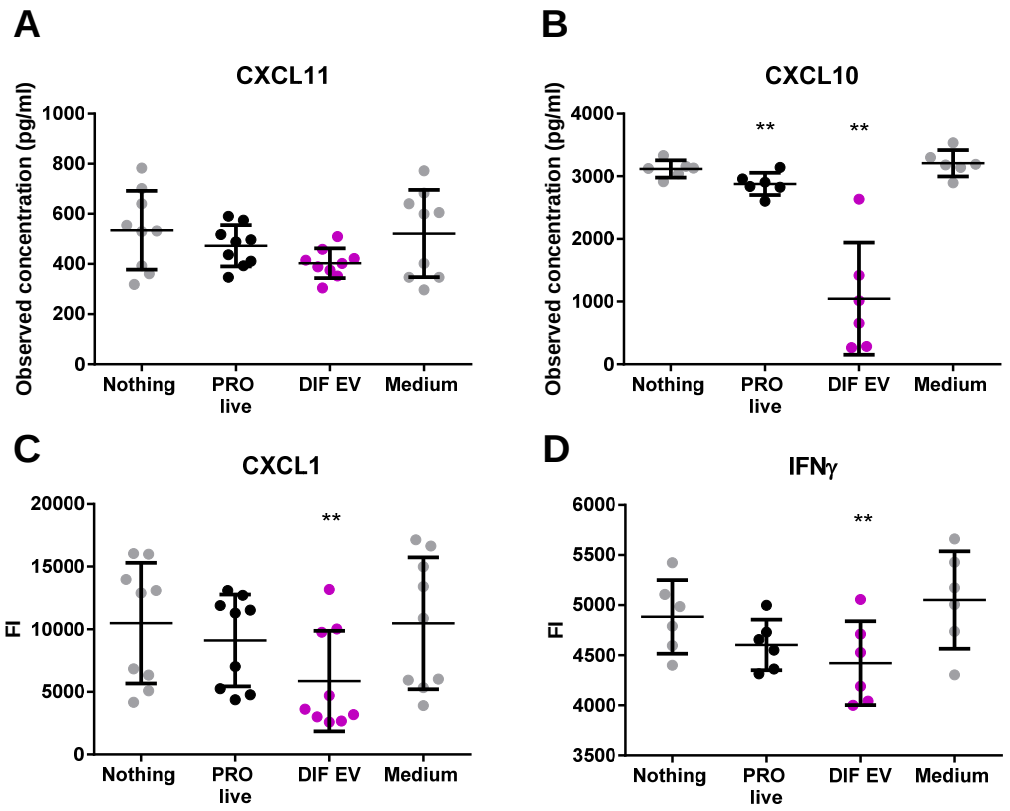

Figure 5.8. Quantitative ELISA cytokine analysis of human macrophages incubated with live *Leishmania* or EVs before LPS/IFNγ stimulation. Experimental details are the same as for Table 5.2. Data for CXCL11 (**A**), CXCL10 (**B**), CXCL1 (**C**) and IFNγ (**D**) secretion from stimulated macrophages are shown; these were the 4 cytokines shown to be dramatically suppressed by *L. mexicana* samples in pre-stimulated macrophages in Fig. 5.4. 9 replicates from three biological repeats are shown, error bars show the mean ± 1 standard deviation. Asterisks show significant differences compared to the medium control as tested by paired t-tests with p values as follows: * p≤0.05; ** p≤ 0.01; *** p≤0.001; **** p≤0.0001.

All significant differences were summarised (Table 5.1, Table 5.2). No substantial significant increases in cytokine production by activated macrophages were observed in response to any *L. mexicana* sample (Table 5.1A, Table 5.2A), while both increases and decreases by unstimulated macrophages were observed (Table 5.1B, Table 5.2B).

The observed decreases in CXCL10, CXCL11 and MIP-1β secretion from stimulated macrophages (Table 5.1A) are consistent with our Proteome Profiler results (Figure 5.3C)

A)

	PRO live	PRO EV	DIF EV
CXCL11	↓	↓	↓
CXCL1	↓	↓	↓
CXCL10	↓	↓	↓
IFNγ	↓	↓	↓
IL8			
IL1ra			
TNFα	↓	↓	
MCP-1			
TGF-β1			
Serpin-E1	↑		
ICAM-1		↓	
IL-1β			
MIP-1α	↓		
IL10			
IL12			
MIP-1β			
IL6			

B)

	PRO live	PRO EV	DIF EV
CXCL11			
CXCL1			
CXCL10	↓	↓	↓
IFNγ			
IL8	↑		↑
IL1ra	↑		↑
TNFα			↑
MCP-1	↓		
TGF-β1		↑	↑
Serpin-E1			
ICAM-1			
IL-1β			↑
MIP-1α			
IL10			
IL12			
MIP-1β			
IL6			

Table 5.1. Summary of quantitative ELISA cytokine analysis of human macrophages incubated with live *Leishmania* or EVs following LPS/IFNγ stimulation. Experimental details are the same as for Fig. 5.4. Whether the levels of each cytokine were significantly increased (↑), decreased (↓) or did not change (left blank) compared to the medium control is summarised for the +LPS/IFNγ (**A**) and –LPS/IFNγ (**B**) samples.

A)

	PRO live	DIF EV
CXCL11		
CXCL1		↓
CXCL10	↓	↓
IFNγ		↓
IL8	↓	↓
IL1ra		
TNFα		
MCP-1		
Serpin-E1		
ICAM-1	↓	↓
IL-1β	↓	↓
MIP-1α		
IL10	↑	
IL12		↓
MIP-1β	↓	↓
IL6		↓

B)

	PRO live	DIF EV
CXCL11		
CXCL1		
CXCL10		
IFNγ		
IL8		
IL1ra		
TNFα		
MCP-1	↓	
Serpin-E1		
ICAM-1		↓
IL-1β		
MIP-1α		↓
IL10		
IL12		
MIP-1β		↓
IL6		

Table 5.2. Summary of quantitative ELISA cytokine analysis of human macrophages incubated with live *Leishmania* or EVs before LPS/IFNγ stimulation. iPSC-derived human macrophages were infected at an MOI of 10 with stationary phase *L. mexicana* Clone 3 promastigotes (PRO live) or incubated with DIF EVs (MOI equivalent of 2500) from the same cell line for 18 h then treated or untreated for 2 days with LPS/IFNγ. As negative controls either nothing or a medium control were added. Macrophage supernatants were collected and the 14 cytokines which were detected by Proteome Profiler analysis as shown in Fig. 5.3 plus IL-12 and IL-10 were quantified by multiplexed Luminex ELISA. Whether the levels of each cytokine were significantly increased, decreased or did not change compared to the medium control, as tested by paired t-test, is summarised for the +LPS/IFNγ (**A**) and –LPS/IFNγ (**B**) samples. Data for CXCL1, CXCL10, CXCL11 and IFNγ are shown in more detail in Fig. 5.8. The data represents nine replicates from three biological repeats.

In these studies so far, *L. mexicana* EV samples with a very high MOI equivalent of 2500 cells had been added to macrophages; in the case of CXCL1, CXCL10, CXCL11 and

IFNγ these EV samples induced the same magnitude of cytokine secretion suppression as PRO live cells at an MOI of 10 (Figure 5.4). We performed a dose-response assay to test how much EV sample was required for the suppressive effect. CXCL11 secretion was still significantly decreased by MOI equivalents of DIF EV sample down to 10 (Figure 5.9A), while the suppressive effects of DIF EVs on CXCL10 (Figure 5.9B) and CXCL1 (Figure 5.9C) were lost at MOI equivalents of 250. IFNγ secretion was not significantly decreased by DIF EVs in this experiment (Figure 5.9D); this may be due to variations between experiments in the extraneous IFNγ added to stimulate the macrophages (the same IFNγ concentrations were added but the potency may have varied depending on the batch and age of sample).

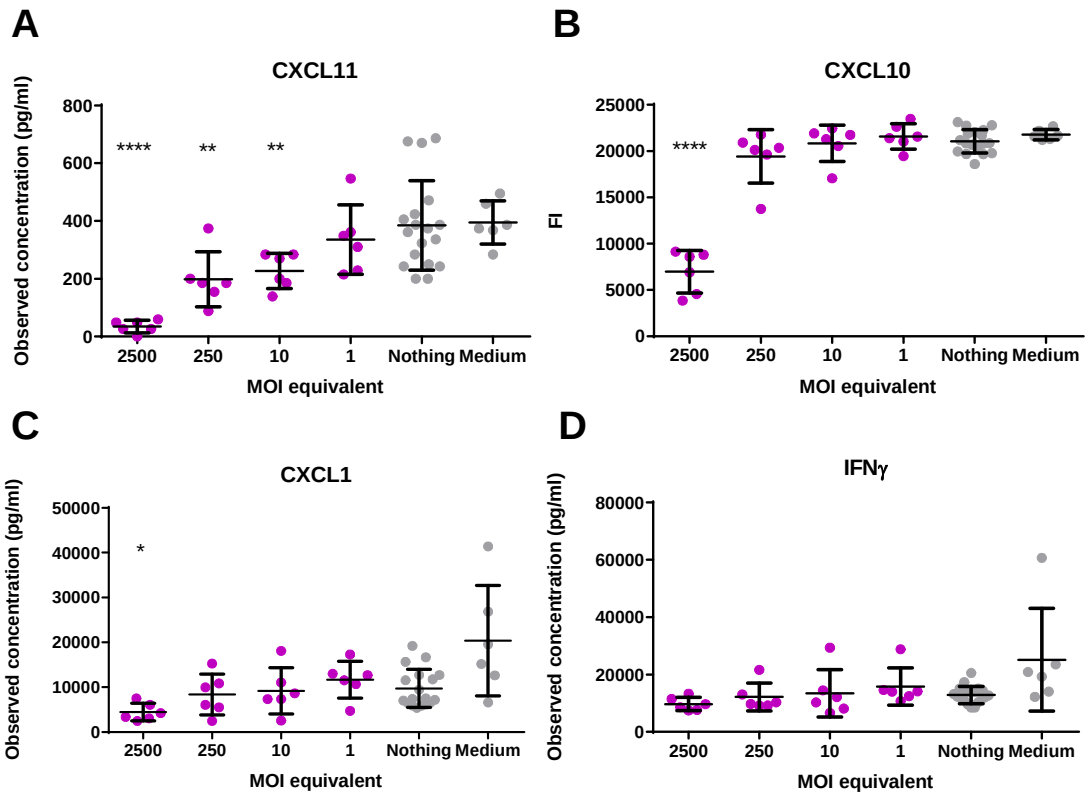

Figure 5.9. Cytokine dose response analysis of human macrophages incubated with EVs. iPSC-

derived human macrophages were treated for 2 days with LPS/IFNγ then incubated with different cell equivalents of DIF EVs from *L. mexicana* Clone 3 cells for 18 h. As negative controls either nothing or a medium control were added. **A-D)** Macrophage supernatants were collected and the 4 cytokines which were shown to be dramatically reduced in Fig. 5.4 were quantified by multiplexed Luminex ELISA. Six replicates from two biological repeats are shown, error bars show the mean ± 1 standard deviation. Asterisks show significant differences compared to the medium control as tested by paired t-tests with p values as follows: * p≤0.05; ** p≤ 0.01; *** p≤0.001; **** p≤0.0001.

5.2.2. LPG contributes to effects on cytokine production

Having detected LPG in our EV samples (Figure 4.1, Chapter 4) we decided to use our LPG-deficient *ΔLPG1* cell line (Figure 4.12, Chapter 4) to investigate whether LPG contributes to the observed effects on macrophage cytokine secretion (Figure 5.4). PRO live cells or DIF EVs from parental, *ΔLPG1* and AB cell lines were added to LPS/IFNγ-stimulated macrophages and CXCL1, CXCL10, CXCL11 and IFNγ secretion was measured, since these cytokines were affected to the greatest extent by non-LPG-deficient *L. mexicana* samples (Figure 5.4). As previously observed, CXCL1 (Figure 5.10A, B), CXCL10 (Figure 5.10C, D) and CXCL11 (Figure 5.10E, F) secretion were decreased by the parental non-LPG-deficient PRO live and DIF EV samples. Suppression of CXCL10 (Figure 5.10C, D) and CXCL11 (Figure 5.10E, F) secretion was reduced in response to *ΔLPG1* PRO live cells and DIF EVs, and these effects were fully restored by the AB samples. In the case of CXCL10, *ΔLPG1* DIF EVs fully restored CXCL10 levels to those of the untreated controls (Figure 5.10D).

As observed in the previous experiment (Figure 5.9D), IFNγ secretion was not significantly decreased by *L. mexicana* samples (Figure 5.10G, H); this may be due to variable concentrations between experiments of extraneous IFNγ added to stimulate the macrophages. The level of CXCL1 secretion was similar in response to PRO live cells (Figure 5.10A) or DIF EVs (Figure 5.10B) from parental, *ΔLPG1* and AB cell lines.

Since human iPSC-derived macrophages are a new model system for *Leishmania*-host interactions studies, we wondered whether the effects of *L. mexicana* samples on cytokine production and their dependency on LPG could be replicated in a more established system: murine BMDMs. CXCL1, CXCL10 and IFNγ secretion were measured, as for the human macrophages. CXCL11 was not measured since the

murine Luminex ELISA assay does not include it, although CXCL11 is present in mice (Widney et al., 2000). IL-10 and TNFα were also included because of their documented regulation in murine macrophages by *Leishmania* samples (Srivastava et al., 2013, Arango Duque et al., 2014). CXCL1 (Figure 5.11A, B) and CXCL10 (Figure 5.11C, D) secretion were both reduced, by ~50% and by ~5-fold respectively, by parental PRO live cells and DIF EVs. In both cases, the suppression of cytokine secretion was reduced but not fully abolished in response to *ΔLPG1* PRO live cells (Figure 5.11A, C) and DIF EVs (Figure 5.11B, D) and these effects were fully restored by the AB samples. Although statistically significant differences were observed, no substantial effects of *L. mexicana* PRO live cells or DIF EVs on IFNγ (Figure 5.11E, F), TNFα (Figure 5.11G, H) or IL-10 (Figure 5.11I, J) secretion were observed. Two different batches of BMDMs from independent labs were used for this experiment, three replicates from one batch and five from the other; this explains the observation that, for all cytokines except CXCL10, there is distinct clustering of cytokine concentrations from the two replicate batches. Importantly, despite the differences in relative levels between batches of BMDMs, all replicates follow the same trends in response to *L. mexicana* samples (Figure 5.11A-J).

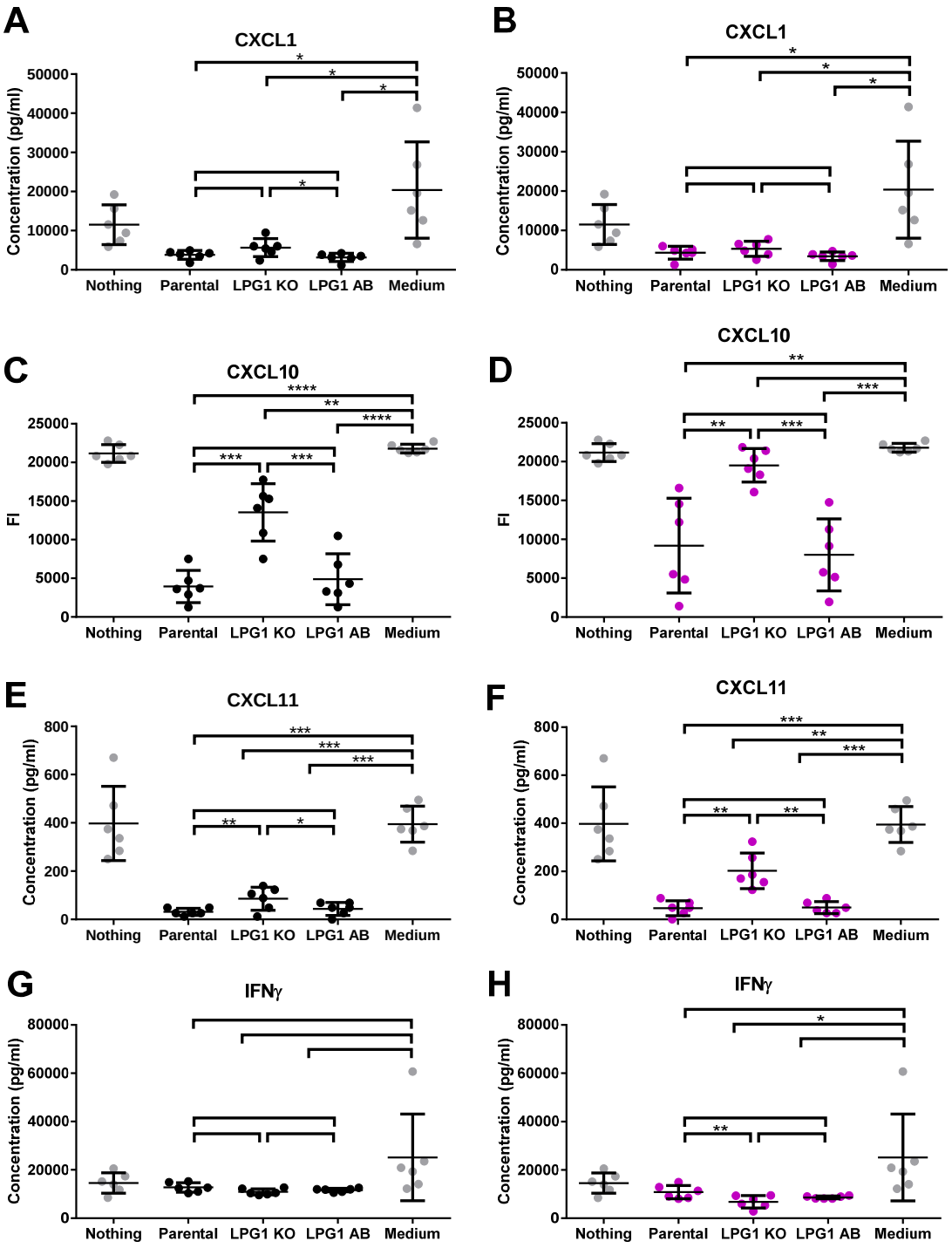
A
CXCL1
Concentration (pg/ml)
50000
40000
30000
20000
10000
0
Nothing
Parental
LPG1 KO
LPG1 AB
Medium
B
CXCL1
Concentration (pg/ml)
C
CXCL10
FI
25000
20000
15000
10000
5000
D
CXCL10
FI
E
CXCL11
Concentration (pg/ml)
800
600
400
200
F
CXCL11
G
IFNγ
80000
60000
40000
20000
H
IFNγ

Figure 5.10. LPG contributes to the effect of *Leishmania* cells and EVs on human macrophage cytokine production. iPSC-derived human macrophages were treated for 2 days with LPS/IFNγ then infected at an MOI of 10 with stationary phase *L. mexicana* promastigotes (**A, C, E, G**) or incubated with DIF EVs at an MOI equivalent of 2500 (**B, D, F, H**) from parental (Cas9 T7 (p)), *ΔLPG1* and *LPG1* AB cell lines. As negative controls either nothing or a medium control were added. After 18 h macrophage supernatants were collected and the 4 cytokines which were shown to be dramatically reduced in Fig. 5.4 were quantified by multiplexed Luminex ELISA. Six replicates from two biological repeats are shown, error bars show the mean ± 1 standard deviation. Asterisks show significant differences compared to the medium control as tested by paired t-tests with p values as follows: * p≤0.05; ** p≤ 0.01; *** p≤0.001; **** p≤0.0001.

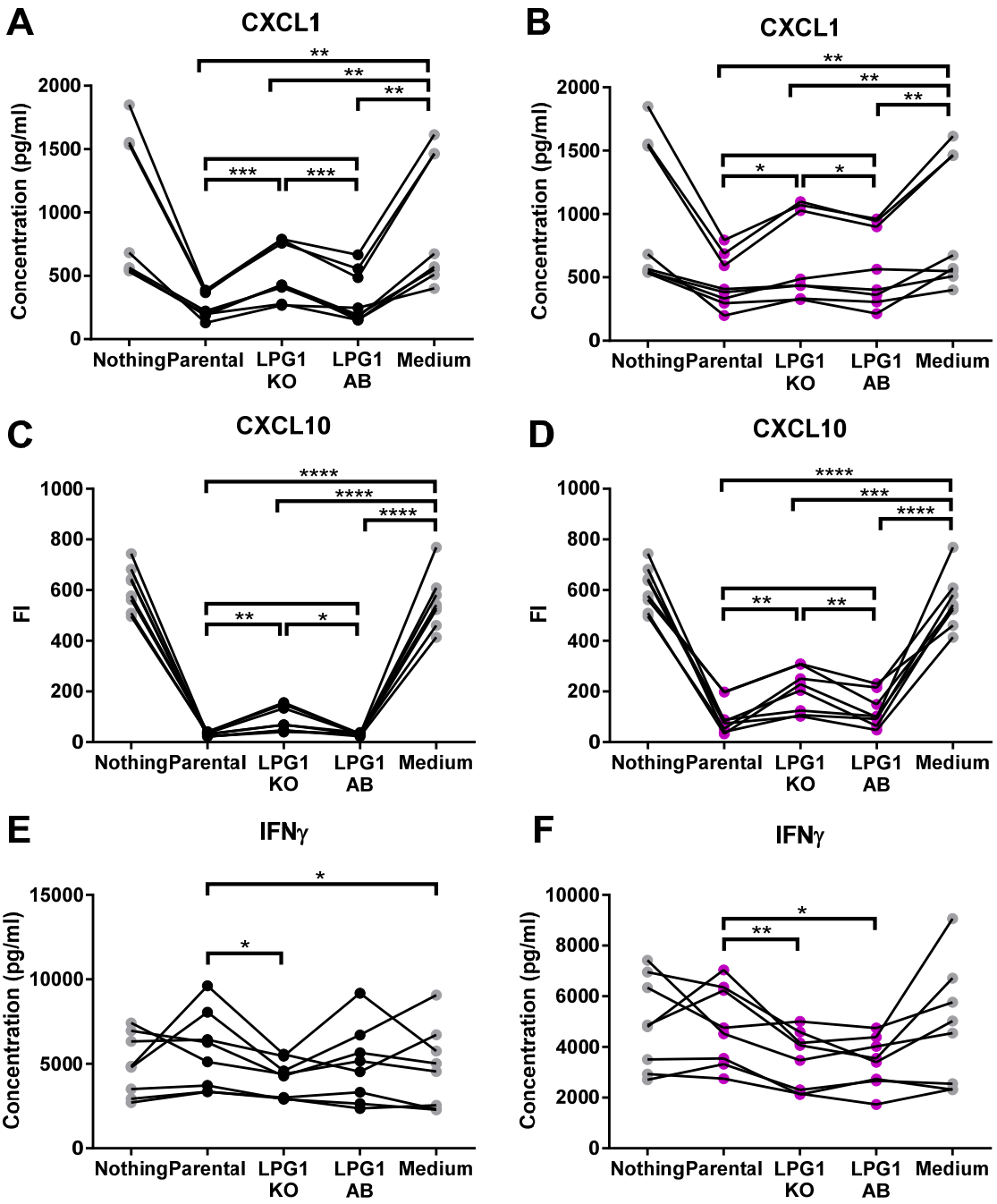
A
CXCL1
Concentration (pg/ml)
2000
1500
1000
500
0
**
**
**
***
***
Nothing
Parental
LPG1 KO
LPG1 AB
Medium
B
CXCL1
Concentration (pg/ml)
2000
1500
1000
500
0
**
**
**
*
*
Nothing
Parental
LPG1 KO
LPG1 AB
Medium
C
CXCL10
FI
1000
800
600
400
200
0
****
****
****
**
*
Nothing
Parental
LPG1 KO
LPG1 AB
Medium
D
CXCL10
FI
1000
800
600
400
200
0
****
***
****
**
**
Nothing
Parental
LPG1 KO
LPG1 AB
Medium
E
IFNγ
Concentration (pg/ml)
15000
10000
5000
0
*
*
Nothing
Parental
LPG1 KO
LPG1 AB
Medium
F
IFNγ
Concentration (pg/ml)
10000
8000
6000
4000
2000
0
*
**
Nothing
Parental
LPG1 KO
LPG1 AB
Medium

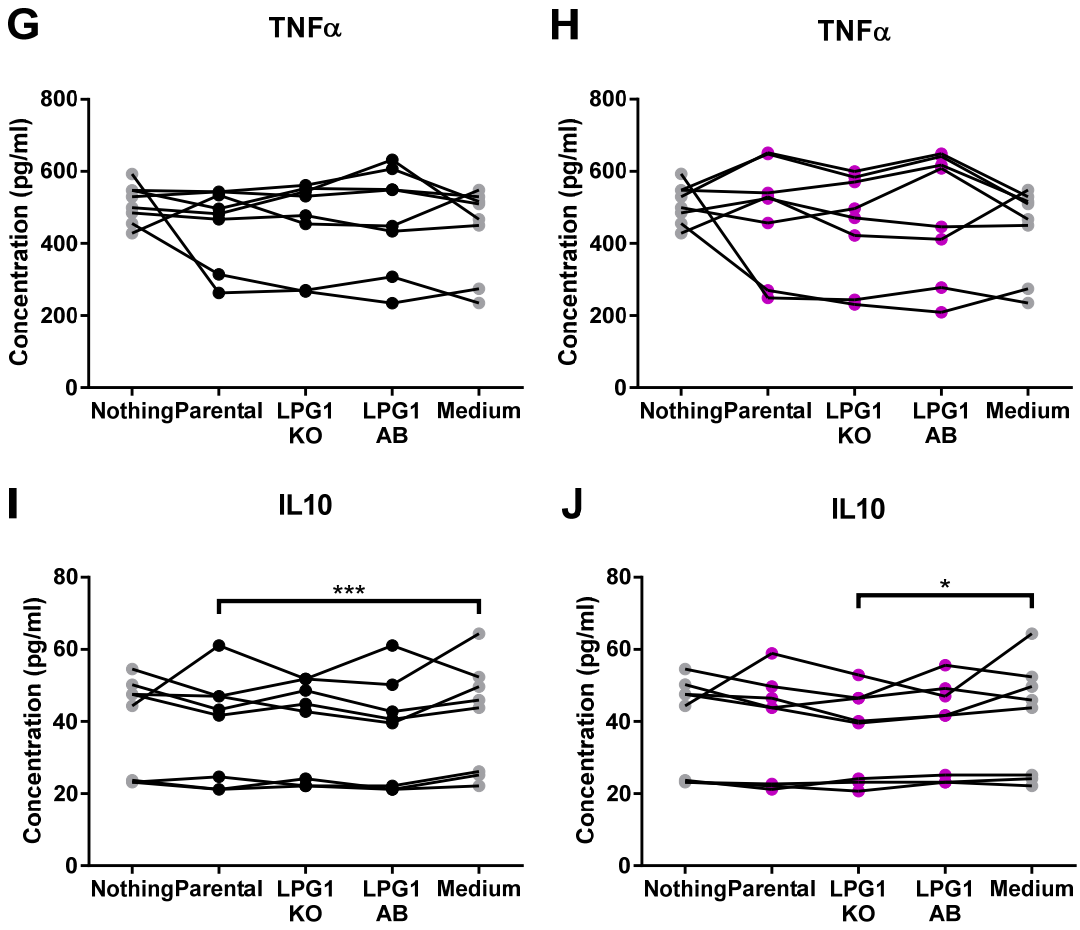

Figure 5.11. *Leishmania* cells and EVs induce similar changes in cytokine production in murine and human macrophages. Murine BMDMs were treated for 2 days with LPS/IFNγ then infected at an MOI of 10 with stationary phase *L. mexicana* promastigotes (**A, C, E, G, I**) or incubated with DIF EVs at an MOI equivalent of 2500 (**B, D, F, H, J**) from parental (Cas9 T7 (p)), *ΔLPG1* and *LPG1* AB cell lines. As negative controls either nothing or a medium control were added. After 18 h macrophage supernatants were collected and IL-10 and TNFα in addition to CXCL1, CXCL10 and IFNγ, which were shown to be dramatically reduced in Fig. 5.4 (CXCL11 not available in murine Luminex assay although present in the mouse), were quantified by multiplexed Luminex ELISA. Eight replicates from three biological repeats are shown with lines between the paired data. Asterisks show significant differences compared to the medium

control as tested by paired t-tests with p values as follows: * p≤0.05; ** p≤ 0.01; *** p≤0.001; **** p≤0.0001.

5.2.3. Fewer EVs are isolated from *ΔLPG1* cells

Given the loss of chemokine suppression in response to EVs from *ΔLPG1* cells, we wanted to check whether the number of EVs released from *ΔLPG1* cells is comparable to parental cells. Using NTA, the number of EVs released from *ΔLPG1* cells was 2-6-fold lower than parental cells, with a mean of 3-fold, and the parental level of EV release was restored in AB cells (Figure 5.12A, B).

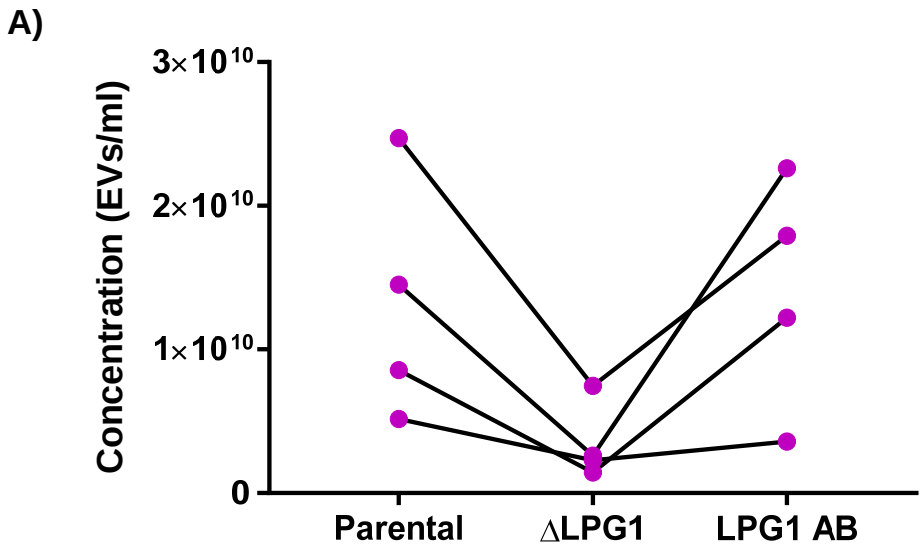

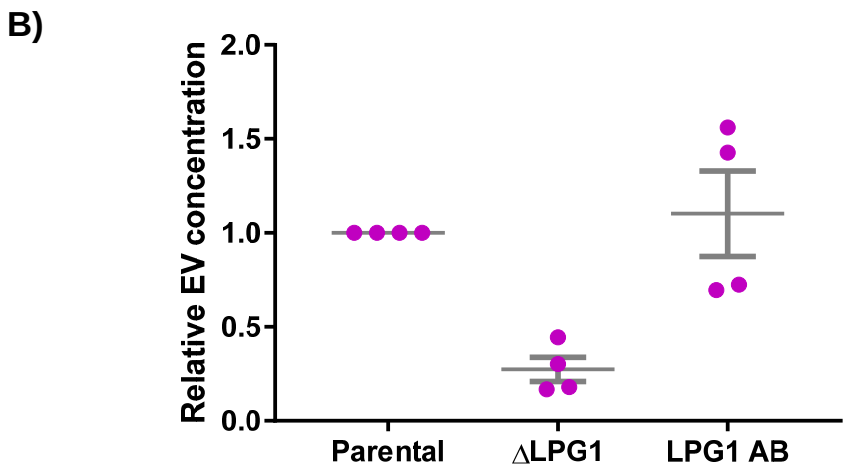

Figure 5.12. Fewer EVs are isolated from *ΔLPG1* parasites. DIF EVs were isolated from equal numbers of parental (*L. mexicana* Cas9 T7 (p)), *ΔLPG1* and *LPG1* AB cell lines and EV concentrations were measured by NTA. Four biological repeats were carried out: **A)** raw data with lines between the paired data points **B)** data normalised to the parental values with error bars ± SEM. Statistical analysis by unpaired one-way ANOVA indicated statistically significant differences between the samples with a p value of 0.0039.

5.2.4. *ΔLPG1* cells are able to survive inside human macrophages

L. mexicana ΔLPG1 cells have been shown to have undiminished virulence compared to WT cells in murine macrophages and mice (Ilg, 2000), but these experiments have not been carried out in human macrophages. We sought to compare the infection levels of parental, *ΔLPG1* and AB cell lines in human iPSC-derived macrophages. We carried out the infections in both unstimulated macrophages and macrophages pre-stimulated with LPS and IFNγ, since the latter condition is expected to enhance parasite killing by macrophages (Green et al., 1990, Mukbel et al., 2007). The DNA dye Draq5 was used to stain *L. mexicana* and macrophage nuclei and quantify infection levels (Figure 5.13A). Both with and without LPS and IFNγ, the absolute initial infection

level (both *Leishmania* per 100 macrophages and % infected macrophages) was lower in the parental sample than the *ΔLPG1* sample (~2-fold fewer *Leishmania* per 100 macrophages) with the AB falling in between the two (Figure 5.13B). The initial number of *Leishmania* per 100 macrophages was roughly 50 parasites lower for each sample in the LPS and IFNγ-treated macrophages compared to the untreated (within a range of 100-300), and after 48 h was roughly 100 lower for the *ΔLPG1* and AB cell lines and 30 lower for the parental cell line (Figure 5.13B). In both treated and untreated samples, the % infected macrophages fell in the first 24-48 h, then rose up to 72 h before decreasing again (Figure 5.13B). A similar pattern was seen for *Leishmania* per 100 macrophages, except with the parental cell line which increased up to 72 h in the untreated macrophage sample and up to 24 h before decreasing in the LPS and IFNγ treated sample (Figure 5.13B). When infection levels were normalised to the 0 h time point, the parental cell line had increased infection levels compared to the *ΔLPG1* or AB cell lines at all subsequent time points (both *Leishmania* per 100 macrophages and % infected macrophages) (Figure 5.13C). The difference between the cell lines in terms of *Leishmania* per 100 macrophages was enhanced in the LPS and IFNγ-treated samples; at 24 h, for example, the number of parental *Leishmania* per 100 macrophages was ~20% higher than *ΔLPG1 Leishmania* in the untreated sample, compared to ~120% higher in the LPS and IFNγ-treated sample (Figure 5.13C).

The major conclusion from this data is that LPG is not essential for *L. mexicana* to survive and replicate in human macrophages, but there may be subtle differences in the dynamics of infection between parental and LPG-deficient parasites.

A)

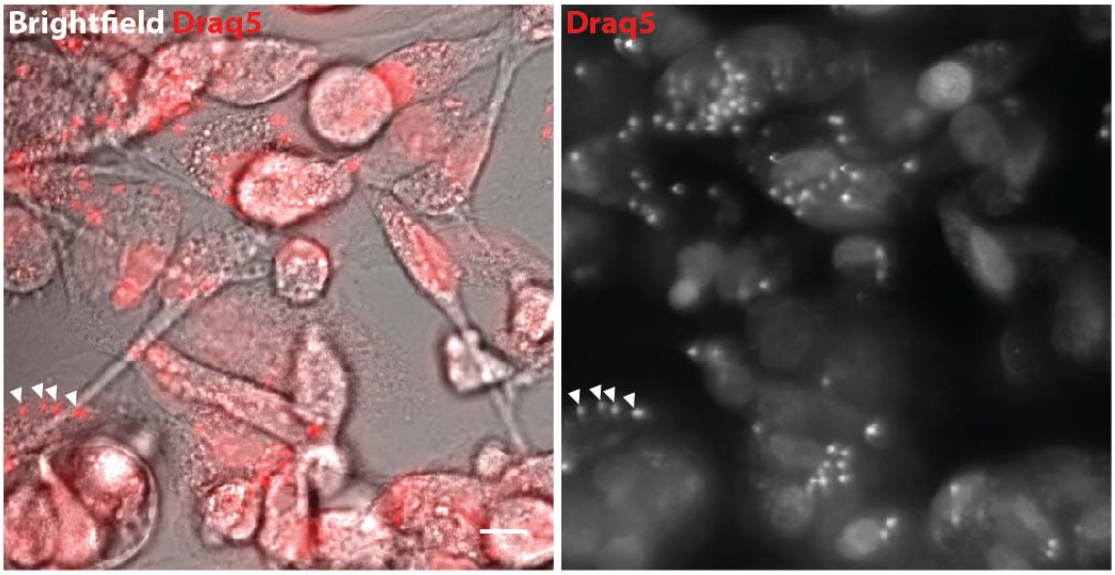

B)

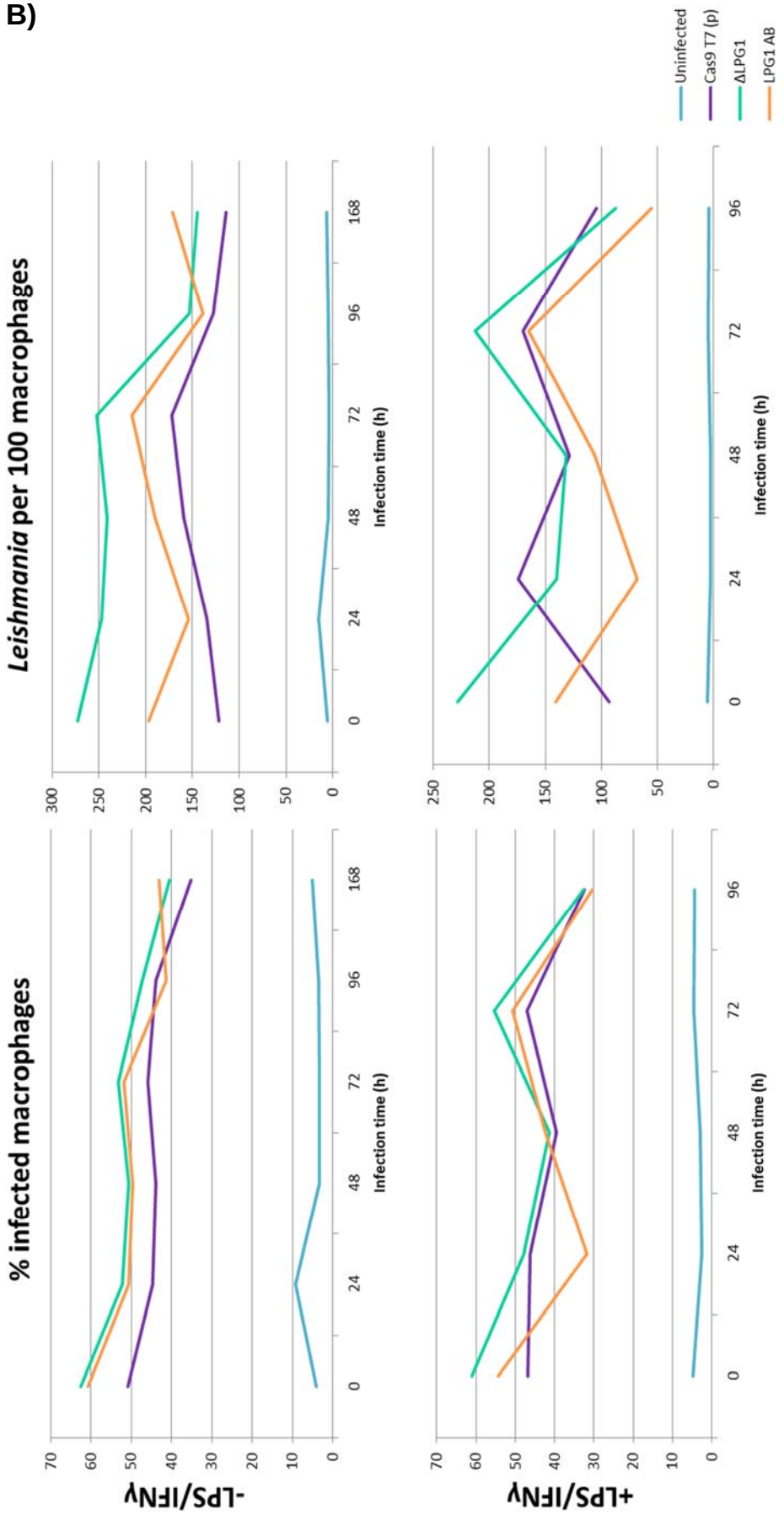
% infected macrophages
Leishmania per 100 macrophages
-LPS/IFNγ
+LPS/IFNγ
Infection time (h)
Uninfected
Cas9 T7 (p)
ΔLPG1
LPG1 AB

C)

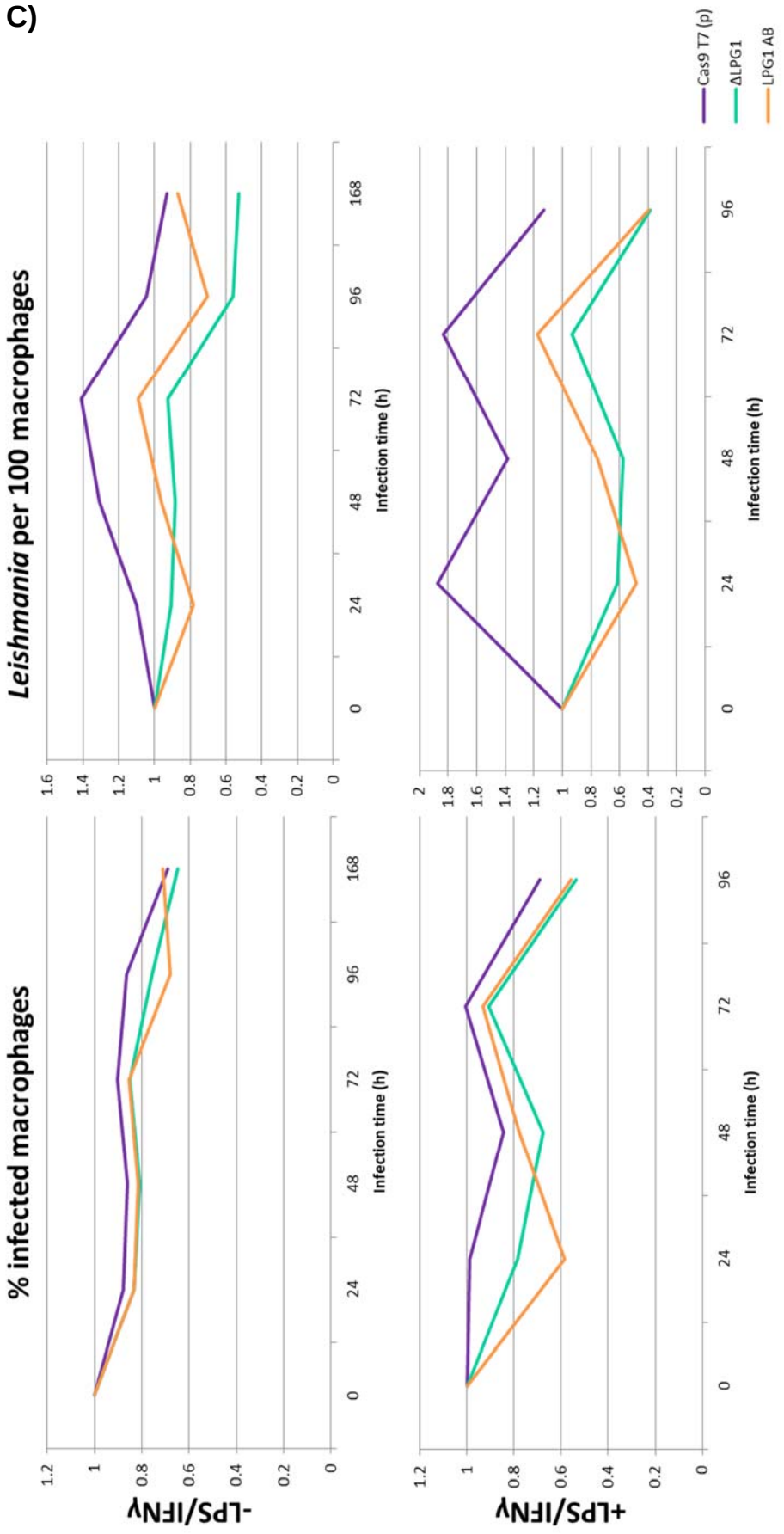
Cas9 T7 (p)
ΔLPG1
LPG1 AB
% infected macrophages
Leishmania per 100 macrophages
-LPS/IFNγ
+LPS/IFNγ
Infection time (h)

Figure 5.13. Time course of infection of human macrophages with *ΔLPG1* parasites. Human iPSC-derived macrophages which had been treated or untreated for 3 days with LPS and IFNγ were infected with stationary phase parental (*L. mexicana* Cas9 T7 (p)), *ΔLPG1* clone F3 or *LPG1* AB cells at a MOI of 10. An uninfected control was also analysed. At 2 h post-infection (the "0 h sample") all samples were washed, and one set of eight samples (three cell lines and uninfected control ± LPS/IFNγ) was stained with the DNA dye Draq5 and imaged live on an inverted fluorescence microscope. The remaining sets of samples were stained and imaged subsequently at 24, 48, 72, 96 and 168 h (the +LPS/IFNγ samples could not be imaged at 168 h due to macrophage death). The Draq5 channel was used to manually select macrophage and parasite nuclei, then these selections were analysed using an ImageJ Macro (developed by Jessica Valli) to determine how many parasites were inside each macrophage. **A)** An example of an image used to count macrophage and parasite nuclei (24 h, Cas9 T7 (p), -LPS/IFNγ sample). Four of the parasites are indicated by arrowheads to illustrate how they appear with Draq5 staining. Scale bar 10 μm. **B** and **C**) Time courses showing the percentage of infected macrophages and the number of parasites in every 100 macrophages. The raw data (**B**) and data normalised to the 0 h time point (**C**) are shown.

5.2.5. Analysis of effects of infective promastigotes and EVs on macrophage signalling pathways

Given that we found suppressive effects of *L. mexicana* PRO live cells and DIF EVs on CXCL- chemokine secretion (Figure 5.4) and these effects appear to be partially LPG-dependent (Figure 5.10, Figure 5.11), we decided to investigate the signalling pathways responsible which LPG might target in the macrophage. Signalling phosphoproteins Erk1/2 and p38 were chosen for study because they are regulated by LPG (Balaraman et al., 2005, de Veer et al., 2003). STAT3 is implicated in CXCL11 expression (Yang et al., 2007a), and forms signalling complexes with STAT1 in

response to IFNγ. Finally, STAT4 is inducibly expressed in macrophages and regulates the expression of pro-inflammatory cytokines (Fukao et al., 2001, Schindler et al., 2001). Expression of the active phosphoproteins in human iPSC-derived macrophages was first tested by WB under conditions known to induce expression (addition of LPS or a cytokine) with unstimulated cells as negative controls. All phosphoproteins were robustly expressed within 1 h of macrophage stimulation (Figure 5.14A, C, D, E), except STAT4. Erk1/2, but not STAT1, STAT3 or p38, was detected in unstimulated macrophages (Figure 5.14A, C, D, E). Although faint products of approximately the expected molecular weight of STAT4 were detected in all conditions (Figure 5.14B), it was not clear whether any of the bands correspond to STAT4 since there was no increase as expected upon IL-12 stimulation. Therefore, STAT4 was not taken forward for further study.

The expression of STAT1, STAT3, Erk1/2 and p38 were measured by WB at several time points during an 18 h incubation of LPS/IFNγ-stimulated human macrophages with *L. mexicana* DIF EVs from parental, *ΔLPG1* and AB cells. All phosphoproteins were detected in the negative control macrophage sample (Figure 5.15). This is likely because these phosphoproteins are induced in LPS and/or IFNγ stimulated macrophages; this has been shown in our own experiments for STAT1, p38 and Erk1/2 (Figure 5.14), and STAT3 is also documented to be induced by IFNγ (Yang et al., 2007a). It is not clear why two bands were present in the anti-p38 positive control and only the lower band was present in all other samples (Figure 5.15), however it is the lower band which is the expected molecular weight of activated phospho-p38 (T180/y182). All phosphoproteins were detected at all time points and in response to all samples (Figure 5.15). Differences in band intensity between the time points (for example, all

the phosphoprotein bands are stronger at the 0.5 h time point) are likely to be due to technical issues rather than biological effects; samples from different time points were present on different membranes and were therefore exposed under slightly different conditions. We looked for a pattern of phosphoprotein expression which mirrored the differences observed in chemokine levels in response to *ΔLPG1* versus parental and AB samples (Figure 5.10 and Figure 5.11). However, no consistent differences in phosphoprotein expression between macrophages incubated with parental, *ΔLPG1* or AB DIF EVs were observed (Figure 5.15).

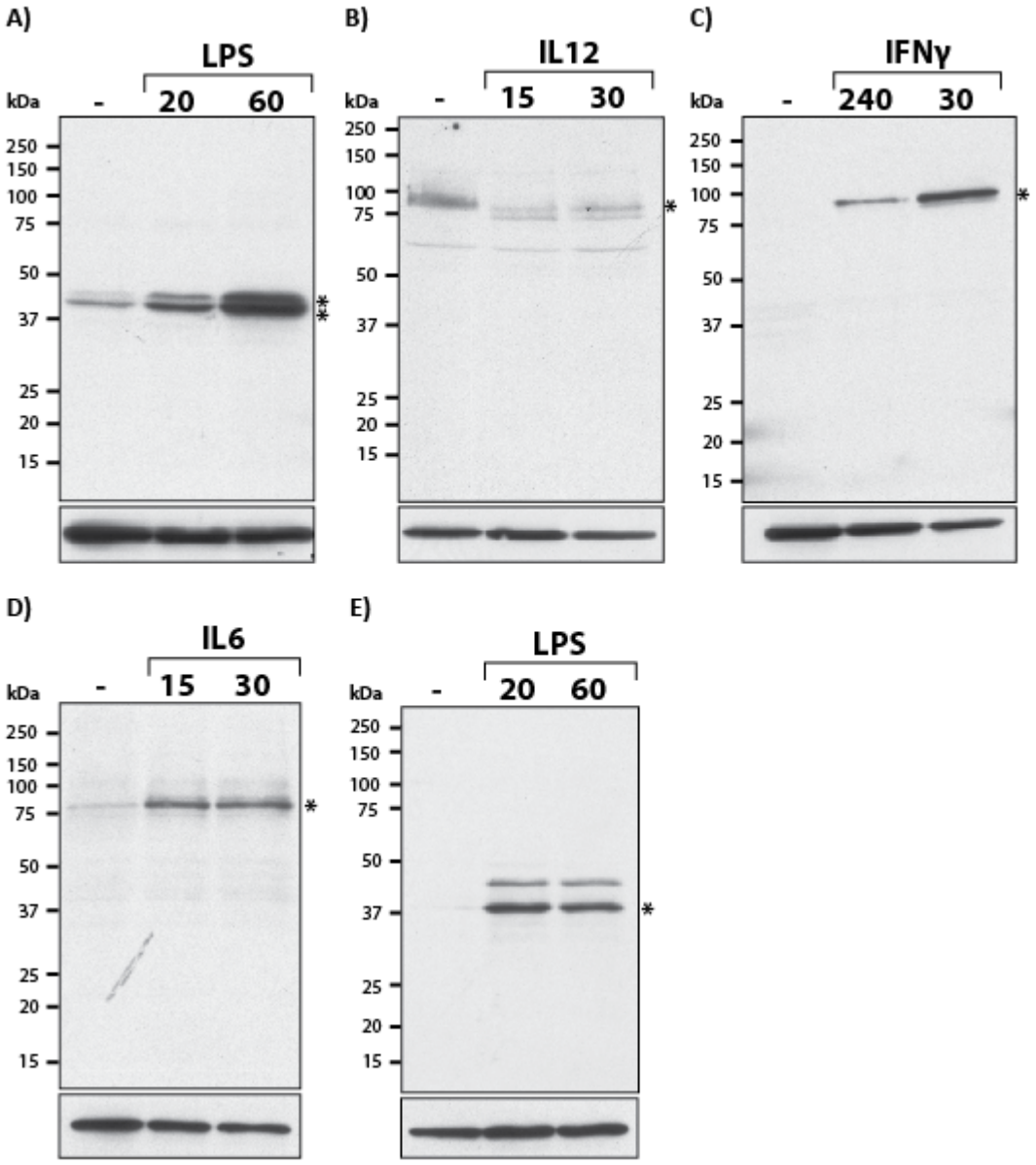

Figure 5.14. Western blotting of human macrophage WCLs for phosphorylated signalling proteins. iPSC-derived human macrophage WCLs were probed for the active phosphorylated versions of various intracellular signalling proteins: **A)** Erk1 (T202/Y204)/Erk2 (T185/Y187) **B)** STAT4 (Y693) **C)** STAT1 (Y701) **D)** STAT3(Y705) **E)** p38 (T180/Y182). Untreated macrophage WCLs were used as negative controls (-). Positive controls were done by stimulating macrophages with the appropriate cytokine or PAMP as shown and stimulation times in minutes are indicated. Asterisks indicate the correct size of the expected product. The bottom

panels show the same membranes probed for α tubulin as a loading control. Antibody details in Table 2.2 in Materials and Methods.

A)

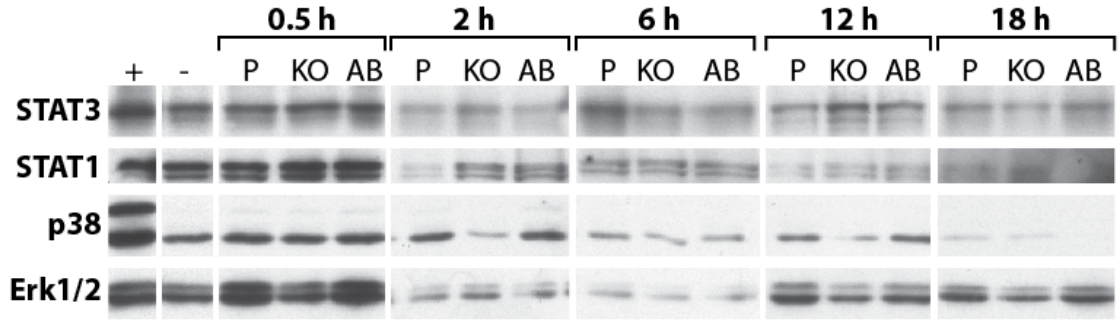

B)

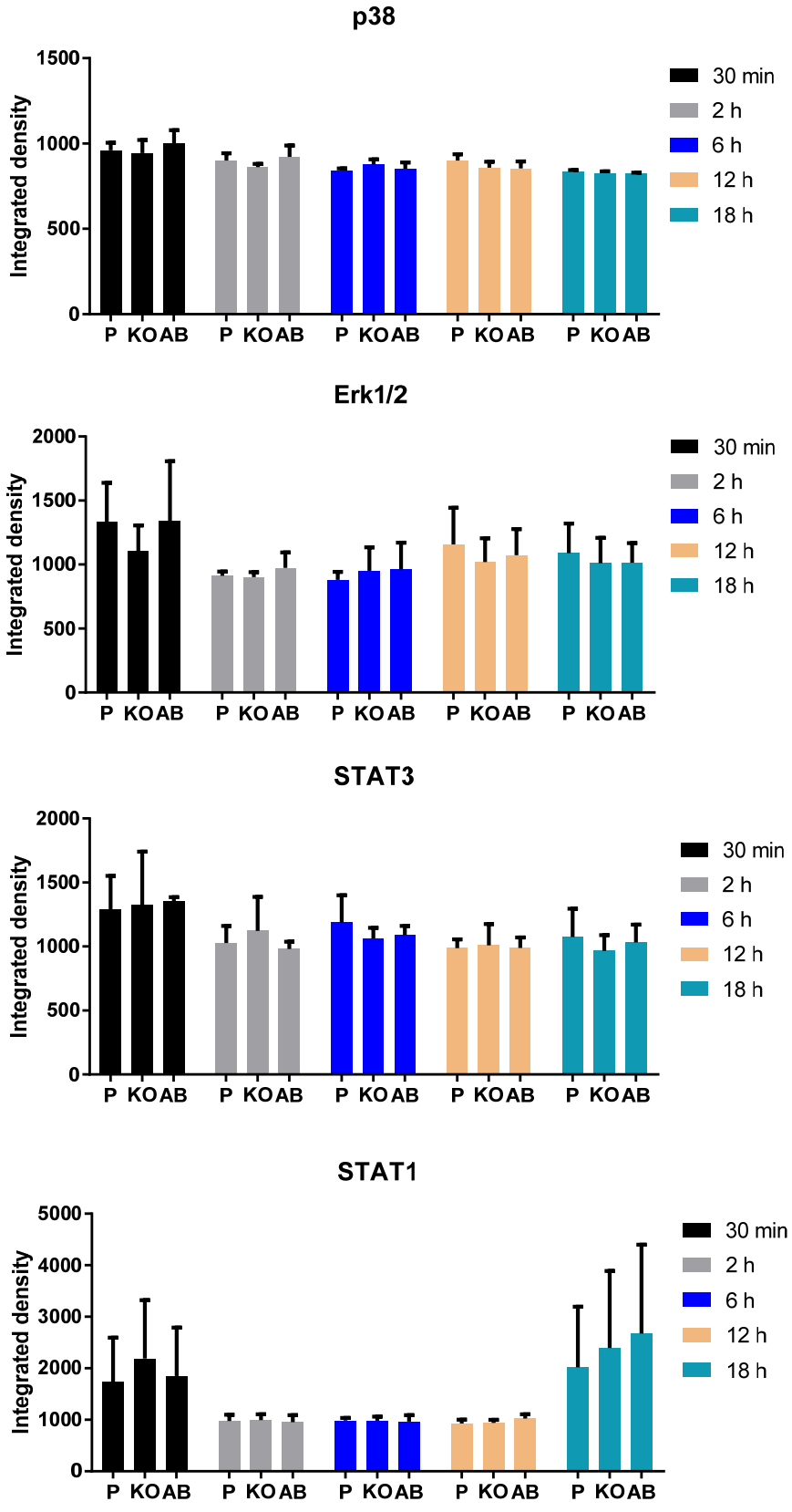
p38
Integrated density
1500
1000
500
0
P KO AB P KO AB P KO AB P KO AB P KO AB
30 min
2 h
6 h
12 h
18 h
Erk1/2
Integrated density
2000
1500
1000
500
0
P KO AB P KO AB P KO AB P KO AB P KO AB
30 min
2 h
6 h
12 h
18 h
STAT3
Integrated density
2000
1500
1000
500
0
P KO AB P KO AB P KO AB P KO AB P KO AB
30 min
2 h
6 h
12 h
18 h
STAT1
Integrated density
5000
4000
3000
2000
1000
0
P KO AB P KO AB P KO AB P KO AB P KO AB
30 min
2 h
6 h
12 h
18 h

Figure 5.15. Western blotting of human macrophage WCLs incubated with *Leishmania* EVs for phosphorylated signalling proteins. iPSC-derived human macrophage were treated for 2 days with LPS/IFNγ then incubated with DIF EVs at an MOI equivalent of 2500 from Cas9 T7 (p) (P), *ΔLPG1* (KO) and *LPG1* AB cell lines or nothing was added as negative controls (-). Macrophage WCLs were collected at the indicated time points post-infection and probed for the active phosphorylated versions of various intracellular signalling proteins: STAT3(Y705), STAT1 (Y701), p38 (T180/Y182) and Erk1 (T202/Y204)/Erk2 (T185/Y187). Positive controls (+) were as described in Fig. 5.14. **A)** This Western blot data is representative of triplicate data from three iPSC-derived macrophage donor cell lines. **B)** Triplicate Western blot data was analysed in a semi-quantitative way by measuring the integrated pixel density (IntDen, the product of the area and mean grey value) of equal-sized areas surrouding each protein band using ImageJ software. The error bars show the mean ± SEM. Antibody details in Table 2.2 in Materials and Methods.

Since no obvious effects of *L. mexicana* DIF EVs on STAT1, STAT3, p38 or Erk1/2 macrophage expression were found, we next chose to investigate the transcription factors NFκB and AP-1. As discussed in *Section 1.2.4*, NFκB has been identified as a driver of CXCL1 (Kanayama et al., 2015), CXCL10 (Brownell et al., 2014) and CXCL11 (Yang et al., 2007a) expression, and both NFκB (Becker et al., 2003) and AP-1 activity (Balaraman et al., 2005) are regulated by LPG. RAW-Blue^{TM} macrophages were used as a reporter cell line to quantify the levels of NFκB and/or AP-1 transcription (Figure 5.16). PRO live cells slightly induced NFκB and/or AP-1 activity at both 34°C (Figure 5.17A) and 37°C (Figure 5.17B), and the effect was slightly reduced in response to *ΔLPG1* cells compared to parental or AB (Figure 5.17A, B). We also decided to investigate the effect of lysed cells on transcription, as a control for the possibility that

any effect of EV samples could be due to contaminating factors from whole or lysed cells. Lysed cells induced a very small but significant increase in NFκB and/or AP-1 activity (Figure 5.17C). Like PRO live cells, DIF EVs induced a small but significant increase in NFκB and/or AP-1 activity, but with no differences between the parental, *ΔLPG1* and AB samples (Figure 5.17D). Neither PRO live cells (Figure 5.18A) nor DIF EVs (Figure 5.18B) had any effect on NFκB and/or AP-1 activity in LPS/IFNγ-stimulated macrophages.

In summary, roles for the macrophage signalling proteins STAT3, STAT1, p38, Erk1/2, AP-1 and NFκB in LPG-dependent suppression of chemokines is not supported by our data.

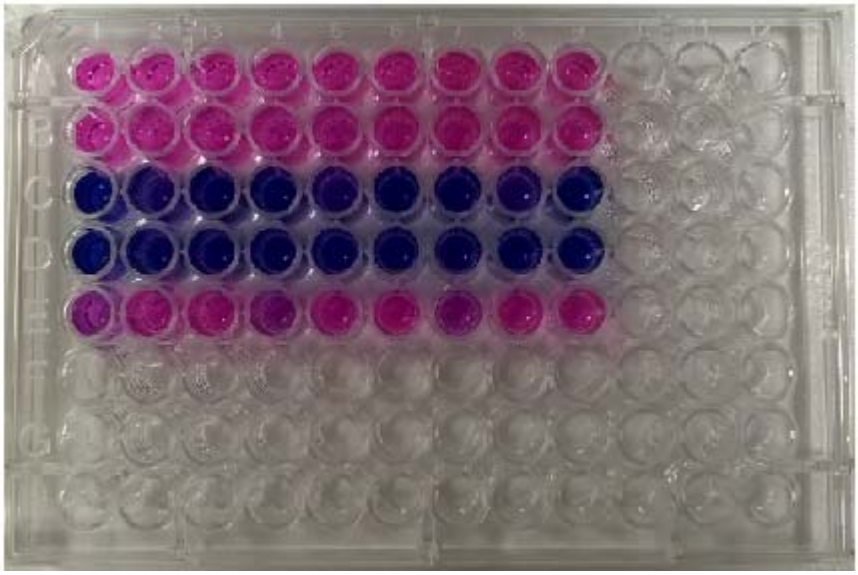

Figure 5.16. RAW-Blue™ macrophages as a reporter system for NFκB and/or AP-1 transcription. RAW-Blue™ macrophages transcribe and secrete alkaline phosphatase when NFκB and/or AP-1 transcription is activated. The amount of alkaline phosphatase secreted can be quantified by incubation with QuantiBlue™, where the absorbance at ~630 nm correlates with the level of NFκB/AP-1 transcriptional activation, as shown here where the positive wells appear blue.

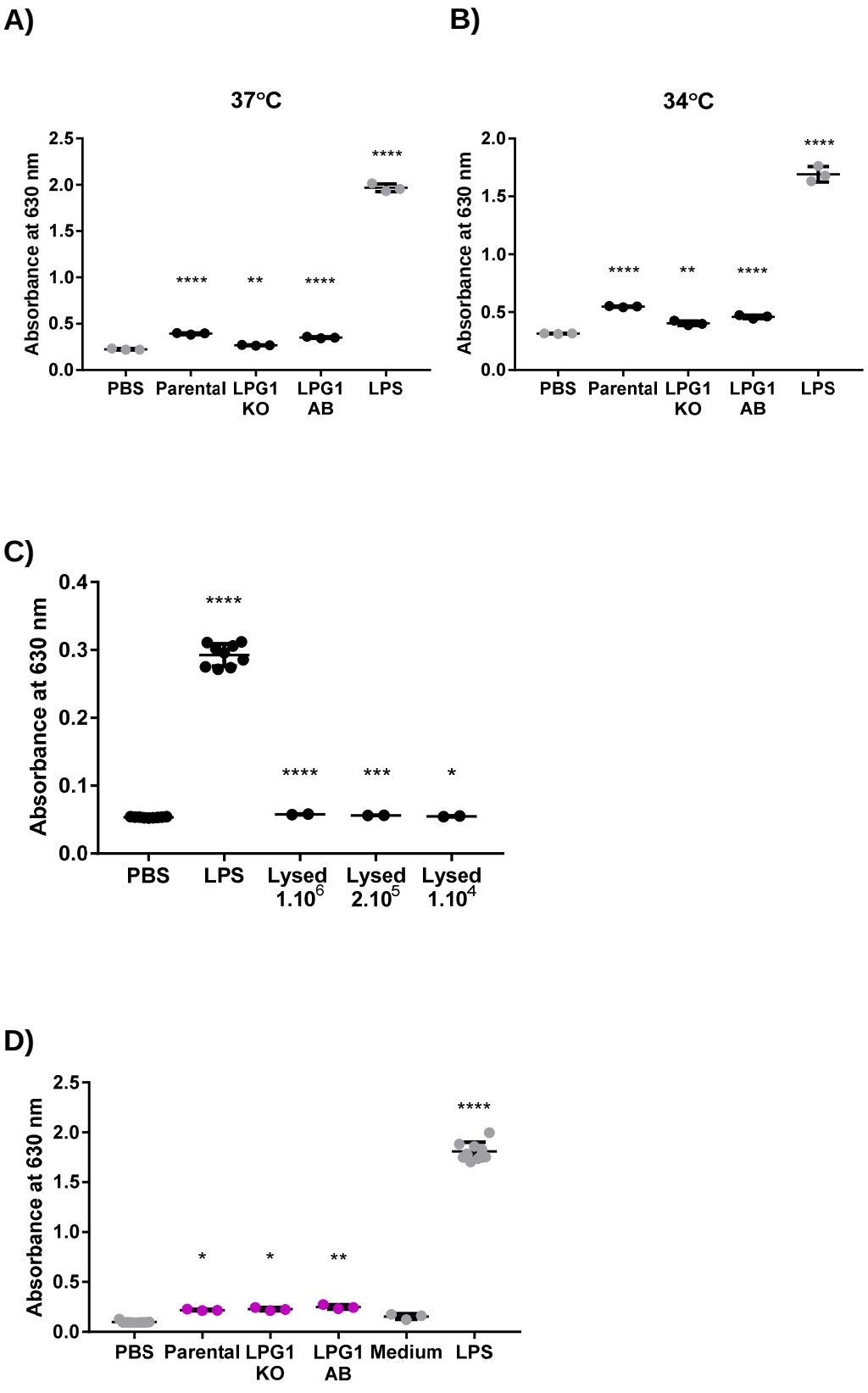
A)
37°C
Absorbance at 630 nm
2.5
2.0
1.5
1.0
0.5
0.0
****
****
**
****
PBS
Parental
LPG1 KO
LPG1 AB
LPS
B)
34°C
Absorbance at 630 nm
2.0
1.5
1.0
0.5
0.0
****
****
**
****
PBS
Parental
LPG1 KO
LPG1 AB
LPS
C)
Absorbance at 630 nm
0.4
0.3
0.2
0.1
0.0
****
****
***
*
PBS
LPS
Lysed 1.10^6
Lysed 2.10^5
Lysed 1.10^4
D)
Absorbance at 630 nm
2.5
2.0
1.5
1.0
0.5
0.0
****
*
*
**
PBS
Parental
LPG1 KO
LPG1 AB
Medium
LPS

Figure 5.17. *Leishmania* cells and EVs induce weak NFκB/AP-1 activation in RAW macrophages. RAW-Blue™ macrophages were infected at an MOI of 10 with stationary phase *L. mexicana* parental (Cas9 T7 (p)), *ΔLPG1* or *LPG1* AB promastigotes at 34°C (**A**) or 37°C (**B**). **C)** Freeze-thaw-lysed stationary phase Cas9 T7 (p) promastigotes were added at the indicated MOI equivalents. **D)** DIF EVs were added at an MOI equivalent of 2500 from parental (Cas9 T7 (p)), *ΔLPG1* and *LPG1* AB cell lines. As negative controls either PBS or a medium control were added. LPS was used as a positive control. After 18 h at 37°C (unless otherwise specified) macrophage supernatants were collected, incubated with QuantiBlue™ reagent and absorbance at 630 nm was measured. **A, B, C)** Duplicate or triplicate data from one biological repeat are shown. (**D)** These data are representative of two biological repeats. Asterisks show significant differences compared to the medium or PBS control as tested by unpaired t-tests with p values as follows: * p≤0.05; ** p≤ 0.01; *** p≤0.001; **** p≤0.0001.

A)

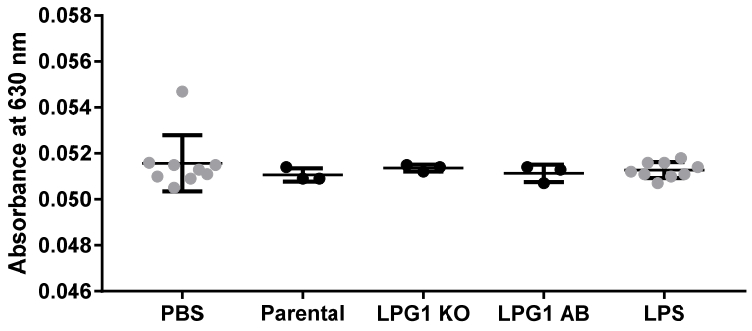

B)

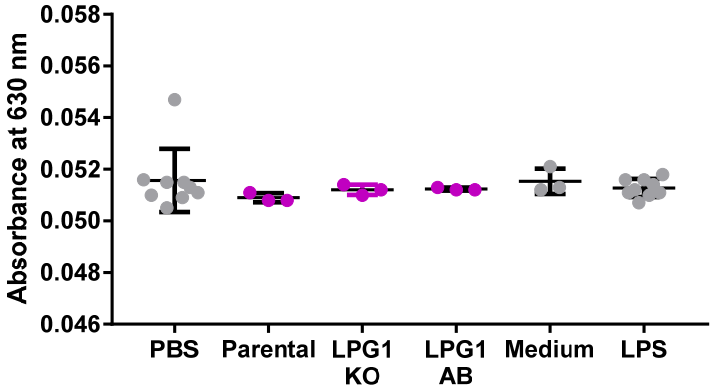

Figure 5.18. *Leishmania* cells and EVs induce no NFκB/AP-1 activation in LPS/IFNγ-treated RAW macrophages. RAW-Blue™ macrophages were treated for 1 day with LPS/IFNγ then infected at an MOI of 10 with stationary phase *L. mexicana* promastigotes (**A**) or incubated with DIF EVs at an MOI equivalent of 2500 (**B**) from parental (Cas9 T7 (p)), *ΔLPG1* and *LPG1* AB cell lines. After 18 h at 37°C macrophage supernatants were collected, incubated with QuantiBlue™ reagent and absorbance at 630 nm was measured. These data are representative of two biological repeats. There were no significant differences between samples and the medium or PBS control as tested by unpaired t-tests with p values of >0.05.

5.3. Discussion

5.3.1. Macrophage cytokine regulation by *L. mexicana* promastigotes and EVs

While the cytokine screening array we used contains only 36 cytokines and immune response genes out of more than 100 potential cytokines of interest (Dinarello, 2007), it nevertheless constitutes a much broader and less biased survey than the majority of *Leishmania* studies. To our knowledge only one other similarly broad cytokine screening study has been performed (Filardy et al., 2014). This study screened for 40 murine cytokines in response to *L. major* infection of unstimulated resident murine macrophages; TNFα, IL-6, TIMP-1, IL-1ra, G-CSF, TREM, CXCL1, MIP-1α, MIP-1β, MCP-1, and MIP-2 were all upregulated (Filardy et al., 2014). This broad approach allowed us to search for human macrophage cytokines of interest which had not been previously reported to be regulated by *Leishmania* under unstimulated versus LPS/IFNγ-stimulated conditions, while also checking for results consistent with previously published *Leishmania*-dependent effects on cytokines.

IL-12. The major effect which has been consistently reported of *Leishmania* promastigote infection on cytokine production from stimulated macrophages is inhibition of IL-12 (Belkaid et al., 1998). While we observe a slight decrease in IL-12 secretion from macrophages which have been stimulated following incubation with DIF EVs (Table 5.2A), we do not see inhibition of IL-12 secretion by *L. mexicana* promastigote infection under any of the conditions tested (Figure 5.7B, Table 5.2A, B). This could be due to different experimental timings; in most published studies *Leishmania* promastigotes were added at the same time as LPS and/or IFNγ stimulation (Belkaid et al., 1998), whereas in our experiments macrophages were

treated for two or three days prior to addition of *Leishmania* samples, or for two days following an 18 h incubation with *Leishmania* samples.

IL-8 and IL-1ra. Regarding effects on cytokines from unstimulated macrophages, we confirm that IL-8 and IL-1ra are increased in response to *L. mexicana* promastigote infection (Figure 5.5A, B), as had been reported for *L. donovani* (Silverman et al., 2010a) and *L. major* (Filardy et al., 2014) infection respectively. Interestingly, increased IL-1ra levels are also observed in response to DIF but not PRO EVs, although this increase is very small (Figure 5.5B). Increased secretion of IL-8 has been shown from both monocytes and macrophages in response to *L. donovani* and *L. major* EVs (Silverman et al., 2010a) and this is the main published effect of *Leishmania* EVs on macrophage cytokine production thus far. In our hands, IL-8 is increased by both *L. mexicana* promastigotes and DIF EVs from both unstimulated macrophages (Figure 5.5A) and macrophages stimulated with LPS/IFNγ for two days following *L. mexicana* sample incubation (Table 5.2A), although the changes are very small.

TNFα and IL-6. Increases in macrophage TNFα and IL-6 secretion were reported in response to *L. donovani* and *L. major* infection (Arango Duque et al., 2014), but while we observe higher TNFα levels in response to DIF EVs (Figure 5.5D), we do not see higher levels of either cytokine in response to *L. mexicana* promastigote infection (Figure 5.5D, Figure 5.7D).

Overall, we confirm the published trend that cytokine production in response to *Leishmania* samples is lowered in activated macrophages and increased in un-activated macrophages. This could be due to cytokines already being maximally produced in response to LPS and IFNγ stimulation.

5.3.2. *L. mexicana* samples decrease CXCL1, CXCL10 and CXCL11 levels in macrophages

The cytokine changes discussed so far are significant but small. The major finding is the substantial decrease in CXCL1, CXCL10 and CXCL11 levels in both human (Figure 5.4) and murine (Figure 5.11) LPS/IFNγ-stimulated macrophages in response to *L. mexicana* promastigote infection and also to PRO and DIF EVs. The reduction in CXCL10 levels is particularly dramatic, being reduced ~8-fold and ~5-fold in human (Figure 5.4C) and murine (Figure 5.11C, D) macrophages respectively, and was highly reproducible. IFNγ levels were also decreased in human macrophages (Figure 5.4E) but this result was not reproducible (Figure 5.9, Figure 5.10) and therefore shall not be discussed further. While there is mounting evidence that CXCL10, and to some extent CXCL11 (Moafi et al., 2017), is protective in *Leishmania* infection and enhances macrophage killing (Vasquez and Soong, 2006), reduced macrophage CXCL10 secretion in response to *Leishmania* infection or EVs has not been reported to our knowledge. Given the potential protective role of CXCL10, it is possible that our results reflect an *L. mexicana* mechanism to reduce CXCL10 levels and create an environment conducive to parasite survival. Surprisingly, the suppressive effects of *L. mexicana* promastigotes and EVs on CXCL- chemokine levels are reduced when human macrophages are stimulated with LPS and IFNγ after (Figure 5.8) rather than before (Figure 5.4) *L. mexicana* sample incubation. In the former case, for example, (Figure 5.8B) CXCL10 levels are reduced to ~1000 pg/ml by *Leishmania* EVs compared to control levels of ~3000 pg/ml; in the latter case (Figure 5.4C) CXCL10 levels are reduced to ~1000 pg/ml by *Leishmania* samples compared to control levels of ~8000 pg/ml. The lower control levels of CXCL10 when macrophages were LPS/IFNγ-stimulated after *Leishmania* sample incubation may reflect the shorter LPS/IFNγ-

stimulation time of two days (Figure 5.8) compared to three days (Figure 5.4). Therefore it is not clear whether the smaller relative reduction in chemokine levels (Figure 5.8) is due to smaller suppressive effects of the *Leishmania* samples under these conditions, or decreased chemokine induction. Furthermore, *L. mexicana* DIF EVs have a greater suppressive effect on CXCL10 levels than promastigote infection when macrophages are stimulated after sample incubation (Figure 5.8B). These data could suggest that *L. mexicana* samples predominantly reduce CXCL- chemokine levels by uptake or degradation following macrophage activation rather than inhibiting their initial release, and that EVs are better at inhibiting CXCL10 release than promastigotes.

5.3.3. Physiological context of EV sample concentration

In most cases, *L. mexicana* promastigote infection and PRO and DIF EVs have very similar effects on macrophage cytokine production (Figure 5.4, Table 5.1A, B). There are some differences between the effects of PRO and DIF EVs, including the increase in IL-8, IL-1ra, TNFα and IL-1β levels in unstimulated macrophages induced by DIF but not PRO EVs (Table 5.1B). The fact that DIF EVs seem to induce higher levels of pro-inflammatory cytokines than PRO EVs supports our hypothesis that PRO and DIF EVs could be functionally different and that DIF EVs are enriched for virulence factors (see Chapter 3). However, the effects induced by DIF but not PRO EVs are very small in magnitude, (Figure 5.5A, B, D, Figure 5.6D) therefore we cannot draw strong conclusions from these results. The similar effects of promastigotes and EVs is surprising given that the EV samples added to macrophages contain at least 5-fold less protein (as measured by Bradford assay, data not shown) than the promastigotes, suggesting that key parasite factors are enriched in EV samples. In our studies, the

amount of EV sample added per macrophage corresponded to the amount of EVs isolated from 2500 *Leishmania* cells, which seems very high compared to the likely *in vivo* situation. However, this is assuming an unlikely 100% EV recovery. We do not know exactly what proportion of EVs are lost during EV isolation but it is likely that the true MOI equivalent is much less than 2500. Based on measurements of DIF EVs which contain ~0.5 µg protein per 10^9 cell equivalents (Figure 4.4), and given that 2.5×10^8 cell equivalents are added per well of macrophages in 200 µl, the estimated protein concentration of EVs which macrophages were exposed to is ~0.625 µg/ml. This rough estimate is well below the figure of 50 µg/ml which has been proposed as a physiologically relevant EV concentration (Silverman et al., 2010b), and below the EV concentrations which are commonly used in *Leishmania* cytokine studies (Silverman et al., 2010b, Hassani et al., 2014). Therefore, based on available evidence, the EV concentrations used in this study appear to be below what might be physiologically relevant, suggesting that our observed effects are likely to be an under- rather than an over- estimation. However, further data to back up this statement are required, including measurements of our EV yields and the ratio of secreted to vesicle-associated protein in EV samples. The relevance of discussing exogenous EV concentration, however, is debatable since we hypothesise that EVs are released from differentiating *Leishmania* inside PVs, where the effective concentration of EVs would be much higher. We find that decreasing EV concentration 10-fold is enough to abolish the suppressive activity of *L. mexicana* DIF EVs on CXCL1 and CXCL10, but that even a 250-fold diluted EV sample retains the suppressive effect on CXCL11, (Figure 5.9) suggesting a very potent effect of EVs on this chemokine.

5.3.4. LPG contributes to suppression of CXCL- chemokines

We find by comparing the effects of *L. mexicana* parental, *ΔLPG1* and AB samples that LPG contributes to the suppression of CXCL10 and CXCL11, but not CXCL1, in human macrophages (Figure 5.10) and to the suppression of CXCL1 and CXCL10 (CXCL11 not measured) in murine macrophages (Figure 5.11). The effect of LPG on CXCL10 is greater in human than murine macrophages; in DIF EVs, LPG seems to account for the entire effect on CXCL10 levels in human macrophages since DIF EVs from *ΔLPG1* cells have no significant effect on CXCL10 levels (Figure 5.10D). This difference between the macrophage species is interesting given that *L. mexicana* LPG is thought to be dispensable for virulence in mice (Ilg, 2000) but it is not known whether it is essential in humans. No increase in TNFα or IL-10 secretion from murine macrophages was observed in response to *L. mexicana* promastigotes or EVs (Figure 5.11), in contrast with the published ability of purified *L. shawi* and *L. mexicana* LPG to induce these cytokines. This result highlights the fact that LPG appears to have different effects when purified or when cell-associated.

5.3.5. Effect of LPG may be direct or indirect

We show that LPG is not only likely to be EV cargo, but may influence EV release. *ΔLPG1* cells release approximately three-fold fewer particles as measured by NTA than parental cells (Figure 5.12). Several explanations could account for this result: firstly, NTA measures particles which we assume are EVs, but it is possible that *ΔLPG1* cells simply release less of some other particulate such as aggregrated protein; secondly, the presence or absence of LPG, which is negatively charged (Mangoni et al., 2005, Turco et al., 1987), is likely to change the surface charge or adhesivity of EVs which may then adsorb more or less well to the surface of tubes during EV isolation, resulting

in different EV yields. Finally, it is possible that LPG regulates EV biogenesis via unknown mechanisms. Our NTA experiments do not measure particles <50 nm in diameter, therefore we do not know whether LPG affects the isolation of particles in this size range.

Intriguingly, our data suggest that the effect of DIF EV-associated LPG on both CXCL10 and CXCL11 secretion in human macrophages is greater (Figure 5.10D, F) than promastigote-associated LPG (Figure 5.10C, E), perhaps indicating that secreted LPG accounts for a major proportion of its effects on these chemokines. However, our observation that ~three-fold fewer EVs, or at least particles, are isolated from *ΔLPG1* cells than parental or AB cells complicates the interpretation of these data (Figure 5.12). Since the differences in chemokine level in response to parental and *ΔLPG1* DIF EV samples are no more than 3-fold (Figure 5.10, Figure 5.11), it is possible that these differences and the apparent LPG-dependency are due to the addition of fewer EVs, which may contain some other unknown factor which is responsible for chemokine suppression. While we know that adding ten-fold fewer EVs abolishes the effect of DIF EVs on CXCL1 and CXCL10 (Figure 5.9), further experiments would have to be done to determine the effect of adding three-fold fewer. We hypothesise that the isolation of fewer EVs or particles from *ΔLPG1* than parental cells may be due to technical reasons. However, that cannot account for the apparent LPG-dependency of chemokine changes observed in response to *L. mexicana* promastigote samples, which have not undergone EV isolation (Figure 5.10C, E, Figure 5.11A, C). There are several possibilities: *ΔLPG1* promastigotes release fewer EVs containing a factor other than LPG which induces chemokine suppression, or the loss of cell-associated and/or

secreted LPG is directly responsible for the reduction in chemokine suppression. Alternatively, the protein cargo of EVs from *ΔLPG1* cells compared to parental EVs may be altered, as has been shown for HSP100 and GP63 knockouts (Silverman et al., 2010b, Hassani et al., 2014); this could mean that another virulence factor responsible for the effects is down-regulated. The first step in resolving these open questions would be to determine whether fewer EVs are truly released from *ΔLPG1* cells without carrying out EV isolation; a fluorescence or luciferase assay could be developed to monitor real-time EV release into culture medium (Long et al., 2016). Despite these unresolved questions, the parental and *ΔLPG1* promastigote data (Figure 5.10C, E, Figure 5.11A, C) tell us that *L. mexicana* LPG plays a definite role in chemokine suppression, whether direct or indirect.

5.3.6. *ΔLPG1* cells survive and replicate in human macrophages

We show that in human macrophages, as has been previously shown in murine macrophages (Ilg, 2000), *ΔLPG1* cells are able to survive and replicate. Initial infection rates of *ΔLPG1* cells are higher than parental, although it is not clear whether this is due to technical error or a real superiority at macrophage invasion. While parental infection levels increase within the first 24 h of infection, *ΔLPG1* infection levels decrease suggesting that LPG may play a role in early *L. mexicana* survival inside human macrophages. Interestingly, this effect is enhanced by macrophage activation with LPS/IFNγ (Figure 5.13) which likely leads to increased parasite killing (Green et al., 1990, Mukbel et al., 2007), suggesting that the use of LPS/IFNγ activation may be a useful tool to reveal more subtle infection phenotypes. The *LPG1* AB did not fully restore infection levels to those of the parental. While the AB cell line appears to produce comparable levels of LPG to parental (Figure 4.12E), the levels and pattern of

PPG and SAP are more comparable to the *ΔLPG1* cell line (Figure 4.12E). These differences, and possible changes in expression level of other factors we are not aware of, could account for the intermediate infection phenotype of the AB. However, any differences in macrophage infection level between the cell lines were small and this experiment was carried out only once, therefore to be confident in the differences observed replicates would be required. Overall, we can state that *L. mexicana* LPG is not essential for human macrophage infection.

5.3.7. The macrophage signalling proteins responsible for CXCL- chemokine suppression are unknown

Despite the published ability of purified LPG from several *Leishmania* species to induce p38 and Erk1/2 phosphorylation and activation (Balaraman et al., 2005), de Veer, Curtis et al. 2003, Rojas-Bernabe, Garcia-Hernandez et al. 2014), we find no obvious differences in the levels of phosphorylated p38 and Erk1/2 between LPS/IFNγ-stimulated human macrophages incubated with EVs from parental or *ΔLPG1 L. mexicana* cells (Figure 5.15). Furthermore, no obvious differences in STAT1 or STAT3 expression are observed (Figure 5.15). This experiment was carried out at time points over 18 h, the time in which DIF EVs induce suppression of CXCL- chemokines (Figure 5.4, Figure 5.10). It seems likely, therefore, that these signalling proteins and transcription factors are not responsible for the LPG-dependent effects observed on human macrophage CXCL- chemokine secretion. However, no loading control was included in this experiment (Ponceau staining of the WB membranes was carried out but was too weak to be useful as a loading control) and it is possible that subtle changes in phosphoprotein level are present but not detectable due to small differences in sample loading. In addition, the fact that samples from different time

points are present on different membrane and therefore their band intensities cannot be directly compared, means that it is not possible to tell whether the levels of phosphoprotein change during the time course.

Published data show that both *Leishmania* infection and purified LPG induce NFκB nuclear translocation and activation and that purified LPG induces AP-1 activation in macrophages. Consistent with these data, we show that *L. mexicana* promastigotes (Figure 5.17A, B) and DIF EVs (Figure 5.17D) induce a slight increase in NFκB and/or AP-1 activity in unstimulated murine macrophages, and that this effect is slightly decreased in response to *ΔLPG1* promastigotes compared to parental or AB (Figure 5.17A, B). Two observations make it likely that this slight NFκB and/or AP-1 activation is not responsible for LPG-dependent suppression of macrophage CXCL- chemokines: firstly, no effect of *L. mexicana* promastigotes (Figure 5.18A) or DIF EVs (Figure 5.18B) on NFκB and/or AP-1 is observed in LPS/IFNγ-stimulated macrophages which is the condition where we see the effects on CXCL- chemokines; secondly, unlike CXCL-chemokine levels, there is no difference between NFκB and/or AP-1 levels in response to DIF EVs from parental versus *ΔLPG1* cells (Figure 5.17D).

5.3.8. Suppression of CXCL- chemokines is likely due to uptake and/or degradation

The fact that *L. mexicana* promastigotes (Figure 5.17A, B), EVs (Figure 5.17D) and the positive control LPS (a PAMP) (Figure 5.17) are able to induce NFκB and/or AP-1 activation in unstimulated but not in LPS/IFNγ-stimulated macrophages (Figure 5.18A, B) is reminiscent of LPS tolerance. The phenomenon whereby prolonged exposure to LPS induces a 'tolerant' state where subsequent LPS exposure has greatly reduced pro-inflammatory effects is well established (Foster et al., 2007, Frankenberger et al., 1995, Medvedev et al., 2000, Nomura et al., 2000, Tominaga et al., 1999, Virca et al.,

1989). LPS tolerance occurs both systemically *in vivo* and in *in vitro* cell lines including macrophages (Seeley and Ghosh, 2017). The suppression of pro-inflammatory signals after a long exposure to a PAMP such as LPS is thought to be an important mechanism for controlling harmful levels of tissue damage and inflammation during infection. Stimulation with LPS for around 16-48 h is required to induce tolerance (Seeley and Ghosh, 2017); IL-6 secretion from murine macrophages was measured after a 24 h LPS stimulation following pre-stimulation with LPS for between 0 and 96 h (Foster et al., 2007). Pre-stimulation for 24 and 48 h induced the strongest tolerance, i.e. suppression of IL-6 secretion, while pre-stimulation for longer or shorter times progressively reduced the induction of tolerance (Foster et al., 2007). Our studies use LPS/IFNγ pre-stimulation times from 24 h (Figure 5.18) to 72 h (Figure 5.4), which fall within the time frame of inducing macrophage tolerance. Consistent with our results (Figure 5.18), tolerant murine macrophages have reduced NFκB and AP-1 activation upon the second LPS stimulation (Medvedev et al., 2000).

Two classes of LPS-induced genes involved in LPS tolerance have been identified; one includes classical pro-inflammatory genes such as IL-6 and expression of these genes is suppressed following a second LPS stimulation after a prolonged LPS exposure. The other class of genes which are mostly antimicrobial and non-inflammatory are primed to be expressed at higher levels upon the second LPS stimulation (Foster et al., 2007). This system is thought to allow a sustained antimicrobial response through increased expression of antimicrobial genes such as *Cnlp* during an infection, while also limiting the expression of pro-inflammatory genes which would cause tissue damage if expressed at high levels for a long period of time.

CXCL10 is among the genes whose mRNA expression is suppressed upon a second LPS stimulation (Medvedev et al., 2000); another study showed that CXCL1 and CXCL11 also belong to this group of genes (Foster et al., 2007). Therefore, it seems likely that under the condition of prolonged macrophage pre-stimulation where addition of *L. mexicana* samples leads to a reduction in CXCL1, CXCL10 and CXCL11 levels (Figure 5.4, Figure 5.10, Figure 5.11), the macrophages are in a tolerant state and unable to express further levels of these chemokines. If this is true, then our observation of reduced CXCL-chemokine levels in response to *L. mexicana* samples would reflect a reduction in the levels of existing secreted chemokines, rather than an inhibition of further secretion. This model would explain why we do not see changes in signalling proteins and transcription factors in pre-stimulated macrophages in response to *L. mexicana* samples. It would also explain why we do not observe the expected reduction in IL-12 levels in LPS/IFNγ-pre-stimulated macrophages (Figure 5.7B), since IL-12 is also suppressed during LPS tolerance (Wysocka et al., 2001). To test this theory, the experiments using LPS/IFNγ–stimulation prior to addition of *Leishmania* samples could be repeated, with an additional macrophage washing step to wash away any existing secreted chemokines prior to addition of fresh LPS/IFNγ-containing medium with or without *L. mexicana* samples, to see if CXCL-chemokines are newly secreted or not.

5.3.9. Mechanisms of chemokine uptake and degradation

There are two potential mechanisms for reducing existing levels of secreted chemokines: degradation or increased uptake, which in our experimental case would be uptake by macrophages. There are precedents for both mechanisms. Cytokines, including chemokines, are common targets for bacterial proteases (Potempa and Pike,

2009); *S. pyogenes* ScpC, for example, cleaves and renders IL-8 inactive (Hidalgo-Grass et al., 2006). While we are not aware of any *Leishmania* proteases that target host cytokines, the *Leishmania* genome encodes over 150 predicted proteases, some of which are important virulence factors (reviewed in (Mottram et al., 2004)) and many of which have unknown functions (Besteiro et al., 2007). Mechanisms are needed to down-regulate pro-inflammatory signalling by ligand-bound chemokine receptors to tissue damage; this is mediated by either G-protein uncoupling leading to signal termination, or by internalisation of the ligand-bound receptor leading to recycling or degradation (Colvin et al., 2004). Internalisation of ligand-bound receptors represents a mechanism for chemokine uptake which can lead to reduced concentrations of extracellular chemokine. CXCR3, the receptor for CXCL9, CXCL10 and CXCL11, is expressed on macrophages (Zhou et al., 2010, Butler et al., 2017) and has been shown to significantly reduce extracellular chemokine concentrations both in circulation (Cardona et al., 2008) and in salivary glands (Sfriso et al., 2006); CXCR3 is therefore a candidate for reducing CXCL- chemokine levels in our studies. However, the ability of typical chemokine receptors such as CXCR3 to undergo down-regulation to dampen pro-inflammatory signalling means they are not generally very efficient at removing extracellular chemokines (Colvin et al., 2004). An atypical class of chemokine receptors have been described which do not induce chemotactic activity and their primary function appears to be chemokine scavenging, thanks to their ability to continuously recycle back to the surface following internalisation (Hansell et al., 2006, Weber et al., 2004). Atypical chemokine receptors could therefore be good candidates for chemokine uptake leading to the reductions observed in CXCL-chemokine, and particularly CXCL10, levels (Figure 5.4). CXCL11 is scavenged by atypical chemokine

receptor CXCR7 (Benredjem et al., 2017, Naumann et al., 2010), and CXCL1 (Wan et al., 2015) and CXCL10 (Nibbs and Graham, 2013) are bound by ACKR1. Future experiments to investigate the mechanism underlying our CXCL- chemokine observations could test whether CXCR3, CXCR7, ACKR1 or any other chemokine receptors of interest are up-regulated by pre-stimulated macrophages in response to *L. mexicana* samples. Fluorescent chemokines could also be used to monitor uptake and degradation (Ford et al., 2013).

5.3.10. Conclusions and outlook

We present a broad analysis of the effects of *L. mexicana* promastigotes and PRO and DIF EVs on human macrophage cytokine levels under three conditions: no macrophage stimulation (Table 5.1B), pre-stimulation with LPS and IFNγ prior to *L. mexicana* sample addition (Table 5.1A), and LPS and IFNγ stimulation following *L. mexicana* sample incubation (Table 5.2A). We found minimal cytokine regulation of unstimulated macrophages in response to *L. mexicana* promastigotes or EVs (Table 5.1B, Table 5.2B). We show that in pre-stimulated macrophages, secreted CXCL1, CXCL10 and CXCL11 are strongly down-regulated by promastigotes and PRO and DIF EVs (Figure 5.4), which to our knowledge are not effects which have been previously published. These effects are absent or weaker in macrophages which are stimulated following *L. mexicana* sample incubation (Figure 5.8). CXCL1 and CXCL10 levels are also suppressed in murine macrophages (Figure 5.11), showing these effects are robust and conserved between species.

We show using parental and *ΔLPG1* cell lines that CXCL-chemokine suppression is partially dependent on the well-studied glycoconjugate LPG (Figure 5.10, Figure 5.11), which is present in promastigotes and EV samples. We show that *ΔLPG1* cells are able

to survive and replicate in human macrophages and we identify the potential of LPS and IFNγ activated macrophages in mutant infection studies to enhance the effects of subtle phenotypes. Intriguingly, fewer EVs are isolated from *ΔLPG1* cells than parental. This result may be due to technical issues or may suggest that LPG plays a role in EV biogenesis or cargo selection, which would be previously undescribed functions of LPG. The effect of LPG on macrophage chemokine levels may therefore be direct or may be due to EV dose regulation and requires further investigation.

The molecular basis for the reduction in CXCL- chemokine levels remains unknown. However, there is reason to suspect that conventional macrophage signalling pathways which are targeted to modulate cytokine expression and secretion are not responsible for these effects (Figure 5.15, Figure 5.18). We speculate that pre-stimulated macrophages are in a state of LPS-induced tolerance, therefore addition of *L. mexicana* samples is likely to reduce CXCL- chemokine levels via uptake and/or degradation rather than inhibition of secretion. If confirmed through further studies, this would represent a novel mechanism of cytokine regulation by *Leishmania*.

6. Final discussion

6.1. The *L. mexicana* flagellum is a source of EVs

The overarching aim was to determine whether EVs from the *L. mexicana* flagellum deliver virulence factors to modulate the host macrophage response. Firstly, we addressed the subcellular origin of *L. mexicana* EVs and whether the flagellum is a source of EVs. Imaging of EVs from a tagged *L. mexicana* cell line strongly suggested that both the cell body and flagellar membranes are sources of EVs. Flagellar EVs appear to be more abundant than cell body-derived EVs: the ratio of flagellar to cell body EVs was around 5:1 in promastigote samples and around 200:1 in samples from differentiating *Leishmania* (Figure 3.21B). Therefore, while acknowledging that other populations of EVs may be present which were not visible using this method because they contained neither GT2 nor SMP1 hence no fluorescent label, it seems likely that the flagellum is not only a source but the major source EVs. To comprehensively determine the proportion of flagellar-derived EVs as a fraction of total EVs, one approach would be immuno-precipitation of EVs from a tagged cell line with an epitope specifically present on the outside of flagellar-derived EVs, in combination with NTA.

6.2. Flagellar EVs are released within infected macrophages

EVs were directly observed being released from live flagella within infected macrophages (Figure 3.8), showing that flagellar-derived EVs are present in a physiologically relevant context. A major open question is whether these EVs reach the macrophage cytoplasm and if so, how? It is known that *Leishmania* EV-associated proteins, including GP63, can be detected in the macrophage cytoplasm (Gomez et al., 2009, Atayde et al., 2015, Silverman and Reiner, 2011), but how they are able to

cross the PV membrane if released inside the phagolysosome or cross the macrophage PM if released from extracellular *Leishmania* remains unknown. Possibly *Leishmania* factors on the surface of EVs could bind macrophage membrane receptors and elicit a signalling response without the need to physically cross the membrane. It is unclear whether isolated EVs delivered to macrophage medium (as in our experimental setup) would reach the same intracellular destination and exert the same effects as EVs released by parasites within the PV. There is no simple way to compare these two routes without the confounding factor of the parasites themselves; mutant parasites which cannot release EVs or chemical inhibition of EV release would help to dissect this question if such tools were available.

6.3. *L. mexicana* EV release and flagellar shortening are linked

Live imaging supports a link between flagellar shortening and EV release (Figure 3.8), since EV shedding appears to leave behind shorter flagella. However, further imaging is required to gain a clearer idea of the frequency of such events. Further evidence supporting this conclusion is that increased EV release (Figure 3.22), as well as an increased ratio of FM-derived to cell body membrane-derived EVs (Figure 3.21B), occurs during promastigote to amastigote differentiation when flagellar shortening takes place. We therefore expand the current understanding of the EV field that a link between flagellar shortening and EV release is conserved between diverse eukaryotes, namely mammalian cells (Nager et al., 2016), *C. reinhardtii* (Dentler, 2013) and now *L. mexicana,* suggesting that EV shedding plays a conserved role in removing excess membrane during flagellar shortening or disassembly. We have gained insights into the structural mechanisms of *L. mexicana* flagellar EV release by showing that EVs are released from FM blebs and nanotubes (Figure 3.8), in a manner

which may be analogous to pearling (McConnell and Tyska 2007, Yue, Zhang et al. 2014, Jelercic and Gov 2015). We have generated nine KO cell lines for candidate EV biogenesis and flagellar length control proteins but all of these still undergo flagellar shortening and form FM nanotubes. We have therefore not fulfilled our aim of uncovering the underlying molecular mechanisms of *L. mexicana* FM shedding. In further studies on these mutants, it would however be interesting to test whether they regulate the release of other classes of *Leishmania* EVs or the frequency of nanotube formation. (Figure 3.13).

Whether EV release is the main mechanism driving flagellar shortening in *L. mexicana* is unclear; it is also possible that increased endocytosis from the FP reduces FM surface area. However, based on our estimates of flagellar surface area and the total surface area of shed EVs isolated from cells during flagellar shortening (Chapter 3 Discussion), EV release alone could account for excess FM loss. Total and flagellar EV release increases during differentiation (Figure 3.21B, Figure 3.22), and virulence factors including GP63 and EF-1α are present in EV samples (Table 4.2); this is consistent with our hypothesis that EVs from the shortening flagellum deliver virulence factors. What is missing from this argument is data comparing the protein composition of flagellar-derived *L. mexicana* EVs to EVs from other subcellular sources. There are at least two ways in which the flagellum could deliver virulence factors via EVs: i) as a specialised membrane domain for enrichment and shedding of virulence factors or (ii) assuming a homogenous distribution of virulence factors across the parasite surface, EV release during flagellar shortening could facilitate virulence factor delivery. Again, the ability to specifically isolate flagellar-derived EVs would enable this comparative analysis.

6.4. *L. mexicana* promastigotes and EVs have similar effects on macrophage cytokines

Next, we carried out macrophage cytokine analysis comparing the effects of *L. mexicana* infective promastigotes, to isolated EVs from promastigotes and differentiating *Leishmania*. This study provides the first broad macrophage cytokine analysis comparing the effects of live parasites and EVs under the same experimental conditions. Strikingly, all three biological samples induce similar cytokine changes when incubated with macrophages (Figures 5.4-5.7). This raises several interesting questions. Does this mean that the effects of promastigotes are largely due to EV release, since EVs alone induce the same effects? Or, are the effects due to *Leishmania* factors/PAMPs which are equally present in whole cells and EV samples? Mutant cell lines which cannot release EVs would help address this question. Secondly, although the ratio of flagellar to cell body-derived EVs is much greater in DIF than PRO EVs (Figure 3.21B), PRO and DIF EVs have similar effects on macrophage cytokine production. Therefore the factor(s) responsible is unlikely to be enriched in flagellar EVs. This would support scenario (ii) (above) whereby flagellar shortening facilitates the release of virulence factors which are localised throughout the cell, and is consistent with our identification of LPG, which localises across the parasite surface, as a major contributor to cytokine effects. This is also consistent with our MS analysis, which does not reveal striking differences in proteomic composition (particularly regarding the most abundant proteins) between PRO and DIF EVs (Appendix 1, Table 4.2). Stationary phase promastigotes are enriched in infective metacyclic parasites which, like subsequent differentiating parasites, are present at the early stages of mammalian infection; therefore it is not surprising that EVs from both life cycle stages induce similar effects on macrophages and perhaps play similar roles in establishing

infection. To fully address whether flagellar-derived EVs are functionally different to other EVs, it would be necessary to isolate EV sub-populations from different subcellular origins to compare their effects on cytokine production.

DIF cells release ~45% more EVs than PRO cells (Figure 3.22), therefore ~45% more DIF EVs than PRO EVs were incubated with macrophages before cytokine analysis, yet both samples induced similar effects (Figure 5.4-5.7). Our data does not therefore support the biological significance of increased EV production during differentiation and flagellar shortening. However, it is possible that the effects on macrophage cytokine production may be saturating at the EV concentrations used here (which we believe are likely to be physiologically relevant, see Chapter 5 Discussion), such that a 45% difference in EV numbers would not elicit changes in cytokine production. We conclude that all three *L. mexicana* samples have similar capacities to induce changes in macrophage cytokine production and are therefore likely to contain common virulence factors.

6.5. Chemokine downregulation in response to *L. mexicana* samples

The key observation is the consistent reduction in CXCL1, CXCL11 and CXCL10 levels in LPS/IFNγ-stimulated macrophages in response to *L. mexicana* promastigotes and EVs. This effect is robust and consistent across murine BMDMs (Figure 5.11) and human iPSC-derived macrophages (Figure 5.4). The CXCL10 effect is the most dramatic, with *Leishmania* samples inducing up to an 8-fold reduction in levels (Figure 5.4); to our knowledge this is the first report of *Leishmania*-dependent downregulation of CXCL10 levels. Crucially, is an 8-fold change in CXCL10 level likely to have an effect *in vivo*? A study in C57BL/6 mice found that a 10-fold increase in CXCL10 concentration administered by injection leads to a 5-fold increase in CD8 T cell

(other cell types were not investigated) recruitment to the lungs (Campanella et al., 2006), suggesting that an 8-fold change could also have substantial effects. CD8 T cells are thought to play an important role in an effective Th1 immune response and parasite clearance during *Leishmania* infection (da Silva Santos and Brodskyn, 2014).

6.6. Chemokine downregulation is partially dependent on virulence factor LPG

We met our goal of identifying parasite factors responsible for inducing changes in cytokine production: LPG contributes to chemokine downregulation (Figure 5.10, Figure 5.11). Regarding EV-dependent downregulation of CXCL10 in human macrophages, LPG appears to account for the entire effect (Figure 5.10D). We show for the first time that LPG is present in EV samples (Figure 4.1G) and affects the macrophage cytokine response when delivered via crude EV preparations (Figure 5.10, Figure 5.11). This suggests that EVs are a major delivery route for LPG; the delivery route has until now been a major open question in the *Leishmania* field. However, this conclusion comes with the caveat that LPG may be present in EV samples as a freely secreted molecule rather than an integral EV component. An important future experiment would be to incubate macrophages with purified LPG to see whether LPG alone reduces secreted chemokine levels. Although immuno-gold staining suggests that at least a fraction of LPG in EV samples is EV-associated (Figure 4.16), further investigation is needed. Interestingly, we show that fewer EVs are consistently isolated from LPG-deficient *L. mexicana* cells (Figure 5.12), either because fewer EVs are released initially or for technical reasons relating to differences in surface charge. The EV sample volume added to macrophages for cytokine analysis was always calculated based on the number of cells from which the EVs were isolated, rather than EV numbers in the final sample. Therefore we cannot tell whether the

contribution of LPG to chemokine downregulation is due to lack of LPG in EVs or reduced delivery of EVs containing another factor. Live promastigotes also show the same LPG-dependent effect, however, therefore whatever the mechanism, LPG has a biological effect on macrophage cytokine production. This could again be due to the lack of LPG in EVs or reduced promastigote EV release. To address this, equal numbers of EVs from parental and LPG-deficient cells could added to macrophages to see whether they induce the same effects.

We find, consistent with published murine studies (Ilg, 2000), that LPG-deficient *L. mexicana* parasites are able to survive and replicate in human macrophages, albeit with slightly different infection kinetics from parental parasites (Figure 5.13). This raises doubt about the biological significance of LPG-dependent changes in chemokine levels during infection. However, macrophage studies cannot be used to infer conclusions about the importance of LPG during systemic infection. Furthermore, the main action of macrophage chemokines is regulating chemotaxis of other cell types, (T cells in the case of CXCL10) (Dufour et al., 2002). Therefore, it is not surprising that changes in chemokine secretion do not impact on *L. mexicana* survival within isolated macrophages.

6.7. Molecular mechanisms of macrophage chemokine downregulation

We aimed to elucidate the signalling targets in the macrophage responsible for chemokine downregulation by *Leishmania* samples. Phosphoproteins Erk1/2, STAT1, STAT3 and p38 (Figure 5.15) and transcription factors NFκB and AP-1 do not appear to be responsible (Figure 5.17, Figure 5.18), therefore the signalling targets in the macrophage remain unknown. However, we speculate that under the conditions where chemokine downregulation is observed, it is likely that the LPS/IFNγ-

prestimulated macrophages are in a state of LPS tolerance (Seeley and Ghosh, 2017) and therefore cannot secrete further amounts of certain cytokines, including CXCL10, after the addition of *Leishmania* samples. Therefore, for *Leishmania* samples to reduce secreted chemokine levels, we reason it would be via removal of existing secreted chemokine rather than inhibition of *de novo* synthesis and secretion. We propose that future studies under these experimental conditions should focus on determining to what extent degradation and uptake from the medium modulate extracellular chemokine levels.

6.8. The importance of CXCL10 in *Leishmania* infection and therapeutic potential

Our finding that levels of secreted macrophage CXCL10 are reduced by *L. mexicana* samples is of interest in the context of the literature (discussed in the Chapter 5 Introduction) showing that in mice CXCL10 promotes a protective Th1 response and *Leishmania* parasite clearance (Vasquez and Soong, 2006, Figueiredo et al., 2017). It therefore makes sense that *Leishmania* parasites would have mechanisms to reduce CXCL10 levels; we show for the first time that this is the case in macrophages. A recent study investigated the therapeutic potential of CXCL10-based treatment of murine *L. major* infection (Montakhab-Yeganeh et al., 2017). Either a plasmid encoding CXCL10 or live *Leishmania tarentolae* (*L. tarentolae*, a non-pathogenic species which infects lizards) parasites expressing murine CXCL10 were used; plasmids were injected once a week and *L. tarentolae* twice a week into *L. major*-infected footpads over six weeks (regular injection is necessary because *L. tarantolae* is usually cleared within days). Both treatments reduced parasite burden by ~30-fold after three weeks (Montakhab-Yeganeh et al., 2017). Importantly, this reduction was comparable to that induced by the positive control, liposomal amphotericin B, which is a second-line drug used to

treat cutaneous leishmaniasis. Treatments with CXCL10-expressing *L. tarentolae* were particularly effective at enhancing the protective Th1 response (Montakhab-Yeganeh et al., 2017). Efficacy of *L. tarentolae* expressing CXCL10 has also been shown by the same lab in the treatment of breast cancer in mice (Taslimi et al., 2016). Independent corroboration of the efficacy of CXCL10-expressing *L. tarentolae* as an immunotherapeutic would bolster the case for taking it forward to clinical trials. While CXCL10 is considered a promising immunotherapy candidate based on its efficacy in animal studies in treating cancer as well as viral, bacterial and leishmanial infections (Mohit and Rafati, 2012) and chemokine immunotherapy more widely is considered to be a promising approach (Nagarsheth et al., 2017), to our knowledge no CXCL10-based treatments are currently approved for human use.

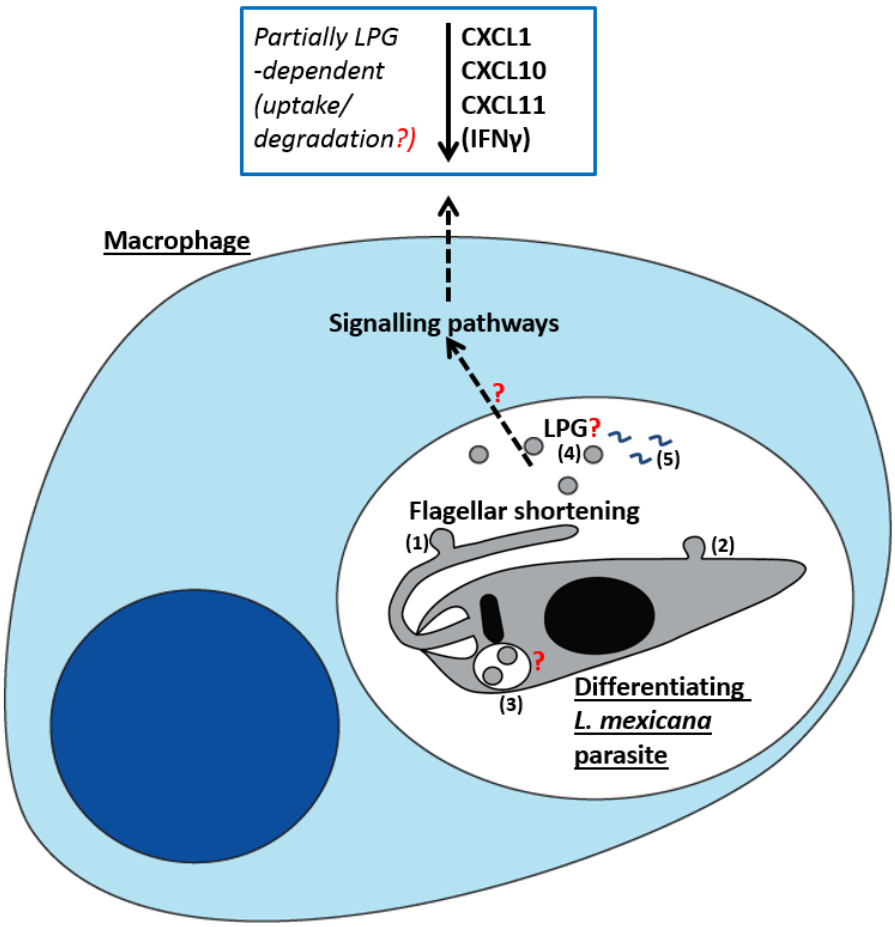

Figure 6.1. Summary of thesis conclusions. *L. mexicana* parasites release EVs from their flagellum (1), as well as from the cell body membrane (2), inside the PV of host macrophages. Exosomes may also be released from multi-vesicular bodies (3), but the presence of these organelles in *L. mexicana* is uncertain. During the early time-points of infection, when infective promastigotes are differentiating to amastigotes and undergoing flagellar shortening, there is also an increase in the release EVs and the ratio of flagellar- to cell body membrane- derived EVs. *L. mexicana* EV samples contain virulence factors including LPG (4), which may be present as a secreted factor (5) or an integral EV component. EVs and/or secreted factors released inside the PV signal via unknown signalling pathways in an LPG-dependent manner to the macrophage, resulting in decreased levels of secreted CXCL1, CXCL10, CXCL11 and possibly IFNγ. Downregulation of these cytokine levels is likely to be via increased uptake and/or degradation.

6.9. Conclusions

We show that the *L. mexicana* flagellum is a source of EVs. Flagellar-derived EVs appear to constitute a major fraction of total EVs, the cell body membrane is the source of a less abundant population of EVs and the abundance of MVB-derived exosomes, if they exist in *Leishmania*, is unknown. The functional and compositional differences between *L. mexicana* EVs from different subcellular sources remains an interesting open question. We place *L. mexicana* alongside *C. reinhardtii* and mammalian cells in displaying the recently described phenomenon that flagellar shortening and EV release are linked. The extent to which this is a causal link and the underlying molecular mechanisms remain to be elucidated in *L. mexicana*. The major finding from this study is the previously undescribed reduction in secreted levels of CXCL- chemokines, including CXCL10, from LPS/IFNγ stimulated macrophages after exposure to *Leishmania* promastigotes or isolated EVs. This is consistent with the published protective role of CXCL10 in *Leishmania* infection, suggesting a benefit to the parasite in reducing host CXCL10 levels. Our data suggests that the well-studied virulence factor LPG may be delivered to macrophages via EVs, although further work is required to confirm this. Chemokine downregulation is partially LPG-dependent. This could be due to the direct action of LPG or to LPG-dependent modulation of *L. mexicana* EV properties and/or release. We speculate that novel mechanisms of chemokine downregulation such as degradation and uptake are responsible.

Acknowledgments

Most of all, thank you Eva Gluenz for making this PhD as stress-free as a supervisor could and for always perfectly counteracting my lack of attention to detail. Thank you to the Wellcome Trust for generous funding and support. Thank you to Sally Cowley in the James Martin Stem Cell Facility for the wonderful iPSC collaboration. I am grateful to Chris Tang for helpful discussions and support throughout my PhD. Errin Johnson made all the EM analysis possible and I thank her for all the support along the way. Thank you to Svenja Hester and Ben Thomas who advised on sample preparation and carried out all the MS analysis and to Shabaz Mohammed for help with the Proteome Discoverer analysis. Thank you to Amin Moghaddam in the Quentin Sattentau lab for help and advice with the cytokine and RAW-Blue assays, including use of lab equipment and the generous gift of RAW-Blue RAW macrophages, which made the most important experiments of this thesis possible. Helder Carmen and David Vaux kindly allowed me to use their NanoSight and thank you to Helder for giving up your time to train me. Thank you to Patrizia Abrusci for help with ultracentrifugation. Lewis Taylor and Theodoros Kapellos in the David Greaves lab helped me out in several macrophage crises and kindly donated both RAW macrophages and BMDMs. Thank you to the animal facility for mice and help with dissection.

Thank you to the Gull lab for sharing equipment and Keith Gull for helpful comments on experiments. I cannot thank the Gull lab post-docs Jack Sunter, Sam Dean, Vlado Varga, Helen Farr, Richard Wheeler and lab manager Helen Banks enough for all kinds of daily help in the lab, especially when I was new and hopeless. I would honestly have been lost without you, and thank you for coffee breaks: the highlight! And thank you Karen Billington, who swooped in at the end and brightened the lab.

To the Gluenz lab: thank you Ross Madden and most of all Tom Beneke for loads of help with genetic manipulation (not my forte) and for bringing Crispr-Cas9 to the lab. Thank you Jessica Valli for all your help, and in particular for developing the macrophage infection analysis and help with Airyscan imaging. Most importantly, thank you guys for the banter and Gluenz lab love.

Thanks Mum, Dad and Anna for your love and support always. Thank you Olivia for lunch breaks which always left me uplifted. And to Iain, the only person listed here who made it harder, but that's only because I missed you so darn much – thank you for still being there at the end.

References

ABDOLI, A., MASPI, N. & GHAFFARIFAR, F. 2017. Wound healing in cutaneous leishmaniasis: A double edged sword of IL-10 and TGF-beta. *Comp Immunol Microbiol Infect Dis,* 51**,** 15-26.

ABOU FAKHER, F. H., RACHINEL, N., KLIMCZAK, M., LOUIS, J. & DOYEN, N. 2009. TLR9-dependent activation of dendritic cells by DNA from Leishmania major favors Th1 cell development and the resolution of lesions. *J Immunol,* 182**,** 1386-96.

ABU-DAYYEH, I., HASSANI, K., WESTRA, E. R., MOTTRAM, J. C. & OLIVIER, M. 2010. Comparative study of the ability of Leishmania mexicana promastigotes and amastigotes to alter macrophage signaling and functions. *Infect Immun,* 78**,** 2438-45.

AGRAWAL, N., DASARADHI, P. V., MOHMMED, A., MALHOTRA, P., BHATNAGAR, R. K. & MUKHERJEE, S. K. 2003. RNA interference: biology, mechanism, and applications. *Microbiol Mol Biol Rev,* 67**,** 657-85.

AJDARY, S., ALIMOHAMMADIAN, M. H., ESLAMI, M. B., KEMP, K. & KHARAZMI, A. 2000. Comparison of the immune profile of nonhealing cutaneous Leishmaniasis patients with those with active lesions and those who have recovered from infection. *Infect Immun,* 68**,** 1760-4.

AKERS, J. C., RAMAKRISHNAN, V., NOLAN, J. P., DUGGAN, E., FU, C. C., HOCHBERG, F. H., CHEN, C. C. & CARTER, B. S. 2016. Comparative Analysis of Technologies for Quantifying Extracellular Vesicles (EVs) in Clinical Cerebrospinal Fluids (CSF). *PLoS One,* 11**,** e0149866.

ALEXANDER, J. & BRYSON, K. 2005. T helper (h)1/Th2 and Leishmania: paradox rather than paradigm. *Immunol Lett,* 99**,** 17-23.

ANDERSON, C. F., LIRA, R., KAMHAWI, S., BELKAID, Y., WYNN, T. A. & SACKS, D. 2008. IL-10 and TGF-beta control the establishment of persistent and transmissible infections produced by Leishmania tropica in C57BL/6 mice. *J Immunol,* 180**,** 4090-7.

ANDERSON, P. 2008. Post-transcriptional control of cytokine production. *Nat Immunol,* 9**,** 353-9.

ARANGO DUQUE, G. & DESCOTEAUX, A. 2014. Macrophage cytokines: involvement in immunity and infectious diseases. *Front Immunol,* 5**,** 491.

ARANGO DUQUE, G., FUKUDA, M. & DESCOTEAUX, A. 2013. Synaptotagmin XI regulates phagocytosis and cytokine secretion in macrophages. *J Immunol,* 190**,** 1737-45.

ARANGO DUQUE, G., FUKUDA, M., TURCO, S. J., STAGER, S. & DESCOTEAUX, A. 2014. Leishmania promastigotes induce cytokine secretion in macrophages through the degradation of synaptotagmin XI. *J Immunol,* 193**,** 2363-72.

ARGUETA-DONOHUE, J., CARRILLO, N., VALDES-REYES, L., ZENTELLA, A., AGUIRRE-GARCIA, M., BECKER, I. & GUTIERREZ-KOBEH, L. 2008. Leishmania mexicana: participation of NF-kappaB in the differential production of IL-12 in dendritic cells and monocytes induced by lipophosphoglycan (LPG). *Exp Parasitol,* 120**,** 1-9.

ARIFFIN, J. K. & SWEET, M. J. 2013. Differences in the repertoire, regulation and function of Toll-like Receptors and inflammasome-forming Nod-like Receptors between human and mouse. *Curr Opin Microbiol,* 16**,** 303-10.

ARTHUR, J. S. & LEY, S. C. 2013. Mitogen-activated protein kinases in innate immunity. *Nat Rev Immunol,* 13**,** 679-92.

ATAYDE, V. D., ASLAN, H., TOWNSEND, S., HASSANI, K., KAMHAWI, S. & OLIVIER, M. 2015. Exosome Secretion by the Parasitic Protozoan Leishmania within the Sand Fly Midgut. *Cell Rep,* 13**,** 957-67.

AVIDOR-REISS, T., MAER, A. M., KOUNDAKJIAN, E., POLYANOVSKY, A., KEIL, T., SUBRAMANIAM, S. & ZUKER, C. S. 2004. Decoding cilia function: defining

specialized genes required for compartmentalized cilia biogenesis. *Cell,* 117**,** 527-39.

AVILAN, L., GUALDRON-LOPEZ, M., QUINONES, W., GONZALEZ-GONZALEZ, L., HANNAERT, V., MICHELS, P. A. & CONCEPCION, J. L. 2011. Enolase: a key player in the metabolism and a probable virulence factor of trypanosomatid parasites-perspectives for its use as a therapeutic target. *Enzyme Res,* 2011**,** 932549.

BABST, M., WENDLAND, B., ESTEPA, E. J. & EMR, S. D. 1998. The Vps4p AAA ATPase regulates membrane association of a Vps protein complex required for normal endosome function. *Embo j,* 17**,** 2982-93.

BAHR, V., STIERHOF, Y. D., ILG, T., DEMAR, M., QUINTEN, M. & OVERATH, P. 1993. Expression of lipophosphoglycan, high-molecular weight phosphoglycan and glycoprotein 63 in promastigotes and amastigotes of Leishmania mexicana. *Mol Biochem Parasitol,* 58**,** 107-21.

BAIETTI, M. F., ZHANG, Z., MORTIER, E., MELCHIOR, A., DEGEEST, G., GEERAERTS, A., IVARSSON, Y., DEPOORTERE, F., COOMANS, C., VERMEIREN, E., ZIMMERMANN, P. & DAVID, G. 2012. Syndecan-syntenin-ALIX regulates the biogenesis of exosomes. *Nat Cell Biol,* 14**,** 677-85.

BALARAMAN, S., SINGH, V. K., TEWARY, P. & MADHUBALA, R. 2005. Leishmania lipophosphoglycan activates the transcription factor activating protein 1 in J774A.1 macrophages through the extracellular signal-related kinase (ERK) and p38 mitogen-activated protein kinase. *Mol Biochem Parasitol,* 139**,** 117-27.

BANGS, J. D., UYETAKE, L., BRICKMAN, M. J., BALBER, A. E. & BOOTHROYD, J. C. 1993. Molecular cloning and cellular localization of a BiP homologue in Trypanosoma brucei. Divergent ER retention signals in a lower eukaryote. *J Cell Sci,* 105 (Pt 4)**,** 1101-13.

BARBI, J., BROMBACHER, F. & SATOSKAR, A. R. 2008. T cells from Leishmania major-susceptible BALB/c mice have a defect in efficiently up-regulating CXCR3 upon activation. *J Immunol,* 181**,** 4613-20.

BARRON, T. L. & TURCO, S. J. 2006. Quantitation of Leishmania lipophosphoglycan repeat units by capillary electrophoresis. *Biochim Biophys Acta,* 1760**,** 710-4.

BAYER-SANTOS, E., LIMA, F. M., RUIZ, J. C., ALMEIDA, I. C. & DA SILVEIRA, J. F. 2014. Characterization of the small RNA content of Trypanosoma cruzi extracellular vesicles. *Mol Biochem Parasitol,* 193**,** 71-4.

BAYER-SANTOS, E., MARINI, M. M. & DA SILVEIRA, J. F. 2017. Non-coding RNAs in Host-Pathogen Interactions: Subversion of Mammalian Cell Functions by Protozoan Parasites. *Front Microbiol,* 8**,** 474.

BECKER, I., SALAIZA, N., AGUIRRE, M., DELGADO, J., CARRILLO-CARRASCO, N., KOBEH, L. G., RUIZ, A., CERVANTES, R., TORRES, A. P., CABRERA, N., GONZALEZ, A., MALDONADO, C. & ISIBASI, A. 2003. Leishmania lipophosphoglycan (LPG) activates NK cells through toll-like receptor-2. *Mol Biochem Parasitol,* 130**,** 65-74.

BEER, K. B. & WEHMAN, A. M. 2017. Mechanisms and functions of extracellular vesicle release in vivo-What we can learn from flies and worms. *Cell Adh Migr,* 11**,** 135-150.

BELKAID, Y., BUTCHER, B. & SACKS, D. L. 1998. Analysis of cytokine production by inflammatory mouse macrophages at the single-cell level: selective impairment of IL-12 induction in Leishmania-infected cells. *Eur J Immunol,* 28**,** 1389-400.

BENCHIMOL, M. & DE SOUZA, W. 1981. Leishmania mexicana amazonensis: attachment to the membrane of the phagocytic vacuole of macrophages in vivo. *Z Parasitenkd,* 66**,** 25-9.

BENEKE, T., MADDEN, R., MAKIN, L., VALLI, J., SUNTER, J. & GLUENZ, E. 2017. A CRISPR Cas9 high-throughput genome editing toolkit for kinetoplastids. *R Soc Open Sci,* 4**,** 170095.

BENEKE;, T. 2017. *LeishGEdit* [Online]. Available: http://www.leishgedit.net/Home.html.
BENREDJEM, B., GIRARD, M., RHAINDS, D., ST-ONGE, G. & HEVEKER, N. 2017. Mutational Analysis of Atypical Chemokine Receptor 3 (ACKR3/CXCR7) Interaction with Its Chemokine Ligands CXCL11 and CXCL12. *J Biol Chem,* 292**,** 31-42.
BESTEIRO, S., WILLIAMS, R. A., COOMBS, G. H. & MOTTRAM, J. C. 2007. Protein turnover and differentiation in Leishmania. *Int J Parasitol,* 37**,** 1063-75.
BESTEIRO, S., WILLIAMS, R. A., MORRISON, L. S., COOMBS, G. H. & MOTTRAM, J. C. 2006. Endosome sorting and autophagy are essential for differentiation and virulence of Leishmania major. *J Biol Chem,* 281**,** 11384-96.
BLAINEAU, C., TESSIER, M., DUBESSAY, P., TASSE, L., CROBU, L., PAGES, M. & BASTIEN, P. 2007. A novel microtubule-depolymerizing kinesin involved in length control of a eukaryotic flagellum. *Curr Biol,* 17**,** 778-82.
BOONSTRA, A., RAJSBAUM, R., HOLMAN, M., MARQUES, R., ASSELIN-PATUREL, C., PEREIRA, J. P., BATES, E. E., AKIRA, S., VIEIRA, P., LIU, Y. J., TRINCHIERI, G. & O'GARRA, A. 2006. Macrophages and myeloid dendritic cells, but not plasmacytoid dendritic cells, produce IL-10 in response to MyD88- and TRIF-dependent TLR signals, and TLR-independent signals. *J Immunol,* 177**,** 7551-8.
BOSE, M., BARMAN, B., GOSWAMI, A. & BHATTACHARYYA, S. N. 2017. Spatiotemporal Uncoupling of MicroRNA-Mediated Translational Repression and Target RNA Degradation Controls MicroRNP Recycling in Mammalian Cells. *Mol Cell Biol,* 37.
BRIGHTBILL, H. D., PLEVY, S. E., MODLIN, R. L. & SMALE, S. T. 2000. A prominent role for Sp1 during lipopolysaccharide-mediated induction of the IL-10 promoter in macrophages. *J Immunol,* 164**,** 1940-51.
BROOKS, P., FUERTES, G., MURRAY, R. Z., BOSE, S., KNECHT, E., RECHSTEINER, M. C., HENDIL, K. B., TANAKA, K., DYSON, J. & RIVETT, J. 2000. Subcellular localization of proteasomes and their regulatory complexes in mammalian cells. *Biochem J,* 346 Pt 1**,** 155-61.
BROWN, L., WOLF, J. M., PRADOS-ROSALES, R. & CASADEVALL, A. 2015. Through the wall: extracellular vesicles in Gram-positive bacteria, mycobacteria and fungi. *Nat Rev Microbiol,* 13**,** 620-30.
BROWNELL, J., BRUCKNER, J., WAGONER, J., THOMAS, E., LOO, Y. M., GALE, M., JR., LIANG, T. J. & POLYAK, S. J. 2014. Direct, interferon-independent activation of the CXCL10 promoter by NF-kappaB and interferon regulatory factor 3 during hepatitis C virus infection. *J Virol,* 88**,** 1582-90.
BUCK, A. H., COAKLEY, G., SIMBARI, F., MCSORLEY, H. J., QUINTANA, J. F., LE BIHAN, T., KUMAR, S., ABREU-GOODGER, C., LEAR, M., HARCUS, Y., CERONI, A., BABAYAN, S. A., BLAXTER, M., IVENS, A. & MAIZELS, R. M. 2014. Exosomes secreted by nematode parasites transfer small RNAs to mammalian cells and modulate innate immunity. *Nat Commun,* 5**,** 5488.
BUNNELL, T. M., BURBACH, B. J., SHIMIZU, Y. & ERVASTI, J. M. 2011. beta-Actin specifically controls cell growth, migration, and the G-actin pool. *Mol Biol Cell,* 22**,** 4047-58.
BUTLER, K. L., CLANCY-THOMPSON, E. & MULLINS, D. W. 2017. CXCR3+ monocytes/macrophages are required for establishment of pulmonary metastases. *Sci Rep,* 7**,** 45593.
BUTTON, L. L. & MCMASTER, W. R. 1988. Molecular cloning of the major surface antigen of leishmania. *J Exp Med,* 167**,** 724-9.
BUXBAUM, L. U., DENISE, H., COOMBS, G. H., ALEXANDER, J., MOTTRAM, J. C. & SCOTT, P. 2003. Cysteine protease B of Leishmania mexicana inhibits host Th1 responses and protective immunity. *J Immunol,* 171**,** 3711-7.

CABRA, V. & SAMSO, M. 2015. Do's and don'ts of cryo-electron microscopy: a primer on sample preparation and high quality data collection for macromolecular 3D reconstruction. *J Vis Exp*, 52311.

CAMERON, P., MCGACHY, A., ANDERSON, M., PAUL, A., COOMBS, G. H., MOTTRAM, J. C., ALEXANDER, J. & PLEVIN, R. 2004. Inhibition of lipopolysaccharide-induced macrophage IL-12 production by Leishmania mexicana amastigotes: the role of cysteine peptidases and the NF-kappaB signaling pathway. *J Immunol,* 173, 3297-304.

CAMPANELLA, G. S., GRIMM, J., MANICE, L. A., COLVIN, R. A., MEDOFF, B. D., WOJTKIEWICZ, G. R., WEISSLEDER, R. & LUSTER, A. D. 2006. Oligomerization of CXCL10 is necessary for endothelial cell presentation and in vivo activity. *J Immunol,* 177, 6991-8.

CARDONA, A. E., SASSE, M. E., LIU, L., CARDONA, S. M., MIZUTANI, M., SAVARIN, C., HU, T. & RANSOHOFF, R. M. 2008. Scavenging roles of chemokine receptors: chemokine receptor deficiency is associated with increased levels of ligand in circulation and tissues. *Blood,* 112, 256-63.

CARTER, S. L., MULLER, M., MANDERS, P. M. & CAMPBELL, I. L. 2007. Induction of the genes for Cxcl9 and Cxcl10 is dependent on IFN-gamma but shows differential cellular expression in experimental autoimmune encephalomyelitis and by astrocytes and microglia in vitro. *Glia,* 55, 1728-39.

CASANOVA, M., CROBU, L., BLAINEAU, C., BOURGEOIS, N., BASTIEN, P. & PAGES, M. 2009. Microtubule-severing proteins are involved in flagellar length control and mitosis in Trypanosomatids. *Mol Microbiol,* 71, 1353-70.

CASGRAIN, P. A., MARTEL, C., MCMASTER, W. R., MOTTRAM, J. C., OLIVIER, M. & DESCOTEAUX, A. 2016. Cysteine Peptidase B Regulates Leishmania mexicana Virulence through the Modulation of GP63 Expression. *PLoS Pathog,* 12, e1005658.

CASTELLANO, L. R., FILHO, D. C., ARGIRO, L., DESSEIN, H., PRATA, A., DESSEIN, A. & RODRIGUES, V. 2009. Th1/Th2 immune responses are associated with active cutaneous leishmaniasis and clinical cure is associated with strong interferon-gamma production. *Hum Immunol,* 70, 383-90.

CHACON-HESZELE, M. F., CHOI, S. Y., ZUO, X., BAEK, J. I., WARD, C. & LIPSCHUTZ, J. H. 2014. The exocyst and regulatory GTPases in urinary exosomes. *Physiol Rep,* 2.

CHAIROUNGDUA, A., SMITH, D. L., POCHARD, P., HULL, M. & CAPLAN, M. J. 2010. Exosome release of beta-catenin: a novel mechanism that antagonizes Wnt signaling. *J Cell Biol,* 190, 1079-91.

CHARRIN, S., JOUANNET, S., BOUCHEIX, C. & RUBINSTEIN, E. 2014. Tetraspanins at a glance. *J Cell Sci,* 127, 3641-8.

CHOI, D. S., CHOI, D. Y., HONG, B. S., JANG, S. C., KIM, D. K., LEE, J., KIM, Y. K., KIM, K. P. & GHO, Y. S. 2012. Quantitative proteomics of extracellular vesicles derived from human primary and metastatic colorectal cancer cells. *J Extracell Vesicles,* 1.

CHOUDHURI, K., LLODRA, J., ROTH, E. W., TSAI, J., GORDO, S., WUCHERPFENNIG, K. W., KAM, L. C., STOKES, D. L. & DUSTIN, M. L. 2014. Polarized release of T-cell-receptor-enriched microvesicles at the immunological synapse. *Nature,* 507, 118-23.

CIVINI, S., JIN, P., REN, J., SABATINO, M., CASTIELLO, L., JIN, J., WANG, H., ZHAO, Y., MARINCOLA, F. & STRONCEK, D. 2013. Leukemia cells induce changes in human bone marrow stromal cells. *J Transl Med,* 11, 298.

CLOUTIER, S., LAVERDIERE, M., CHOU, M. N., BOILARD, N., CHOW, C. & PAPADOPOULOU, B. 2012. Translational control through eIF2alpha phosphorylation during the Leishmania differentiation process. *PLoS One,* 7, e35085.

COLOMBO, M., MOITA, C., VAN NIEL, G., KOWAL, J., VIGNERON, J., BENAROCH, P., MANEL, N., MOITA, L. F., THERY, C. & RAPOSO, G. 2013. Analysis of ESCRT functions in exosome biogenesis, composition and secretion highlights the heterogeneity of extracellular vesicles. *J Cell Sci,* 126**,** 5553-65.

COLOMBO, M., RAPOSO, G. & THERY, C. 2014. Biogenesis, secretion, and intercellular interactions of exosomes and other extracellular vesicles. *Annu Rev Cell Dev Biol,* 30**,** 255-89.

COLVIN, R. A., CAMPANELLA, G. S., SUN, J. & LUSTER, A. D. 2004. Intracellular domains of CXCR3 that mediate CXCL9, CXCL10, and CXCL11 function. *J Biol Chem,* 279**,** 30219-27.

CONTRERAS, I., GOMEZ, M. A., NGUYEN, O., SHIO, M. T., MCMASTER, R. W. & OLIVIER, M. 2010. Leishmania-induced inactivation of the macrophage transcription factor AP-1 is mediated by the parasite metalloprotease GP63. *PLoS Pathog,* 6**,** e1001148.

CORBETTA, S., RAIMONDO, F., TEDESCHI, S., SYREN, M. L., REBORA, P., SAVOIA, A., BALDI, L., BETTINELLI, A. & PITTO, M. 2015. Urinary exosomes in the diagnosis of Gitelman and Bartter syndromes. *Nephrol Dial Transplant,* 30**,** 621-30.

CUERVO, P., DE JESUS, J. B., SABOIA-VAHIA, L., MENDONCA-LIMA, L., DOMONT, G. B. & CUPOLILLO, E. 2009. Proteomic characterization of the released/secreted proteins of Leishmania (Viannia) braziliensis promastigotes. *J Proteomics,* 73**,** 79-92.

CUVILLIER, A., REDON, F., ANTOINE, J. C., CHARDIN, P., DEVOS, T. & MERLIN, G. 2000. LdARL-3A, a Leishmania promastigote-specific ADP-ribosylation factor-like protein, is essential for flagellum integrity. *J Cell Sci,* 113 (Pt 11)**,** 2065-74.

CVJETKOVIC, A., JANG, S. C., KONECNA, B., HOOG, J. L., SIHLBOM, C., LASSER, C. & LOTVALL, J. 2016. Detailed Analysis of Protein Topology of Extracellular Vesicles-Evidence of Unconventional Membrane Protein Orientation. *Sci Rep,* 6**,** 36338.

D'ANGELO, M. A., MONTAGNA, A. E., SANGUINETI, S., TORRES, H. N. & FLAWIA, M. M. 2002. A novel calcium-stimulated adenylyl cyclase from Trypanosoma cruzi, which interacts with the structural flagellar protein paraflagellar rod. *J Biol Chem,* 277**,** 35025-34.

DA SILVA SANTOS, C. & BRODSKYN, C. I. 2014. The Role of CD4 and CD8 T Cells in Human Cutaneous Leishmaniasis. *Front Public Health,* 2**,** 165.

DAVID M. HORN, ILYAS SINGEC & BRILL, L. *Quantitative Analysis of Large Phosphopeptide Datasets Using Proteome Discoverer 2.0* [Online]. Available: https://tools.thermofisher.com/content/sfs/posters/PN-64491-LIMS-Proteome-Discoverer-Phosphopeptide-Datasets-ASMS2015-PN64491-EN.pdf.

DE MENEZES, J. P., GUEDES, C. E., PETERSEN, A. L., FRAGA, D. B. & VERAS, P. S. 2015. Advances in Development of New Treatment for Leishmaniasis. *Biomed Res Int,* 2015**,** 815023.

DE SANTA, F., TOTARO, M. G., PROSPERINI, E., NOTARBARTOLO, S., TESTA, G. & NATOLI, G. 2007. The histone H3 lysine-27 demethylase Jmjd3 links inflammation to inhibition of polycomb-mediated gene silencing. *Cell,* 130**,** 1083-94.

DE VEER, M. J., CURTIS, J. M., BALDWIN, T. M., DIDONATO, J. A., SEXTON, A., MCCONVILLE, M. J., HANDMAN, E. & SCHOFIELD, L. 2003. MyD88 is essential for clearance of Leishmania major: possible role for lipophosphoglycan and Toll-like receptor 2 signaling. *Eur J Immunol,* 33**,** 2822-31.

DEAN, S., SUNTER, J., WHEELER, R. J., HODKINSON, I., GLUENZ, E. & GULL, K. 2015. A toolkit enabling efficient, scalable and reproducible gene tagging in trypanosomatids. *Open Biol,* 5**,** 140197.

DENNY, P. W., LEWIS, S., TEMPERO, J. E., GOULDING, D., IVENS, A. C., FIELD, M. C. & SMITH, D. F. 2002. Leishmania RAB7: characterisation of terminal endocytic stages in an intracellular parasite. *Mol Biochem Parasitol,* 123**,** 105-13.

DENTLER, W. 2013. A role for the membrane in regulating Chlamydomonas flagellar length. *PLoS One,* 8**,** e53366.

DESJARDINS, M. & DESCOTEAUX, A. 1997. Inhibition of phagolysosomal biogenesis by the Leishmania lipophosphoglycan. *J Exp Med,* 185**,** 2061-8.

DILLON, L. A., SURESH, R., OKRAH, K., CORRADA BRAVO, H., MOSSER, D. M. & EL-SAYED, N. M. 2015. Simultaneous transcriptional profiling of Leishmania major and its murine macrophage host cell reveals insights into host-pathogen interactions. *BMC Genomics,* 16**,** 1108.

DINARELLO, C. A. 2007. Historical insights into cytokines. *Eur J Immunol,* 37 Suppl 1**,** S34-45.

DJACZENKO, W., FILADORO, F. & PEZZI, R. 1969. On the presence of multivesicular bodies in Leishmania donovani. *Experientia,* 25**,** 666-7.

DODGE, M. A., WALLER, R. F., CHOW, L. M., ZAMAN, M. M., COTTON, L. M., MCCONVILLE, M. J. & WIRTH, D. F. 2004. Localization and activity of multidrug resistance protein 1 in the secretory pathway of Leishmania parasites. *Mol Microbiol,* 51**,** 1563-75.

DUFOUR, J. H., DZIEJMAN, M., LIU, M. T., LEUNG, J. H., LANE, T. E. & LUSTER, A. D. 2002. IFN-gamma-inducible protein 10 (IP-10; CXCL10)-deficient mice reveal a role for IP-10 in effector T cell generation and trafficking. *J Immunol,* 168**,** 3195-204.

EICHELBAUM, K. & KRIJGSVELD, J. 2014. Rapid temporal dynamics of transcription, protein synthesis, and secretion during macrophage activation. *Mol Cell Proteomics,* 13**,** 792-810.

EIRIN, A., ZHU, X. Y., PURANIK, A. S., WOOLLARD, J. R., TANG, H., DASARI, S., LERMAN, A., VAN WIJNEN, A. J. & LERMAN, L. O. 2016. Comparative proteomic analysis of extracellular vesicles isolated from porcine adipose tissue-derived mesenchymal stem/stromal cells. *Sci Rep,* 6**,** 36120.

ELIAZ, D., KANNAN, S., SHAKED, H., ARVATZ, G., TKACZ, I. D., BINDER, L., WALDMAN BEN-ASHER, H., OKALANG, U., CHIKNE, V., COHEN-CHALAMISH, S. & MICHAELI, S. 2017. Exosome secretion affects social motility in Trypanosoma brucei. *PLoS Pathog,* 13**,** e1006245.

EMBL, PROTEOMICS, CORE & FACILITY. *Sample preparation* [Online]. Available: https://www.embl.de/proteomics/proteomics_services/user_guide/faq/.

ERDMANN, M., SCHOLZ, A., MELZER, I. M., SCHMETZ, C. & WIESE, M. 2006. Interacting protein kinases involved in the regulation of flagellar length. *Mol Biol Cell,* 17**,** 2035-45.

FARIA, M. S., REIS, F. C., AZEVEDO-PEREIRA, R. L., MORRISON, L. S., MOTTRAM, J. C. & LIMA, A. P. 2011. Leishmania inhibitor of serine peptidase 2 prevents TLR4 activation by neutrophil elastase promoting parasite survival in murine macrophages. *J Immunol,* 186**,** 411-22.

FAUGHT, E., HENRICKSON, L. & VIJAYAN, M. M. 2017. Plasma exosomes are enriched in Hsp70 and modulated by stress and cortisol in rainbow trout. *J Endocrinol,* 232**,** 237-246.

FAVILA, M. A., GERACI, N. S., JAYAKUMAR, A., HICKERSON, S., MOSTROM, J., TURCO, S. J., BEVERLEY, S. M. & MCDOWELL, M. A. 2015. Differential Impact of LPG-and PG-Deficient Leishmania major Mutants on the Immune Response of Human Dendritic Cells. *PLoS Negl Trop Dis,* 9**,** e0004238.

FERNANDES, M. C., DILLON, L. A., BELEW, A. T., BRAVO, H. C., MOSSER, D. M. & EL-SAYED, N. M. 2016. Dual Transcriptome Profiling of Leishmania-Infected Human Macrophages Reveals Distinct Reprogramming Signatures. *MBio,* 7.

FERNANDEZ-LEIRO, R. & SCHERES, S. H. 2016. Unravelling biological macromolecules with cryo-electron microscopy. *Nature,* 537**,** 339-46.
FIEBIG, M., KELLY, S. & GLUENZ, E. 2015. Comparative Life Cycle Transcriptomics Revises Leishmania mexicana Genome Annotation and Links a Chromosome Duplication with Parasitism of Vertebrates. *PLoS Pathog,* 11**,** e1005186.
FIGUEIREDO, W. M. E., VIANA, S. M., ALVES, D. T., GUERRA, P. V., COELHO, Z. C. B., BARBOSA, H. S. & TEIXEIRA, M. J. 2017. Protection mediated by chemokine CXCL10 in BALB/c mice infected by Leishmania infantum. *Mem Inst Oswaldo Cruz,* 112**,** 561-568.
FILARDY, A. A., COSTA-DA-SILVA, A. C., KOELLER, C. M., GUIMARAES-PINTO, K., RIBEIRO-GOMES, F. L., LOPES, M. F., HEISE, N., FREIRE-DE-LIMA, C. G., NUNES, M. P. & DOSREIS, G. A. 2014. Infection with Leishmania major induces a cellular stress response in macrophages. *PLoS One,* 9**,** e85715.
FORD, L. B., HANSELL, C. A. & NIBBS, R. J. 2013. Using fluorescent chemokine uptake to detect chemokine receptors by fluorescent activated cell sorting. *Methods Mol Biol,* 1013**,** 203-14.
FORESTIER, C. L., GAO, Q. & BOONS, G. J. 2014. Leishmania lipophosphoglycan: how to establish structure-activity relationships for this highly complex and multifunctional glycoconjugate? *Front Cell Infect Microbiol,* 4**,** 193.
FORGET, G., GREGORY, D. J., WHITCOMBE, L. A. & OLIVIER, M. 2006. Role of host protein tyrosine phosphatase SHP-1 in Leishmania donovani-induced inhibition of nitric oxide production. *Infect Immun,* 74**,** 6272-9.
FORGET, G., SIMINOVITCH, K. A., BROCHU, S., RIVEST, S., RADZIOCH, D. & OLIVIER, M. 2001. Role of host phosphotyrosine phosphatase SHP-1 in the development of murine leishmaniasis. *Eur J Immunol,* 31**,** 3185-96.
FOSTER, S. L., HARGREAVES, D. C. & MEDZHITOV, R. 2007. Gene-specific control of inflammation by TLR-induced chromatin modifications. *Nature,* 447**,** 972-8.
FRANK, B., MARCU, A., DE OLIVEIRA ALMEIDA PETERSEN, A. L., WEBER, H., STIGLOHER, C., MOTTRAM, J. C., SCHOLZ, C. J. & SCHURIGT, U. 2015. Autophagic digestion of Leishmania major by host macrophages is associated with differential expression of BNIP3, CTSE, and the miRNAs miR-101c, miR-129, and miR-210. *Parasit Vectors,* 8**,** 404.
FRANKENBERGER, M., PECHUMER, H. & ZIEGLER-HEITBROCK, H. W. 1995. Interleukin-10 is upregulated in LPS tolerance. *J Inflamm,* 45**,** 56-63.
FRANKENBURG, S., LEIBOVICI, V., MANSBACH, N., TURCO, S. J. & ROSEN, G. 1990. Effect of glycolipids of Leishmania parasites on human monocyte activity. Inhibition by lipophosphoglycan. *J Immunol,* 145**,** 4284-9.
FUKAO, T., FRUCHT, D. M., YAP, G., GADINA, M., O'SHEA, J. J. & KOYASU, S. 2001. Inducible expression of Stat4 in dendritic cells and macrophages and its critical role in innate and adaptive immune responses. *J Immunol,* 166**,** 4446-55.
FUKUMOTO, S., HIROI, M., DIRGAHAYU, P., MIURA, K., TADEMOTO, S., OTSUKI, H. & OHMORI, Y. 2012. Suppression of IP-10/CXCL10 gene expression in LPS- and/or IFN-gamma-stimulated macrophages by parasite-secreted products. *Cell Immunol,* 276**,** 101-9.
GAAFAR, A., KHARAZMI, A., ISMAIL, A., KEMP, M., HEY, A., CHRISTENSEN, C. B., DAFALLA, M., EL KADARO, A. Y., EL HASSAN, A. M. & THEANDER, T. G. 1995. Dichotomy of the T cell response to Leishmania antigens in patients suffering from cutaneous leishmaniasis; absence or scarcity of Th1 activity is associated with severe infections. *Clin Exp Immunol,* 100**,** 239-45.
GAIS, P., TIEDJE, C., ALTMAYR, F., GAESTEL, M., WEIGHARDT, H. & HOLZMANN, B. 2010. TRIF signaling stimulates translation of TNF-alpha mRNA via prolonged activation of MK2. *J Immunol,* 184**,** 5842-8.
GALLART-PALAU, X., SERRA, A., WONG, A. S., SANDIN, S., LAI, M. K., CHEN, C. P., KON, O. L. & SZE, S. K. 2015. Extracellular vesicles are rapidly purified

from human plasma by PRotein Organic Solvent PRecipitation (PROSPR). *Sci Rep,* 5**,** 14664.

GALLEGO, C., GOLENBOCK, D., GOMEZ, M. A. & SARAVIA, N. G. 2011. Toll-like receptors participate in macrophage activation and intracellular control of Leishmania (Viannia) panamensis. *Infect Immun,* 79**,** 2871-9.

GARCIA-SILVA, M. R., DAS NEVES, R. F., CABRERA-CABRERA, F., SANGUINETTI, J., MEDEIROS, L. C., ROBELLO, C., NAYA, H., FERNANDEZ-CALERO, T., SOUTO-PADRON, T., DE SOUZA, W. & CAYOTA, A. 2014. Extracellular vesicles shed by Trypanosoma cruzi are linked to small RNA pathways, life cycle regulation, and susceptibility to infection of mammalian cells. *Parasitol Res,* 113**,** 285-304.

GARCOVICH, A., ORMEA, F. & FABRIZI, G. 1975. [Ultrastructural observations on amastigote forms of Leishmania donovani in a case of laryngeal leishmaniasis]. *Minerva Med,* 66**,** 2883-98.

GAUR, U., SHOWALTER, M., HICKERSON, S., DALVI, R., TURCO, S. J., WILSON, M. E. & BEVERLEY, S. M. 2009. Leishmania donovani lacking the Golgi GDP-Man transporter LPG2 exhibit attenuated virulence in mammalian hosts. *Exp Parasitol,* 122**,** 182-91.

GERACI, N. S., TAN, J. C. & MCDOWELL, M. A. 2015. Characterization of microRNA expression profiles in Leishmania-infected human phagocytes. *Parasite Immunol,* 37**,** 43-51.

GERBER, J. S. & MOSSER, D. M. 2001. Reversing lipopolysaccharide toxicity by ligating the macrophage Fc gamma receptors. *J Immunol,* 166**,** 6861-8.

GHALIB, H. W., WHITTLE, J. A., KUBIN, M., HASHIM, F. A., EL-HASSAN, A. M., GRABSTEIN, K. H., TRINCHIERI, G. & REED, S. G. 1995. IL-12 enhances Th1-type responses in human Leishmania donovani infections. *J Immunol,* 154**,** 4623-9.

GHEDIN, E., DEBRABANT, A., ENGEL, J. C. & DWYER, D. M. 2001. Secretory and endocytic pathways converge in a dynamic endosomal system in a primitive protozoan. *Traffic,* 2**,** 175-88.

GHOSH, J., BOSE, M., ROY, S. & BHATTACHARYYA, S. N. 2013. Leishmania donovani targets Dicer1 to downregulate miR-122, lower serum cholesterol, and facilitate murine liver infection. *Cell Host Microbe,* 13**,** 277-88.

GIBBINGS, D. J., CIAUDO, C., ERHARDT, M. & VOINNET, O. 2009. Multivesicular bodies associate with components of miRNA effector complexes and modulate miRNA activity. *Nat Cell Biol,* 11**,** 1143-9.

GLASER, T. A., MOODY, S. F., HANDMAN, E., BACIC, A. & SPITHILL, T. W. 1991. An antigenically distinct lipophosphoglycan on amastigotes of Leishmania major. *Mol Biochem Parasitol,* 45**,** 337-44.

GLUENZ, E., HOOG, J. L., SMITH, A. E., DAWE, H. R., SHAW, M. K. & GULL, K. 2010. Beyond 9+0: noncanonical axoneme structures characterize sensory cilia from protists to humans. *Faseb j,* 24**,** 3117-21.

GLUENZ, E., WHEELER, R. J., HUGHES, L. & VAUGHAN, S. 2015. Scanning and three-dimensional electron microscopy methods for the study of Trypanosoma brucei and Leishmania mexicana flagella. *Methods Cell Biol,* 127**,** 509-42.

GOMES-SILVA, A., DE CASSIA BITTAR, R., DOS SANTOS NOGUEIRA, R., AMATO, V. S., DA SILVA MATTOS, M., OLIVEIRA-NETO, M. P., COUTINHO, S. G. & DA-CRUZ, A. M. 2007. Can interferon-gamma and interleukin-10 balance be associated with severity of human Leishmania (Viannia) braziliensis infection? *Clin Exp Immunol,* 149**,** 440-4.

GOMEZ, M. A., CONTRERAS, I., HALLE, M., TREMBLAY, M. L., MCMASTER, R. W. & OLIVIER, M. 2009. Leishmania GP63 alters host signaling through cleavage-activated protein tyrosine phosphatases. *Sci Signal,* 2**,** ra58.

GOSSAGE, S. M., ROGERS, M. E. & BATES, P. A. 2003. Two separate growth phases during the development of Leishmania in sand flies: implications for understanding the life cycle. *Int J Parasitol,* 33**,** 1027-34.

GREEN, E. R. & MECSAS, J. 2016. Bacterial Secretion Systems: An Overview. *Microbiol Spectr,* 4.

GREEN, S. J., MELTZER, M. S., HIBBS, J. B., JR. & NACY, C. A. 1990. Activated macrophages destroy intracellular Leishmania major amastigotes by an L-arginine-dependent killing mechanism. *J Immunol,* 144**,** 278-83.

GREGORY, D. J., GODBOUT, M., CONTRERAS, I., FORGET, G. & OLIVIER, M. 2008. A novel form of NF-kappaB is induced by Leishmania infection: involvement in macrophage gene expression. *Eur J Immunol,* 38**,** 1071-81.

GUENAT, D., HERMETET, F., PRETET, J. L. & MOUGIN, C. 2017. Exosomes and Other Extracellular Vesicles in HPV Transmission and Carcinogenesis. *Viruses,* 9.

GUERFALI, F. Z., LAOUINI, D., GUIZANI-TABBANE, L., OTTONES, F., BEN-AISSA, K., BENKAHLA, A., MANCHON, L., PIQUEMAL, D., SMANDI, S., MGHIRBI, O., COMMES, T., MARTI, J. & DELLAGI, K. 2008. Simultaneous gene expression profiling in human macrophages infected with Leishmania major parasites using SAGE. *BMC Genomics,* 9**,** 238.

GULL, K. 1999. The cytoskeleton of trypanosomatid parasites. *Annu Rev Microbiol,* 53**,** 629-55.

GUPTA, G., BHATTACHARJEE, S., BHATTACHARYYA, S., BHATTACHARYA, P., ADHIKARI, A., MUKHERJEE, A., BHATTACHARYYA MAJUMDAR, S. & MAJUMDAR, S. 2009. CXC chemokine-mediated protection against visceral leishmaniasis: involvement of the proinflammatory response. *J Infect Dis,* 200**,** 1300-10.

GUPTA, G., MAJUMDAR, S., ADHIKARI, A., BHATTACHARYA, P., MUKHERJEE, A. K., MAJUMDAR, S. B. & MAJUMDAR, S. 2011. Treatment with IP-10 induces host-protective immune response by regulating the T regulatory cell functioning in Leishmania donovani-infected mice. *Med Microbiol Immunol,* 200**,** 241-53.

HALLE, M., GOMEZ, M. A., STUIBLE, M., SHIMIZU, H., MCMASTER, W. R., OLIVIER, M. & TREMBLAY, M. L. 2009. The Leishmania surface protease GP63 cleaves multiple intracellular proteins and actively participates in p38 mitogen-activated protein kinase inactivation. *J Biol Chem,* 284**,** 6893-908.

HALLIDAY, A., BATES, P. A., CHANCE, M. L. & TAYLOR, M. J. 2016. Toll-like receptor 2 (TLR2) plays a role in controlling cutaneous leishmaniasis in vivo, but does not require activation by parasite lipophosphoglycan. *Parasit Vectors,* 9**,** 532.

HANSELL, C. A., SIMPSON, C. V. & NIBBS, R. J. 2006. Chemokine sequestration by atypical chemokine receptors. *Biochem Soc Trans,* 34**,** 1009-13.

HANSON, P. I. & CASHIKAR, A. 2012. Multivesicular body morphogenesis. *Annu Rev Cell Dev Biol,* 28**,** 337-62.

HASSANI, K., ANTONIAK, E., JARDIM, A. & OLIVIER, M. 2011. Temperature-induced protein secretion by Leishmania mexicana modulates macrophage signalling and function. *PLoS One,* 6**,** e18724.

HASSANI, K., SHIO, M. T., MARTEL, C., FAUBERT, D. & OLIVIER, M. 2014. Absence of metalloprotease GP63 alters the protein content of Leishmania exosomes. *PLoS One,* 9**,** e95007.

HAUSSECKER, D., HUANG, Y., LAU, A., PARAMESWARAN, P., FIRE, A. Z. & KAY, M. A. 2010. Human tRNA-derived small RNAs in the global regulation of RNA silencing. *RNA,* 16**,** 673-95.

HEINZEL, F. P., SADICK, M. D., HOLADAY, B. J., COFFMAN, R. L. & LOCKSLEY, R. M. 1989. Reciprocal expression of interferon gamma or interleukin 4 during the resolution or progression of murine leishmaniasis. Evidence for expansion of distinct helper T cell subsets. *J Exp Med,* 169**,** 59-72.

HEMLER, M. E. 2008. Targeting of tetraspanin proteins--potential benefits and strategies. *Nat Rev Drug Discov,* 7**,** 747-58.
HENTZER, B. & KOBAYASI, T. 1977. The ultrastructural changes of Leishmania tropica after treatment with pentamidine. *Ann Trop Med Parasitol,* 71**,** 157-66.
HIDALGO-GRASS, C., MISHALIAN, I., DAN-GOOR, M., BELOTSERKOVSKY, I., ERAN, Y., NIZET, V., PELED, A. & HANSKI, E. 2006. A streptococcal protease that degrades CXC chemokines and impairs bacterial clearance from infected tissues. *EMBO J,* 25**,** 4628-37.
HOFFMANN, E., DITTRICH-BREIHOLZ, O., HOLTMANN, H. & KRACHT, M. 2002. Multiple control of interleukin-8 gene expression. *J Leukoc Biol,* 72**,** 847-55.
HSU, K. S., CHUANG, J. Z. & SUNG, C. H. 2017. The Biology of Ciliary Dynamics. *Cold Spring Harb Perspect Biol,* 9.
HUBEL, A., KROBITSCH, S., HORAUF, A. & CLOS, J. 1997. Leishmania major Hsp100 is required chiefly in the mammalian stage of the parasite. *Mol Cell Biol,* 17**,** 5987-95.
HUEBNER, A. R., SOMPARN, P., BENJACHAT, T., LEELAHAVANICHKUL, A., AVIHINGSANON, Y., FENTON, R. A. & PISITKUN, T. 2015. Exosomes in urine biomarker discovery. *Adv Exp Med Biol,* 845**,** 43-58.
HURLEY, J. H. 2015. ESCRTs are everywhere. *EMBO J,* 34**,** 2398-407.
IBRAIM, I. C., DE ASSIS, R. R., PESSOA, N. L., CAMPOS, M. A., MELO, M. N., TURCO, S. J. & SOARES, R. P. 2013. Two biochemically distinct lipophosphoglycans from Leishmania braziliensis and Leishmania infantum trigger different innate immune responses in murine macrophages. *Parasit Vectors,* 6**,** 54.
IHARA, T., YAMAMOTO, T., SUGAMATA, M., OKUMURA, H. & UENO, Y. 1998. The process of ultrastructural changes from nuclei to apoptotic body. *Virchows Arch,* 433**,** 443-7.
ILG, T. 2000. Lipophosphoglycan is not required for infection of macrophages or mice by Leishmania mexicana. *Embo j,* 19**,** 1953-62.
ILG, T. 2001. Lipophosphoglycan of the protozoan parasite Leishmania: stage- and species-specific importance for colonization of the sandfly vector, transmission and virulence to mammals. *Med Microbiol Immunol,* 190**,** 13-7.
ILG, T., DEMAR, M. & HARBECKE, D. 2001. Phosphoglycan repeat-deficient Leishmania mexicana parasites remain infectious to macrophages and mice. *J Biol Chem,* 276**,** 4988-97.
ILG, T., ETGES, R., OVERATH, P., MCCONVILLE, M. J., THOMAS-OATES, J., THOMAS, J., HOMANS, S. W. & FERGUSON, M. A. 1992. Structure of Leishmania mexicana lipophosphoglycan. *J Biol Chem,* 267**,** 6834-40.
ILG, T., HARBECKE, D., WIESE, M. & OVERATH, P. 1993. Monoclonal antibodies directed against Leishmania secreted acid phosphatase and lipophosphoglycan. Partial characterization of private and public epitopes. *Eur J Biochem,* 217**,** 603-15.
ILG, T., STIERHOF, Y. D., ETGES, R., ADRIAN, M., HARBECKE, D. & OVERATH, P. 1991. Secreted acid phosphatase of Leishmania mexicana: a filamentous phosphoglycoprotein polymer. *Proc Natl Acad Sci U S A,* 88**,** 8774-8.
ILG, T., STIERHOF, Y. D., WIESE, M., MCCONVILLE, M. J. & OVERATH, P. 1994. Characterization of phosphoglycan-containing secretory products of Leishmania. *Parasitology,* 108 Suppl**,** S63-71.
ISMAIL, S. A., CHEN, Y. X., MIERTZSCHKE, M., VETTER, I. R., KOERNER, C. & WITTINGHOFER, A. 2012. Structural basis for Arl3-specific release of myristoylated ciliary cargo from UNC119. *EMBO J,* 31**,** 4085-94.
JACQUIER, A. 2009. The complex eukaryotic transcriptome: unexpected pervasive transcription and novel small RNAs. *Nat Rev Genet,* 10**,** 833-44.
JELERCIC, U. & GOV, N. S. 2015. Pearling instability of membrane tubes driven by curved proteins and actin polymerization. *Phys Biol,* 12**,** 066022.

JULIER, Z., MARTINO, M. M., DE TITTA, A., JEANBART, L. & HUBBELL, J. A. 2015. The TLR4 agonist fibronectin extra domain A is cryptic, exposed by elastase-2; use in a fibrin matrix cancer vaccine. *Sci Rep,* 5**,** 8569.

JUNDI, K. & GREENE, C. M. 2015. Transcription of Interleukin-8: How Altered Regulation Can Affect Cystic Fibrosis Lung Disease. *Biomolecules,* 5**,** 1386-98.

JUNGHAE, M. & RAYNES, J. G. 2002. Activation of p38 mitogen-activated protein kinase attenuates Leishmania donovani infection in macrophages. *Infect Immun,* 70**,** 5026-35.

KAMAU, S. W., GRIMM, F. & HEHL, A. B. 2001. Expression of green fluorescent protein as a marker for effects of antileishmanial compounds in vitro. *Antimicrob Agents Chemother,* 45**,** 3654-6.

KANAYAMA, M., INOUE, M., DANZAKI, K., HAMMER, G., HE, Y. W. & SHINOHARA, M. L. 2015. Autophagy enhances NFkappaB activity in specific tissue macrophages by sequestering A20 to boost antifungal immunity. *Nat Commun,* 6**,** 5779.

KANESHIRO, E. S., JAYASIMHULU, K. & LESTER, R. L. 1986. Characterization of inositol lipids from Leishmania donovani promastigotes: identification of an inositol sphingophospholipid. *J Lipid Res,* 27**,** 1294-303.

KASSI, M., KASSI, M., AFGHAN, A. K., REHMAN, R. & KASI, P. M. 2008. Marring leishmaniasis: the stigmatization and the impact of cutaneous leishmaniasis in Pakistan and Afghanistan. *PLoS Negl Trop Dis,* 2**,** e259.

KELSO, A. 1998. Cytokines: principles and prospects. *Immunol Cell Biol,* 76**,** 300-17.

KEVRIC, I., CAPPEL, M. A. & KEELING, J. H. 2015. New World and Old World Leishmania Infections: A Practical Review. *Dermatol Clin,* 33**,** 579-93.

KIBBE, W. A. 2007. OligoCalc: an online oligonucleotide properties calculator. *Nucleic Acids Res,* 35**,** W43-6.

KIEFFER, C., SKALICKY, J. J., MORITA, E., DE DOMENICO, I., WARD, D. M., KAPLAN, J. & SUNDQUIST, W. I. 2008. Two distinct modes of ESCRT-III recognition are required for VPS4 functions in lysosomal protein targeting and HIV-1 budding. *Dev Cell,* 15**,** 62-73.

KIM, D. K., LEE, J., KIM, S. R., CHOI, D. S., YOON, Y. J., KIM, J. H., GO, G., NHUNG, D., HONG, K., JANG, S. C., KIM, S. H., PARK, K. S., KIM, O. Y., PARK, H. T., SEO, J. H., AIKAWA, E., BAJ-KRZYWORZEKA, M., VAN BALKOM, B. W., BELTING, M., BLANC, L., BOND, V., BONGIOVANNI, A., BORRAS, F. E., BUEE, L., BUZAS, E. I., CHENG, L., CLAYTON, A., COCUCCI, E., DELA CRUZ, C. S., DESIDERIO, D. M., DI VIZIO, D., EKSTROM, K., FALCON-PEREZ, J. M., GARDINER, C., GIEBEL, B., GREENING, D. W., GROSS, J. C., GUPTA, D., HENDRIX, A., HILL, A. F., HILL, M. M., NOLTE-'T HOEN, E., HWANG, D. W., INAL, J., JAGANNADHAM, M. V., JAYACHANDRAN, M., JEE, Y. K., JORGENSEN, M., KIM, K. P., KIM, Y. K., KISLINGER, T., LASSER, C., LEE, D. S., LEE, H., VAN LEEUWEN, J., LENER, T., LIU, M. L., LOTVALL, J., MARCILLA, A., MATHIVANAN, S., MOLLER, A., MORHAYIM, J., MULLIER, F., NAZARENKO, I., NIEUWLAND, R., NUNES, D. N., PANG, K., PARK, J., PATEL, T., POCSFALVI, G., DEL PORTILLO, H., PUTZ, U., RAMIREZ, M. I., RODRIGUES, M. L., ROH, T. Y., ROYO, F., SAHOO, S., SCHIFFELERS, R., SHARMA, S., SILJANDER, P., SIMPSON, R. J., SOEKMADJI, C., STAHL, P., STENSBALLE, A., STEPIEN, E., TAHARA, H., TRUMMER, A., VALADI, H., VELLA, L. J., WAI, S. N., WITWER, K., YANEZ-MO, M., YOUN, H., ZEIDLER, R. & GHO, Y. S. 2014. EVpedia: a community web portal for extracellular vesicles research. *Bioinformatics*.

KING, D. L., CHANG, Y. D. & TURCO, S. J. 1987. Cell surface lipophosphoglycan of Leishmania donovani. *Mol Biochem Parasitol,* 24**,** 47-53.

KLOEHN, J., SAUNDERS, E. C., O'CALLAGHAN, S., DAGLEY, M. J. & MCCONVILLE, M. J. 2015. Characterization of metabolically quiescent

Leishmania parasites in murine lesions using heavy water labeling. *PLoS Pathog,* 11**,** e1004683.
KOPF, M., BROMBACHER, F., KOHLER, G., KIENZLE, G., WIDMANN, K. H., LEFRANG, K., HUMBORG, C., LEDERMANN, B. & SOLBACH, W. 1996. IL-4-deficient Balb/c mice resist infection with Leishmania major. *J Exp Med,* 184**,** 1127-36.
KOWAL, J., ARRAS, G., COLOMBO, M., JOUVE, M., MORATH, J. P., PRIMDAL-BENGTSON, B., DINGLI, F., LOEW, D., TKACH, M. & THERY, C. 2016. Proteomic comparison defines novel markers to characterize heterogeneous populations of extracellular vesicle subtypes. *Proc Natl Acad Sci U S A,* 113**,** E968-77.
KREIMER, S., BELOV, A. M., GHIRAN, I., MURTHY, S. K., FRANK, D. A. & IVANOV, A. R. 2015. Mass-spectrometry-based molecular characterization of extracellular vesicles: lipidomics and proteomics. *J Proteome Res,* 14**,** 2367-84.
KROPF, P., FREUDENBERG, M. A., MODOLELL, M., PRICE, H. P., HERATH, S., ANTONIAZI, S., GALANOS, C., SMITH, D. F. & MULLER, I. 2004. Toll-like receptor 4 contributes to efficient control of infection with the protozoan parasite Leishmania major. *Infect Immun,* 72**,** 1920-8.
KUHN, D. & WIESE, M. 2005. LmxPK4, a mitogen-activated protein kinase kinase homologue of Leishmania mexicana with a potential role in parasite differentiation. *Mol Microbiol,* 56**,** 1169-82.
LACY, P. & STOW, J. L. 2011. Cytokine release from innate immune cells: association with diverse membrane trafficking pathways. *Blood,* 118**,** 9-18.
LAMBERTZ, U., OVIEDO OVANDO, M. E., VASCONCELOS, E., UNRAU, P. J., MYLER, P. J. & REINER, N. E. 2015. Small RNAs derived from tRNAs and rRNAs are highly enriched in exosomes from both old and new world Leishmania providing evidence for conserved exosomal RNA Packaging. *BMC Genomics.*
LANDFEAR, S. M., TRAN, K. D. & SANCHEZ, M. A. 2015. Flagellar membrane proteins in kinetoplastid parasites. *IUBMB Life,* 67**,** 668-76.
LAPARA, N. J., 3RD & KELLY, B. L. 2010. Suppression of LPS-induced inflammatory responses in macrophages infected with Leishmania. *J Inflamm (Lond),* 7**,** 8.
LARRETA, R., SOTO, M., QUIJADA, L., FOLGUEIRA, C., ABANADES, D. R., ALONSO, C. & REQUENA, J. M. 2004. The expression of HSP83 genes in Leishmania infantum is affected by temperature and by stage-differentiation and is regulated at the levels of mRNA stability and translation. *BMC Mol Biol,* 5**,** 3.
LAWRENCE, T. & NATOLI, G. 2011. Transcriptional regulation of macrophage polarization: enabling diversity with identity. *Nat Rev Immunol,* 11**,** 750-61.
LAWSON, C., KOVACS, D., FINDING, E., ULFELDER, E. & LUIS-FUENTES, V. 2017. Extracellular Vesicles: Evolutionarily Conserved Mediators of Intercellular Communication. *Yale J Biol Med,* 90**,** 481-491.
LEE, Y. S., PRESSMAN, S., ANDRESS, A. P., KIM, K., WHITE, J. L., CASSIDY, J. J., LI, X., LUBELL, K., LIM, D. H., CHO, I. S., NAKAHARA, K., PREALL, J. B., BELLARE, P., SONTHEIMER, E. J. & CARTHEW, R. W. 2009. Silencing by small RNAs is linked to endosomal trafficking. *Nat Cell Biol,* 11**,** 1150-6.
LEFEBVRE, F. A. & LECUYER, E. 2017. Small Luggage for a Long Journey: Transfer of Vesicle-Enclosed Small RNA in Interspecies Communication. *Front Microbiol,* 8**,** 377.
LEFEBVRE, P. A., NORDSTROM, S. A., MOULDER, J. E. & ROSENBAUM, J. L. 1978. Flagellar elongation and shortening in Chlamydomonas. IV. Effects of flagellar detachment, regeneration, and resorption on the induction of flagellar protein synthesis. *J Cell Biol,* 78**,** 8-27.

LEHMANN, J., ENSSLE, K. H., LEHMANN, I., EMMENDORFER, A. & LOHMANN-MATTHES, M. L. 2000. The capacity to produce IFN-gamma rather than the presence of interleukin-4 determines the resistance and the degree of susceptibility to Leishmania donovani infection in mice. *J Interferon Cytokine Res,* 20**,** 63-77.

LEMAIRE, J., MKANNEZ, G., GUERFALI, F. Z., GUSTIN, C., ATTIA, H., SGHAIER, R. M., DELLAGI, K., LAOUINI, D. & RENARD, P. 2013. MicroRNA expression profile in human macrophages in response to Leishmania major infection. *PLoS Negl Trop Dis,* 7**,** e2478.

LEUNG, K. F., DACKS, J. B. & FIELD, M. C. 2008. Evolution of the multivesicular body ESCRT machinery; retention across the eukaryotic lineage. *Traffic,* 9**,** 1698-716.

LI, M., ZERINGER, E., BARTA, T., SCHAGEMAN, J., CHENG, A. & VLASSOV, A. V. 2014. Analysis of the RNA content of the exosomes derived from blood serum and urine and its potential as biomarkers. *Philos Trans R Soc Lond B Biol Sci,* 369.

LIEU, Z. Z., LOCK, J. G., HAMMOND, L. A., LA GRUTA, N. L., STOW, J. L. & GLEESON, P. A. 2008. A trans-Golgi network golgin is required for the regulated secretion of TNF in activated macrophages in vivo. *Proc Natl Acad Sci U S A,* 105**,** 3351-6.

LIMA, B. S., DANTAS-TORRES, F., DE CARVALHO, M. R., MARINHO-JUNIOR, J. F., DE ALMEIDA, E. L., BRITO, M. E., GOMES, F. & BRANDAO-FILHO, S. P. 2013. Small mammals as hosts of Leishmania spp. in a highly endemic area for zoonotic leishmaniasis in North-Eastern Brazil. *Trans R Soc Trop Med Hyg,* 107**,** 592-7.

LIN, Y., KIMPLER, L. A., NAISMITH, T. V., LAUER, J. M. & HANSON, P. I. 2005. Interaction of the mammalian endosomal sorting complex required for transport (ESCRT) III protein hSnf7-1 with itself, membranes, and the AAA+ ATPase SKD1. *J Biol Chem,* 280**,** 12799-809.

LIU, J. & ZHANG, W. 2012. *Nanoparticle size measurement by nanoparticle tracking analysis (NTA) method* [Online]. Available: http://www.imeko.org/publications/wc-2012/IMEKO-WC-2012-SS2-P3.pdf.

LIVSHITS, M. A., KHOMYAKOVA, E., EVTUSHENKO, E. G., LAZAREV, V. N., KULEMIN, N. A., SEMINA, S. E., GENEROZOV, E. V. & GOVORUN, V. M. 2015. Isolation of exosomes by differential centrifugation: Theoretical analysis of a commonly used protocol. *Sci Rep,* 5**,** 17319.

LO, S. K., BOVIS, L., MATURA, R., ZHU, B., HE, S., LUM, H., TURCO, S. J. & HO, J. L. 1998. Leishmania lipophosphoglycan reduces monocyte transendothelial migration: modulation of cell adhesion molecules, intercellular junctional proteins, and chemoattractants. *J Immunol,* 160**,** 1857-65.

LODGE, R. & DESCOTEAUX, A. 2005. Modulation of phagolysosome biogenesis by the lipophosphoglycan of Leishmania. *Clin Immunol,* 114**,** 256-65.

LONG, H., ZHANG, F., XU, N., LIU, G., DIENER, D. R., ROSENBAUM, J. L. & HUANG, K. 2016. Comparative Analysis of Ciliary Membranes and Ectosomes. *Curr Biol*.

LYE, L. F., OWENS, K., SHI, H., MURTA, S. M., VIEIRA, A. C., TURCO, S. J., TSCHUDI, C., ULLU, E. & BEVERLEY, S. M. 2010. Retention and loss of RNA interference pathways in trypanosomatid protozoans. *PLoS Pathog,* 6**,** e1001161.

MA, W., LIM, W., GEE, K., AUCOIN, S., NANDAN, D., KOZLOWSKI, M., DIAZ-MITOMA, F. & KUMAR, A. 2001. The p38 mitogen-activated kinase pathway regulates the human interleukin-10 promoter via the activation of Sp1 transcription factor in lipopolysaccharide-stimulated human macrophages. *J Biol Chem,* 276**,** 13664-74.

MAKIN, L. & GLUENZ, E. 2015. cAMP signalling in trypanosomatids: role in pathogenesis and as a drug target. *Trends Parasitol,* 31**,** 373-9.
MALVERN. 2015. *NTA : Nanoparticle Tracking Analysis* [Online]. Available: http://www.sysmex.nl/fileadmin/media/f102/MLS/Academy_docs/Malvern_NTA_Nanosight_presentation.pdf.
MANGONI, M. L., SAUGAR, J. M., DELLISANTI, M., BARRA, D., SIMMACO, M. & RIVAS, L. 2005. Temporins, small antimicrobial peptides with leishmanicidal activity. *J Biol Chem,* 280**,** 984-90.
MANTEL, P. Y., HOANG, A. N., GOLDOWITZ, I., POTASHNIKOVA, D., HAMZA, B., VOROBJEV, I., GHIRAN, I., TONER, M., IRIMIA, D., IVANOV, A. R., BARTENEVA, N. & MARTI, M. 2013. Malaria-infected erythrocyte-derived microvesicles mediate cellular communication within the parasite population and with the host immune system. *Cell Host Microbe,* 13**,** 521-34.
MARR, A. K., MACISAAC, J. L., JIANG, R., AIRO, A. M., KOBOR, M. S. & MCMASTER, W. R. 2014. Leishmania donovani Infection Causes Distinct Epigenetic DNA Methylation Changes in Host Macrophages. *PLoS Pathog,* 10**,** e1004419.
MARTI, M. & JOHNSON, P. J. 2016. Emerging roles for extracellular vesicles in parasitic infections. *Curr Opin Microbiol,* 32**,** 66-70.
MARTIN-URDIROZ, M., DEEKS, M. J., HORTON, C. G., DAWE, H. R. & JOURDAIN, I. 2016. The Exocyst Complex in Health and Disease. *Front Cell Dev Biol,* 4**,** 24.
MARTINEZ, F. O. & GORDON, S. 2014. The M1 and M2 paradigm of macrophage activation: time for reassessment. *F1000Prime Rep,* 6**,** 13.
MASPI, N., ABDOLI, A. & GHAFFARIFAR, F. 2016. Pro- and anti-inflammatory cytokines in cutaneous leishmaniasis: a review. *Pathog Glob Health,* 110**,** 247-260.
MATHEOUD, D., MORADIN, N., BELLEMARE-PELLETIER, A., SHIO, M. T., HONG, W. J., OLIVIER, M., GAGNON, E., DESJARDINS, M. & DESCOTEAUX, A. 2013. Leishmania evades host immunity by inhibiting antigen cross-presentation through direct cleavage of the SNARE VAMP8. *Cell Host Microbe,* 14**,** 15-25.
MATRIXSCIENCE. *Mascot Probability Based Scoring* [Online]. Available: http://www.matrixscience.com/help/scoring_help.html.
MATTE, C. & DESCOTEAUX, A. 2016. Exploitation of the Host Cell Membrane Fusion Machinery by Leishmania Is Part of the Infection Process. *PLoS Pathog,* 12**,** e1005962.
MATTE, C. & OLIVIER, M. 2002. Leishmania-induced cellular recruitment during the early inflammatory response: modulation of proinflammatory mediators. *J Infect Dis,* 185**,** 673-81.
MATTHEWS, D. J., EMSON, C. L., MCKENZIE, G. J., JOLIN, H. E., BLACKWELL, J. M. & MCKENZIE, A. N. 2000. IL-13 is a susceptibility factor for Leishmania major infection. *J Immunol,* 164**,** 1458-62.
MCMAHON-PRATT, D. & ALEXANDER, J. 2004. Does the Leishmania major paradigm of pathogenesis and protection hold for New World cutaneous leishmaniases or the visceral disease? *Immunol Rev,* 201**,** 206-24.
MEDVEDEV, A. E., KOPYDLOWSKI, K. M. & VOGEL, S. N. 2000. Inhibition of lipopolysaccharide-induced signal transduction in endotoxin-tolerized mouse macrophages: dysregulation of cytokine, chemokine, and toll-like receptor 2 and 4 gene expression. *J Immunol,* 164**,** 5564-74.
MEDZHITOV, R. & HORNG, T. 2009. Transcriptional control of the inflammatory response. *Nat Rev Immunol,* 9**,** 692-703.
MENDEZ, S., RECKLING, S. K., PICCIRILLO, C. A., SACKS, D. & BELKAID, Y. 2004. Role for CD4(+) CD25(+) regulatory T cells in reactivation of persistent leishmaniasis and control of concomitant immunity. *J Exp Med,* 200**,** 201-10.

MESTAS, J. & HUGHES, C. C. 2004. Of mice and not men: differences between mouse and human immunology. *J Immunol,* 172**,** 2731-8.
MINCIACCHI, V. R., ZIJLSTRA, A., RUBIN, M. A. & DI VIZIO, D. 2017. Extracellular vesicles for liquid biopsy in prostate cancer: where are we and where are we headed? *Prostate Cancer Prostatic Dis,* 20**,** 251-258.
MIRANDA, K. C., BOND, D. T., LEVIN, J. Z., ADICONIS, X., SIVACHENKO, A., RUSS, C., BROWN, D., NUSBAUM, C. & RUSSO, L. M. 2014. Massively parallel sequencing of human urinary exosome/microvesicle RNA reveals a predominance of non-coding RNA. *PLoS One,* 9**,** e96094.
MOAFI, M., REZVAN, H., SHERKAT, R., TALEBAN, R., ASILIAN, A., ZARKESH-ESFAHANI, S. H., NILFOROUSHZADEH, M. A., JAFFARY, F., MANSOURIAN, M., SOKHANVARI, F. & ANSARI, N. 2017. Comparison of pro-inflammatory cytokines of non-healing and healing cutaneous Leishmaniasis. *Scand J Immunol*.
MOHIT, E. & RAFATI, S. 2012. Chemokine-based immunotherapy: delivery systems and combination therapies. *Immunotherapy,* 4**,** 807-40.
MOHRS, M., HOLSCHER, C. & BROMBACHER, F. 2000. Interleukin-4 receptor alpha-deficient BALB/c mice show an unimpaired T helper 2 polarization in response to Leishmania major infection. *Infect Immun,* 68**,** 1773-80.
MOMEN-HERAVI, F., BALAJ, L., ALIAN, S., MANTEL, P. Y., HALLECK, A. E., TRACHTENBERG, A. J., SORIA, C. E., OQUIN, S., BONEBREAK, C. M., SARACOGLU, E., SKOG, J. & KUO, W. P. 2013. Current methods for the isolation of extracellular vesicles. *Biol Chem,* 394**,** 1253-62.
MONTAKHAB-YEGANEH, H., ABDOSSAMADI, Z., ZAHEDIFARD, F., TASLIMI, Y., BADIRZADEH, A., SALJOUGHIAN, N., TAHERI, T., TAGHIKHANI, M. & RAFATI, S. 2017. Leishmania tarentolae expressing CXCL-10 as an efficient immunotherapy approach against Leishmania major-infected BALB/c mice. *Parasite Immunol,* 39.
MOODY, S. F., HANDMAN, E., MCCONVILLE, M. J. & BACIC, A. 1993. The structure of Leishmania major amastigote lipophosphoglycan. *J Biol Chem,* 268**,** 18457-66.
MORADIN, N. & DESCOTEAUX, A. 2012. Leishmania promastigotes: building a safe niche within macrophages. *Front Cell Infect Microbiol,* 2**,** 121.
MOREIRA, L. O., EL KASMI, K. C., SMITH, A. M., FINKELSTEIN, D., FILLON, S., KIM, Y. G., NUNEZ, G., TUOMANEN, E. & MURRAY, P. J. 2008. The TLR2-MyD88-NOD2-RIPK2 signalling axis regulates a balanced pro-inflammatory and IL-10-mediated anti-inflammatory cytokine response to Gram-positive cell walls. *Cell Microbiol,* 10**,** 2067-77.
MOTTRAM, J. C., COOMBS, G. H. & ALEXANDER, J. 2004. Cysteine peptidases as virulence factors of Leishmania. *Curr Opin Microbiol,* 7**,** 375-81.
MUKBEL, R. M., PATTEN, C., JR., GIBSON, K., GHOSH, M., PETERSEN, C. & JONES, D. E. 2007. Macrophage killing of Leishmania amazonensis amastigotes requires both nitric oxide and superoxide. *Am J Trop Med Hyg,* 76**,** 669-75.
MULCAHY, L. A., PINK, R. C. & CARTER, D. R. 2014. Routes and mechanisms of extracellular vesicle uptake. *J Extracell Vesicles,* 3.
MULLIN, K. A., FOTH, B. J., ILGOUTZ, S. C., CALLAGHAN, J. M., ZAWADZKI, J. L., MCFADDEN, G. I. & MCCONVILLE, M. J. 2001. Regulated degradation of an endoplasmic reticulum membrane protein in a tubular lysosome in Leishmania mexicana. *Mol Biol Cell,* 12**,** 2364-77.
MURAILLE, E., DE TREZ, C., BRAIT, M., DE BAETSELIER, P., LEO, O. & CARLIER, Y. 2003. Genetically resistant mice lacking MyD88-adapter protein display a high susceptibility to Leishmania major infection associated with a polarized Th2 response. *J Immunol,* 170**,** 4237-41.

MURALIDHARAN-CHARI, V., CLANCY, J., PLOU, C., ROMAO, M., CHAVRIER, P., RAPOSO, G. & D'SOUZA-SCHOREY, C. 2009. ARF6-regulated shedding of tumor cell-derived plasma membrane microvesicles. *Curr Biol,* 19**,** 1875-85.

MURRAY, H. W., LUSTER, A. D., ZHENG, H. & MA, X. 2016. IFN-gamma-Regulated Chemokines in Leishmania donovani Infection in the Liver. *Infect Immun*.

MURRAY, H. W., ZHANG, Y., RAMAN, V. S., REED, S. G. & MA, X. 2013. Regulatory actions of Toll-like receptor 2 (TLR2) and TLR4 in Leishmania donovani infection in the liver. *Infect Immun,* 81**,** 2318-26.

MURRAY, R. Z., KAY, J. G., SANGERMANI, D. G. & STOW, J. L. 2005a. A role for the phagosome in cytokine secretion. *Science,* 310**,** 1492-5.

MURRAY, R. Z. & STOW, J. L. 2014. Cytokine Secretion in Macrophages: SNAREs, Rabs, and Membrane Trafficking. *Front Immunol,* 5**,** 538.

MURRAY, R. Z., WYLIE, F. G., KHROMYKH, T., HUME, D. A. & STOW, J. L. 2005b. Syntaxin 6 and Vti1b form a novel SNARE complex, which is up-regulated in activated macrophages to facilitate exocytosis of tumor necrosis Factor-alpha. *J Biol Chem,* 280**,** 10478-83.

NAGARSHETH, N., WICHA, M. S. & ZOU, W. 2017. Chemokines in the cancer microenvironment and their relevance in cancer immunotherapy. *Nat Rev Immunol,* 17**,** 559-572.

NAGER, A. R., GOLDSTEIN, J. S., HERRANZ-PEREZ, V., PORTRAN, D., YE, F., GARCIA-VERDUGO, J. M. & NACHURY, M. V. 2016. An Actin Network Dispatches Ciliary GPCRs into Extracellular Vesicles to Modulate Signaling. *Cell*.

NANDAN, D., YI, T., LOPEZ, M., LAI, C. & REINER, N. E. 2002. Leishmania EF-1alpha activates the Src homology 2 domain containing tyrosine phosphatase SHP-1 leading to macrophage deactivation. *J Biol Chem,* 277**,** 50190-7.

NAUMANN, U., CAMERONI, E., PRUENSTER, M., MAHABALESHWAR, H., RAZ, E., ZERWES, H. G., ROT, A. & THELEN, M. 2010. CXCR7 functions as a scavenger for CXCL12 and CXCL11. *PLoS One,* 5**,** e9175.

NAZIMEK, K., BRYNIARSKI, K., SANTOCKI, M. & PTAK, W. 2015. Exosomes as mediators of intercellular communication: clinical implications. *Pol Arch Med Wewn,* 125**,** 370-80.

NDJAMEN, B., KANG, B. H., HATSUZAWA, K. & KIMA, P. E. 2010. Leishmania parasitophorous vacuoles interact continuously with the host cell's endoplasmic reticulum; parasitophorous vacuoles are hybrid compartments. *Cell Microbiol,* 12**,** 1480-94.

NEININGER, A., KONTOYIANNIS, D., KOTLYAROV, A., WINZEN, R., ECKERT, R., VOLK, H. D., HOLTMANN, H., KOLLIAS, G. & GAESTEL, M. 2002. MK2 targets AU-rich elements and regulates biosynthesis of tumor necrosis factor and interleukin-6 independently at different post-transcriptional levels. *J Biol Chem,* 277**,** 3065-8.

NIBBS, R. J. & GRAHAM, G. J. 2013. Immune regulation by atypical chemokine receptors. *Nat Rev Immunol,* 13**,** 815-29.

NIRUJOGI, R. S., PAWAR, H., RENUSE, S., KUMAR, P., CHAVAN, S., SATHE, G., SHARMA, J., KHOBRAGADE, S., PANDE, J., MODAK, B., PRASAD, T. S., HARSHA, H. C., PATOLE, M. S. & PANDEY, A. 2014. Moving from unsequenced to sequenced genome: reanalysis of the proteome of Leishmania donovani. *J Proteomics,* 97**,** 48-61.

NOBEN-TRAUTH, N., KROPF, P. & MULLER, I. 1996. Susceptibility to Leishmania major infection in interleukin-4-deficient mice. *Science,* 271**,** 987-90.

NOGUEIRA, P. M., ASSIS, R. R., TORRECILHAS, A. C., SARAIVA, E. M., PESSOA, N. L., CAMPOS, M. A., MARIALVA, E. F., RIOS-VELASQUEZ, C. M., PESSOA, F. A., SECUNDINO, N. F., RUGANI, J. N., NIEVES, E., TURCO, S. J., MELO, M. N. & SOARES, R. P. 2016. Lipophosphoglycans from

Leishmania amazonensis Strains Display Immunomodulatory Properties via TLR4 and Do Not Affect Sand Fly Infection. *PLoS Negl Trop Dis,* 10**,** e0004848.
NOLTE-'T HOEN, E. N., BUERMANS, H. P., WAASDORP, M., STOORVOGEL, W., WAUBEN, M. H. & T HOEN, P. A. 2012. Deep sequencing of RNA from immune cell-derived vesicles uncovers the selective incorporation of small non-coding RNA biotypes with potential regulatory functions. *Nucleic Acids Res,* 40**,** 9272-85.
NOMURA, F., AKASHI, S., SAKAO, Y., SATO, S., KAWAI, T., MATSUMOTO, M., NAKANISHI, K., KIMOTO, M., MIYAKE, K., TAKEDA, K. & AKIRA, S. 2000. Cutting edge: endotoxin tolerance in mouse peritoneal macrophages correlates with down-regulation of surface toll-like receptor 4 expression. *J Immunol,* 164**,** 3476-9.
OBITA, T., SAKSENA, S., GHAZI-TABATABAI, S., GILL, D. J., PERISIC, O., EMR, S. D. & WILLIAMS, R. L. 2007. Structural basis for selective recognition of ESCRT-III by the AAA ATPase Vps4. *Nature,* 449**,** 735-9.
ODORIZZI, G. 2006. The multiple personalities of Alix. *J Cell Sci,* 119**,** 3025-32.
OKENWA, C., KUMAR, A., REGO, D., KONARSKI, Y., NILCHI, L., WRIGHT, K. & KOZLOWSKI, M. 2013. SHP-1-Pyk2-Src protein complex and p38 MAPK pathways independently regulate IL-10 production in lipopolysaccharide-stimulated macrophages. *J Immunol,* 191**,** 2589-603.
OPAT, A., NG, K., CURRIE, G., HANDMAN, E. & BACIC, A. 1996. Characterization of lipophosphoglycan from a ricin-resistant mutant of Leishmania major. *Glycobiology,* 6**,** 387-97.
OVALLE-BRACHO, C., FRANCO-MUNOZ, C., LONDONO-BARBOSA, D., RESTREPO-MONTOYA, D. & CLAVIJO-RAMIREZ, C. 2015. Changes in Macrophage Gene Expression Associated with Leishmania (Viannia) braziliensis Infection. *PLoS One,* 10**,** e0128934.
OVERATH, P., STIERHOF, Y. D. & WIESE, M. 1997. Endocytosis and secretion in trypanosomatid parasites - Tumultuous traffic in a pocket. *Trends Cell Biol,* 7**,** 27-33.
PAGAN, J. K., WYLIE, F. G., JOSEPH, S., WIDBERG, C., BRYANT, N. J., JAMES, D. E. & STOW, J. L. 2003. The t-SNARE syntaxin 4 is regulated during macrophage activation to function in membrane traffic and cytokine secretion. *Curr Biol,* 13**,** 156-60.
PAGGETTI, J., HADERK, F., SEIFFERT, M., JANJI, B., DISTLER, U., AMMERLAAN, W., KIM, Y. J., ADAM, J., LICHTER, P., SOLARY, E., BERCHEM, G. & MOUSSAY, E. 2015. Exosomes released by chronic lymphocytic leukemia cells induce the transition of stromal cells into cancer-associated fibroblasts. *Blood,* 126**,** 1106-17.
PAINDAVOINE, P., ROLIN, S., VAN ASSEL, S., GEUSKENS, M., JAUNIAUX, J. C., DINSART, C., HUET, G. & PAYS, E. 1992. A gene from the variant surface glycoprotein expression site encodes one of several transmembrane adenylate cyclases located on the flagellum of Trypanosoma brucei. *Mol Cell Biol,* 12**,** 1218-25.
PALADE, G. E. 1955. A small particulate component of the cytoplasm. *J Biophys Biochem Cytol,* 1**,** 59-68.
PAN, J. & SNELL, W. 2007. The primary cilium: keeper of the key to cell division. *Cell,* 129**,** 1255-7.
PANARO, M. A., BRANDONISIO, O., SISTO, M., ACQUAFREDDA, A., LEOGRANDE, D., FUMAROLA, L. & MITOLO, V. 2001. Nitric oxide production by Leishmania-infected macrophages and modulation by prostaglandin E2. *Clin Exp Med,* 1**,** 137-43.
PANEPINTO, J., KOMPERDA, K., FRASES, S., PARK, Y. D., DJORDJEVIC, J. T., CASADEVALL, A. & WILLIAMSON, P. R. 2009. Sec6-dependent sorting of

fungal extracellular exosomes and laccase of Cryptococcus neoformans. *Mol Microbiol,* 71**,** 1165-76.

PASSERO, L. F., ASSIS, R. R., DA SILVA, T. N., NOGUEIRA, P. M., MACEDO, D. H., PESSOA, N. L., CAMPOS, M. A., LAURENTI, M. D. & SOARES, R. P. 2015. Differential modulation of macrophage response elicited by glycoinositolphospholipids and lipophosphoglycan from Leishmania (Viannia) shawi. *Parasitol Int,* 64**,** 32-5.

PEROVAL, M. Y., BOYD, A. C., YOUNG, J. R. & SMITH, A. L. 2013. A critical role for MAPK signalling pathways in the transcriptional regulation of toll like receptors. *PLoS One,* 8**,** e51243.

PETERS, N. C., EGEN, J. G., SECUNDINO, N., DEBRABANT, A., KIMBLIN, N., KAMHAWI, S., LAWYER, P., FAY, M. P., GERMAIN, R. N. & SACKS, D. 2008. In vivo imaging reveals an essential role for neutrophils in leishmaniasis transmitted by sand flies. *Science,* 321**,** 970-4.

PIPER, R. C. & LEHNER, P. J. 2011. Endosomal transport via ubiquitination. *Trends Cell Biol,* 21**,** 647-55.

POSTBERG, J., FORCOB, S., CHANG, W. J. & LIPPS, H. J. 2010. The evolutionary history of histone H3 suggests a deep eukaryotic root of chromatin modifying mechanisms. *BMC Evol Biol,* 10**,** 259.

POTEMPA, J. & PIKE, R. N. 2009. Corruption of innate immunity by bacterial proteases. *J Innate Immun,* 1**,** 70-87.

PRIVE, C. & DESCOTEAUX, A. 2000. Leishmania donovani promastigotes evade the activation of mitogen-activated protein kinases p38, c-Jun N-terminal kinase, and extracellular signal-regulated kinase-1/2 during infection of naive macrophages. *Eur J Immunol,* 30**,** 2235-44.

PUGACHEVA, E. N., JABLONSKI, S. A., HARTMAN, T. R., HENSKE, E. P. & GOLEMIS, E. A. 2007. HEF1-dependent Aurora A activation induces disassembly of the primary cilium. *Cell,* 129**,** 1351-63.

QI, J., QIAO, Y., WANG, P., LI, S., ZHAO, W. & GAO, C. 2012. microRNA-210 negatively regulates LPS-induced production of proinflammatory cytokines by targeting NF-kappaB1 in murine macrophages. *FEBS Lett,* 586**,** 1201-7.

QUADER, H., CHERNIACK, J. & FILNER, P. 1978. Participation of calcium in flagellar shortening and regeneration in Chlamydomonas reinhardii. *Exp Cell Res,* 113**,** 295-301.

RAI, A. K., THAKUR, C. P., SINGH, A., SETH, T., SRIVASTAVA, S. K., SINGH, P. & MITRA, D. K. 2012. Regulatory T cells suppress T cell activation at the pathologic site of human visceral leishmaniasis. *PLoS One,* 7**,** e31551.

RAIBORG, C. & STENMARK, H. 2009. The ESCRT machinery in endosomal sorting of ubiquitylated membrane proteins. *Nature,* 458**,** 445-52.

RAMACHANDRAN, S. & PALANISAMY, V. 2012. Horizontal transfer of RNAs: exosomes as mediators of intercellular communication. *Wiley Interdiscip Rev RNA,* 3**,** 286-93.

RAN, J., YANG, Y., LI, D., LIU, M. & ZHOU, J. 2015. Deacetylation of alpha-tubulin and cortactin is required for HDAC6 to trigger ciliary disassembly. *Sci Rep,* 5**,** 12917.

RAPOSO, G. & STOORVOGEL, W. 2013. Extracellular vesicles: exosomes, microvesicles, and friends. *J Cell Biol,* 200**,** 373-83.

RASI, M. Q., PARKER, J. D., FELDMAN, J. L., MARSHALL, W. F. & QUARMBY, L. M. 2009. Katanin knockdown supports a role for microtubule severing in release of basal bodies before mitosis in Chlamydomonas. *Mol Biol Cell,* 20**,** 379-88.

REAL, F., FLORENTINO, P. T., REIS, L. C., RAMOS-SANCHEZ, E. M., VERAS, P. S., GOTO, H. & MORTARA, R. A. 2014. Cell-to-cell transfer of Leishmania amazonensis amastigotes is mediated by immunomodulatory LAMP-rich parasitophorous extrusions. *Cell Microbiol,* 16**,** 1549-64.

REYNOLDS, G. & HANIFFA, M. 2015. Human and Mouse Mononuclear Phagocyte Networks: A Tale of Two Species? *Front Immunol,* 6**,** 330.
RICOTE, M., LI, A. C., WILLSON, T. M., KELLY, C. J. & GLASS, C. K. 1998. The peroxisome proliferator-activated receptor-gamma is a negative regulator of macrophage activation. *Nature,* 391**,** 79-82.
ROBBINS, P. D. & MORELLI, A. E. 2014. Regulation of immune responses by extracellular vesicles. *Nat Rev Immunol,* 14**,** 195-208.
RODRIGUEZ-CONTRERAS, D., ASLAN, H., FENG, X., TRAN, K., YATES, P. A., KAMHAWI, S. & LANDFEAR, S. M. 2015. Regulation and biological function of a flagellar glucose transporter in Leishmania mexicana: a potential glucose sensor. *FASEB J,* 29**,** 11-24.
RODRIGUEZ-SOSA, M., MONTEFORTE, G. M. & SATOSKAR, A. R. 2001. Susceptibility to Leishmania mexicana infection is due to the inability to produce IL-12 rather than lack of IL-12 responsiveness. *Immunol Cell Biol,* 79**,** 320-2.
RODRIGUEZ, G. M. & PRADOS-ROSALES, R. 2016. Functions and importance of mycobacterial extracellular vesicles. *Appl Microbiol Biotechnol,* 100**,** 3887-92.
ROGERS, K. A. & TITUS, R. G. 2004. The human cytokine response to Leishmania major early after exposure to the parasite in vitro. *J Parasitol,* 90**,** 557-63.
ROGERS, K. K., WILSON, P. D., SNYDER, R. W., ZHANG, X., GUO, W., BURROW, C. R. & LIPSCHUTZ, J. H. 2004. The exocyst localizes to the primary cilium in MDCK cells. *Biochem Biophys Res Commun,* 319**,** 138-43.
ROGERS, M. E., CHANCE, M. L. & BATES, P. A. 2002. The role of promastigote secretory gel in the origin and transmission of the infective stage of Leishmania mexicana by the sandfly Lutzomyia longipalpis. *Parasitology,* 124**,** 495-507.
ROJAS-BERNABE, A., GARCIA-HERNANDEZ, O., MALDONADO-BERNAL, C., DELEGADO-DOMINGUEZ, J., ORTEGA, E., GUTIERREZ-KOBEH, L., BECKER, I. & AGUIRRE-GARCIA, M. 2014. Leishmania mexicana lipophosphoglycan activates ERK and p38 MAP kinase and induces production of proinflammatory cytokines in human macrophages through TLR2 and TLR4. *Parasitology,* 141**,** 788-800.
ROMER, W., PONTANI, L. L., SORRE, B., RENTERO, C., BERLAND, L., CHAMBON, V., LAMAZE, C., BASSEREAU, P., SYKES, C., GAUS, K. & JOHANNES, L. 2010. Actin dynamics drive membrane reorganization and scission in clathrin-independent endocytosis. *Cell,* 140**,** 540-53.
ROQUE, A. L. & JANSEN, A. M. 2014. Wild and synanthropic reservoirs of Leishmania species in the Americas. *Int J Parasitol Parasites Wildl,* 3**,** 251-62.
ROSSOL, M., HEINE, H., MEUSCH, U., QUANDT, D., KLEIN, C., SWEET, M. J. & HAUSCHILDT, S. 2011. LPS-induced cytokine production in human monocytes and macrophages. *Crit Rev Immunol,* 31**,** 379-446.
RUSSELL, D. G. 1987. The macrophage-attachment glycoprotein gp63 is the predominant C3-acceptor site on Leishmania mexicana promastigotes. *Eur J Biochem,* 164**,** 213-21.
RUSSELL, D. G. & WILHELM, H. 1986. The involvement of the major surface glycoprotein (gp63) of Leishmania promastigotes in attachment to macrophages. *J Immunol,* 136**,** 2613-20.
SACKS, D. L., HIENY, S. & SHER, A. 1985. Identification of cell surface carbohydrate and antigenic changes between noninfective and infective developmental stages of Leishmania major promastigotes. *J Immunol,* 135**,** 564-9.
SACKS, D. L., MODI, G., ROWTON, E., SPATH, G., EPSTEIN, L., TURCO, S. J. & BEVERLEY, S. M. 2000. The role of phosphoglycans in Leishmania-sand fly interactions. *Proc Natl Acad Sci U S A,* 97**,** 406-11.
SACKS, D. L., PIMENTA, P. F., MCCONVILLE, M. J., SCHNEIDER, P. & TURCO, S. J. 1995. Stage-specific binding of Leishmania donovani to the sand fly vector

midgut is regulated by conformational changes in the abundant surface lipophosphoglycan. *J Exp Med,* 181**,** 685-97.

SAHA, S., MONDAL, S., RAVINDRAN, R., BHOWMICK, S., MODAK, D., MALLICK, S., RAHMAN, M., KAR, S., GOSWAMI, R., GUHA, S. K., PRAMANIK, N., SAHA, B. & ALI, N. 2007. IL-10- and TGF-beta-mediated susceptibility in kala-azar and post-kala-azar dermal leishmaniasis: the significance of amphotericin B in the control of Leishmania donovani infection in India. *J Immunol,* 179**,** 5592-603.

SAHASRABUDDHE, A. A., BAJPAI, V. K. & GUPTA, C. M. 2004. A novel form of actin in Leishmania: molecular characterisation, subcellular localisation and association with subpellicular microtubules. *Mol Biochem Parasitol,* 134**,** 105-14.

SAHIN, A., ESPIAU, B., TETAUD, E., CUVILLIER, A., LARTIGUE, L., AMBIT, A., ROBINSON, D. R. & MERLIN, G. 2008. The leishmania ARL-1 and Golgi traffic. *PLoS One,* 3**,** e1620.

SAITO, M., OTSU, W., HSU, K. S., CHUANG, J. Z., YANAGISAWA, T., SHIEH, V., KAITSUKA, T., WEI, F. Y., TOMIZAWA, K. & SUNG, C. H. 2017. Tctex-1 controls ciliary resorption by regulating branched actin polymerization and endocytosis. *EMBO Rep*.

SALHI, A., RODRIGUES, V., JR., SANTORO, F., DESSEIN, H., ROMANO, A., CASTELLANO, L. R., SERTORIO, M., RAFATI, S., CHEVILLARD, C., PRATA, A., ALCAIS, A., ARGIRO, L. & DESSEIN, A. 2008. Immunological and genetic evidence for a crucial role of IL-10 in cutaneous lesions in humans infected with Leishmania braziliensis. *J Immunol,* 180**,** 6139-48.

SAMPEY, G. C., SAIFUDDIN, M., SCHWAB, A., BARCLAY, R., PUNYA, S., CHUNG, M. C., HAKAMI, R. M., ZADEH, M. A., LEPENE, B., KLASE, Z. A., EL-HAGE, N., YOUNG, M., IORDANSKIY, S. & KASHANCHI, F. 2016. Exosomes from HIV-1-infected Cells Stimulate Production of Pro-inflammatory Cytokines through Trans-activating Response (TAR) RNA. *J Biol Chem,* 291**,** 1251-66.

SAMUEL, M., CHISANGA, D., LIEM, M., KEERTHIKUMAR, S., ANAND, S., ANG, C. S., ADDA, C. G., VERSTEEGEN, E., JOIS, M. & MATHIVANAN, S. 2017a. Bovine milk-derived exosomes from colostrum are enriched with proteins implicated in immune response and growth. *Sci Rep,* 7**,** 5933.

SAMUEL, P., FABBRI, M. & CARTER, D. R. F. 2017b. Mechanisms of drug resistance in cancer: The role of extracellular vesicles. *Proteomics*.

SANTRICH, C., MOORE, L., SHERWIN, T., BASTIN, P., BROKAW, C., GULL, K. & LEBOWITZ, J. H. 1997. A motility function for the paraflagellar rod of Leishmania parasites revealed by PFR-2 gene knockouts. *Mol Biochem Parasitol,* 90**,** 95-109.

SATOSKAR, A., BROMBACHER, F., DAI, W. J., MCINNES, I., LIEW, F. Y., ALEXANDER, J. & WALKER, W. 1997. SCID mice reconstituted with IL-4-deficient lymphocytes, but not immunocompetent lymphocytes, are resistant to cutaneous leishmaniasis. *J Immunol,* 159**,** 5005-13.

SCHIERA, G., DI LIEGRO, C. M., SALADINO, P., PITTI, R., SAVETTIERI, G., PROIA, P. & DI LIEGRO, I. 2013. Oligodendroglioma cells synthesize the differentiation-specific linker histone H1 and release it into the extracellular environment through shed vesicles. *Int J Oncol,* 43**,** 1771-6.

SCHINDLER, H., LUTZ, M. B., ROLLINGHOFF, M. & BOGDAN, C. 2001. The production of IFN-gamma by IL-12/IL-18-activated macrophages requires STAT4 signaling and is inhibited by IL-4. *J Immunol,* 166**,** 3075-82.

SCHONEBERG, J., LEE, I. H., IWASA, J. H. & HURLEY, J. H. 2017. Reverse-topology membrane scission by the ESCRT proteins. *Nat Rev Mol Cell Biol,* 18**,** 5-17.

SCHOREY, J. S., CHENG, Y., SINGH, P. P. & SMITH, V. L. 2015. Exosomes and other extracellular vesicles in host-pathogen interactions. *EMBO Rep,* 16**,** 24-43.

SCHRODER, K., IRVINE, K. M., TAYLOR, M. S., BOKIL, N. J., LE CAO, K. A., MASTERMAN, K. A., LABZIN, L. I., SEMPLE, C. A., KAPETANOVIC, R., FAIRBAIRN, L., AKALIN, A., FAULKNER, G. J., BAILLIE, J. K., GONGORA, M., DAUB, C. O., KAWAJI, H., MCLACHLAN, G. J., GOLDMAN, N., GRIMMOND, S. M., CARNINCI, P., SUZUKI, H., HAYASHIZAKI, Y., LENHARD, B., HUME, D. A. & SWEET, M. J. 2012. Conservation and divergence in Toll-like receptor 4-regulated gene expression in primary human versus mouse macrophages. *Proc Natl Acad Sci U S A,* 109**,** E944-53.

SCHUMANN BURKARD, G., JUTZI, P. & RODITI, I. 2011. Genome-wide RNAi screens in bloodstream form trypanosomes identify drug transporters. *Mol Biochem Parasitol,* 175**,** 91-4.

SCIANIMANICO, S., DESROSIERS, M., DERMINE, J. F., MERESSE, S., DESCOTEAUX, A. & DESJARDINS, M. 1999. Impaired recruitment of the small GTPase rab7 correlates with the inhibition of phagosome maturation by Leishmania donovani promastigotes. *Cell Microbiol,* 1**,** 19-32.

SEELEY, J. J. & GHOSH, S. 2017. Molecular mechanisms of innate memory and tolerance to LPS. *J Leukoc Biol,* 101**,** 107-119.

SFRISO, P., OLIVIERO, F., CALABRESE, F., MIORIN, M., FACCO, M., CONTRI, A., CABRELLE, A., BAESSO, I., COZZI, F., ANDRETTA, M., CASSATELLA, M. A., FIOCCO, U., TODESCO, S., KONTTINEN, Y. T., PUNZI, L. & AGOSTINI, C. 2006. Epithelial CXCR3-B regulates chemokines bioavailability in normal, but not in Sjogren's syndrome, salivary glands. *J Immunol,* 176**,** 2581-9.

SHARMA, U. & SINGH, S. 2009. Immunobiology of leishmaniasis. *Indian J Exp Biol,* 47**,** 412-23.

SHELKE, G. V., LASSER, C., GHO, Y. S. & LOTVALL, J. 2014. Importance of exosome depletion protocols to eliminate functional and RNA-containing extracellular vesicles from fetal bovine serum. *J Extracell Vesicles,* 3.

SHIO, M. T., HASSANI, K., ISNARD, A., RALPH, B., CONTRERAS, I., GOMEZ, M. A., ABU-DAYYEH, I. & OLIVIER, M. 2012. Host cell signalling and leishmania mechanisms of evasion. *J Trop Med,* 2012**,** 819512.

SHWEASH, M., ADRIENNE MCGACHY, H., SCHROEDER, J., NEAMATALLAH, T., BRYANT, C. E., MILLINGTON, O., MOTTRAM, J. C., ALEXANDER, J. & PLEVIN, R. 2011. Leishmania mexicana promastigotes inhibit macrophage IL-12 production via TLR-4 dependent COX-2, iNOS and arginase-1 expression. *Mol Immunol,* 48**,** 1800-8.

SILVERMAN, J. M., CHAN, S. K., ROBINSON, D. P., DWYER, D. M., NANDAN, D., FOSTER, L. J. & REINER, N. E. 2008. Proteomic analysis of the secretome of Leishmania donovani. *Genome Biol,* 9**,** R35.

SILVERMAN, J. M., CLOS, J., DE'OLIVEIRA, C. C., SHIRVANI, O., FANG, Y., WANG, C., FOSTER, L. J. & REINER, N. E. 2010a. An exosome-based secretion pathway is responsible for protein export from Leishmania and communication with macrophages. *J Cell Sci,* 123**,** 842-52.

SILVERMAN, J. M., CLOS, J., HORAKOVA, E., WANG, A. Y., WIESGIGL, M., KELLY, I., LYNN, M. A., MCMASTER, W. R., FOSTER, L. J., LEVINGS, M. K. & REINER, N. E. 2010b. Leishmania exosomes modulate innate and adaptive immune responses through effects on monocytes and dendritic cells. *J Immunol,* 185**,** 5011-22.

SILVERMAN, J. M. & REINER, N. E. 2011. Leishmania exosomes deliver preemptive strikes to create an environment permissive for early infection. *Front Cell Infect Microbiol,* 1**,** 26.

SILVESTRE, R., SILVA, A. M., CORDEIRO-DA-SILVA, A. & OUAISSI, A. 2009. The contribution of Toll-like receptor 2 to the innate recognition of a Leishmania infantum silent information regulator 2 protein. *Immunology,* 128**,** 484-99.

SINHA, S., HOSHINO, D., HONG, N. H., KIRKBRIDE, K. C., GREGA-LARSON, N. E., SEIKI, M., TYSKA, M. J. & WEAVER, A. M. 2016. Cortactin promotes exosome secretion by controlling branched actin dynamics. *J Cell Biol,* 214**,** 197-213.

SLACK, E. C., ROBINSON, M. J., HERNANZ-FALCON, P., BROWN, G. D., WILLIAMS, D. L., SCHWEIGHOFFER, E., TYBULEWICZ, V. L. & REIS E SOUSA, C. 2007. Syk-dependent ERK activation regulates IL-2 and IL-10 production by DC stimulated with zymosan. *Eur J Immunol,* 37**,** 1600-12.

SOARES-SILVA, M., DINIZ, F. F., GOMES, G. N. & BAHIA, D. 2016. The Mitogen-Activated Protein Kinase (MAPK) Pathway: Role in Immune Evasion by Trypanosomatids. *Front Microbiol,* 7**,** 183.

SOBIRK, S. K., MORGELIN, M., EGESTEN, A., BATES, P., SHANNON, O. & COLLIN, M. 2013. Human chemokines as antimicrobial peptides with direct parasiticidal effect on Leishmania mexicana in vitro. *PLoS One,* 8**,** e58129.

SOUZA, A. E., WAUGH, S., COOMBS, G. H. & MOTTRAM, J. C. 1992. Characterization of a multi-copy gene for a major stage-specific cysteine proteinase of Leishmania mexicana. *FEBS Lett,* 311**,** 124-7.

SPATH, G. F. & BEVERLEY, S. M. 2001. A lipophosphoglycan-independent method for isolation of infective Leishmania metacyclic promastigotes by density gradient centrifugation. *Exp Parasitol,* 99**,** 97-103.

SPATH, G. F., EPSTEIN, L., LEADER, B., SINGER, S. M., AVILA, H. A., TURCO, S. J. & BEVERLEY, S. M. 2000. Lipophosphoglycan is a virulence factor distinct from related glycoconjugates in the protozoan parasite Leishmania major. *Proc Natl Acad Sci U S A,* 97**,** 9258-63.

SPATH, G. F., LYE, L. F., SEGAWA, H., SACKS, D. L., TURCO, S. J. & BEVERLEY, S. M. 2003. Persistence without pathology in phosphoglycan-deficient Leishmania major. *Science,* 301**,** 1241-3.

SRIVASTAVA, A., SINGH, N., MISHRA, M., KUMAR, V., GOUR, J. K., BAJPAI, S., SINGH, S., PANDEY, H. P. & SINGH, R. K. 2012. Identification of TLR inducing Th1-responsive Leishmania donovani amastigote-specific antigens. *Mol Cell Biochem,* 359**,** 359-68.

SRIVASTAVA, S., PANDEY, S. P., JHA, M. K., CHANDEL, H. S. & SAHA, B. 2013. Leishmania expressed lipophosphoglycan interacts with Toll-like receptor (TLR)-2 to decrease TLR-9 expression and reduce anti-leishmanial responses. *Clin Exp Immunol,* 172**,** 403-9.

STEFANOVA, I., HEMMER, B., VERGELLI, M., MARTIN, R., BIDDISON, W. E. & GERMAIN, R. N. 2003. TCR ligand discrimination is enforced by competing ERK positive and SHP-1 negative feedback pathways. *Nat Immunol,* 4**,** 248-54.

STIERHOF, Y. D., BATES, P. A., JACOBSON, R. L., ROGERS, M. E., SCHLEIN, Y., HANDMAN, E. & ILG, T. 1999. Filamentous proteophosphoglycan secreted by Leishmania promastigotes forms gel-like three-dimensional networks that obstruct the digestive tract of infected sandfly vectors. *Eur J Cell Biol,* 78**,** 675-89.

STIERHOF, Y. D., WIESE, M., ILG, T., OVERATH, P., HANER, M. & AEBI, U. 1998. Structure of a filamentous phosphoglycoprotein polymer: the secreted acid phosphatase of Leishmania mexicana. *J Mol Biol,* 282**,** 137-48.

STOW, J. L., LOW, P. C., OFFENHAUSER, C. & SANGERMANI, D. 2009. Cytokine secretion in macrophages and other cells: pathways and mediators. *Immunobiology,* 214**,** 601-12.

STRAUSS-AYALI, D., BANETH, G., SHOR, S., OKANO, F. & JAFFE, C. L. 2005. Interleukin-12 augments a Th1-type immune response manifested as lymphocyte proliferation and interferon gamma production in Leishmania infantum-infected dogs. *Int J Parasitol,* 35**,** 63-73.

STUCHELL-BRERETON, M. D., SKALICKY, J. J., KIEFFER, C., KARREN, M. A., GHAFFARIAN, S. & SUNDQUIST, W. I. 2007. ESCRT-III recognition by VPS4 ATPases. *Nature,* 449**,** 740-4.

SULLIVAN, R., MARESH, G., ZHANG, X., SALOMON, C., HOOPER, J., MARGOLIN, D. & LI, L. 2017. The Emerging Roles of Extracellular Vesicles As Communication Vehicles within the Tumor Microenvironment and Beyond. *Front Endocrinol (Lausanne),* 8**,** 194.

SUNDAR, S. & SINGH, A. 2016. Recent developments and future prospects in the treatment of visceral leishmaniasis. *Ther Adv Infect Dis,* 3**,** 98-109.

SWIHART, K., FRUTH, U., MESSMER, N., HUG, K., BEHIN, R., HUANG, S., DEL GIUDICE, G., AGUET, M. & LOUIS, J. A. 1995. Mice from a genetically resistant background lacking the interferon gamma receptor are susceptible to infection with Leishmania major but mount a polarized T helper cell 1-type CD4+ T cell response. *J Exp Med,* 181**,** 961-71.

SZATANEK, R., BARAN, J., SIEDLAR, M. & BAJ-KRZYWORZEKA, M. 2015. Isolation of extracellular vesicles: Determining the correct approach (Review). *Int J Mol Med,* 36**,** 11-7.

SZEMPRUCH, A. J., DENNISON, L., KIEFT, R., HARRINGTON, J. M. & HAJDUK, S. L. 2016a. Sending a message: extracellular vesicles of pathogenic protozoan parasites. *Nat Rev Microbiol,* 14**,** 669-675.

SZEMPRUCH, A. J., SYKES, S. E., KIEFT, R., DENNISON, L., BECKER, A. C., GARTRELL, A., MARTIN, W. J., NAKAYASU, E. S., ALMEIDA, I. C., HAJDUK, S. L. & HARRINGTON, J. M. 2016b. Extracellular Vesicles from Trypanosoma brucei Mediate Virulence Factor Transfer and Cause Host Anemia. *Cell,* 164**,** 246-57.

TASLIMI, Y., ZAHEDIFARD, F., HABIBZADEH, S., TAHERI, T., ABBASPOUR, H., SADEGHIPOUR, A., MOHIT, E. & RAFATI, S. 2016. Antitumor Effect of IP-10 by Using Two Different Approaches: Live Delivery System and Gene Therapy. *J Breast Cancer,* 19**,** 34-44.

TEIXEIRA, C., GOMES, R., OLIVEIRA, F., MENESES, C., GILMORE, D. C., ELNAIEM, D. E., VALENZUELA, J. G. & KAMHAWI, S. 2014. Characterization of the early inflammatory infiltrate at the feeding site of infected sand flies in mice protected from vector-transmitted Leishmania major by exposure to uninfected bites. *PLoS Negl Trop Dis,* 8**,** e2781.

TEIXEIRA, M. J., TEIXEIRA, C. R., ANDRADE, B. B., BARRAL-NETTO, M. & BARRAL, A. 2006. Chemokines in host-parasite interactions in leishmaniasis. *Trends Parasitol,* 22**,** 32-40.

TESTA, U., PELOSI, E., CASTELLI, G. & LABBAYE, C. 2017. miR-146 and miR-155: Two Key Modulators of Immune Response and Tumor Development. *Non-Coding RNA,* 3.

THERY, C., DUBAN, L., SEGURA, E., VERON, P., LANTZ, O. & AMIGORENA, S. 2002a. Indirect activation of naive CD4+ T cells by dendritic cell-derived exosomes. *Nat Immunol,* 3**,** 1156-62.

THERY, C., ZITVOGEL, L. & AMIGORENA, S. 2002b. Exosomes: composition, biogenesis and function. *Nat Rev Immunol,* 2**,** 569-79.

THIAKAKI, M., KOLLI, B., CHANG, K. P. & SOTERIADOU, K. 2006. Down-regulation of gp63 level in Leishmania amazonensis promastigotes reduces their infectivity in BALB/c mice. *Microbes Infect,* 8**,** 1455-63.

TIEDJE, C., HOLTMANN, H. & GAESTEL, M. 2014. The role of mammalian MAPK signaling in regulation of cytokine mRNA stability and translation. *J Interferon Cytokine Res,* 34**,** 220-32.

TOMINAGA, K., SAITO, S., MATSUURA, M. & NAKANO, M. 1999. Lipopolysaccharide tolerance in murine peritoneal macrophages induces downregulation of the lipopolysaccharide signal transduction pathway through

mitogen-activated protein kinase and nuclear factor-kappaB cascades, but not lipopolysaccharide-incorporation steps. *Biochim Biophys Acta,* 1450**,** 130-44.
TONDELEIR, D., LAMBRECHTS, A., MULLER, M., JONCKHEERE, V., DOLL, T., VANDAMME, D., BAKKALI, K., WATERSCHOOT, D., LEMAISTRE, M., DEBEIR, O., DECAESTECKER, C., HINZ, B., STAES, A., TIMMERMAN, E., COLAERT, N., GEVAERT, K., VANDEKERCKHOVE, J. & AMPE, C. 2012. Cells lacking beta-actin are genetically reprogrammed and maintain conditional migratory capacity. *Mol Cell Proteomics,* 11**,** 255-71.
TRUDGIAN, D. C., RIDLOVA, G., FISCHER, R., MACKEEN, M. M., TERNETTE, N., ACUTO, O., KESSLER, B. M. & THOMAS, B. 2011. Comparative evaluation of label-free SINQ normalized spectral index quantitation in the central proteomics facilities pipeline. *Proteomics,* 11**,** 2790-7.
TULL, D., NADERER, T., SPURCK, T., MERTENS, H. D., HENG, J., MCFADDEN, G. I., GOOLEY, P. R. & MCCONVILLE, M. J. 2010. Membrane protein SMP-1 is required for normal flagellum function in Leishmania. *J Cell Sci,* 123**,** 544-54.
TURCO, S. J., HULL, S. R., ORLANDI, P. A., JR., SHEPHERD, S. D., HOMANS, S. W., DWEK, R. A. & RADEMACHER, T. W. 1987. Structure of the major carbohydrate fragment of the Leishmania donovani lipophosphoglycan. *Biochemistry,* 2*6***,** 6233-8.
UENO, N. & WILSON, M. E. 2012. Receptor-mediated phagocytosis of Leishmania: implications for intracellular survival. *Trends Parasitol,* 2*8***,** 335-44.
UNTERGASSER, A., CUTCUTACHE, I., KORESSAAR, T., YE, J., FAIRCLOTH, B. C., REMM, M. & ROZEN, S. G. 2012. Primer3--new capabilities and interfaces. *Nucleic Acids Res,* 40**,** e115.
VAN WILGENBURG, B., BROWNE, C., VOWLES, J. & COWLEY, S. A. 2013. Efficient, long term production of monocyte-derived macrophages from human pluripotent stem cells under partly-defined and fully-defined conditions. *PLoS One,* 8**,** e71098.
VANNIER-SANTOS, M. A., URBINA, J. A., MARTINY, A., NEVES, A. & DE SOUZA, W. 1995. Alterations induced by the antifungal compounds ketoconazole and terbinafine in Leishmania. *J Eukaryot Microbiol,* 42**,** 337-46.
VARGAS-INCHAUSTEGUI, D. A., HOGG, A. E., TULLIANO, G., LLANOS-CUENTAS, A., AREVALO, J., ENDSLEY, J. J. & SOONG, L. 2010. CXCL10 production by human monocytes in response to Leishmania braziliensis infection. *Infect Immun,* 78**,** 301-8.
VARGAS-INCHAUSTEGUI, D. A., TAI, W., XIN, L., HOGG, A. E., CORRY, D. B. & SOONG, L. 2009. Distinct roles for MyD88 and Toll-like receptor 2 during Leishmania braziliensis infection in mice. *Infect Immun,* 77**,** 2948-56.
VASQUEZ, R. E. & SOONG, L. 2006. CXCL10/gamma interferon-inducible protein 10-mediated protection against Leishmania amazonensis infection in mice. *Infect Immun,* 74**,** 6769-77.
VAURE, C. & LIU, Y. 2014. A comparative review of toll-like receptor 4 expression and functionality in different animal species. *Front Immunol,* 5**,** 316.
VEGA, V. L., RODRIGUEZ-SILVA, M., FREY, T., GEHRMANN, M., DIAZ, J. C., STEINEM, C., MULTHOFF, G., ARISPE, N. & DE MAIO, A. 2008. Hsp70 translocates into the plasma membrane after stress and is released into the extracellular environment in a membrane-associated form that activates macrophages. *J Immunol,* 180**,** 4299-307.
VINCE, J. E., TULL, D., LANDFEAR, S. & MCCONVILLE, M. J. 2011. Lysosomal degradation of Leishmania hexose and inositol transporters is regulated in a stage-, nutrient- and ubiquitin-dependent manner. *Int J Parasitol,* 41**,** 791-800.
VINET, A. F., FUKUDA, M., TURCO, S. J. & DESCOTEAUX, A. 2009. The Leishmania donovani lipophosphoglycan excludes the vesicular proton-ATPase from phagosomes by impairing the recruitment of synaptotagmin V. *PLoS Pathog,* 5**,** e1000628.

VIRCA, G. D., KIM, S. Y., GLASER, K. B. & ULEVITCH, R. J. 1989. Lipopolysaccharide induces hyporesponsiveness to its own action in RAW 264.7 cells. *J Biol Chem,* 264**,** 21951-6.

VOGEL, R., COUMANS, F. A., MALTESEN, R. G., BOING, A. N., BONNINGTON, K. E., BROEKMAN, M. L., BROOM, M. F., BUZAS, E. I., CHRISTIANSEN, G., HAJJI, N., KRISTENSEN, S. R., KUEHN, M. J., LUND, S. M., MAAS, S. L., NIEUWLAND, R., OSTEIKOETXEA, X., SCHNOOR, R., SCICLUNA, B. J., SHAMBROOK, M., DE VRIJ, J., MANN, S. I., HILL, A. F. & PEDERSEN, S. 2016. A standardized method to determine the concentration of extracellular vesicles using tunable resistive pulse sensing. *J Extracell Vesicles,* 5**,** 31242.

VON STEBUT, E., EHRCHEN, J. M., BELKAID, Y., KOSTKA, S. L., MOLLE, K., KNOP, J., SUNDERKOTTER, C. & UDEY, M. C. 2003. Interleukin 1alpha promotes Th1 differentiation and inhibits disease progression in Leishmania major-susceptible BALB/c mice. *J Exp Med,* 198**,** 191-9.

WALL, E. A., ZAVZAVADJIAN, J. R., CHANG, M. S., RANDHAWA, B., ZHU, X., HSUEH, R. C., LIU, J., DRIVER, A., BAO, X. R., STERNWEIS, P. C., SIMON, M. I. & FRASER, I. D. 2009. Suppression of LPS-induced TNF-alpha production in macrophages by cAMP is mediated by PKA-AKAP95-p105. *Sci Signal,* 2**,** ra28.

WAN, W., LIU, Q., LIONAKIS, M. S., MARINO, A. P., ANDERSON, S. A., SWAMYDAS, M. & MURPHY, P. M. 2015. Atypical chemokine receptor 1 deficiency reduces atherogenesis in ApoE-knockout mice. *Cardiovasc Res,* 106**,** 478-87.

WANG, J., SILVA, M., HAAS, L. A., MORSCI, N. S., NGUYEN, K. C., HALL, D. H. & BARR, M. M. 2014. C. elegans ciliated sensory neurons release extracellular vesicles that function in animal communication. *Curr Biol,* 24**,** 519-25.

WANG, J., WAKEHAM, J., HARKNESS, R. & XING, Z. 1999. Macrophages are a significant source of type 1 cytokines during mycobacterial infection. *J Clin Invest,* 103**,** 1023-9.

WANG, Z. E., REINER, S. L., ZHENG, S., DALTON, D. K. & LOCKSLEY, R. M. 1994. CD4+ effector cells default to the Th2 pathway in interferon gamma-deficient mice infected with Leishmania major. *J Exp Med,* 179**,** 1367-71.

WEBER, M., BLAIR, E., SIMPSON, C. V., O'HARA, M., BLACKBURN, P. E., ROT, A., GRAHAM, G. J. & NIBBS, R. J. 2004. The chemokine receptor D6 constitutively traffics to and from the cell surface to internalize and degrade chemokines. *Mol Biol Cell,* 15**,** 2492-508.

WEISE, F., STIERHOF, Y. D., KUHN, C., WIESE, M. & OVERATH, P. 2000. Distribution of GPI-anchored proteins in the protozoan parasite Leishmania, based on an improved ultrastructural description using high-pressure frozen cells. *J Cell Sci,* 113 Pt 24**,** 4587-603.

WELTON, J. L., BRENNAN, P., GURNEY, M., WEBBER, J. P., SPARY, L. K., CARTON, D. G., FALCON-PEREZ, J. M., WALTON, S. P., MASON, M. D., TABI, Z. & CLAYTON, A. 2016. Proteomics analysis of vesicles isolated from plasma and urine of prostate cancer patients using a multiplex, aptamer-based protein array. *J Extracell Vesicles,* 5**,** 31209.

WHEELER, R. J., GLUENZ, E. & GULL, K. 2011. The cell cycle of Leishmania: morphogenetic events and their implications for parasite biology. *Mol Microbiol,* 79**,** 647-62.

WHEELER, R. J., GLUENZ, E. & GULL, K. 2015. Basal body multipotency and axonemal remodelling are two pathways to a 9+0 flagellum. *Nat Commun,* 6**,** 8964.

WHITAKER, S. M., COLMENARES, M., PESTANA, K. G. & MCMAHON-PRATT, D. 2008. Leishmania pifanoi proteoglycolipid complex P8 induces macrophage cytokine production through Toll-like receptor 4. *Infect Immun,* 76**,** 2149-56.

WHO. 2017. *Leishmaniasis fact sheet* [Online]. Available: http://www.who.int/mediacentre/factsheets/fs375/en/.
WIDNEY, D. P., XIA, Y. R., LUSIS, A. J. & SMITH, J. B. 2000. The murine chemokine CXCL11 (IFN-inducible T cell alpha chemoattractant) is an IFN-gamma- and lipopolysaccharide-inducible glucocorticoid-attenuated response gene expressed in lung and other tissues during endotoxemia. *J Immunol,* 164**,** 6322-31.
WIESE, M., KUHN, D. & GRUNFELDER, C. G. 2003. Protein kinase involved in flagellar-length control. *Eukaryot Cell,* 2**,** 769-77.
WILLMS, E., JOHANSSON, H. J., MAGER, I., LEE, Y., BLOMBERG, K. E., SADIK, M., ALAARG, A., SMITH, C. I., LEHTIO, J., EL ANDALOUSSI, S., WOOD, M. J. & VADER, P. 2016. Cells release subpopulations of exosomes with distinct molecular and biological properties. *Sci Rep,* 6**,** 22519.
WILSON, M. E., PAETZ, K. E., RAMAMOORTHY, R. & DONELSON, J. E. 1993. The effect of ongoing protein synthesis on the steady state levels of Gp63 RNAs in Leishmania chagasi. *J Biol Chem,* 268**,** 15731-6.
WINZEN, R., KRACHT, M., RITTER, B., WILHELM, A., CHEN, C. Y., SHYU, A. B., MULLER, M., GAESTEL, M., RESCH, K. & HOLTMANN, H. 1999. The p38 MAP kinase pathway signals for cytokine-induced mRNA stabilization via MAP kinase-activated protein kinase 2 and an AU-rich region-targeted mechanism. *EMBO J,* 18**,** 4969-80.
WOLF, M. & MOSER, B. 2012. Antimicrobial activities of chemokines: not just a side-effect? *Front Immunol,* 3**,** 213.
WOOD, C. R., HUANG, K., DIENER, D. R. & ROSENBAUM, J. L. 2013. The cilium secretes bioactive ectosomes. *Curr Biol,* 23**,** 906-11.
WOOD, C. R. & ROSENBAUM, J. L. 2015. Ciliary ectosomes: transmissions from the cell's antenna. *Trends Cell Biol*.
WYSOCKA, M., ROBERTSON, S., RIEMANN, H., CAAMANO, J., HUNTER, C., MACKIEWICZ, A., MONTANER, L. J., TRINCHIERI, G. & KARP, C. L. 2001. IL-12 suppression during experimental endotoxin tolerance: dendritic cell loss and macrophage hyporesponsiveness. *J Immunol,* 166**,** 7504-13.
YANG, C. H., WEI, L., PFEFFER, S. R., DU, Z., MURTI, A., VALENTINE, W. J., ZHENG, Y. & PFEFFER, L. M. 2007a. Identification of CXCL11 as a STAT3-dependent gene induced by IFN. *J Immunol,* 178**,** 986-92.
YANG, Z., MOSSER, D. M. & ZHANG, X. 2007b. Activation of the MAPK, ERK, following Leishmania amazonensis infection of macrophages. *J Immunol,* 178**,** 1077-85.
YAO, C., DONELSON, J. E. & WILSON, M. E. 2003. The major surface protease (MSP or GP63) of Leishmania sp. Biosynthesis, regulation of expression, and function. *Mol Biochem Parasitol,* 132**,** 1-16.
YOKOI, A., YOSHIOKA, Y. & OCHIYA, T. 2015. Towards the realization of clinical extracellular vesicle diagnostics: challenges and opportunities. *Expert Rev Mol Diagn,* 15**,** 1555-66.
YOSHIOKA, Y., KONISHI, Y., KOSAKA, N., KATSUDA, T., KATO, T. & OCHIYA, T. 2013. Comparative marker analysis of extracellular vesicles in different human cancer types. *J Extracell Vesicles,* 2.
YOUNG, R. W. 1971. The renewal of rod and cone outer segments in the rhesus monkey. *J Cell Biol,* 49**,** 303-18.
ZANGGER, H., MOTTRAM, J. C. & FASEL, N. 2002. Cell death in Leishmania induced by stress and differentiation: programmed cell death or necrosis? *Cell Death Differ,* 9**,** 1126-39.
ZHANG, D., CAO, X., LI, J. & ZHAO, G. 2015. MiR-210 inhibits NF-kappaB signaling pathway by targeting DR6 in osteoarthritis. *Sci Rep,* 5**,** 12775.
ZHOU, J., TANG, P. C., QIN, L., GAYED, P. M., LI, W., SKOKOS, E. A., KYRIAKIDES, T. R., POBER, J. S. & TELLIDES, G. 2010. CXCR3-dependent accumulation

and activation of perivascular macrophages is necessary for homeostatic arterial remodeling to hemodynamic stresses. *J Exp Med,* 207**,** 1951-66.

ZHOU, W., ZHU, P., WANG, J., PASCUAL, G., OHGI, K. A., LOZACH, J., GLASS, C. K. & ROSENFELD, M. G. 2008. Histone H2A monoubiquitination represses transcription by inhibiting RNA polymerase II transcriptional elongation. *Mol Cell,* 29**,** 69-80.

ZHU, Z., ZHANG, D., LEE, H., MENON, A. A., WU, J., HU, K. & JIN, Y. 2017. Macrophage-derived apoptotic bodies promote the proliferation of the recipient cells via shuttling microRNA-221/222. *J Leukoc Biol,* 101**,** 1349-1359.

ZWEEMER, A. J., FRENCH, C. B., MESFIN, J., GORDONOV, S., MEYER, A. S. & LAUFFENBURGER, D. A. 2017. Apoptotic Bodies Elicit Gas6-mediated Migration of AXL-expressing Tumor Cells. *Mol Cancer Res*.